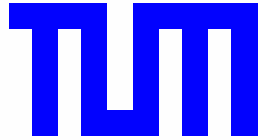

**Institut für Humangenetik,
Technische Universität München und
GSF-Forschungszentrum für Umwelt und Gesundheit**



**Functional Proteome Analysis of
Pathophysiological Variants of the AAA-
ATPase Cdc48p/VCP**

Dipl.-Biochem. Ralf Josef Braun

Vollständiger Abdruck der von der Fakultät Wissenschaftszentrum Weihenstephan für Ernährung, Landnutzung und Umwelt der Technischen Universität München zur Erlangung des akademischen Grades eines

Doktors der Naturwissenschaften

genehmigten Dissertation.

Vorsitzender: Univ.-Prof. Dr. Erwin Grill

Prüfer der Dissertation: 1. apl. Prof. Dr. Jerzy Adamski
2. Univ.-Prof. Dr. Bertold Hock, em.
3. Univ.-Prof. Dr. Frank Madeo,
Karl-Franzens-Universität Graz/Österreich

Die Dissertation wurde am 05.10.2006 bei der Technischen Universität München eingereicht und durch die Fakultät Wissenschaftszentrum Weihenstephan für Ernährung, Landnutzung und Umwelt am 21.12.2006 angenommen.

Meinen Eltern,
meinem Bruder
und meiner Angelika

Table of Contents

A. ABBREVIATIONS	9
B. SUMMARY.....	13
C. ZUSAMMENFASSUNG	15
D. INTRODUCTION.....	17
1. PROTEOMICS AND FUNCTIONAL PROTEOMICS	17
1.1 Proteome and proteomics	17
1.1.1 Proteomics describes the dynamic protein expression pattern of a cell	17
1.1.2 Proteome analyses were enabled by the development of new techniques	17
1.1.3 Combination of complementary techniques and reducing complexity of protein samples facilitate the full description of a proteome	18
1.2 Functional proteomics.....	19
2. STRUCTURE AND CELLULAR ROLE OF THE AAA-ATPASE CDC48P/VCP	21
2.1 Historical overview	21
2.2 Cdc48p/VCP is a ubiquitous highly conserved protein	21
2.3 Cdc48p/VCP is a member of the AAA-ATPase family	22
2.4 The Cdc48p/VCP-ATPase is controlled by ubiquitin	24
2.5 Cdc48p/VCP participates in a variety of different cellular processes	25
2.5.1 Protein degradation.....	25
2.5.2 ER-associated protein degradation (ERAD).....	25
2.5.3 Cell cycle regulation.....	28
2.5.4 Transcriptional control.....	28
2.5.5 Membrane fusion	29
2.5.6 Chaperone activity.....	29
2.5.7 DNA repair	30
3. ROLE OF CDC48P/VCP UNDER PATHOPHYSIOLOGICAL CONDITIONS	31
3.1 Mutant VCP causes the rare dominant multisystem disorder IBMPFD	31
3.2 Wild-type VCP and human protein deposit disorders.....	31
3.3 Cdc48p/VCP and apoptosis: From humans to yeast	33
4. YEAST AS A MODEL	35
4.1 Yeast as a model for conserved cellular processes in eukaryotes.....	35
4.2 Yeast as a model for the analysis of evolutionary conserved mechanisms of apoptotic cell death	35
5. AIM OF THE STUDY	39
E. MATERIAL AND METHODS	41
1. MATERIAL.....	41
1.1 Chemicals.....	41
1.2 General equipment.....	41
1.3 Protein chemistry	41
1.3.1 Special equipment.....	41
1.3.2 Kits	42
1.4 Molecular biology	42
1.4.1 Special equipment.....	42
1.4.2 Kits	42
1.4.3 E. coli strains.....	42
1.4.4 Enzymes	42
1.4.5 Oligonucleotides.....	42
1.4.6 Plasmids and constructs	43
1.4.6.1 Plasmids	43
1.4.6.2 Constructs.....	44
1.5 Analysis of yeast and mammalian cell cultures.....	44
1.5.1 Special equipment.....	44
1.5.2 Kits	44
1.5.3 Yeast strains and mammalian cell lines.....	45
1.5.3.1 Yeast strains	45
1.5.3.2 Mammalian cell lines	45
1.5.4 Antibodies.....	45
1.6 Software and databases	46
1.6.1 Software.....	46

1.6.2 Databases	46
2. METHODS	47
2.1 Protein chemistry	47
2.1.1 Determination of protein concentration	47
2.1.2 Protein precipitation	47
2.1.3 SDS-PAGE	48
2.1.4 Staining of SDS gels	49
2.1.4.1 Silver staining	49
2.1.4.2 Coomassie staining	50
2.1.4.3 Colloidal Coomassie staining	50
2.1.4.4 Ruthenium-II-bathophenanthroline disulfonate chelate (RuBP) staining	51
2.1.4.5 Digitalizing and drying of SDS gels	52
2.1.5 Western blot analysis	52
2.1.6 Two-dimensional gel electrophoresis (2-DE)	54
2.1.6.1 Sample preparation	54
2.1.6.2 Rehydration and sample loading	55
2.1.6.3 Isoelectric focusing (IEF)	56
2.1.6.4 Casting of the polyacrylamide gels for the second dimension	56
2.1.6.5 Equilibration and transfer of the IPG strips	57
2.1.6.6 Second dimension: SDS-PAGE	58
2.1.6.7 Image analysis	58
2.1.7 16-BAC/SDS gel electrophoresis	59
2.1.7.1 First dimension: 16-BAC-PAGE	59
2.1.7.2 Casting of SDS gels	60
2.1.7.3 Equilibration and transfer of the 16-BAC gel strips	61
2.1.7.4 Second dimension: SDS-PAGE	61
2.1.8 MALDI-ToF mass spectrometry	62
2.1.8.1 Destaining, reduction, alkylation of gel plugs and in-gel proteolysis	62
2.1.8.2 MALDI-TOF mass spectrometry	63
2.1.8.3 Peptide mass fingerprinting (PMF) and database searching	64
2.2 Molecular biology	66
2.2.1 <i>E. coli</i> cultures	66
2.2.1.1 Liquid cultures	66
2.2.1.2 Plating cultures	66
2.2.1.3 Cryo cultures	66
2.2.1.4 Generation of chemically competent <i>E. coli</i>	66
2.2.2 Chemical transformation of <i>E. coli</i>	67
2.2.3 Plasmid DNA preparation	67
2.2.4 DNA sequencing	68
2.2.5 Agarose gel electrophoresis	69
2.2.6 Polymerase chain reaction (PCR)	69
2.2.7 DNA restriction	70
2.2.8 DNA ligation	70
2.2.9 TOPO cloning	70
2.2.10 DNA cloning	71
2.2.10.1 Subcloning	71
2.2.10.2 PCR-based cloning	71
2.2.10.3 TOPO-based cloning	71
2.2.11 Site-directed mutagenesis	72
2.2.12 Generation of VCP constructs	72
2.3 Analysis of yeast cultures	75
2.3.1 Yeast culture	75
2.3.1.1 Liquid cultures	75
2.3.1.2 Plating cultures	75
2.3.1.3 Cryo cultures	75
2.3.1.4 Determination of cell density	75
2.3.2 Generation of ρ^0 strains	76
2.3.3 Culture conditions for the induction of apoptosis	76
2.3.4 Viability of yeast cultures	76
2.3.4.1 Survival plating assay	76
2.3.4.2 Differential plating assay	77
2.3.5 Test for apoptosis	77
2.3.5.1 TUNEL Assay	77
2.3.5.2 Staining of reactive oxygen species (ROS) in yeast cells	78
2.3.5.3 <i>In vivo</i> measurement of caspase-like enzymatic activity in yeast cells	79
2.3.6 <i>In vivo</i> fluorescence microscopy	79
2.3.7 Electron microscopy (EM)	79
2.3.8 Preparation of cell extracts and cell fractionation	80

2.3.8.1 Preparation of cell extracts	80
2.3.8.2 Cell fractionation	81
2.3.9 Analysis of mitochondria by zone-electrophoresis in a free-flow device	83
2.3.9.1 Principle of zone-electrophoresis in a free-flow device (ZE-FFE)	83
2.3.9.2 Quality tests for correct instrument assembly and flow profile	83
2.3.9.3 Analysis of mitochondria by ZE-FFE	84
2.4 Analysis of mammalian cell cultures	85
2.4.1 Growth and maintenance of mammalian cell cultures	85
2.4.2 Transient transfection of mammalian cell cultures	85
2.4.3 Generation of protein extracts	86
2.4.4 Fluorescence microscopy	86
2.4.5 Immunofluorescence microscopy	86
2.4.6 Cell viability assay (Live-Dead Assay)	88
F. RESULTS	89
1. ANALYSIS OF CDC48P VARIANTS IN YEAST	89
1.1 Cell viability and apoptosis in the <i>cdc48^{S565G}</i> strain	89
1.1.1 Cell viability is decreased and susceptibility for apoptotic cell death is increased upon CDC48 mutation in yeast	89
1.2 Differential 2-DE analysis of the <i>cdc48^{S565G}</i> strain	92
1.2.1 Distinct alterations are observed in mitochondrial extracts of <i>cdc48^{S565G}</i> cells compared to wild-type cells under apoptotic growth conditions	92
1.2.3 Cdc48p-S565G and other proteins associated with the NE-ER accumulate in mitochondrial extracts of <i>cdc48^{S565G}</i> cells	95
1.3 Crucial mitochondrial impairment in the <i>cdc48^{S565G}</i> strain	99
1.3.1 Mitochondria in <i>cdc48^{S565G}</i> cells are enlarged compared to wild-type cells under apoptotic growth conditions	99
1.3.2 <i>Cdc48^{S565G}</i> cells show respiratory deficiency under apoptotic growth conditions	99
1.3.3 Cytochrome c accumulates in the cytosol of <i>cdc48^{S565G}</i> cells under early apoptotic growth conditions	102
1.3.4 Reactive oxygen species (ROS) accumulate in <i>cdc48^{S565G}</i> cells under early apoptotic growth conditions	102
1.3.5 Accumulating ROS are predominantly produced by the mitochondrial cytochrome bc ₁ complex	104
1.3.6 ρ^0 strains generated from wild-type and <i>cdc48^{S565G}</i> strains are unable to produce ROS and demonstrate highly similar viability under apoptotic growth conditions	105
1.3.7 Caspase-like enzymatic activity emerges in <i>cdc48^{S565G}</i> cells under early apoptotic growth conditions	106
1.4 Cdc48p-S565G dysfunction in ERAD is paralleled by increased association of NE-ER and mitochondria	110
1.4.1 CDC48 mutation (<i>cdc48^{S565G}</i>) leads to accumulation of polyubiquitinated proteins and ER stress	110
1.4.2 Polyubiquitinated proteins, Cdc48p-S565G and microsomes stably co-migrate with mitochondria in the <i>cdc48^{S565G}</i> strain under apoptotic growth conditions	111
1.4.3 Zone-electrophoresis in a free-flow device (ZE-FFE) allows the separation of a NE-ER-containing mitochondrial side fraction from the mitochondrial main fraction in wild-type and <i>cdc48^{S565G}</i> strain	113
1.4.4 Polyubiquitinated proteins and Cdc48p-S565G accumulate in the mitochondrial side fraction enriched with NE-ER-derived microsomes	120
1.4.5 In <i>cdc48^{S565G}</i> cells NE-ER and mitochondria demonstrate a significantly increased spatial proximity	121
2. ANALYSIS OF VCP VARIANTS IN MAMMALIAN CELL CULTURE	125
2.1 Selection of VCP variants and generation of constructs suitable for expression in mammalian cell culture	125
2.2 Influence of the expression of VCP variants on cell viability and cell death in mammalian cell culture	128
2.2.1 Expression of ATPase-deficient VCP-K524A and of VCP-S555G but not of the IBMPFD-associated mutation VCP-R155H has severe effects on cell viability	128
2.2.2 Expression of VCP-K524A and VCP-S555G leads to cytoplasmic vacuolization and condensation and fragmentation of nuclei	129
2.2.3 Increased cell death upon ATPase domain mutations in VCP is paralleled by accumulation of polyubiquitinated proteins	131
2.3 Dysfunction of VCP variants in the degradation of rhodopsin – a potential ERAD substrate	134
2.3.1 Rhodopsin and rhodopsin-P23H, a frequent variant causative for the human disorder retinitis pigmentosa, can be efficiently expressed in mammalian cell cultures	134
2.3.2 Mutation of VCP leads to accumulation and increased aggregation of the ERAD substrate rhodopsin	136
G. DISCUSSION	138
1. ANALYSIS OF CDC48P VARIANTS IN YEAST	138
1.1 Functional proteome analysis of apoptotic <i>cdc48^{S565G}</i> yeast	138
1.2 Crucial mitochondrial impairment upon CDC48 mutation in apoptotic yeast	141

<i>1.3 CDC48 mutation is paralleled by increased association of ubiquitinated NE-ER and mitochondria</i>	144
<i>1.4 Model of Cdc48p-mediated apoptosis in yeast</i>	146
2. ANALYSIS OF VCP VARIANTS IN MAMMALIAN CELL CULTURE	149
<i>2.1 VCP mutations in the major ATPase domain of VCP severely impair cell viability and cell morphology and result in cell death</i>	149
<i>2.2 VCP mutations in the ATPase domain and the most common IBMPFD-causing mutation result in impairment of ERAD</i>	151
3. PERSPECTIVES	153
H. REFERENCES	155
I. ANNEX	175
<i>1. FIGURE INDEX</i>	175
<i>2. TABLE INDEX</i>	176
<i>3. PUBLICATIONS AND PRESENTATIONS</i>	177
<i>4. ACKNOWLEDGMENTS</i>	179
<i>5. CURRICULUM VITAE</i>	182

A. Abbreviations

1D	One-dimensional
16-BAC	16-benzyltrimethyl- <i>n</i> -hexadecylammonium chloride
16-BAC/SDS-PAGE	16-BAC/SDS polyacrylamide gel electrophoresis
2D	Two-dimensional
2-DE	Two-dimensional gel electrophoresis
AAA	ATPase associated with various cellular activities
ACTH	Adenocorticotrophic hormone clip 18-39
ADH	Alcohol dehydrogenase
AIF	Apoptosis-inducing factor
APS	Ammonium peroxodisulfate
ATP	Adenosine triphosphate
BiP	Binding protein/GRP78
bp	Base pair
BRCA1	Breast cancer type 1 susceptibility protein
BSA	Bovine serum albumine
CA	Carrier ampholyte
CHAPS	3-[(3-Cholamidopropyl)-dimethyl-ammonio]-1-propansulfonate
<i>CDC48</i>	Cell division cycle gene 48
Cdc48p	Cell division cycle protein 48
<i>cdc48</i> ^{S565G}	Cell division cycle gene 48 mutant
Cdc48p-S565G	Cell division cycle protein 48 variant
cDNA	Coding DNA
CFU	Colony forming unit
CPY	Carboxypeptidase Y
Cue1p	Coupling of ubiquitin conjugation to ER degradation protein 1
DAPI	4,6-diaminodiphenyl-2-phenylindole
ddH ₂ O	Ultra-pure water
ddNTP	Dideoxynucleotide triphosphate
Der1p	Degradation of endoplasmic reticulum protein 1
Dfm1p	Der1-like family protein member 1
dH ₂ O	Deionized water
DHR123	Dihydrorhodamine 123
DMEM	Dulbecco's modified Eagle's medium
DMSO	Dimethylsulfoxide
DNA	Deoxyribonucleic acid
dNTPs	Deoxynucleotide triphosphate
Doa10p	Degradation of alpha2-10 protein (E3 enzyme)
DTE	Dithioerythritol
DTT	Dithiothreitol
DUF	DNA unwinding factor
E1	Ubiquitin-activating enzyme
E2	Ubiquitin-conjugating enzyme
E3	Ubiquitin ligase
E4	Multiubiquitylation enzyme
ECL	Enhanced chemiluminescence
EDTA	Ethylendiaminetetraacetate
EM	Electron microscopy
ER	Endoplasmic reticulum
ERAD	ER-associated protein degradation

EtOH	Ethanol
ex-polyQ	Proteins with expanded polyglutamine stretches
FCS	Fetal calf serum
FITC	Fluorescein isothiocyanate
FTD	Frontotemporal dementia
Gal	Galactose
GFP	Green-fluorescent protein
Glc	Glucose
GRP78	78 kDa glucose-regulated protein
HAc	Acetic acid
HCCA	α -cyano-4-hydroxycinnamic acid
HCMV	Human cytomegalovirus
Hrd	Hydroxymethylglutaryl-CoA reductase degradation protein
HRP	Horseradish peroxidase
Hsp	Heat shock protein
IBM	Inclusion body myopathy
IBMPFD	Inclusion body myopathy associated with Paget disease of bone and frontotemporal dementia
IEF	Isoelectric focusing
IF	Immunofluorescence
I κ B α	Inhibitor of NF κ B
IPG	Immobilized pH gradient
kb	kilo base
kDa	kilo Dalton, molecular mass
KFY	Kai-Uwe-Fröhlich-Yeast
KPB	Potassium phosphate buffer
Lac	Lactate
LB	Luria-Bertani
LC	Liquid chromatography
LC-MS/MS	Liquid chromatography coupled with tandem mass spectrometry
MALDI	Matrix-assisted laser desorption ionization
MALDI/TOF-MS	Matrix-assisted laser desorption ionization/Time-of-flight mass spectrometry
MAM	Mitochondria-associated membranes
MDLC	Multi-dimensional liquid chromatography
MeOH	Methanol
MHC 1	Major histocompatibility complex I
Mmf1p	Maintenance of mitochondrial function
Mmi1p	Microtubule and mitochondria interacting protein
MOPS	3-(N-morpholino)propanesulfonic acid
mRNA	messenger RNA
MS	Mass spectrometry
MS/MS	Tandem mass spectrometry
mtDNA	Mitochondrial DNA
NE	Nuclear envelope
NE-ER	Nuclear envelope-endoplasmic reticulum network
NF κ B	Nuclear factor kappa B
Npl4	Nuclear protein localization gene 4
NSF	N-ethylmaleimide sensitive factor

OD	Optical density
Otu1	Ovarian tumor protein family 1
p47	47 kDa protein
p97	97 kDa protein/VCP
p.A.	pro analysis grade
PAF	Paraformaldehyde
PBS	Phosphate-buffered saline
PBST	PBS-Tween
PCR	Polymerase chain reaction
PDB	Paget disease of bone
pI	Isoelectric point
PI	Protease inhibitor mix
PLGS	ProteinLynx Globalsever
PMF	Peptide mass fingerprinting
PMSF	Phenylmethylsulfonylfluorid
ppm	Parts per million
PVDF	Polyvinylidene difluoride
RFU	Relative fluorescence unit
RNA	Ribonucleic acid
ROS	Reactive oxygen species
rpm	Rounds per minute
RT	Room temperature
RuBP	Ruthenium-II-bathophenanthroline disulfonate chelate
s.d.	Standard deviation
SDS	Sodium dodecyl sulfate
SDS-PAGE	SDS-polyacrylamide gel electrophoresis
Sec61p	Secretory pathway protein 61
SET	Sucrose-EDTA-Tris buffer
s-IBM	Sporadic inclusion body myopathy
SNARE	Soluble NSF attachment protein receptor
SRH	Second region of homology
TAE	Tris-acetic acid-EDTA buffer
TB-RBP	Testis brain RNA-binding protein
TCTP	Translationally controlled tumor protein homologue
TdT	T4 terminal deoxynucleotidyl transferase
TEMED	N, N, N', N'-tetraethylmethylendiamine
TFA	Trifluoroacetic acid
TOF	Time-of-flight
Tris	Tris-(hydroxymethyl)-aminomethan
TUNEL	TdT-mediated terminal dUTP nick end labeling
U	Unit/enzymatic activity
Ubc	Ubiquitin-conjugating enzyme
Ubx	Ubiquitin regulatory X domain-containing protein
Ufd	Ubiquitin-fusion degradation protein
UPR	Unfolded protein response
UPS	Ubiquitin-proteasome system
UV	Ultra-violet radiation
VCP	Valosin-containing protein
VIMP	VCP-interacting membrane protein

vol	Volume
W	Western
WRN	Werner syndrome helicase
X-gal	5-bromo-4-chloro-3-indoyl- β -D-galactopyranoside
YCA-1	Yeast caspase 1
YPGal	Yeast galactose full medium
YPGlc	Yeast glucose full medium
YPLac	Yeast lactate full medium

B. Summary

The yeast ‘cell division cycle protein 48’ (Cdc48p) and its highly conserved human orthologue ‘valosin-containing protein’ (VCP) are ubiquitin-controlled AAA-ATPases (ATPases associated with various cellular activities). Cdc48p/VCP is involved in different cellular processes, such as ER-associated protein degradation (ERAD), membrane fusion and cell cycle control. VCP has been proposed as a sensor for misfolded proteins associated with neurodegenerative disorders, such as Machado-Joseph, Parkinson and Alzheimer disease. Upon mutation human VCP is causative for ‘inclusion body myopathy associated with Paget disease of bone and frontotemporal dementia’ (IBMPFD), a hereditary disease characterized by protein deposits in either myofibrils or brain. Mutation of Cdc48p/VCP leads to apoptotic cell death in mammalian cells, in zebrafish, *Caenorhabditis elegans* and in the unicellular organism *Saccharomyces cerevisiae*. However, the cellular mechanisms of apoptotic cell death upon mutation of Cdc48p/VCP and the pathophysiological role of this protein in the progression of human degenerative disorders have remained unresolved.

In this study, a systematic proteome analysis of the apoptotic *cdc48*^{S565G} mutant yeast strain was performed, in order to reveal apoptosis-associated proteome alterations that may help to elucidate cellular mechanisms underlying Cdc48p/VCP-mediated cell death. Differential two-dimensional gel electrophoresis (2-DE) of the apoptotic *cdc48*^{S565G} mutant and the *CDC48* wild-type yeast strain resulted in significant protein spot alterations in mitochondrial extracts. Both altered amounts of mitochondrial proteins and accumulation of Cdc48p-S565G itself and other proteins associated with the NE-ER (nuclear envelope-endoplasmic reticulum) were observed in mitochondrial extracts of the *cdc48*^{S565G} strain. Starting from these results, mitochondria were demonstrated to play a pivotal role during apoptotic cell death in the *cdc48*^{S565G} strain: Depletion of mitochondrial proteins essential for mitochondrial function was found to be associated with mitochondrial swelling, respiratory deficiency of yeast cells, release of cytochrome *c* into the cytosol, and accumulation of reactive oxygen species (ROS) produced by mitochondria. Generating yeast strains completely lacking functional mitochondria (ρ^0 strains) resulted in the assimilation of the viabilities of wild-type and *cdc48*^{S565G} cells under apoptotic growth conditions, confirming a deleterious role of mitochondria during apoptotic cell death. The increased co-purification of Cdc48p-S565G and other NE-ER-associated proteins with mitochondria as observed by 2-DE was demonstrated to be due to an augmented co-migration of microsomes with mitochondria in mitochondrial extracts. Ultrastructural analysis by electron microscopy revealed augmented proximity of NE-ER membranes and mitochondria in *cdc48*^{S565G} cells, indicating an increased

association of NE-ER and mitochondria in apoptotic *cdc48*^{S565G} cells. Increased amounts of polyubiquitinated proteins in total cell extracts and microsomal extracts point to a dysfunction of Cdc48p-S565G in ERAD. Polyubiquitinated proteins were found to be strongly associated with a subset of mitochondria, whereas the majority of mitochondria were not affected. The polyubiquitinated mitochondrial fraction comprised markedly increased amounts of Cdc48p-S5656, ER stress marker Kar2p and microsomes. The observed increased association of NE-ER and mitochondria in *cdc48*^{S565G} cells demonstrates for the first time that cellular stress localized at the NE-ER due to mutation in *CDC48* and dysfunction of ERAD is transmitted to mitochondria. This may result in mitochondrial damage that initiates mitochondria to produce ROS and thus triggering apoptotic cell death.

In order to verify if the results obtained in the *cdc48*^{S565G} yeast strain are relevant for events in VCP-mediated cell death, a mammalian cell culture system expressing human VCP variants was established. Decreased cell viability, increased apoptotic cell death and accumulation of polyubiquitinated proteins was observed in cells expressing the dominant ATPase-deficient human VCP variant VCP-K524A and the VCP variant VCP-S555G, the homologous variant to yeast Cdc48p-S565G. Coexpression of VCP and of the ERAD substrate rhodopsin resulted in the accumulation of aggregated rhodopsin in the case of VCP-K524A and VCP-S555G, showing the defect of these variants in ERAD. Since these are highly similar features as observed in the *cdc48*^{S565G} yeast strain, these data obtained in mammalian cell culture validate the use of the yeast model system. In contrast, in mammalian cells expression of the IBMPFD-causing VCP variant VCP-R155H did not affect cell viability. However, VCP-R155H demonstrated deficiency in ERAD but much less severe compared to VCP-K524A and VCP-S555G. Thus, ERAD deficiency upon Cdc48p/VCP mutation is *per se* not sufficient to trigger cell death. However, the ERAD deficiency of VCP-R155H might become deleterious and may result in the induction of apoptotic cell death upon enrichment of proteins during ageing. Based on the results obtained in the *cdc48*^{S565G} yeast strain, a crucial mitochondrial involvement during apoptosis in cells with dysfunctional VCP and ERAD should be evaluated in the future.

C. Zusammenfassung

Das Hefe-Zellzyklusprotein 48 (Cdc48p) und dessen hochkonserviertes menschliches Ortholog, Valosin-enhaltendes Protein' (VCP), sind Ubiquitin-kontrollierte AAA-ATPasen (ATPasen assoziiert mit verschiedenen zellulären Aktivitäten). Cdc48p/VCP ist in verschiedenen zellulären Prozessen beteiligt, wie z.B. im ER-assoziierten Proteinabbau (ERAD), bei Membranfusionsprozessen und bei der Zellzykluskontrolle. VCP wurde als Sensor für falschgefaltete Proteine vorgeschlagen, die mit neurodegenerativen Erkrankungen, wie z.B. Machado-Joseph-, Parkinson- und Alzheimer-Erkrankung, in Zusammenhang gebracht werden. Nach Mutation ist VCP ursächlich für die Erbkrankheit IBMPFD, die durch das Auftreten von Proteinablagerungen in Muskelgewebe oder Gehirn charakterisiert ist und zu Muskelschwäche, zur Paget'schen Knochenerkrankung und zu frontotemporaler Demenz führen kann. Mutationen von Cdc48p/VCP führen in Säugerzellen, in Zebrafischen, in *Caenorhabditis elegans* und im Einzeller *Saccharomyces cerevisiae* zu apoptotischem Zelltod. Die molekularen Mechanismen des Zelltods ausgelöst durch Mutationen in Cdc48p/VCP und die pathophysiologische Rolle dieses Proteines im Verlauf menschlicher Erkrankungen blieben jedoch ungeklärt.

In dieser Studie wurde eine systematische Proteomanalyse des apoptotischen Hefestamms *cdc48^{S565G}* durchgeführt, um apoptoseassoziierte proteomische Veränderungen zu identifizieren, die helfen könnten, den Mechanismus des Cdc48p/VCP-vermittelten Zelltodes aufzulösen. Vergleichende zwei-dimensionale Gelelektrophorese (2-DE) des apoptotischen Stammes *cdc48^{S565G}* und des Wildtyp-Stammes *CDC48* ergab signifikante Proteinveränderungen in mitochondrialen Extrakten. Sowohl veränderte Mengen an mitochondrialen Proteinen als auch eine Anreicherung von Cdc48p-S565G und anderen Proteinen, die mit dem NE-ER (Kernhülle und endoplasmatisches Retikulum) assoziiert sind, konnten in mitochondrialen Extrakten des *cdc48^{S565G}*-Stammes beobachtet werden. Ausgehend von diesen Ergebnissen wurde eine entscheidende Rolle von Mitochondrien im apoptotischen Zelltod im *cdc48^{S565G}*-Stamm gezeigt: Eine Abreicherung mitochondrialer Proteine, die essenziell für die mitochondriale Funktionstüchtigkeit sind, konnte genauso beobachtet werden wie ein Anschwellen der Mitochondrien, die Unfähigkeit von *cdc48^{S565G}*-Zellen zur Atmung, die Freigabe von Cytochrom *c* in das Zytosol und die Anreicherung von in Mitochondrien hergestellten reaktiven Sauerstoffspezies (ROS). Die Herstellung von Hefestämmen, die frei von funktionstüchtigen Mitochondrien sind (ρ^0 -Stämme) ergab eine Angleichung der Überlebensfähigkeit von Wildtyp- und *cdc48^{S565G}*-Zellen unter apoptotischen Wachstumsbedingungen, was die schädliche Rolle von Mitochondrien während

der Apoptose bestätigt. Die bei 2-DE-Analysen beobachtete verstärkte Aufreinigung von Cdc48p-S565G und anderen NE-ER-assoziierten Proteinen mit Mitochondrien konnte auf eine verstärkte Komigration von Mikrosomen mit Mitochondrien zurückgeführt werden. Die durch Elektronenmikroskopie beobachtete größere Nähe von NE-ER-Membranen und Mitochondrien in *cdc48^{S565G}*-Zellen zeigt deshalb eine zunehmende Assoziation von NE-ER und Mitochondrien. Größere Mengen an polyubiquitinylierten Proteinen in Gesamtzell- und mikrosomalen Extrakten weisen auf eine Dysfunktion von Cdc48p-S565G im ERAD. Polyubiquitinylierte Proteine wurden stark assoziiert in einer Untergruppe von Mitochondrien gefunden, in der deutlich erhöhte Mengen an Cdc48p-S565G, am ER-Stressmarker Kar2p und an Mikrosomen gefunden wurden. Die beobachtete verstärkte Assoziation von NE-ER und Mitochondrien in *cdc48^{S565G}*-Zellen zeigt zum ersten Mal, dass am NE-ER lokalisierter zellulärer Stress, aufgrund der Mutation in *CDC48* und der Dysfunktion von ERAD, auf Mitochondrien übertragen werden könnte. Die daraus folgende Schädigung der Mitochondrien könnte zur Herstellung von ROS und zur Auslösung von apoptotischem Zelltod führen.

Um zu überprüfen, ob die Ergebnisse, die mit Hilfe des *cdc48^{S565G}*-Stammes gewonnen wurden, übertragbar sind auf die Vorgänge beim VCP-vermittelten Zelltod, wurden Säugerzellkulturen analysiert, die menschliche VCP-Varianten exprimierten. Expression der dominanten ATPase-defizienten Variante VCP-K524A und der zur Hefemutante Cdc48p-S565G homologen Variante VCP-S555G führte zu einer abnehmenden Zellviabilität, zunehmendem Zelltod und zu einer zellulären Anreicherung an polyubiquitinylierten Proteinen. Weiterhin zeigen Koexpressionsstudien von VCP und dem ERAD-Substrat Rhodopsin eine Anreicherung von Rhodopsinaggregaten bei Koexpression mit VCP-K524A und VCP-S555G, was auf einen Defekt dieser Varianten im ERAD hin deutet. Diese zum *cdc48^{S565G}*-Stamm sehr ähnlichen Ergebnisse unterstützen den Nutzen des Hefemodells. Die Expression der IBMPFD-auslösenden Variante VCP-R155H hat keinen Einfluss auf die Überlebensfähigkeit der Zellkultur. Allerdings zeigt diese Variante eine, wenn auch zu VCP-K524A und VCP-S555G deutlich weniger ausgeprägte, Defizienz im ERAD. Demnach ist ERAD-Defizienz allein nicht ausreichend zur Einleitung des Zelltodes. Die ERAD-Defizienz von VCP-R155H könnte jedoch schädlich werden und zu apoptotischem Zelltod führen, wenn sich falsch gefaltete Proteine in Alterungsprozessen anreichern. In Zukunft sollte nun anhand der Ergebnisse des *cdc48^{S565G}*-Hefemodells eine kritische mitochondriale Beteiligung an der Apoptose von Zellen mit dysfunktionalem VCP bzw. ERAD untersucht werden.

D. Introduction

1. Proteomics and Functional Proteomics

1.1 Proteome and proteomics

1.1.1 Proteomics describes the dynamic protein expression pattern of a cell

The ‘proteome’ was initially defined as ‘the proteins expressed by a genome or a tissue’ (Wilkins et al., 1996; Wilkins et al., 1997). Since this definition does not consider that protein expression depends apart from the genome on many other factors, such as cell type, differentiation, stress, and nutrition, a more precise definition was proposed: ‘The proteome is the quantitative protein expression pattern of a cell under strictly defined conditions’ (Lottspeich, 2006).

Proteome analysis systematically investigates protein expression patterns of a cell. But why are proteome analyses useful? (i) The genome does not contain any information about dynamic processes at the protein level. (ii) There is no compelling correlation between gene expression, as measured for example by the abundance of specific mRNAs (transcriptome analysis), with the amounts of the respective proteins within the cell especially in the case of low-abundant proteins (Anderson and Seilhamer, 1997; Gygi et al., 1999). Regulation and kinetics of processes like protein translation, maturation, processing, modification and degradation result in altered cellular amounts of individual protein species in addition to their gene expression rates. (iii) Individual proteins are subject to a variety of co- and post-translational modifications, such as phosphorylation, glycosylation, farnesylation, ubiquitination, and acetylation, significantly increasing the number of protein species compared to the number of protein-coding genes.

Due to the resultant high complexity of the proteome, proteomic subdisciplines emerged that deal solely with subpools of the cellular proteome. Organelle proteomics investigates the protein contents of purified organelles (*e.g.*, mitochondria (Sickmann et al., 2003b)), whereas glycoproteomics and phosphoproteomics aims at analyzing phosphorylated and glycosylated proteins of a cell, respectively (Hirabayashi, 2004; Reinders and Sickmann, 2005).

1.1.2 Proteome analyses were enabled by the development of new techniques

In order to allow the analysis of complex protein expression patterns of a cell, major improvements of existing techniques, *e.g.*, two-dimensional gel electrophoresis (2-DE), and invention of new techniques, especially mass spectrometric methods allowing reliable and large-scale identification of proteins, became necessary. With high-resolution 2-DE, which

separates proteins in the first dimension according to their charge and in the second dimension according to their apparent molecular weight, it is now possible to reproducibly and simultaneously separate markedly more than 1000 different proteins (Görg et al., 1988; Görg et al., 2004). Subsequent mass spectrometric analysis linked with searches in public protein and gene databases (*e.g.*, SwissProt) allows the identification of individual proteins (Sickmann et al., 2003a).

As alternatives to the gel-based 2-DE, gel-free methods, such as liquid chromatography coupled with mass spectrometry (LC-MS/MS), were developed to analyze the proteome of a given sample (Baggerman et al., 2005). Each of the applied techniques has advantages and disadvantages, *e.g.*, 2-DE has the tendency to lose highly hydrophobic proteins (Santoni et al., 2000), and none of these techniques allows the description of a complete proteome.

1.1.3 Combination of complementary techniques and reducing complexity of protein samples facilitate the full description of a proteome

A combination of several complementary techniques, *e.g.*, gel-based 2-DE and gel-free LC-MS/MS, is a promising but expensive and elaborate approach to get a most complete proteome of a given sample. An alternative approach to circumvent the loss of major parts of the proteome is to reduce the complexity of a proteome prior to analysis. The proteome of a cell can be divided into discrete subproteomes by prefractionation. This can be achieved by either isolation of distinct organelles (*e.g.*, mitochondria) or suborganellar structures (*e.g.*, outer mitochondrial membrane). Alternatively, complex protein samples may be subfractionated in fractions enriched with membrane proteins and fractions enriched with soluble proteins by means of carbonate extraction (Fujiki et al., 1982), or cellular phosphoproteomes may be enriched from complex samples by the use of phosphopeptide-binding columns (Reinders and Sickmann, 2005). In this study, the proteomes of apoptotic *cdc48*^{S565G} yeast cells and of *CDC48* wild-type cells was compared by 2-DE. Here, sample complexity was markedly reduced by analyzing the mitochondrial and cytosolic subproteomes.

Both strategies, applying complementary techniques and reducing of sample complexity, were used to characterize the full protein inventory of a cell or organelle under defined conditions. For example the proteome of yeast mitochondria is now one of the best described and most complete organellar proteomes with an inventory of 700-800 individual proteins (Prokisch et al., 2006; Prokisch et al., 2004). Purified mitochondria were analyzed by

gel-based SDS-PAGE and 2-DE, and gel-free LC-MS/MS and MDLC (multidimensional liquid chromatography)-MS (Ohlmeier et al., 2004; Prokisch et al., 2004; Sickmann et al., 2003b). Furthermore, the proteome of mitochondrial subfractions with decreased complexity, such as the total mitochondrial membrane fraction or, more specifically, the outer mitochondrial membrane fraction, were investigated in detail (Zahedi et al., 2005; Zahedi et al., 2006). Applying similar approaches, the archaea *Halobacterium salinarum* has now one of the best described proteomes of a whole organism (Bisle et al., 2006; Klein et al., 2005; Tebbe et al., 2005).

However, as described above, the proteome is highly dynamic, and a protein inventory of a cell or organelle under defined conditions is only a snap shot of these cellular dynamics. Therefore, proteomics now tries to evolve from a limited descriptive level of analysis to a level that may help to elucidate cellular mechanisms and protein function.

1.2 Functional proteomics

Classically, proteomics tries to characterize complete protein inventories of cells or organelles under given conditions. Functional proteomics aims at elucidating dynamics at the protein level including protein expression, interaction dynamics or topology, in order to illuminate both protein function and cellular mechanisms (Domon and Broder, 2004; Hubbard, 2002). In order to fulfill this task, proteomic strategies are now highly integrative to biochemistry and cell biology, providing an elaborate technological platform for these classical biological disciplines. Structural proteomics links proteomics with structural biology because the three-dimensional structure of a protein or a protein complex is highly useful for elucidating its function (Sali et al., 2003). High-throughput and *in silico* strategies for the determination of protein structures are thus now evolving (Tickle et al., 2004; Vinarov and Markley, 2005). Interaction proteomics highlights the fact that proteins do not act alone but in stable or transient (multi) protein complexes or molecular machines (Monti et al., 2005). For example high-throughput tandem-affinity purification strategies (Gavin et al., 2002) or determination of protein complexes of whole organelles by native gel electrophoresis methods are now applied (an example for mitochondria using two-dimensional blue native/SDS-PAGE: (Reifschneider et al., 2006)). Topological proteomics considers that cells are much more compartmentalized than the classical subdivision of cells into organelles might suggest (Sali et al., 2003; Schubert, 2003). Quantitative proteomics aims at the quantitative assessment of dynamics of the proteome under different conditions, in order to delineate cellular mechanisms (Stults and Arnott, 2005).

In this study, such a differential approach was conducted applying 2-DE. The proteome and the mitochondrial and cytosolic subproteomes of a yeast strain (*cdc48*^{S565G}) with high susceptibility to undergo apoptotic cell death (Madeo et al., 1997) was compared with the isogenic wild-type strain (*CDC48*) grown under identical conditions. Different growth conditions were chosen, in order to allow time-resolved protein dynamics associated with apoptotic cell death.

2. Structure and Cellular Role of the AAA-ATPase Cdc48p/VCP

Cdc48p/VCP is a ubiquitous highly conserved protein and a member of the AAA-ATPase family (for review: Dreveny et al., 2004; Halawani and Latterich, 2006; Wang et al., 2004; Woodman, 2003; Ye, 2006). Activity of this ATPase is controlled by ubiquitin. Binding of different co-factors link Cdc48p/VCP to a variety of different cellular functions, such as protein degradation and ER-associated protein degradation (ERAD), homotypic ER fusion, Golgi and nuclear reassembly after mitotic disassembly, spindle disassembly at the end of mitosis, transcriptional control, cell cycle control and DNA repair. An introduction into the structure and regulation of this versatile protein will be given in this chapter that may allow a better understanding of its seemingly unrelated cellular roles.

2.1 Historical overview

Two decades ago *CDC48* was discovered in a genetic screen as gene no. 48 that causes arrest in the cell division cycle (*cdc*) in *S. cerevisiae* upon mutation (Moir et al., 1982). The mammalian homologue of Cdc48p (the protein encoded by the *CDC48* gene) is called valosin-containing protein (VCP), since it was initially characterized as a precursor protein for valosin, a small peptide isolated from pig intestine (Koller and Brownstein, 1987). Although further work demonstrated that valosin is an artifact of purification and is unrelated to VCP, the name VCP is still widely used. The *Xenopus* homologue of Cdc48p was discovered as a ubiquitous ATPase in *Xenopus* extracts and named p97 for its relative molecular mass in sucrose gradient sedimentation (Peters et al., 1990). The names Cdc48p, VCP and p97 are widely used in literature, also as synonyms. In this work Cdc48p refers to the yeast protein, VCP to its mammalian counterpart, and Cdc48p/VCP to describe conserved functions of these homologous proteins.

2.2 Cdc48p/VCP is a ubiquitous highly conserved protein

Cdc48p/VCP is one of the most highly evolutionary conserved proteins. Human VCP shows a 70% sequence identity to yeast Cdc48p (Fröhlich et al., 1991). Highly conserved Cdc48p/VCP orthologues were also found in worms (e.g., *C. elegans* C41C4.8 and C06A1.1, Yamanaka et al., 2004), in insects (e.g., *Drosophila* TER94, Pinter et al., 1998), in protozoan parasites (e.g., *Trypanosoma brucei* TbVCP, Roggy and Bangs, 1999), in plants (e.g., *Arabidopsis thaliana* AtCDC48, Feiler et al., 1995), and even in archaea (e.g., *Thermoplasma acidophilum* VAT, Pamnani et al., 1997).

Cdc48p/VCP is ubiquitously expressed in all eukaryotic cells and is one of the most abundant proteins in cells accounting for more than 1% of the total cellular protein (Wang et al., 2004; Ye, 2006), underlining its essential cellular role. It is a predominantly cytoplasmic protein, in which a significant portion is found to be associated with cellular membranes, such as the ER and the Golgi membrane (Acharya et al., 1995; Latterich et al., 1995; Rabouille et al., 1995). Small amounts of yeast Cdc48p were also found in the nucleus dependent on the cell cycle (Madeo et al., 1998).

2.3 Cdc48p/VCP is a member of the AAA-ATPase family

Cdc48p/VCP is a member of the type II AAA (ATPases associated with various cellular activities) ATPase family, which are characterized by the presence of two conserved ATPase domains, also called AAA domains (Lupas and Martin, 2002; Patel and Latterich, 1998; Zwickl and Baumeister, 1999). Cdc48p/VCP consists of 834 and 806 amino acids for yeast Cdc48p and human VCP, respectively (Fröhlich et al., 1991), and is made up of four domains: the N-terminal domain, the ATPase domains D1 and D2 comprising the conserved AAA motifs Walker A, Walker B and the ‘second region of homology’ (SRH), and the C-terminal domain (Wang et al., 2004) (Fig. 1A). The N-terminal domain is involved in binding of cofactors and substrates (Wang et al., 2004). Indeed, all known cofactors, except for Ufd2 and Ufd3 (ubiquitin fusion degradation protein 2 and 3, respectively), bind to the N-terminal domain of Cdc48p/VCP (Rumpf and Jentsch, 2006; Ye, 2006). The D1 domain demonstrates marked ATPase activity only under unphysiological elevated temperatures but has been shown to be crucially involved in oligomerization of Cdc48p/VCP (Song et al., 2003; Wang et al., 2004). Although a matter of debate, the major ATPase activity of Cdc48p/VCP has been assigned to the D2 domain (Song et al., 2003; Wang et al., 2004). Recently, distinct amino acid residues of the D2 domain have been attributed to be involved in substrate binding (DeLaBarre et al., 2006; Halawani and Latterich, 2006), so that substrate binding might take place at both the N-terminal and D2 domain of Cdc48p/VCP. The C-terminal domain of Cdc48p/VCP binds the cofactors Ufd2 and Ufd3 (Rumpf and Jentsch, 2006) and is involved, at least for yeast Cdc48p, in the phosphorylation-dependent nuclear localization of this protein (Madeo et al., 1998).

Similar to other AAA-ATPases, Cdc48p/VCP assembles into a stable homo-hexameric barrel structure with a small central channel that runs through the entire span of the hexamer (Fig. 1B) (DeLaBarre and Brunger, 2003; Huyton et al., 2003; Peters et al., 1992; Rouiller et al., 2000; Zhang et al., 2000b). The homo-hexamers are built up of two ring-shaped layers

made of the respective D1 and D2 domains (Fig. 1C). D1 and D2 have highly similar shapes and are aligned above each other in a head-to-tail manner. The N-terminal domains crucially involved in substrate and cofactor binding (Fig. 1A) are arranged at the outside of the ring formed by the D1 domains of the subunits (D1 ring) (Figs. 1B and C).

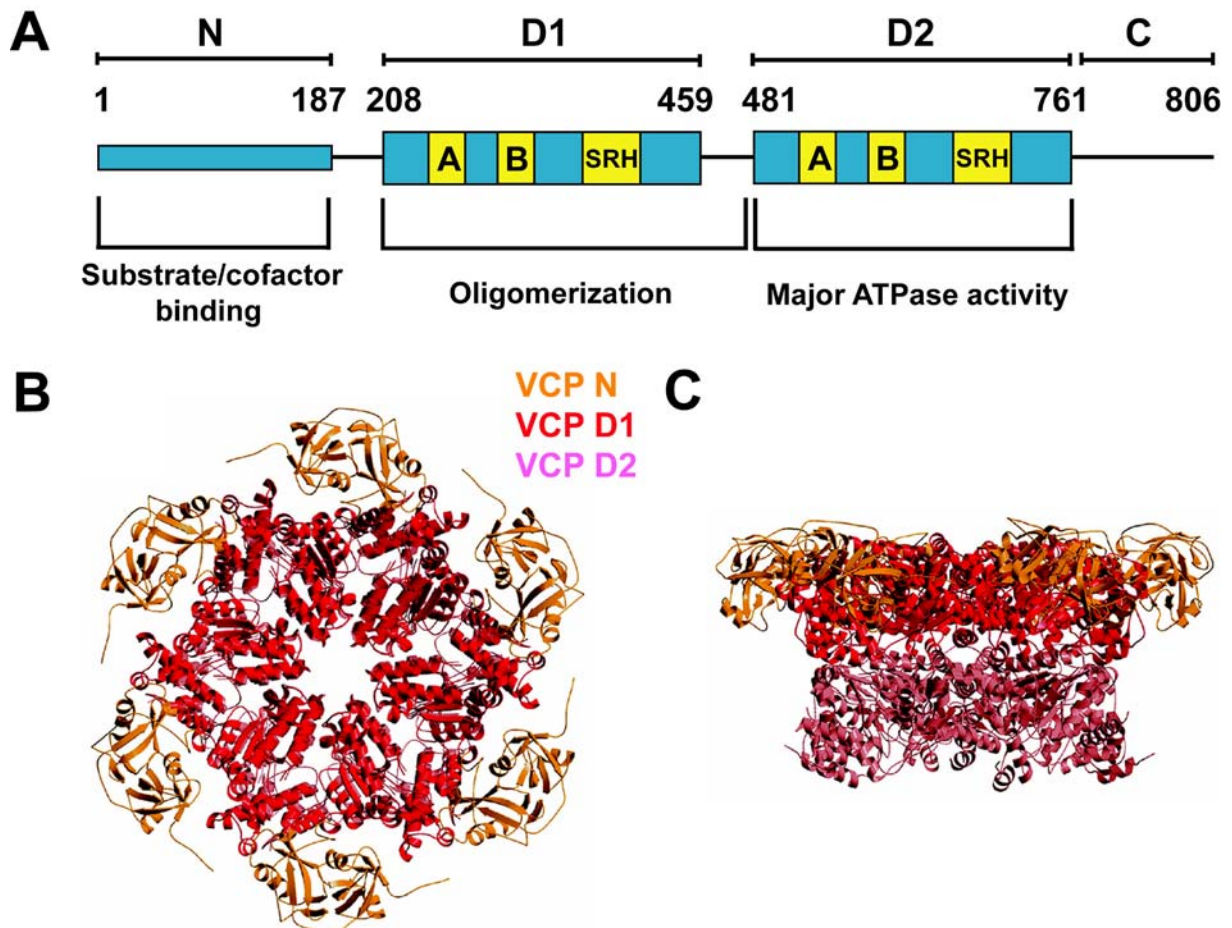


Figure 1: Structure of the AAA-ATPase Cdc48p/VCP.

(A) Domain structure of Cdc48p/VCP. Cdc48p/VCP consists of four domains, the N-terminal domain (N), the ATPase domains D1 and D2 comprising the motifs Walker A, Walker B and the ‘second region of homology’ (SRH) motif, and the C-terminal domain (C). In Cdc48p/VCP the major ATPase activity is located in the D2 domain, whereas the D1 domain is responsible for oligomerization. The N-terminal domain is involved in the binding of substrates and cofactors. This figure is essentially based on (Wang et al., 2004) with permission from Elsevier.

(B, C) Crystal structure of Cdc48p/VCP. Ribbon representation of full-length murine Cdc48p/VCP (<http://www.rcsb.org/pdb/explore.do?structureId=1R7R>, pdb (protein data bank) code 1R7R, Huyton et al. (2003)) is shown in top (B) and side view (C). Cdc48p/VCP forms stable barrel-like, homo-hexamers that comprise two ring-shaped layers made of the D1 and D2 AAA modules aligned above each other in a head-to-tail manner. Due to its high flexibility the C-terminal domain is not visible. The VCP hexamer has a diameter of ~ 160 Å at one end, ~ 120 Å at the other end, and a height of ~ 85 Å (see side view). A central pore, with an overall length of ~ 70 Å and complex interior shape, runs through the entire span of the hexamer (see top view). The N-D1 domain occupies the wider layer of the structure, and has the N domains sticking out at positions $\sim 30^\circ$ from the apex of the D1 and D2 domains. This figure is based on Dreveny et al. (2004) with permission from Portland Press.

2.4 The Cdc48p/VCP-ATPase is controlled by ubiquitin

The Cdc48p/VCP homo-hexameric, especially the ring formed by the D2 domains of the subunits (D2 ring), undergoes drastic conformational changes during its nucleotide hydrolysis cycle (Beuron et al., 2003; DeLaBarre and Brunger, 2005; Rouiller et al., 2002; Wang et al., 2003b). These conformational changes upon ATP hydrolysis presumably generate the mechanical force to dissociate large protein complexes. Disassembling of protein complexes, unfolding and refolding of proteins are typical characteristics for AAA-ATPases (Lupas and Martin, 2002). Concerning the AAA-ATPase Cdc48p/VCP a paradigm is emerging that all the diverse cellular processes Cdc48p/VCP is involved in (see below) are controlled by ubiquitin and ubiquitination (Ye, 2006). In this general model, a protein substrate is bound by Cdc48p/VCP and ubiquitinated by the sequential activity of the ubiquitin-activating enzyme (E1), an ubiquitin-conjugating enzyme (E2) and a substrate-specific ubiquitin ligase (E3) (Fig. 2). Binding of the ubiquitinated protein substrate to Cdc48p/VCP initiates ATP hydrolysis, resulting in the dissociation of this substrate from the rest of the complex or from certain intracellular structures such as the ER membrane. In this model, substrate specificity and the cellular role (*e.g.*, protein degradation and membrane fusion) are defined by binding of different cofactors and interacting proteins for Cdc48p/VCP.

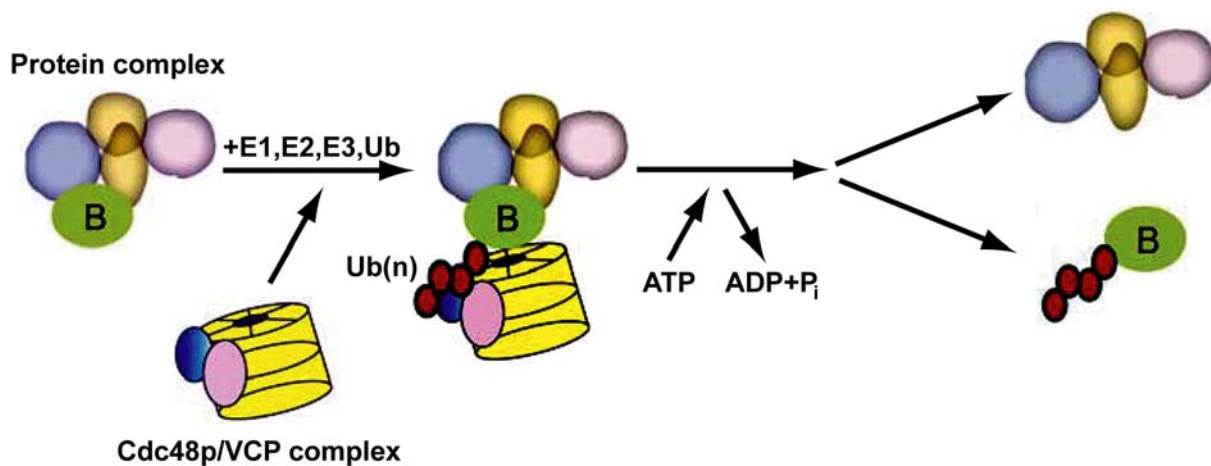


Figure 2: Specific disassembly of protein complexes by the AAA-ATPase Cdc48p/VCP.

A protein subunit of a protein complex destined for dissociation is labelled by a polyubiquitin chain by the sequential action of E1 (ubiquitin-activating enzyme), E2 (ubiquitin-conjugating enzymes), and substrate-specific E3 (ubiquitin ligases) enzymes. Binding of the Cdc48p/VCP complex to the polyubiquitinated protein subunit triggers ATP hydrolysis. The Cdc48p/VCP complex undergoes major structural alterations, ultimately leading to segregation of the bound polyubiquitinated protein subunit from the rest of the complex. This figure is essentially based on Ye (2006) with permission from Elsevier.

2.5 Cdc48p/VCP participates in a variety of different cellular processes

Cdc48p/VCP is involved in a number of seemingly unrelated cellular functions, such as protein degradation, membrane fusion, and cell cycle control (for review: Dreveny et al., 2004; Halawani and Latterich, 2006; Wang et al., 2004; Woodman, 2003; Ye, 2006). However, all these processes appear to be regulated by ubiquitination and seem to fit into the general model of Cdc48p/VCP action (Fig. 2).

2.5.1 Protein degradation

Cdc48p/VCP plays a key role in the proteasomal degradation and processing of certain protein substrates (Dai et al., 1998; Dai and Li, 2001; Ghislain et al., 1996; Jarosch et al., 2002; Ye et al., 2001). In this particular function, Cdc48p/VCP acts with its cofactors Ufd1 (ubiquitin fusion degradation protein 1) and Npl4 (nuclear protein localization gene 4) (Meyer et al., 2000; Ye et al., 2001). The Cdc48p/VCP-Ufd1-Npl4 complex captures the protein substrate. After polyubiquitination of the substrate by E1 and substrate-specific E2 and E3 enzymes, the Cdc48p/VCP-Ufd1-Npl4 complex delivers the polyubiquitinated substrate to the proteasome for degradation (Richly et al., 2005). During the escort pathway to the proteasome, the Cdc48p/VCP-Ufd1-Npl4 complex may bind additional cofactors that can modulate proteasomal degradation of the bound substrate. In yeast, binding of Ufd2, an E4 multiubiquitylation enzyme that adds further ubiquitin moieties to the preformed ubiquitin conjugates, promotes degradation (Richly et al., 2005; Rumpf and Jentsch, 2006), whereas binding of Ufd3, that competes with Ufd2 for the same site at the C-terminal domain of Cdc48p, and binding of the deubiquitylation enzyme Otu1 (ovarian tumor protein family 1), leads to disassembly of multiubiquitin chains and inhibits proteasomal degradation of the bound substrate (Rumpf and Jentsch, 2006).

2.5.2 ER-associated protein degradation (ERAD)

The degradation of ER luminal and ER membrane proteins in the ER-associated protein degradation (ERAD) pathway crucially depends on the activity of the Cdc48p/VCP-Ufd1-Npl4 complex (Jarosch et al., 2002; Ye, 2005; Ye et al., 2001) (Fig. 3).

The aggregation-prone variant of yeast carboxypeptidase Y* (CPY*) is degraded via the ubiquitin-proteasome pathway (Hiller et al., 1996) and has been extensively used as a ER luminal model substrate of ERAD (Elkabetz et al., 2004; Hoyer et al., 2004; Jarosch et al., 2002) (Fig. 3A). Here, CPY* is recognized by the ER luminal chaperone Kar2p/GRP78 (78 kDa glucose regulated protein) (Fig. 3A, step 1). Kar2p/GRP78 delivers the misfolded

protein to a retrotranslocation channel comprising Sec61p (secretory pathway protein 61), Der1p (degradation of endoplasmic reticulum protein 1) or Dfm1p (Der1-like family protein member 1) (Fig. 3A, step 2). The constitution of the retrotranslocation channel is a matter of debate and may differ from substrate to substrate (Römisch, 2006; Schubert and Buchberger, 2005; Ye, 2006). CPY* is partially moved out into the cytosol through this channel by an unknown mechanism and is then captured by the Cdc48p/VCP-Ufd1-Npl4 complex that is attached to the ER membrane through interaction with the ER membrane protein Ubx2 (ubiquitin-regulatory X domain containing protein 2) (Fig. 3A, step 3) (Neuber et al., 2005; Schubert and Buchberger, 2005). Subsequently, ubiquitination of CPY* occurs via the E2 Ubc7p (ubiquitin-conjugating enzyme 7) and the E3s Hrd1p/Hrd3p (hydroxymethylglutaryl-CoA reductase degradation 1 and 3). Binding of the Cdc48p/VCP-Ufd1-Npl4 complex to the polyubiquitin moieties of CPY* initiates ATP hydrolysis, resulting in the dissociation of the ubiquitinated protein substrate from the ER membrane into the cytosol (Fig. 3A, step 4) prior delivery to the proteasome for degradation (Fig. 3A, step 5).

In a highly similar manner, proteins resident in the ER membrane are captured by the Cdc48p/VCP-Ufd1-Npl4 complex, polyubiquitinated and extracted by Cdc48p/VCP-Ufd1-Npl4 upon ATP hydrolysis (Figs. 3B and 3C). Ste6p* is an aberrant form of the yeast ATP-binding cassette transporter protein Ste6p, a multispanning plasma membrane protein, that retains within the ER membrane upon mutation in a cytosolic domain and is therefore degraded via the ERAD pathway (Huyer et al., 2004; Loayza et al., 1998) (Fig. 3B). Ste6p* is bound by the Cdc48p/VCP-Ufd1-Npl4 complex and ubiquitinated by the E2s Ubc6p/Ubc7p and the E3 Doa1p (degradation of alpha2-10) (Fig. 3B, step 1). Subsequent extraction of ubiquitinated Ste6p* via Cdc48p/VCP-Ufd1-Npl4 appears to start from a cytosolic domain of Ste6p* (Fig. 3B, step 2) before release into the cytosol for proteasomal degradation (Fig. 3B, step 3). It is unclear whether the extraction of Ste6p* proceeds through a retrotranslocation channel as described for the degradation of CPY* and MHC class I heavy chain (see below).

MHC (major histocompatibility complex) class I is a plasma membrane protein required for immune surveillance in humans (Alberts et al., 1994b). ERAD can be hijacked by the human cytomegalovirus (HCMV) to target newly synthesized MHC class I heavy chain for retrotranslocation and proteasomal degradation (Tortorella et al., 2000; Ye, 2006; Ye et al., 2005; Ye et al., 2004) (Fig. 3C). The HCMV-encoded ER membrane protein US11 delivers MHC class I heavy chain to the retrotranslocation channel comprising the

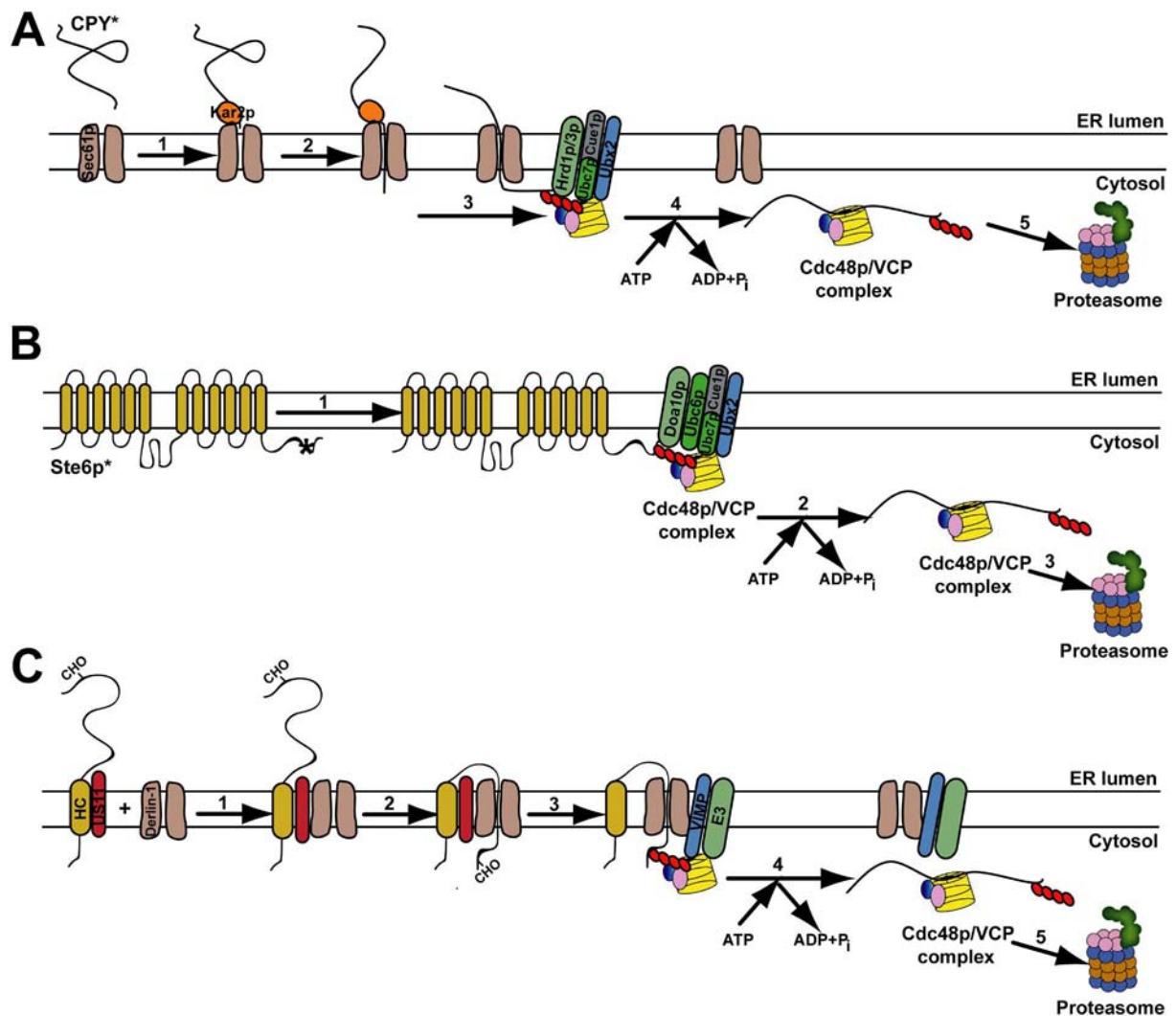


Figure 3: Role of Cdc48p/VCP in ER-associated protein degradation (ERAD).

(A) Degradation of the ER luminal ERAD substrate CPY* in *S. cerevisiae*. The ER luminal chaperone Kar2p/GRP78 targets CPY* to the retrotranslocation channel comprising Sec61p (step 1) and initiates the retrotranslocation of the CPY* peptide (step 2). The emerging polypeptide is captured by Cdc48p/VCP-Ufd1-Npl4 localized to the ER membrane via interaction with the ER membrane protein Ubx2. CPY* is ubiquitinated by the cytosolic E2 ubiquitin-conjugating enzyme Ubc7p bound to the ER membrane through interaction with the ER membrane protein Cue1p (coupling of ubiquitin conjugation to ER degradation 1) and the ER membrane E3 ubiquitin-ligases Hrd1p and Hrd3p (step 3). ATP hydrolysis of the Cdc48p/VCP complex is initiated, resulting in the retranslocation of the polyubiquitinated CPY* into the cytosol (step 4) and its delivery to the proteasome for degradation (step 5). The model of CPY* degradation depicted here is based on Elkabetz et al. (2004), Huyer et al. (2004) and Jarosch et al. (2002).

(B) Degradation of the ER membrane ERAD substrate Ste6p* in *S. cerevisiae*. Ste6p* becomes ubiquitinated via the the E3 Doa10p in conjunction with the ER membrane E2 Ubc6p and the cytosolic E2 Ubc7p that is localized to the ER membrane via interaction with Cue1p (step 1). Cdc48p/VCP-Ufd1-Npl4, associated to the ER membrane through binding to Ubx2, captures polyubiquitinated Ste6p*. ATP hydrolysis results in retrotranslocation of Ste6p* starting from its cytosolic domain into the cytosol (step 2) prior proteasomal degradation (step 3). The model of Ste6p* degradation depicted here is mainly based on Huyer et al. (2004).

(C) The US11-dependent retrotranslocation of MHC class I heavy chain (HC) in human cells. The HCMV-encoded viral protein US11 targets glycosylated (CHO) HC to the retrotranslocation channel comprising Derlin-1 (step 1), initiating the retrotranslocation of the ER luminal domain of HC through the channel into the cytosol (step 2). The emerging polypeptide is deglycosylated and captured by Cdc48p/VCP-Ufd1-Npl4 bound to the ER membrane protein VIMP (step 3). After polyubiquitination via an unknown E3, ATP hydrolysis by Cdc48p/VCP-Ufd1-Npl4 results in the release of HC from the ER membrane into the cytosol (step 4) and its delivery to the proteasome for degradation (step 5). This model is essentially based on Ye (2006) with permission from Elsevier.

multispanning membrane protein Derlin-1, the human homologue of yeast Der1p (Fig. 3C, step 1). In contrast to the degradation of Ste6p*, retrotranslocation of MHC class I heavy chain is initiated by the translocation of the ER luminal domain of this protein into the cytosol through this channel (Fig. 3C, step 2). MHC class I heavy chain is then bound to the Cdc48p/VCP-Ufd1-Npl4 complex that is attached to the ER membrane through interaction with VIMP (VCP-interacting membrane protein) (Fig. 3C, step 3). After ubiquitination by unknown E3s, MHC class I heavy chain is then extracted by Cdc48p/VCP-Ufd1-Npl4 upon ATP hydrolysis into the cytosol (Fig. 3C, step 4) prior proteasomal degradation (Fig. 3C, step 5). In the degradation of both ER luminal and ER membrane proteins, the Cdc48p/VCP-mediated delivery of the ubiquitinated substrate to the proteasome is regulated as described in 2.5.1.

2.5.3 Cell cycle regulation

Despite the fact that *cdc48* was originally characterized as a cell cycle mutant more than two decades ago (Moir et al., 1982), its role in cell cycle regulation has remained unresolved for a long time. Meanwhile, Cdc48p/VCP has been shown to be involved in the ubiquitin-dependent degradation of critical cell cycle regulators such as cyclin E (Dai and Li, 2001), the G1-cyclin-dependent kinase inhibitor Far1p (Fu et al., 2003), and the proteins securin and separase that control chromosome segregation during mitosis (Yuasa et al., 2004). Increased stability of these cell cycle regulators upon Cdc48p/VCP dysfunction in protein degradation might explain the cell cycle defects found in cells expressing mutated Cdc48p/VCP (Ye, 2006).

Moreover, the Cdc48p/VCP-Ufd1-Npl4 complex has been shown to be required for spindle disassembly during mitotic exit (Cao et al., 2003). Here, Cdc48p/VCP dissociates the microtubule-associated proteins XMAP215 and TPX2 that are involved in spindle maintenance from the spindle, allowing its disassembly. In line with the general model of Cdc48p/VCP function (Fig. 2), this dissociation is dependent on ubiquitination of these factors (Cao et al., 2003).

2.5.4 Transcriptional control

Cdc48p/VCP is also involved in transcriptional control. In yeast, Cdc48p participates in the proteasomal processing of the dormant ER membrane-associated transcription factor precursor Spt23 that is involved in fatty acid synthesis (Hitchcock et al., 2001; Rape et al., 2001). Here, the Cdc48p-Ufd1-Npl4 complex dissociates the proteasomal-processed and

ubiquitinated Spt23 transcription factor from the ER membrane, allowing its translocation into the nucleus. Mammalian VCP has been shown to interact with I κ B α , an inhibitor of the transcription factor NF κ B (nuclear factor kappa B) (Asai et al., 2002; Dai et al., 1998). I κ B α becomes phosphorylated and ubiquitinated, the VCP-Ufd1-Npl4 complex dissociates this factor from NF κ B and delivers it to the proteasome for degradation, thereby activating NF κ B-mediated gene expression.

2.5.5 Membrane fusion

Cdc48p/VCP is involved in proteasomal degradation, ER-associated protein degradation, cell cycle regulation and transcriptional control with its cofactors Ufd1-Npl4. The cofactor p47 (or Shp1 in yeast) competes with Ufd1-Npl4 for the same binding site in the N-terminal domain of Cdc48p/VCP (Meyer et al., 2000). Although a matter of debate (Schuberth et al., 2004), it is believed that binding of the cofactor p47 directs Cdc48p/VCP to its role in membrane fusion events. Cdc48p/VCP-p47 is crucially involved in homotypic fusion of ER vesicles (Latterich et al., 1995), in the assembly of transitional ER (Roy et al., 2000), it participates in the reassembly of the Golgi apparatus after its mitotic disassembly (Acharya et al., 1995; Kondo et al., 1997; Rabouille et al., 1995) and in the reformation of the nuclear envelope during mitosis (Hetzer et al., 2001). Interestingly, in the latter case both Cdc48p/VCP-p47 and Cdc48p/VCP-Ufd1-Npl4 are necessary for rebuilding of the nuclear envelope.

The fusion of vesicles with their target membrane is catalyzed by the formation of a highly stable SNARE (soluble NSF attachment protein receptor) complex that forms between the v(vesicle)- and the t(target)-SNARE proteins upon fusion (McNew et al., 2000; Weber et al., 1998). There is evidence that Cdc48p/VCP similar to the closely related AAA-ATPase NSF (*N*-ethylmaleimide sensitive factor) is able to disassemble SNARE protein complexes, in order to allow further rounds of fusion (Brunger and DeLaBarre, 2003; Latterich et al., 1995; Meyer, 2005). Recent results implicate that a cycle of ubiquitination and de-ubiquitination underlie the Cdc48p/VCP-p47-mediated processes in membrane fusion events (Meyer, 2005). In this case, ubiquitination appears to have a regulatory role and is independent of proteasomal degradation.

2.5.6 Chaperone activity

VAT, the archaea homologue of Cdc48p/VCP, is involved in both protein unfolding and protein folding (Golbik et al., 1999). Yeast Cdc48p is able to recognize unfolded

polypeptides and suppress their aggregation in a cell free system (Thoms, 2002). These data suggest that Cdc48p/VCP can act as a chaperone similar to many other members of the AAA-ATPase family (Lupas and Martin, 2002; Patel and Latterich, 1998; Zwickl and Baumeister, 1999). Notably, the *C. elegans* homologues of Cdc48p/VCP are able to suppress polyglutamine-induced protein aggregation (Yamanaka et al., 2004). However, the relevance of this basic chaperone activity of Cdc48p/VCP on cellular function remains to be resolved.

2.5.7 DNA repair

Cdc48p/VCP interacts with DUF (DNA unwinding factor), TB-RBP (testis brain RNA-binding protein), WRN (Werner syndrome helicase), and BRCA1 (breast cancer type 1 susceptibility protein), proteins involved in DNA replication, DNA recombination and DNA repair (Indig et al., 2004; Partridge et al., 2003; Wu et al., 1999b; Yamada et al., 2000; Zhang et al., 2000a). These data suggest a role of Cdc48p/VCP in these cellular processes. However, the function of the AAA-ATPase and of ubiquitin in these processes is poorly understood.

3. Role of *Cdc48p/VCP* under pathophysiological conditions

3.1 Mutant *VCP* causes the rare dominant multisystem disorder IBMPFD

Point mutations in the *VCP* gene have been described as causative for ‘inclusion body myopathy (IBM) associated with Paget disease of bone (PDB) and frontotemporal dementia (FTD)’ (IBMPFD), a rare human multisystem disorder (OMIM 605382) (Kimonis and Watts, 2005; Schröder et al., 2005; Watts et al., 2004) (Fig. 4A). IBMPFD is characterized by adult-onset proximal and distal muscle weakness, early onset Paget disease of bone, a metabolic bone disease that is characterized by overactive osteoclasts containing nuclear inclusions (Mills and Singer, 1976), and in most cases premature frontotemporal dementia (Kimonis et al., 2000; Kovach et al., 2001). Affected individuals suffer at least from one of these features (Fig. 4A). IBMPFD is inherited in an autosomal dominant fashion (Fig. 4A). Both females and males are affected with similar frequency and the offspring of one affected parent has a high risk (about 50%) to develop features of the disease. In IBMPFD *VCP* was found in large or small rounded protein aggregates in affected scattered muscle fibers (Watts et al., 2004) (Fig. 4B e and 4B f, respectively) or in neuronal nuclear inclusions comprising aggregated ubiquitinated proteins (Schröder et al., 2005). These authors therefore proposed that dysfunction of *VCP* in its role in ubiquitin-dependent protein quality control upon mutation might be causative for the disorder.

3.2 Wild-type *VCP* and human protein deposit disorders

IBMPFD is a rare human disorder characterized by aberrant protein deposits. However, formation of protein aggregates, intranuclear or cytoplasmic inclusion bodies and extracellular plaques is a hallmark of many human degenerative disorders, especially in the pathogenesis of common neurodegenerative disorders such as Alzheimer, Parkinson, and Huntington diseases (Bossy-Wetzel et al., 2004; Taylor et al., 2002). Endogenous wild-type *VCP* co-localizes *in situ* with abnormal cellular protein aggregates and inclusions in motor neuron disease with dementia, in Creutzfeldt-Jacob disease (Fig. 4C d), in Alzheimer (Fig. 4C a), Parkinson (Fig. 4C e-g), Huntington and Machado-Joseph diseases (Hirabayashi et al., 2001; Mizuno et al., 2003). From these data, *VCP* has been proposed as a sensor protein for misfolded and aggregated proteins associated with human degenerative disorders (Hirabayashi et al., 2001; Mizuno et al., 2003).

Huntington and Machado-Joseph diseases both belong to a class of inherited neurodegenerative disorders characterized by the expansion of polyglutamine stretches (ex-

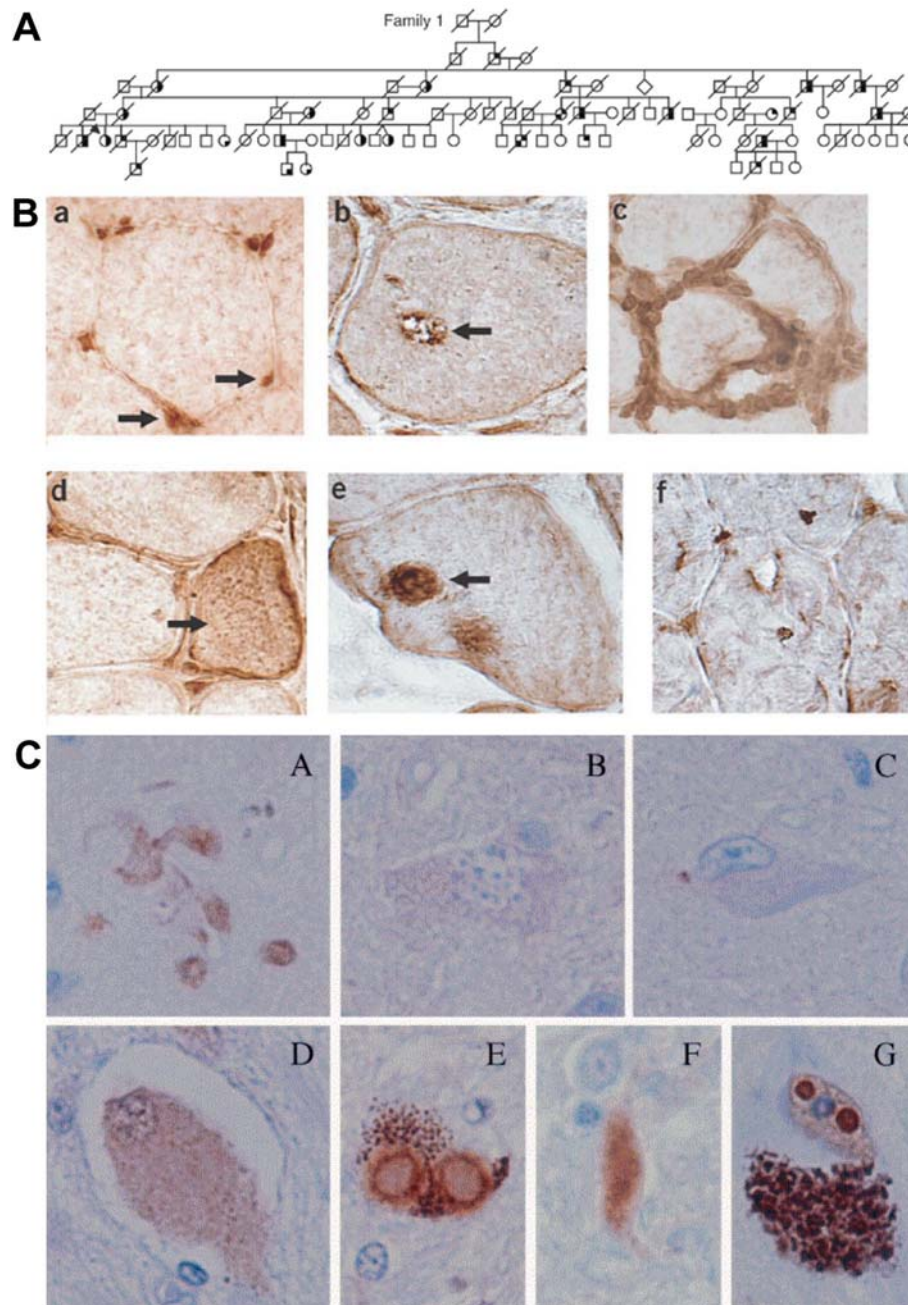


Figure 4: VCP causes upon mutation the protein deposit disorder IBMPFD and endogenous VCP is a sensor of aggregated proteins causative for neurodegenerative disorders.

(A) Pedigree of a family with IBMPFD. Squares indicate males, and circles indicate females. Arrows indicate probands, and symbols with a slash indicate deceased family members. The filled upper right quadrant indicates inclusion body myopathy (IBM), filled lower right quadrant indicates Paget disease of bone (PDB), and filled lower left quadrant indicates frontotemporal dementia (FTD). Reprinted from Watts et al. (2004) with permission from Nature Publishing Group.

(B) Staining of normal and diseased human muscle with polyclonal antibody to VCP. (a) Normal muscle. VCP is prominently located in small endomysial capillaries (right arrow). In muscle fibers, VCP accumulates with lipofuscin granules (left arrow) at the periphery and more diffusely, at low levels, in the cytoplasm. (b) Muscle with s(sporadic)-IBM. VCP is present in material in a vacuole (arrow) and in small accumulations in the muscle fiber cytoplasm. (c) Muscle with s-IBM. VCP is strongly stained in endomysial inflammatory cells surrounding a muscle fiber. (d) Muscle with s-IBM. VCP is upregulated in regenerating muscle fibers (arrow). (e) Muscle with IBMPFD. Large focal inclusion (arrow) in muscle fiber contains VCP. (f) Muscle with IBMPFD. Multiple small foci are present within a muscle fiber. Magnification: 540x. Reprinted from Watts et al. (2004) with permission from Nature Publishing Group.

(C) VCP immunoreactivity in the dystrophic neurites of the (a) senile plaque, (b) granulovacuolar degeneration, and (c) neurofibrillary tangles in the hippocampus, (d) ballooned neurons in the temporal cortex, and (e) Lewy bodies, (f) Lewy neurites and (g) Marinesco bodies in the substantia nigra. Dystrophic neurites, ballooned neurons, Lewy neurites, and Marinesco bodies were immunostained with VCP, while granules of granulovacuolar degeneration and neurofibrillary tangles were not labelled. Magnification 400x. a-c: Alzheimer disease, d: Creutzfeld-Jacob disease, e-g: Parkinson disease. Reprinted from Mizuno et al. (2003) with permission from Elsevier.

polyQ) in those proteins responsible for each disorder. These expansions frequently lead to aggregation of these proteins (La Spada and Taylor, 2003). In this context, VCP has been identified as an ex-polyQ interacting protein *in vitro* and *in vivo* (Hirabayashi et al., 2001). In *C. elegans* the two identified VCP homologues modulate the aggregation of ex-polyQ proteins (Yamanaka et al., 2004). A genetic screening of a *Drosophila* model for human polyglutamine diseases demonstrated the *Drosophila* homologue of VCP (*ter94*) as a modulator of apoptotic cell death (Higashiyama et al., 2002), leading these authors to propose VCP as a pathological effector for ex-polyQ-induced neurodegeneration.

3.3 Cdc48p/VCP and apoptosis: From humans to yeast

Whereas endogenous VCP is involved in human degenerative disorders, increased levels of VCP have been linked to increased proliferation. In certain types of cancer tissues, *e.g.*, colorectal carcinomas, pancreatic endocrine neoplasms, and follicular thyroid cancer, the expression level of VCP is markedly elevated and has been shown to be associated with poor prognosis, proposing VCP expression levels as useful marker for the progression of these cancers (Tsujiyama et al., 2004; Yamamoto et al., 2004a; Yamamoto et al., 2004b; Yamamoto et al., 2004c; Yamamoto et al., 2004d; Yamamoto et al., 2003a; Yamamoto et al., 2004e; Yamamoto et al., 2004f; Yamamoto et al., 2003b; Yamamoto et al., 2005).

Whereas elevated levels of VCP are correlated with cancer, *i.e.*, uncontrolled proliferation characterized by a decreased capability to undergo apoptotic cell death, cellular expression of mutated VCP results in decreased cell proliferation due to an increased occurrence of cell death (Hirabayashi et al., 2001; Shirogane et al., 1999).

Increased cell death and the emergence of apoptotic phenotypes in cells expressing mutated Cdc48p/VCP have originally been described in budding yeast (Madeo et al., 1997), and were thereafter confirmed in mammalian cell cultures (Hirabayashi et al., 2001; Shirogane et al., 1999), in trypanosomes (Lamb et al., 2001), in zebrafish (Imamura et al., 2003), and in *C. elegans* (Wu et al., 1999a). These findings confirm the essential cellular role of this evolutionary highly conserved protein for cell death and survival.

Cdc48p was the first apoptotic mediator found in *S. cerevisiae* (Madeo et al., 1997). The expression of a point mutated *CDC48* gene (*cdc48*^{S565G}) leads to a characteristic apoptotic phenotype: phosphatidylserine externalization to the outer leaflet of the plasma membrane, DNA fragmentation, chromatin condensation, nuclear fragmentation, vacuolization and emergence of reactive oxygen species (ROS) (Madeo et al., 1997; Madeo et

al., 1999). These results obtained in the *cdc48*^{S565G} strain initiated the establishment of yeast as a model to study evolutionary conserved mechanisms of apoptotic regulation (see 4.2).

4. Yeast as a model

4.1 Yeast as a model for conserved cellular processes in eukaryotes

Saccharomyces cerevisiae or baker's yeast is a unicellular eukaryotic organism that has been widely used for the elucidation of biochemical, cell biological and genetic processes since 1860, when Louis Pasteur identified fermentation as a cellular process taking place in yeast cells. The elucidation of eukaryotic metabolic pathways, gene regulation and expression, organelle biogenesis, protein sorting (Nobel prize for Medicine 1999), cell cycle control (Nobel prize for Medicine 2001), and ubiquitin-dependent protein degradation (Nobel prize for Chemistry 2004), are significantly based on results obtained in yeast.

S. cerevisiae is a non-toxic organism that can be kept in culture very easily. Under optimal condition, yeast has high cell proliferation with about 90 min between two cell divisions, allowing the generation of high yields of cell material for further experiments. Genetic analysis and manipulation of yeast cells is also advantageous: (i) Yeast can be grown in both diploid and haploid form facilitating the generation of mutant yeast strains, since only one allele has to be exchanged, (ii) the capability of yeast cells to undergo homologous recombination enables the specific exchange of whole genomic sections with foreign DNA (Rothstein, 1991), (iii) a plethora of genetic methods for the manipulation of yeast has been established (Fink and Guthrie, 1992), and (iv) a collection of precise deletion mutants of nearly every gene in the genome is available (EUROFAN consortium: European network for functional analysis of yeast genes) (Dujon, 1998).

In 1997 the complete genome of *S. cerevisiae* was published (Cherry et al., 1997). *S. cerevisiae* contains about 6000 genes on 16 chromosomes. For 30% of all genes known to be involved in human diseases, homologous genes exist in yeast, and 50% of all yeast genes have homologous genes in the human genome (Botstein et al., 1997), *e.g.*, the human *VCP* is the highly conserved homologue of yeast *CDC48* in both sequence and function (Fröhlich et al., 1991; Ye, 2006). Thus, examination of the cellular roles of conserved genes and proteins in yeast may give important insights in the role and function of their human homologues, as already demonstrated by many studies (*e.g.*, for review of yeast models as tools to study human neurodegenerative disorders: (Sherman and Muchowski, 2003)).

4.2 Yeast as a model for the analysis of evolutionary conserved mechanisms of apoptotic cell death

Apoptosis is a form of physiological cell death first described by Kerr, Wyllie and Currie (Kerr et al., 1972) that can be distinguished from necrosis, the pathological form of cell

death. In contrast to necrosis, removal of cells during apoptosis takes place quickly without damage to the cellular environment. It is an active process depending on gene expression and on the induction of cellular apoptotic cascades (*e.g.*, caspases as specific enzymes that become activated during apoptosis) and therefore also described as programmed cell death (Steller, 1995). In higher eukaryotes apoptosis is an essential mechanism dealing with cell homeostasis, *i.e.*, removal of mutated, infected or superfluous cells (Uren and Vaux, 1996). In cancer proliferating cells lost the capability to undergo apoptosis, whereas in degenerative disorders apoptotic cell death is often increased.

Classically, apoptosis is characterized through distinct morphological and cellular hallmarks: (i) Exposition of the phospholipid phosphatidylserine to the outer leaflet of the plasma membrane (Martin et al., 1995), (ii) condensation of chromatin to the nuclear envelope and fragmentation of the nucleus (Kerr et al., 1972), (iii) DNA fragmentation (Wyllie, 1980), and (iv) disruption of the cell into membrane-enclosed apoptotic bodies (Kerr et al., 1972).

All these morphological and cellular hallmarks of apoptosis can also be observed in the unicellular organism *S. cerevisiae* (Madeo et al., 1997). Moreover, apoptosis can be prevented by inhibiting protein translation, demonstrating that cell death is dependent on gene expression and therefore programmed (Madeo et al., 1999). These data strongly hint to a highly conserved basic mechanism of apoptotic cell death in yeast (for review: Ludovico et al., 2005; Madeo et al., 2004; Weinberger et al., 2003).

Yeast cells have the capability to age as total population (chronological ageing Fabrizio and Longo, 2003), as well as to age individually due to asymmetric cell division (replicative ageing, Bitterman et al., 2003). Replicatively aged yeast cells accumulate ROS and demonstrate morphological and cellular markers of apoptotic cell death (Laun et al., 2001). Chronologically aged yeast cells undergo apoptosis as well and demonstrate accumulation of ROS and the activation of the yeast caspase YCA-1 (yeast caspase-1) (Herker et al., 2004), which has been characterized to have highly similar activity to caspases in higher eukaryotes and which is activated upon oxidative stress (Madeo et al., 2002b). Disruption of the YCA-1 gene results in a marked delay in age-related cell death, but the surviving cells lose the ability for regrowth, indicating the accumulation of predamaged cells in the absence of apoptotic cell removal (Herker et al., 2004). Thus, yeast apoptosis appears to guarantee the selective removal of damaged and unfit individual yeast cells of a yeast clone, *i.e.*, a culture consisting of isogenic cells, which is of long-term benefit for the survival of the clone. Similarly, yeast cells that are unable to undergo mating (sexual reproduction) upon

pheromone α -factor treatment were selectively killed by apoptosis (Severin and Hyman, 2002).

Yeast cells undergo apoptosis not only upon ageing but also under stress conditions. Oxidative stress (Madeo et al., 1999), acidic stress (Ludovico et al., 2001), salt stress (Huh et al., 2002), starvation (*e.g.*, nitrogen starvation, (Madeo et al., 2002a), and UV radiation (Del Carratore et al., 2002) induce apoptotic cell death in individual yeast cells, suggesting that apoptosis is widely used to guarantee ‘homeostasis of a yeast clone’ similar to higher eukaryotes that use apoptosis to provide homeostasis of tissues.

Although the yeast genome appears to lack homologues of important mammalian proteins involved in the progression and regulation of apoptosis, such as members of the Bax/Bcl-2-family that crucially participate in mitochondria-dependent apoptotic pathways (Green and Kroemer, 2004), emerging data reveal striking similarities between the molecular progression of yeast and mammalian apoptosis. ROS play an important role in both yeast and mammalian apoptosis (Green and Kroemer, 2004; Madeo et al., 2002a). For example in yeast, quenching of ROS by growth in media containing radical scavengers or by growth under oxygen free conditions prevents apoptotic cell death (Madeo et al., 1999). Caspases are important effector enzymes in apoptotic cascades in mammalian apoptosis (Green and Kroemer, 2004). The recent identification of the yeast caspase 1 (YCA-1) demonstrated a similar role of caspase activity in yeast (Madeo et al., 2002b). Apoptosis-inducing factor (AIF) is an important pro-apoptotic regulator in mammalian apoptosis (Susin et al., 1999). Similar to mammalian AIF, the yeast homologue AIF-1, translocates during apoptosis from mitochondria to the nucleus and has nuclease activity (Wissing et al., 2004). Cytochrome *c* mediates mitochondria-dependent apoptosis in mammalian cells (Green and Kroemer, 2004). Disruption of cytochrome *c* in yeast cells prohibits apoptotic cell death, suggesting a key role of cytochrome *c* and mitochondria in yeast apoptosis (Ludovico et al., 2002; Severin and Hyman, 2002).

Heterologous expression of the mammalian pro-apoptotic protein Bax in yeast results in apoptotic cell death. It induces the release of cytochrome *c* from mitochondria (Manon et al., 1997) and leads to a high conductance channel in mitochondria (Pavlov et al., 2001), similar to the permeability transition pore in mitochondria-dependent apoptosis in mammalian cells (Green and Kroemer, 2004). Applying the cytotoxicity of Bax on yeast, yeast mutations were identified that prevent cell death. For example mutations in the yeast mitochondrial F_0F_1 ATPase inhibit the progression of Bax-dependent cell death in yeast and this modulating protein could further be validated to play a similar role in mammalian cells (Matsuyama et al.,

1998). Thus, yeast is a highly valuable model for the analysis of conserved mechanisms of apoptotic cell death.

In this study a functional proteome analysis of an apoptotic yeast strain harboring a mutation in *CDC48* (*cdc48*^{S565G}), one of the most highly evolutionary conserved genes (Fröhlich et al., 1991), was performed, in order to get insights in the underlying mechanisms of cell death that might be relevant for human disorders mediated by the human orthologue VCP.

5. Aim of the study

In the beginning of this study, Cdc48p/VCP was known to be one of the evolutionary highly conserved proteins with nearly identical cellular features from yeast to humans. In both species, the crucial role of Cdc48p/VCP in membrane fusion events and proteasomal protein degradation, especially in ERAD, was proposed. In 2001, there was first evidence that human VCP binds abnormal protein aggregates comprised of misfolded proteins causative for polyglutamine disorders, such as Machado-Joseph disease (Hirabayashi et al., 2001). Further studies suggested that VCP is involved in cellular processes underlying cell death in these degenerative disorders (Higashiyama et al., 2002; Kobayashi et al., 2002). Mutations of Cdc48p/VCP were known to cause apoptotic cell death in mammalian cells (Shirogane et al., 1999), in *C. elegans* (Wu et al., 1999a) and in *S. cerevisiae* (Madeo et al., 1997), with the at first and in most detail described apoptotic phenotype in the *cdc48^{S565G}* yeast strain (Madeo et al., 1997; Madeo et al., 1999). However, the pathophysiological mechanisms of Cdc48p/VCP-mediated cell death, in both human degenerative disorders and cells expressing mutated Cdc48p/VCP, have remained unknown. This study aimed at understanding the cellular consequences of pathophysiological mutations of Cdc48p/VCP, in order to resolve mechanisms of cell death that might be relevant for the progression of cell death in human disease.

Using the apoptotic *cdc48^{S565G}* mutant yeast strain as model system, a systematic proteome analysis applying differential two-dimensional gel electrophoresis (2-DE) of the *cdc48^{S565G}* and the *CDC48* wild-type strain was performed.

Objective 1: Discovery of protein alterations that might give insights into the unknown molecular cell death mechanism upon *CDC48* mutation (*cdc48^{S565G}*) in yeast.

Beside total cell extracts, mitochondrial and cytosolic extracts of the *cdc48^{S565G}* strain and the wild-type strain were examined by 2-DE under apoptotic growth conditions (Braun, 2002, and this study). The markedly reduced complexities of the protein contents of these subcellular fractions facilitated a more detailed analysis of the proteome. 2-DE of mitochondrial extracts revealed (i) alterations, both depletion and accumulation, of mitochondrial proteins, and (ii) accumulation of Cdc48p-S565G and other proteins associated with the NE-ER, especially the two proteasomal subunits PRE3 and Y7. Based on the result of this proteome analysis, the following questions were raised:

Objective 2: Are mitochondria impaired upon apoptosis and do these organelles play a pivotal role in apoptotic cell death in *cdc48^{S565G}* cells?

Objective 3: Is the accumulation of Cdc48p-S565G, proteasomal subunits and other NE-ER-associated proteins accompanied by a dysfunction of Cdc48p-S565G in the proteasomal ERAD pathway? Is there a link between dysfunction of Cdc48p-S565G in ERAD and mitochondrial impairment in apoptotic *cdc48*^{S565G} cells?

In the course of this study, mutations of human VCP were discovered to be causative for the human degenerative disorder IBMPFD (Watts et al., 2004). Meanwhile, wild-type VCP has been proposed to be a general sensor for misfolded and aggregated proteins causative for various neurodegenerative disorders, such as Parkinson and Alzheimer diseases (Mizuno et al., 2003). Therefore, the aim was to initiate the evaluation of the results obtained in the yeast model system in a mammalian cell culture system that is more appropriate for the description of cellular mechanisms in human VCP-mediated disorders.

Objective 4: Establishment of a mammalian cell culture system expressing VCP variants including the most common IBMPFD-causing variant and the homologous variant to yeast Cdc48p-S565G.

Objective 5: Evaluation of the influence of different VCP variants on cell viability, cell morphology and cell death upon expression in mammalian cell culture.

Objective 6: Correlation of cell viability and cell death with the functionality of the different VCP variants in ubiquitin-dependent protein degradation, *e.g.*, ERAD.

E. Material and Methods

1. Material

1.1 Chemicals

All chemicals were purchased from Sigma-Aldrich (Sigma, Fluka, Aldrich; Taufkirchen, Germany) and VWR International (Darmstadt, Germany) if not otherwise stated. In this study dH₂O is referred to deionized water, ddH₂O is referred to ultra-pure water (Milli-Q Biocell, Millipore, Eschborn, Germany).

1.2 General equipment

Autoclave Bioclav	Schütt Labortechnik, Göttingen, Germany
Autoclave Systec 5075 ELV	Systec, Wettengel, Germany
Analysis scales BP221S	Sartorius, Göttingen, Germany
Precision scales Basic Plus BP2100	Sartorius
Optima TLX ultracentrifuge with TLA110 rotor	Beckman Coulter, Krefeld, Germany
Sigma Laboratory Centrifuges 6K15 and 4K15C and rotors	Sigma Laborzentrifugen, Osterode, Germany
Table top centrifuge 5415D with standard rotor	Eppendorf, Hamburg, Germany
Shaker Duomax 1030	Heidolph Instruments, Schwabach, Germany
Shaker KS260 basic	IKA Labortechnik, Staufen, Germany
Magnetic stirrer RH basic	IKA Labortechnik
Milli-Q Biocell	Millipore
SpeedVac SPD111V, freeze drying chamber for lyophilization and ValuPump VLP80	Savant, Fisher Scientific, Schwerte, Germany
Ultra-low temperature freezer (-80°C) VIP™ series	Sanyo Scientific, IL, USA
Ultrasonic bath Transsonic 310/H	Elma Ultrasonic, Singen, Germany
Ultraspec 3300 pro UV/Vis photometer	GE Healthcare, Freiburg, Germany
Vortex Genie 2	Scientific Industries, VWR
Water bath HRB 4 digital	IKA Labortechnik

1.3 Protein chemistry

1.3.1 Special equipment

Power Supply Power Pac 3000	Bio-Rad, Munich, Germany
Mini Protean 3 for SDS-PAGE	Bio-Rad
Protean II for SDS-PAGE	Bio-Rad
GelAir dryer	Bio-Rad
GS-710 Calibrated Imaging Densitometer	Bio-Rad
Fuji FLA-3000 scanner	Fuji, Düsseldorf, Germany
Mini Trans Blot Electrophoretic Transfer Cell for Western blot	Bio-Rad
Agfa Curix 60 Developer	Agfa, Cologne, Germany
Rehydration chamber for IPG strips	GSF workshop
Multiphor II for isoelectric focusing (IEF)	GE Healthcare
Equilibration chamber for IPG strips	GSF workshop
Ettan Dalt II Gel Caster System for 2-DE	GE Healthcare
Ettan Dalt II Electrophoresis Chamber for 2-DE	GE Healthcare
MALDI/TOF Reflectron	Waters, Eschborn, Germany

MALDI/TOF Bruker Reflex III
MALDI-TOF/TOF mass spectrometer ABI 4700
Proteomics Analyzer

Bruker Daltonics, Bremen, Germany
Applied Biosystems, Foster City, CA,
USA

1.3.2 Kits

Bio-Rad Protein Assay Kit
Enhanced chemiluminescence kit, ECLplus

Bio-Rad
GE Healthcare

1.4 Molecular biology

1.4.1 Special equipment

SubCell GT chambers for agarose gel electrophoresis
UV transilluminator UVT-40M
ABI Prism 3100 Genetic Analyzer for DNA sequencing
PCR DNA Engine Tetrad Gradient Cycler PTC-225
Incubator for *E. coli*
GFL Incubator Shaker for *E. coli*

Bio-Rad
Herolab, Wiesloch, Germany
Applied Biosystems
MJ Research, Bio-Rad
Memmert, Schwabach, Germany
Burgwedel, Germany

1.4.2 Kits

Big Dye Terminator v3.1 Cycle Sequencing Kit
PureYield Plasmid Midiprep System
QIAquick Gel Extraction Kit
QIAquick PCR purification Kit
QIAprep Spin Plasmid Miniprep Kit
QuikChange II Site-Directed Mutagenesis Kit
TOPO TA Cloning Kit

Applied Biosystems
Promega, Mannheim, Germany
Qiagen, Hilden, Germany
Qiagen
Qiagen
Stratagene, Amsterdam, Netherlands
Invitrogen, Karlsruhe, Germany

1.4.3 *E. coli* strains

DH5 α
DH10B
TOP10
XL1-Blue supercompetent cells

Invitrogen
Invitrogen
Invitrogen
Stratagene

1.4.4 Enzymes

Restriction enzymes and DNA ladders were purchased from New England Biolabs (Frankfurt a.M., Germany), T4 DNA ligase, Taq DNA polymerase, Calf Intestine Alkaline Phosphatase were purchased from MBI Fermentas (St. Leon-Rot, Germany).

1.4.5 Oligonucleotides

Primer for cloning and sequencing were ordered from a GSF-intern producer, whereas HPLC-purified primer for site-directed mutagenesis were purchased from Metabion (Martinsried, Germany).

Table 1: Primer for cloning of VCP

Primer name	Used restriction site	Sequence
VCP_Kozak_BamHI_fw	<i>Bam</i> HI	5'-AATAGGATCCGCCACCATGGCTTCTGGA GCCGATTC-3'
VCP_EcoRI_rv2	<i>Eco</i> RI site upstream of primer binding site	5'-CTCGGCATCAATGGTCTCATCCTC-3'
VCP_EcoRI_fw2	<i>Eco</i> RI site downstream of primer binding site	5'-GCTAGATGCCATCGCTCCCAAAG-3'
VCP_NoStop_NotI_HindIII_rv	<i>Not</i> I	5'-TATTAAGCTTGC GGCCGCGCCATACAGG TCATCATCATTGTCTTCTG-3'

Table 2: Mutagenesis primer

Primer name	Sequence
humanVCP_K524A_fw	5'-GACCTCCTGGCTGTGGGGCAACTTTGTTGGC-3'
humanVCP_K524A_rv	5'-GCCAACAAGTTGCCACAGCCAGGAGGTC-3'
humanVCP_P605L_WT_fw	5'-GTCATCAACCAGATCCGACAGAAATGGATGGC-3'
humanVCP_P605L_WT_rv	5'-GCCATCCATTTCTGTCCAGGATCTGGTTGATGAC-3'
humanVCP_R155H_fw	5'-GACATTTTTCTTGTCCATGGTGGGATGCGTGC-3'
humanVCP_R155H_rv	5'-GCACGCATCCCACCATGGACAAGAAAAATGTC-3'
humanVCP_S555G_fw	5'-CATGTGGTTTGGGGAGGGTGAGGCCAATGTCAG-3'
humanVCP_S555G_rv	5'-CTGACATTGGCCTCACCTCCCAAACCACATG-3'

Table 3: Sequencing and PCR primer

Primer name	Sequence
pcDNA3_fw	5'-GCGGTAGGCGTGTACGGTGGG-3'
pcDNA3_rv	5'-GGGCAAACAACAGATGGCTGGC-3'
seqVCP1a_fw	5'-CGGTTAATTGTTGATGAAGCC-3'
seqVCP2_fw	5'-GTGGAGTTCAAAGTGGTGGGA-3'
seqVCP3_fw	5'-TGTTGACCCTCATGGATGGC-3'
seqVCP4_fw	5'-ATCCTGTGGAGCACCCAGAC-3'
seqVCP5_fw	5'-TAACCTGCGCAAGTCCCCAG-3'
seqVCP6_fw	5'-GGGAACCAGGGTGGAGC-3'
M13_fw	5'-TGTAACACGACGGCCAGT-3'
M13_rv	5'-CAGGAAACAGCTATGAC-3'

1.4.6 Plasmids and constructs

1.4.6.1 Plasmids

Table 4: Plasmids

Plasmid	Description	Resistance	Provider
pcDNA3	mammalian expression vector	Ampicillin (100 µg/mL)	Invitrogen
pcDNA3-Strep-GFP	pcDNA3 plasmid with C-terminal streptavidin (Strep)-green fluorescent protein (GFP)-tag	Ampicillin (100 µg/mL)	C. J. Gloeckner, GSF, Munich-Neuherberg, Germany
pCR2.1-TOPO	TOPO vector, TOPO TA Cloning Kit	Kanamycin (50 µg/mL), Ampicillin (100 µg/mL)	Invitrogen
pOTB7	library vector	Chloramphenicol (27 µg/mL)	RZPD, Berlin, Germany
pRC/CMV	mammalian expression vector	Ampicillin (100 µg/mL)	Invitrogen

1.4.6.2 Constructs

Table 5: Constructs

Construct name	cDNA	Plasmid	Provider
pcDNA3-VCP-WT	VCP-WT	pcDNA3	this study
pcDNA3-VCP-R155H	VCP-R155H	pcDNA3	this study
pcDNA3-VCP-K524A	VCP-K524A	pcDNA3	this study
pcDNA3-VCP-S555G	VCP-S555G	pcDNA3	this study
pcDNA3-VCP-WT-GFP	VCP-WT	pcDNA3-Strep-GFP	this study
pcDNA3-VCP-R155H-GFP	VCP-R155H	pcDNA3-Strep-GFP	this study
pcDNA3-VCP-K524A-GFP	VCP-K524A	pcDNA3-Strep-GFP	this study
pcDNA3-VCP-S555G-GFP	VCP-S555G	pcDNA3-Strep-GFP	this study
pOTB7-VCP IRALp962D0522Q2	VCP	pOTB7	RZPD
pOTB7-VCP IRALp962J231Q2	VCP	pOTB7	RZPD
pOTB7-VCP IRALp962O029Q2	VCP	pOTB7	RZPD
pOTB7-VCP complete	VCP	pOTB7	this study
pRC/CMV-Rhodopsin-WT	Rhodopsin-WT	pRC/CMV	V. Marigo, TIGEM, Napoli, Italy
pRC/CMV-Rhodopsin-P23H	Rhodopsin-P23H	pRC/CMV	V. Marigo
pRC/CMV-Rhodopsin-P347S	Rhodopsin-P347S	pRC/CMV	V. Marigo

1.5 Analysis of yeast and mammalian cell cultures*1.5.1 Special equipment*

Leica inverse table top microscope DMIL	Leica Microsystems, Wetzlar, Germany
Leica inverse fluorescence microscope (DMIRE2, CTRMic) with camera DC250	Leica Microsystems
Zeiss Axioskop 2 with AxioCam HRc	Zeiss, Göttingen, Germany
Zeiss ApoTome™ with AxioCam HRc	Zeiss
Zeiss electron microscope EM 10	Zeiss
Ultramicrotome Ultratome III	LKB, Bromma, Sweden
Synergy HT microplate reader	Biotek, Bad Friedrichshall, Germany
GENios Pro™ microplate reader	Tecan, Grödig, Austria
CO ₂ incubator	Sanyo, Munich, Germany
Laminar flow	BDK, Sonnenbühl-Genkingen, Germany
Polyscience water bath	Polyscience, Niles, IL, USA
Rotanta 46RS Centrifuge	Hettich-Zentrifugen, Tuttlingen, Germany
Rotator Stuart Rotator SB3	VWR
Infors HT Multitron Incubator Shaker for Yeast	Infors HT, Bottmingen, Switzerland
Free flow electrophoresis (FFE) apparatus, Octopus	Dr. Weber GmbH, Kirchheim, Germany
FACS Calibur	BD Biosciences, Heidelberg, Germany
Liquid Nitrogen Tank Chronos, ADURβ	Messer, Sulzbach, Germany
Potter S	B. Biotech International, Melsungen, Germany

1.5.2 Kits

CaspACE™ FITC-VAD-FMK <i>in situ</i> marker	Promega
<i>In situ</i> cell death detection kit for TUNEL assay	Roche Applied Sciences, Mannheim, Germany
Effectene Transfection Reagent for lipofection	Qiagen

1.5.3 Yeast strains and mammalian cell lines

1.5.3.1 Yeast strains

Table 6: Yeast strains

Strain	Genotype	Provider
KFY417	<i>MAT a, his4-619, leu2-3,112, ura3-52, cdc48::URA3; YEp52-CDC48</i>	Kai-Uwe Fröhlich, University of Graz, Austria
KFY437	<i>MAT a, his4-619, leu2-3,112, ura3-52, cdc48::URA3; YEp52-cdc48^{S565G}</i>	Kai-Uwe Fröhlich

1.5.3.2 Mammalian cell lines

Table 7: Mammalian cell lines

Cell line	Description	Provider
HEK293	Human embryonic kidney, ACC 305	DSMZ, Braunschweig, Germany

1.5.4 Antibodies

Table 8: Antibodies against yeast proteins

Antibody	Species	Dilution	Provider
Anti-40 kDa microsomal protein	rabbit, polyclonal	1:1000 W	G. Daum, TU Graz, Graz, Austria
Anti-55 kDa cytosolic protein	mouse, monoclonal	1:20 W	G. Blobel, Rockefeller University, NY, USA
Anti-AAC2	rabbit, polyclonal	1:1000 W	W. Neupert, University of Munich, Germany
Anti-Cdc48p	rabbit, polyclonal	1:5000 W	F. Madeo, University of Graz, Austria
Anti-Cytochrome <i>c</i>	rabbit, polyclonal	1:1000 W	F. Sherman, University of Rochester, NY, USA
Anti-DPM1	mouse, monoclonal	4 µg/mL W	Molecular Probes, Invitrogen
Anti-Kar2p	rabbit, polyclonal	1:10000 W	R. Schekman, University of California, CA, USA
Anti-TOM70	rabbit, polyclonal	1:1000 W	W. Neupert
Anti-Ubiquitin	mouse, monoclonal	1:8000 W	BD Biosciences, Heidelberg, Germany

W: Western

Table 9: Antibodies against mammalian proteins

Antibodies	Species	Dilution	Provider
Anti-GAPDH	mouse, monoclonal	1:1000 W	Chemicon, Hampshire, UK
Anti-GFP	rabbit, polyclonal	1:10000 W	Molecular Probes, Invitrogen
Anti-p97-ATPase (VCP)	mouse, monoclonal	1:1000 W	BD Biosciences
Anti-PARP cleaved	rabbit, polyclonal	1:1000 W	Cell Signaling Technology, New England Biolabs
Anti-Rhodopsin (4D2)	mouse, monoclonal	1:4000 IF	R. Molday, University of British Columbia, Canada
Anti-Rhodopsin (ABR)	rabbit, polyclonal	1:1000 W 1:100 IF	Dianova, Hamburg, Germany
Anti-Rhodopsin (1D4)	mouse, monoclonal	1:1000 W	Sigma-Aldrich
Anti-β-Tubulin	mouse, monoclonal	1:500 IF	Sigma-Aldrich
Anti-Ubiquitin	mouse, monoclonal	1:8000 W	BD Biosciences

IF: Immunofluorescence, W: Western

Table 10: Secondary antibodies

Antibodies	Species	Dilution	Provider
Anti-Mouse IgG HRP-conjugated	goat, polyclonal	1:15000 W	Jackson ImmunoResearch Laboratories, Dianova
Anti-Rabbit IgG HRP-conjugated	goat, polyclonal	1:15000 W	Jackson ImmunoResearch Laboratories, Dianova
Anti-Mouse IgG Alexa Fluor 488-conjugated	goat, polyclonal	1:1000 IF	Molecular Probes, Invitrogen
Anti-Mouse IgG Alexa Fluor 568-conjugated	goat, polyclonal	1:1000 IF	Molecular Probes, Invitrogen
Anti-Rabbit IgG Alexa Fluor 488-conjugated	goat, polyclonal	1:1000 IF	Molecular Probes, Invitrogen
Anti-Rabbit IgG Alexa Fluor 568-conjugated	goat, polyclonal	1:1000 IF	Molecular Probes, Invitrogen

IF: Immunofluorescence, W: Western

1.6 Software and databases

1.6.1 Software

Adobe Illustrator 10.0	Adobe Systems, Seattle WA, USA
Adobe Photoshop 7.0	Adobe
AxioVision LE 4.0-4.5 for fluorescence and electron microscopy	Zeiss
Cell Quest analysis software for FACS analysis	BD Biosciences
GPS Explorer 2.0 for analysis of MalDI-TOF/TOF MS	Applied Biosystems
Mascot 1.7 search engine	Matrix Science, London, UK
MassLynx V.3.5	Waters
MS Office 2002 (Word, Excel, Powerpoint)	Microsoft, Redmond, WA, USA
ProteinLynx Globalserver V.1.1 for analysis of MalDI-TOF MS	Waters
ProteomWeaver V.1-V.2 for 2-DE image analysis	Definiens, Munich, Germany
QuantityOne 4.2 for quantification of Western blots	Bio-Rad
SigmaPlot 8.0/9.0 for illustration of quantitative data	Systat, Cranes Software, Bangalore, India
Vector NTI Suite 9.0/10.0 for molecular biology	Invitrogen
X-tof 5.0.1 for analysis of MalDI-TOF MS	Bruker Daltonik

1.6.2 Databases

NCBI	http://www.ncbi.nlm.nih.gov/
PubMed	http://www.ncbi.nlm.nih.gov/entrez/query.fcgi
Protein	http://www.ncbi.nlm.nih.gov/entrez/query.fcgi?db=protein
Nucleotide	http://www.ncbi.nlm.nih.gov/entrez/query.fcgi?db=nucleotide
Scopus	http://www.scopus.com/scopus/home.url
Swiss-Prot	http://us.expasy.org/sprot/
RZPD	http://www.rzpd.de/
Mips	http://mips.gsf.de/projects/fungi
Mitop2	http://ihg.gsf.de/mitop2/start.jsp

2. Methods

2.1 Protein chemistry

2.1.1 Determination of protein concentration

The concentration of proteins in extracts was determined according to Bradford (1976). This assay is based on the binding of the dye Coomassie Brilliant Blue G-250 to proteins leading to a shift in the absorption maximum of the dye from 465 nm to 595 nm. This shift is presumably caused by the stabilization of the dye in its un-protonated, anionic sulfonated form by complex formation between dye and protein. The dye binds unspecifically to cationic and non-polar, hydrophobic side chains of proteins (mainly arginine and aromatic amino acids). The Bradford method shows a high sensitivity (1 µg protein/mL reaction solution) and is not disturbed by reducing agents such as dithiothreitol (DTT) and β-mercaptoethanol. In contrast, the measurement is compromised by detergents such as sodium dodecyl sulfate (SDS), strong basic reagents and high urea concentrations (see below). The Bio-Rad Protein Assay Kit (Bio-Rad) was used for the Bradford assay following the manufacturer's instructions. 1 vol of Dye Reagent Concentrate was diluted with 4 vol of dH₂O. 1 mL of the diluted reagent was mixed with 1-10 µL of the protein sample and incubated for 5 min at room temperature (RT). Diluted reagent was used as blank. Absorption was measured at 595 nm in a photometer (Ultraspec 3300 pro, GE Healthcare). Protein concentrations were calculated using a standard regression curve with bovine serum albumin (BSA) as protein standard (2-10 µg BSA). 2-DE lysis buffer contains high amounts of urea, a reagent disturbing the Bradford assay. Determination of the concentration of proteins in 2-DE lysis buffer was therefore done using BSA diluted in 2-DE lysis buffer. All samples (protein samples and BSA samples) were added with 2-DE lysis buffer to 10 µL to ensure same amounts of urea in all cuvettes. 10 µL 2-DE lysis buffer was used as blank.

2.1.2 Protein precipitation

In order to enrich proteins from diluted protein extracts or to remove disturbing components in the sample buffers (*e.g.*, sucrose), proteins were precipitated using a denaturing chloroform-methanol method (Wessel and Flügge, 1984). Precipitation of proteins by this method is rather insensitive against lipids, salts, β-mercaptoethanol and detergents such as SDS. Moreover, precipitation is quantitative over a wide concentration range. 0.4 mL methanol (p.A.) was added to 0.1 mL of aqueous protein sample. The solution was vortexed and centrifuged for 10 sec (16000 g, RT). 0.1 mL chloroform (p.A.) was added, and the solution was mixed and centrifuged (10 sec, 16000 g, RT). By adding 0.3 mL ddH₂O

and thoroughly vortexing and centrifugation (1 min, 16000 g, RT), phase separation was induced leading to accumulation of denaturated proteins in the interphase. The upper (aqueous) phase was carefully removed and the remaining solution was mixed with 0.3 mL methanol. Denaturated proteins were then pelleted (2 min, 16000 g, RT) and air-dried after discarding the supernatant. The pellet was dissolved in SDS sample buffer for further analysis by SDS-PAGE (see 2.1.3) and Western blot (see 2.1.5).

2.1.3 SDS-PAGE

In order to separate protein mixtures one-dimensional SDS-polyacrylamide gel electrophoresis (1D-SDS-PAGE) was used (Laemmli, 1970). In this method proteins bind the negatively charged denaturing detergent SDS in a relation of 1.4 g SDS per g protein. SDS confers a high negative charge density to the proteins masking their own charge. This leads to a nearly constant charge-to-mass ratio of the SDS-protein complexes, in which the proteins are in a denaturated form. Electrophoresis of proteins in a SDS-containing gel therefore separates the SDS-protein complexes according to their molecular masses, whereby smaller proteins move faster through the pores of the polyacrylamide matrix. In the used discontinuous gel system, a stacking gel with large pores was polymerized on top of the separating gel. The pH value of the stacking gel (pH 6.8) is in the range of the pI value (isoelectric point) of glycine, a major component of the electrophoresis buffer. At this pH value glycine is nearly in its netto-uncharged zwitterionic form, leading to the reduction of charged molecules in the stacking gel. The remaining charged molecules are the chloride ions of the stacking gel buffer and the SDS-protein complexes. The latter focus (stack) according to their electrophoretic mobility immediately behind the leading chloride ions and before the lagging glycine ions (isotachopheresis effect). Passing the alkaline separating gel (pH 8.8), glycine becomes negatively charged. This leads to a strong accumulation of charged molecules. The SDS-protein complexes are now separated in the small pores of the separating gel according their molecular masses.

Gels were casted separately using casting chambers for Mini Protean 3 (Bio-Rad) for mini gels and Protean II (Bio-Rad) for 18 cm gels, respectively, with 0.75 mm spacers. The casting chamber was filled with separating gel solution (Table 11) that was overlaid with isopropanol. Formation of the polyacrylamide matrix was done by a radical polymerization reaction of the monomers acrylamide and bisacrylamide induced by adding N, N, N', N'-tetraethylmethylenediamine (TEMED) and the polymerization starter ammonium peroxydisulfate (APS). After polymerization isopropanol was removed and the top of the

separating gel was washed with ddH₂O. The separating gel was overlaid by the stacking gel solution (Table 12) and the combs were inserted. Different concentrations of acrylamide were used for separating gels (8 to 16%).

Table 11: Gel solution for SDS separating gel (60 mL)

	8%	10%	12%	14%	16%
ddH ₂ O	28 mL	24 mL	20 mL	16 mL	12 mL
1.5 M Tris-HCl pH 8.8	15 mL	15 mL	15 mL	15 mL	15 mL
Acrylamide:bisacrylamide (37.5%:1%)	16 mL	20 mL	24 mL	28 mL	32 mL
10% (w/v) SDS	600 µL	600 µL	600 µL	600 µL	600 µL
TEMED	60 µL	60 µL	60 µL	60 µL	60 µL
10% (w/v) APS	300 µL	300 µL	300 µL	300 µL	300 µL

Table 12: Gel solution for SDS stacking gel (15 mL)

	4%
ddH ₂ O	11.65 mL
1.5 M Tris-HCl pH 6.8	1.25 mL
Acrylamide:bisacrylamide (37.5%:1%)	2.0 mL
10% (w/v) SDS	150 µL
TEMED	30 µL
10% (w/v) APS	150 µL

Gels were placed into the gel chambers (MiniProtean 3 and Protean II, respectively) and the buffer chambers were filled with SDS electrophoresis buffer (50 mM Tris, 384 mM glycine, 0.2% (w/v) SDS). Protein extracts were treated with SDS sample buffer (5x buffer: 5% (w/v) SDS, 250 mM Tris-HCl pH 6.8, 50% (v/v) glycerol, 500 mM β-mercaptoethanol, 0.025% (w/v) bromophenol blue) and heated to 96°C for 3 min. For the analysis of membrane proteins, *i.e.*, hydrophobic aggregation-prone proteins, protein extracts treated with SDS sample buffer were incubated for 1 h on ice. After loading the extracts onto the gel, electrophoresis was done 15 min with 15 mA or 100 V (MiniProtean 3 and Protean II, respectively) and was then changed to 25 mA or 10 W, respectively. Electrophoresis was stopped after the bromophenol blue front reached the end of the separating gel. As protein standard pre-stained protein markers were used (*e.g.*, PageRuler Prestained Protein Ladder, Fermentas).

2.1.4 Staining of SDS gels

2.1.4.1 Silver staining

Silver staining of SDS gels is based on the reduction of silver ions to silver by formaldehyde under alkaline conditions (Shevchenko et al., 1996). Since silver ions form complexes with proteins, this process leads to visualization of protein spots or bands. Silver

staining is highly sensitive (1 ng per protein band). It is 100-fold more sensitive than standard staining with Coomassie Brilliant Blue R-250 (see 2.1.4.2).

After finishing electrophoresis, SDS gels were incubated twice for 30 min in fixation solution (50% (v/v) methanol, 12% (v/v) acetic acid, 500 μ L/L 37% formaldehyde). The cross-linker formaldehyde was used to reduce loss of polypeptides. Gels were then incubated three times for 20 min in 50% (v/v) ethanol. Incubation in ethanol solution led to shrinking of the gels due to dehydration. In the next step, gels were rehydrated for 30 sec in an aqueous 0.02% (w/v) sodium thiosulfate ($\text{Na}_2\text{S}_2\text{O}_3$) solution followed by two washing steps in dH_2O . Shrinking and swelling of the gels was done in order to remove SDS from the gel matrix. Sodium thiosulfate was used in order to remove oxidating groups and radicals within the gel that may increase background staining. Gels were then incubated for 20 min in silver nitrate (AgNO_3) solution (0.2% (w/v) silver nitrate, 750 μ L/L 37% formaldehyde). Gels were then placed in developer solution (6% (w/v) sodium carbonate (Na_2CO_3), 0.005% (w/v) sodium thiosulfate, 500 μ L/L 37% formaldehyde). This treatment led to a shift from the acidic towards the alkaline pH range. Formaldehyde was then able to reduce silver ions complexed by proteins. After protein bands or spots were visualized, staining was stopped by incubation for 10 min in fixation solution. Gels were equilibrated in storage solution (20% (v/v) ethanol, 2% (v/v) glycerol) for at least 15 min and could then be scanned and dried (see 2.1.4.5).

2.1.4.2 Coomassie staining

Coomassie staining is based on the binding of Coomassie Brilliant Blue R-250 to proteins. This staining method is fast but much less sensitive (about 100 ng per protein band) than silver (see 2.1.4.1) and RuBP staining (see 2.1.4.4). After finishing electrophoresis, SDS gels were incubated in fixation solution (40% (v/v) methanol, 10% (v/v) acetic acid) for 15 min. Visualization of protein bands was accomplished by incubation in staining solution (40% (v/v) methanol, 10% (v/v) acetic acid, 0.1% (w/v) Coomassie Brilliant Blue R-250) for 1 h at RT. Background staining was removed by equilibrating the gels in fixation solution. Fixation solution was exchanged until a clear protein pattern could be observed. Gels could then be scanned and dried (see 2.1.4.5).

2.1.4.3 Colloidal Coomassie staining

This method allows a more sensitive staining of proteins with Coomassie Brilliant Blue G-250. The sensitivity is in between that of Coomassie and silver stain. Coomassie Brilliant Blue G-250 is able to form microprecipitates (colloids) in acidic media containing

ammonium sulfate ((NH₄)₂SO₄) (Candiano et al., 2004; Neuhoff et al., 1988; Rabilloud and Charmont, 2000), *i.e.*, there is a very low concentration of free dye resulting in minimal background staining. The colloids act as a reservoir of dye molecules, so that enough dye is present to occupy all binding sites of the proteins, provided that staining is prolonged to the steady state.

After electrophoresis, the gels were incubated twice for 30 min in fixation solution (20% (v/v) methanol, 10% (v/v) phosphoric acid). Gels were washed three times for 20 min in (10% (v/v) phosphoric acid), and were equilibrated for 30 min in a solution containing (10% (v/v) phosphoric acid, 20% (v/v) methanol and 10% (w/v) ammonium sulfate). Staining of the gels was done by adding 1.2% (v/v) of a solution containing 2 g Coomassie Brilliant Blue G-250 in 100 mL (prepared in hot dH₂O under stirring and filtrated through a fluted filter (Schleicher&Schuell) after cooling). The gels were incubated until staining had reached the steady-state (24 to 72 h). Background destaining and depletion of surplus ammonium sulfate was done by equilibrating the gels three times in dH₂O for 10 min. Gels could then be scanned and dried (see 2.1.4.5).

2.1.4.4 Ruthenium-II-bathophenanthroline disulfonate chelate (RuBP) staining

Silver staining is a highly sensitive protein stain (1 ng per protein band) but shows rather poor linearity and interferes with protein identification using mass spectrometry. Staining of proteins using RuBP is less sensitive compared to silver staining (10 ng per protein band) but markedly more sensitive than Colloidal Coomassie staining. It shows high linearity and good compatibility to mass spectrometry (Lamanda et al., 2004; Rabilloud et al., 2001).

2.1.4.4.1 Preparation of the fluorescence probe ruthenium-II-bathophenanthroline disulfonate chelate (RuBP)

RuBP was prepared as described by Rabilloud et al. (2001). 0.2 g of potassium pentachloro aqua ruthenate (K₂Cl₅Ru·H₂O, 26.9% ruthenium, Alfa Aesar, Karlsruhe, Germany) were dissolved under reflux in 20 mL boiling dH₂O. 0.94 g (three molar equivalents) of the di-sodium salt of bathophenanthroline disulfonate (Fluka) were added to the solution that was subsequently kept under reflux for 20 min. 5 mL of a 500 mM sodium ascorbate solution (freshly prepared) were added into the refluxing mixture that was kept under reflux for additional 20 min. After cooling, the pH was adjusted to 7 with sodium

hydroxide and the volume was adjusted to 26 mL with dH₂O resulting in a 20 mM stock solution that could be stored at 4°C.

2.1.4.4.2 Standard RuBP staining protocol

All solutions and buffers for RuBP staining were done with ddH₂O. After electrophoresis gels were incubated overnight in fixation solution (30% (v/v) ethanol, 10% (v/v) acetic acid). Gels were washed four times for 30 min in 20% (v/v) ethanol in order to remove acetic acid quantitatively (acids may interfere with the fluorescence of the ruthenium chelate). Staining was accomplished by incubating the gels 6 h in staining solution (20% (v/v) ethanol, 200 nM ruthenium chelate). Gels were equilibrated twice for 10 min in ddH₂O and digitalized using the Fuji FLA-3000 scanner (settings: Laser 473 nm, Filter R675, Pixel size 100 μ, Bits per pixel 16, Sensitivity 1000).

2.1.4.4.3 Enhanced RuBP staining protocol

An additional destaining step can improve the sensitivity of the RuBP staining method by reducing background staining (Lamanda et al., 2004). After equilibrating the stained gels in ddH₂O, the gels were subsequently incubated in RuBP destaining solution (40% (v/v) ethanol, 10% (v/v) acetic acid) overnight, equilibrated twice for 10 min in ddH₂O and scanned as described in 2.1.4.4.2. RuBP stained gels could then be stained with colloidal Coomassie (see 2.1.4.3).

2.1.4.5 Digitalizing and drying of SDS gels

SDS gels stained with silver, Coomassie or colloidal Coomassie were digitalized using a GS-710 Calibrated Imaging Densitometer (Bio-Rad) and Adobe Photoshop 7.0 software package. SDS gels can subsequently be packed air bubble-free between two wet cellophane foils (Bio-Rad) and dried in a gel drier (Bio-Rad) at 50°C for 3 h.

2.1.5 Western blot analysis

SDS-protein complexes separated by SDS-PAGE can be transferred electrophoretically onto membranes for immunodetection of individual proteins using specific antibodies (Towbin et al., 1979). In this study, blotting of SDS gels to Hybond-P polyvinylidene difluoride (PVDF) transfer membranes (GE Healthcare) by a wet blotting apparatus (Mini Trans Blot Electrophoretic Transfer Cell, Bio-Rad) was carried out according to manufacturer's protocol. After electrophoresis, SDS gels were incubated in blotting buffer

(12 mM Tris, 96 mM glycine, 10% (v/v) methanol p.A.) for 5 min. PVDF membranes were activated with methanol (p.A.), rinsed in dH₂O and incubated in blotting buffer for 5 min. Cut up filter papers (Whatman, Dassel, Germany) and fiber pads were soaked in blotting buffer prior use. A fiber pad, one filter paper and the PVDF membrane were laid on the anodal side of the gel holder cassette. The SDS gel was then placed air bubble-free on top of the membrane, followed by a filter paper and a fiber pad. The gel holder cassette was closed and placed into the blotting module. The blotting module and the cooling unit were inserted into the blotting tank. Proteins were transferred with 175 mA for 2 h or 25 mA overnight at 4°C. After blotting, the membranes were stained for 10 min in Ponceau staining solution (0.5% (w/v) Ponceau S, 1% (v/v) acetic acid). Background staining was removed incubating the membranes three times in Ponceau destaining solution (10% (v/v) acetic acid, 40% (v/v) ethanol) for 5 min. Protein band patterns on the membranes were digitalized using the GS-710 Calibrated Imaging Densitometer (Bio-Rad) and Adobe Photoshop 7.0 software package. Membranes were destained in PBST (137 mM NaCl, 2.7 mM KCl, 10 mM Na₂HPO₄, 2 mM KH₂PO₄, 0.1% (v/v) Tween-20), blocked for 1 h at RT using 5% (w/v) milk powder (Blotting Grade Blocker Non-Fat Dry Milk, Bio-Rad) in PBST, incubated with the first antibody in an appropriate dilution (see 1.5.4, Tables 8 and 9) in 5% (w/v) milk powder in PBST for 3 h at RT or overnight at 4°C. Membranes were washed five times for 5 min with PBST to remove unbound antibody and were then incubated with the appropriate horseradish-peroxidase (HRP)-coupled secondary antibody (see 1.5.4, Table 10) in a 1:15000 dilution in 5% (w/v) milk powder in PBST for 1 h. Membranes were washed five times for 5 min with PBST. Immunodetection was done using the enhanced chemiluminescence plus kit (ECL plus, GE Healthcare) according to manufacturer's protocol. 2 mL of solution A was mixed with 50 µL solution B immediately before use. Membranes were incubated for 5 min at RT with the mixed solution and subsequently put into a developer cassette (Hypercassette, GE Healthcare). Under red light conditions, Hyperfilm ECL films (GE Healthcare) were put into the cassette for an appropriate time and were then developed using the Agfa Curix 60 developer (Agfa). The films were afterwards digitalized using the GS-710 Calibrated Imaging Densitometer (Bio-Rad) and Adobe Photoshop 7.0 software package. Immunoreactive bands were quantified applying the QuantityOne[®] V.4.2 software package (Bio-Rad), after adjusting the images using the levels function in Photoshop 7.0. With QuantityOne software adjusted volumes of the immunoreactive bands were determined using the global or local background subtraction method. Extremely weak bands and saturated bands were discarded from the

analysis. Relative quantification and statistics (paired and unpaired Student's t-test, respectively) were done using MS Excel 2002 or SigmaPlot 8.0 (Systat) software packages.

For reprobing of the membranes antibodies bound to PVDF membranes could be destroyed by equilibrating the membranes in stripping buffer (2% (w/v) SDS, 50 mM Tris-HCl pH 6.8, 100 mM β -mercaptoethanol) for 15 min at 55°C under gently shaking. Membranes were washed in PBST and subsequently blocked, incubated with the first and second antibody as described above.

2.1.6 Two-dimensional gel electrophoresis (2-DE)

For differential analysis of complex protein mixtures high-resolution 2-DE was applied according to Rabilloud et al. (1997) using immobilized pH gradients (IPG-Dalt) based on the protocol of Görg et al. (1988). In the first dimension, denaturated proteins were separated by isoelectric focusing (IEF) according to their charge. Here, proteins migrate in a stable pH gradient upon high voltage to the pH value in which their net charges become zero (isoelectric point, pI). Commercially available IPG strips consist of a polyacrylamide matrix with large pores attached to a plastic surface. The matrix is prepared by co-polymerization of acrylamide-bisacrylamide with acidic and basic acrylamide derivatives leading to an immobilized pH gradient. In order to increase the buffer capacity of the pH gradient, carrier ampholytes (CA), *i.e.*, low molecular ampholytes, were added to the 2-DE rehydration buffer.

In the second dimension separation of proteins was done according to their apparent molecular mass by SDS-PAGE. Here, IPG strips were laid on top of the SDS gels. In order to get a maximal separation, gradient gels were used. Separated proteins could be visualized as protein spots by staining of the gel via silver (see 2.1.4.1), standard RuBP (see 2.1.4.4) or colloidal Coomassie staining (see 2.1.4.3).

2.1.6.1 Sample preparation

Proteins to be separated by IPG-Dalt had to be solubilized, denaturated and reduced. Samples applied on the focusing strips must not contain salts and charged detergents such as SDS, since they would migrate in the electric field, thereby interfering with focusing of the proteins. Solubilization and denaturation of proteins was accomplished using 2-DE lysis buffer, containing high molar concentrations of urea and thiourea, as well as the non-ionic detergent 3-[(3-cholamidopropyl)-dimethyl-ammonio]-1-propansulfonate (CHAPS). For reduction 2-DE lysis buffer was supplemented with dithioerythritol (DTE).

2-DE lysis and 2-DE rehydration buffer (see 2.1.6.2) were always prepared freshly as follows: 5.4 g urea (p.A.) and 1.9 g thiourea (p.A.) were filled up with ddH₂O to 10 mL and stirred at RT until urea and thiourea were completely dissolved resulting in a highly concentrated urea/thiourea solution (9.5 M urea, 2.5 M thiourea). 0.2 g Duolite ionexchanger beads (MB-6113, VWR) were added in order to remove remaining salts. After 10 min stirring, the solution was filtered through a fluted filter (Schleicher & Schuell). 2-DE lysis buffer was obtained by adding 4% (w/v) CHAPS and 1% (w/v) DTE. 2-DE rehydration buffer was obtained from the highly concentrated urea/thiourea solution by adding 2% (w/v) CHAPS, 0.5% (w/v) DTE, 10 µL/mL Pharmalyte (carrier ampholytes pH 3-10 for IEF, 0.36 meq/mL pH, GE Healthcare), 5 µL/mL Orange G solution (saturated in ddH₂O) and 40 µL/mL 1 M Tris.

Aqueous mitochondrial protein extracts (see 2.3.8.2.2) were lyophilized overnight (Freeze drying chamber and ValuPump, Savant). Dried protein extracts were solubilized in 2-DE lysis buffer (150 µL lysis buffer per 500 µg protein extract), stirred for 2 h at RT and incidentally sonicated in order to destroy urea crystals. After centrifugation (20 min, 30000 g, RT), supernatants were used for determination of protein concentration by Bradford assay (see 2.1.1). Cytosolic protein extracts contained high concentration of sorbitol (0.6 M, see 2.3.8.2.2) a component that interferes with isoelectric focusing. Therefore, cytosolic extracts were precipitated (see 2.1.2) prior dissolution in 2-DE lysis buffer.

2.1.6.2 Rehydration and sample loading

In order to get a high resolution in IEF over a broad pI range, 24 cm IPG strips with a non-linear pH gradient covering pH values from 3-10 with a flat pH gradient at neutral pH values were used (GE Healthcare). The dried and frozen (-20°C) IPG strips were prepared for IEF by equilibrating them up-side-down in 2-DE rehydration buffer (480 µL per strip) in a rehydration chamber (GSF workshop). The gel matrices of the IPG strips were equally covered with 2-DE rehydration buffer. IPG strips were overlaid with 3 mL gas-free mineral oil (DryStrip Cover Fluid, GE Healthcare), in order to exclude drying and formation of urea crystals. IPG strips were equilibrated in the rehydration chamber overnight at RT. In this study, proteins were loaded onto the IPG strips applying the in-gel rehydration method. Thus, protein samples dissolved in 2-DE lysis buffer were diluted in 2-DE rehydration buffer resulting in 150 µg and 400 µg protein per strip for analytical and preparative 2-DE gels, respectively.

2.1.6.3 Isoelectric focusing (IEF)

IEF was done using the Multiphor II apparatus (GE Healthcare). The tank of the electrophoresis unit was filled with dH₂O and the cooling plate was put into the tank. In order to guarantee equal cooling, the Dry Strip Kit was laid air bubble-free onto the cooling plate with 5 mL mineral oil in between. The focusing strip aligner was laid air bubble-free into the Dry Strip Kit with 8 mL mineral oil in between. Rehydrated IPG strips were rinsed with ddH₂O and laid onto a wet filter paper (Whatman) with the plastic side facing the paper. A second wet filter paper was pressed gently on top of the gel matrix of the strips and removed carefully. This step was done in order to remove surplus mineral oil, urea crystals and proteins that were not moved into the gel matrix during the in-gel rehydration step. IPG strips were then laid gel-side-up into the grooves of the aligner. Wet electrode strips (GE Healthcare) were pressed gently at the anodic and cathodic ends of the strips, respectively. Electrodes were positioned and IPG strips were overlaid with mineral oil. Small plastic bowls containing sodium hydroxide (NaOH) pellets were put onto the cooling plate, in order to remove CO₂ carboxylates proteins. Focusing was done under cooling at 20 to 23°C. In the beginning, a low voltage step (150 V) was applied, in order to remove remaining salts from the strips. At higher voltages (2000 to 8000 V) proteins began to focus in the stable pH gradient. Equal velocity of the Orange G front (a negatively charged dye) ensures highly comparable currents through the different strips. Focusing was continued until 120 kWh were reached. At this time point the steady state phase was reached, *i.e.*, the time point at which all the proteins were focused. After focusing, IPG strips were used either immediately for the second dimension or were frozen at -20°C until further use.

2.1.6.4 Casting of the polyacrylamide gels for the second dimension

For the second dimension, SDS-PAGE was applied using gradient gels (24 cm x 20 cm, 0.75 mm spacer). Casting of the gels was done using the Ettan Dalt II Gel Caster System allowing the simultaneous casting of 14 gels. Gel solutions (Table 13, without APS and TEMED) were filtrated using a fluted filter (Schleicher & Schuell) and air bubbles were removed for 15 min applying vacuum using an oil pump. To the gel solution with the lower concentration of acrylamide (8%) APS and TEMED were added and the solution was immediately filled into the gradient mixer. Air bubbles were removed from the tubes and the gradient mixer. After adding APS and TEMED, the gradient mixer was filled with the higher concentrated gel solution (16%). The pump of the gel caster system now pressed the lower concentrated gel solution from below into the casting chamber. The connection of the higher

concentrated gel solution to the mixture chamber was opened, leading to filling of the casting chamber with a progressively higher concentrated gel solution. After the chamber was filled, the gels were overlaid with 1.5 mL *n*-butanol per gel. Polymerization was done overnight. Gels could be stored for up to two weeks submerged in SDS gel storage buffer (375 mM Tris-HCl pH 8.8) at 4°C.

Table 13: Gel solutions for second dimension in 2-DE

	8%	16%
30% (w/v) Acrylamide:bisacrylamide (37.5:1, Serva)	100 mL	200 mL
1.5 M Tris-HCl pH 8.8 (USB)	94.2 mL	94.2 mL
ddH ₂ O	178.5 mL	53 mL
Glycerol p.A.	0 mL	25.5 mL
12.5% (w/v) Sodium thiosulfate	940 µL	940 µL
TEMED (Bio-Rad)	125 µL	125 µL
10% (w/v) APS – freshly prepared	1.25 mL	1.25 mL

2.1.6.5 Equilibration and transfer of the IPG strips

After IEF, IPG strips were rinsed with ddH₂O and incubated in two steps in 2-DE equilibration solution for the second dimension (SDS-PAGE). In order to prevent electroendosmotic effects during the protein transfer from the focusing strip into the SDS gel, 2-DE equilibration solutions contained urea and glycerol (50 mM Tris-HCl pH 6.8, 6 M urea, 30% (v/v) glycerol, 2% (w/v) SDS; solution stable at RT for up to 1 month). In the first step, IPG strips were incubated for 15 min at RT in reducing 2-DE equilibration solution containing 1% (w/v) DTE (freshly prepared) using an equilibration chamber (GSF workshop). Under these reducing conditions, existing disulfide bonds between the sulfhydryl groups of the polypeptides were cleaved and (re)formation of disulfide bonds was prohibited. After rinsing the strips with ddH₂O, equilibration was done for 15 min at RT in the alkylating 2-DE equilibration buffer (4.8 (w/v) 2-iodoacetamide and one tip of bromophenol blue in 2-DE equilibration buffer, freshly prepared). In this step, free sulfhydryl groups of surplus DTE and of cysteine residues were alkylated, preventing reoxidation to disulfide bonds. This step was necessary, in order to prevent the emergence of non-protein “ghost bands” from DTE side products between 50 and 70 kDa when staining the gel with a silver staining procedure. IPG strips were then rinsed with ddH₂O and laid on edge on a wet filter paper (Whatman). SDS gels were overlaid with SDS electrophoresis buffer (50 mM Tris, 384 mM glycine, 0.2% (w/v) SDS). IPG strips were dipped in SDS electrophoresis buffer and transferred on top of the SDS gels with the plastic side facing to the bigger glass plate of the gel and the acidic end of the strips oriented to the left side of the gel. IPG strips were gently pressed on top of the SDS gel and air bubbles between strips and gel had to be removed. Surplus SDS

electrophoresis buffer was removed and IPG strips were fixed with boiled agarose solution (0.5% (w/v) agarose in SDS electrophoresis buffer).

2.1.6.6 Second dimension: SDS-PAGE

SDS gels were put into the Ettan Dalt II Electrophoresis chamber (GE Healthcare) and electrophoresis was done under cooling at 4°C, in order to reduce diffusion effects. In the beginning, 20 mA per gel were applied for 45 min. After the proteins were transferred from the IPG gel matrices into the SDS gels, as evidenced by the bromophenol blue front, gels were run with 15 W per gel until the bromophenol blue front reached the end of the gels (about 7 to 9 h). After electrophoresis, analytical gels were stained by the silver staining method (see 2.1.4.1), whereas preparative gels were stained applying the standard RuBP (see 2.1.4.4) followed by the colloidal Coomassie staining method (see 2.1.4.3).

2.1.6.7 Image analysis

Analysis of 2D gels was done visually assisted by ProteomWeaver™ V.2 software package (Definiens AG, Munich, Germany). Two gels of two different conditions, *i.e.*, *CDC48* wild-type and *cdc48*^{S565G} mutant protein extracts, were laid side by side and analyzed for visible alterations in their protein patterns, *i.e.*, decrease or increase of the intensity of single protein spots. Since technical variability of protein patterns between different gels of the same electrophoretic run and the same condition had to be taken into consideration, all observed alterations were validated by analyzing all the gels of the same 2-DE separation set. Confirmed alterations were then compared with alterations observed in independent 2-DE separation sets, each consisting of several gels. Protein spot alterations were regarded to be reliable, if they were confirmed at least in two independent 2-DE separation sets. These protein spot alterations were then quantified using ProteomWeaver™ V.2 software package and evaluated statistically using MS Excel 2002. The intensities of a single protein spot were quantified in the gels of both conditions considering all 2-DE separation sets. Subsequently, the ratio of the mean values of the intensities of this spot between both conditions was determined. This ratio reflected the quantitative alteration in a single protein spot between both analyzed conditions. Significance of a protein spot alteration was evaluated using the unpaired Student's t-test. Here, all protein spot intensities of one condition were compared with all protein spot intensities of the second condition. A p-value below 0.05 was considered to reflect a statistically significant protein spot alteration.

2.1.7 16-BAC/SDS gel electrophoresis

Integral membrane proteins, particularly those with more than one transmembrane domain, are difficult to separate by 2-DE. Due to their high hydrophobicity, these proteins do not solubilize well in non-ionic detergents (such as CHAPS) and urea used in 2-DE. Moreover, they have a high tendency for precipitation after reaching their isoelectric point (pI) during IEF. Membrane proteins can be solubilized using ionic detergents, such as the anionic detergent SDS or the cationic detergent 16-benzyltrimethyl-*n*-hexadecylammonium chloride (16-BAC) and subsequently separated by one-dimensional (1D) gel electrophoresis by SDS-PAGE (Laemmli, 1970) (see 2.1.3) and by 16-BAC-PAGE (Macfarlane, 1983), respectively. However, 1D-PAGE has limitations in the resolution of complex protein mixtures. Therefore, two-dimensional gel electrophoresis with discontinuous 16-BAC-PAGE as first and discontinuous SDS-PAGE as second dimension that allows a higher resolution of complex protein mixtures enriched with membrane proteins (Hartinger et al., 1996; Islinger et al., 2006; Macfarlane, 1989; Zahedi et al., 2005) was used.

2.1.7.1 First dimension: 16-BAC-PAGE

Gels were casted separately using casting chambers for 18 cm gels (Protean II, Bio-Rad), respectively, with 0.75 mm spacers. The casting chamber was filled with separating gel solution (Table 14) that was overlaid with *n*-butanol. Formation of the polyacrylamide matrix was done by a radical polymerization reaction of the monomers acrylamide and bisacrylamide. Formation of radicals under the applied acidic conditions was conducted by the Fenton's reaction, *i.e.*, the oxidation of Fe²⁺ ions to Fe³⁺ ions in aqueous solutions containing hydrogen peroxide (H₂O₂), resulting in highly reactive hydroxyl radicals (OH·).

Table 14: Gel solution for 16-BAC separating gel (40 mL)

	10%
Urea	7.2 g
500 mM KPB pH 2.1	6.0 mL
30% (w/v) Acrylamide:bisacrylamide (37.5:1, Serva)	13.3 mL
2% Bisacrylamide	1.58 mL
250 mM 16-BAC	400 µL
5 mM FeSO ₄ (freshly prepared)	64 µL
80 mM Ascorbic acid (freshly prepared)	2.0 mL
ddH ₂ O	ad 38.4 mL
H ₂ O ₂ (1:1200-dilution of a 30% stock solution, freshly prepared)	1.6 mL

Table 15: Gel solution for 16-BAC stacking gel (10 mL)

	4%
Urea	1 g
500 mM KPB pH 4.1	2.5 mL
30% (w/v) Acrylamide:bisacrylamide (37.5:1, Serva)	1.33 mL
2% Bisacrylamide	1.17 mL
250 mM 16-BAC	70 μ L
5 mM FeSO ₄ (freshly prepared)	8.5 μ L
80 mM Ascorbic acid (freshly prepared)	0.5 mL
ddH ₂ O	ad 9.5 mL
H ₂ O ₂ (1:750-dilution of a 30% stock solution, freshly prepared)	0.5 mL

After polymerization *n*-butanol was removed and the top of the separating gel was washed with dH₂O. The separating gel was overlaid by the stacking gel solution (Table 15) and the combs were inserted. Polymerization of the gels was done overnight.

16-BAC sample buffer (2x) was always prepared freshly as follows: 4.5 g urea and 1 g 16-BAC were mixed with 1 mL 100% glycerol and 4 mL ddH₂O. The mixture was carefully heated at 60°C until dissolution. 750 μ L 1 M DTT and 100 μ L 5% (w/v) Pyronin Y were added and the solution was filled up to 10 mL with ddH₂O. 1x 16-BAC sample buffer, generated by diluting 1 vol 2x 16-BAC sample buffer with 1 vol ddH₂O, could be stored at RT until use.

Gels were put into the gel chambers, the buffer chambers were filled with 16-BAC electrophoresis buffer (50 mM phosphoric acid, 150 mM glycine, 2.5 mM 16-BAC), and wells were thoroughly washed with 16-BAC electrophoresis buffer. Protein extracts were treated with 1x 16-BAC sample buffer and incubated for 1 h at RT. After short centrifugation (30 sec, 16000 g, RT), the extracts were loaded onto the gel. The remaining wells were filled up with 1x 16-BAC sample buffer and electrophoresis was carried out towards the cathode (opposite to SDS-PAGE!) at 4°C with 25 mA per gel. After 1 h the 16-BAC electrophoresis buffer in the upper buffer chamber was renewed. Electrophoresis was stopped after the Pyronin Y dye front (*i.e.*, the Schlieren line) has nearly completely left the end of the separating gel. 16-BAC gels were subsequently stained by Coomassie (see 2.1.4.2) and digitalized (see 2.1.4.5). 16-BAC gels were stored at -20°C prior transfer to the second dimension.

2.1.7.2 Casting of SDS gels

Casting of SDS gels for the second dimension of 16-BAC/SDS-PAGE was done as described for 2-DE (see 2.1.6.4) with the following modifications: (i) the multicasting chamber for the Protean II gel system (18 cm gels, Bio-Rad) was used coupled with the

gradient maker of the Ettan Dalt II Gel Caster System (GE Healthcare), (ii) 1.5 mm instead of 0.75 mm spacers were used, (iii) the separating gel (8-16% gradient, see 2.1.6.4, Table 13) was overlaid with a 4% stacking gel (see 2.1.3, Table 12).

2.1.7.3 Equilibration and transfer of the 16-BAC gel strips

Coomassie-stained 16-BAC gels were cut into strips using a long razor blade. Gel strips were then rinsed with ddH₂O and incubated in four steps in equilibration solution for the second dimension (SDS-PAGE) (see 2.1.6.5, equilibration and transfer of focusing strips in 2-DE) using an equilibration chamber (GSF workshop). In the first step, 16-BAC strips were equilibrated twice in 16-BAC/SDS equilibration solution (50 mM Tris-HCl pH 6.8, 1.5 M urea, 30% (v/v) glycerol, 2% (w/v) SDS; solution stable at RT for up to 1 month) for 15 min at RT. The second step was the incubation of the 16-BAC strips in reducing 16-BAC/SDS equilibration solution containing 1% (w/v) DTT (freshly prepared) for 15 min at RT. In the third step, 16-BAC strips were equilibrated in alkylating 16-BAC/SDS equilibration solution (4.8 (w/v) 2-iodoacetamide and one tip of bromophenol blue in 16-BAC/SDS equilibration buffer, freshly prepared) for 15 min at RT. Finally, 16-BAC gel strips were equilibrated for 15 min at RT in 16-BAC/SDS equilibration solution containing one tip of bromophenol blue. SDS gels were overlaid with SDS electrophoresis buffer (50 mM Tris, 384 mM glycine, 0.2% (w/v) SDS). 16-BAC gel strips were rinsed with ddH₂O and then with SDS electrophoresis buffer and transferred on top of the SDS gels. 10 µL protein ladder (*e.g.*, PageRuler Prestained Protein Ladder, Fermentas) were pipetted on small strips of Whatman paper. The Whatman strips were placed next to the 16-BAC strips on top of the stacking gel. 16-BAC gel strips were gently pressed on top of the SDS gel and air bubbles between strips and gel had to be removed. Surplus SDS electrophoresis buffer was removed and 16-BAC gel strips were fixed with boiled agarose solution (0.5% (w/v) agarose in SDS electrophoresis buffer).

2.1.7.4 Second dimension: SDS-PAGE

SDS-PAGE was done as described in 2.1.3 with 9 mA per gel overnight at 4°C. 16-BAC/SDS gels were stained with enhanced RuBP staining (see 2.1.4.4) followed by enhanced colloidal Coomassie staining (see 2.1.4.3).

2.1.8 Maldi-Tof mass spectrometry

2.1.8.1 Destaining, reduction, alkylation of gel plugs and in-gel proteolysis

Protein spots and protein bands of interest were excised with a scalpel from dried or wet RuBP and colloidal Coomassie stained 2D gels and 16-BAC/SDS gels, or Coomassie stained 1D gels. Gel plugs were equilibrated twice for 20 min in 1 mL ddH₂O and the cellophane foil was removed from the gel matrix. Plugs were transferred into a 96-well plate (Falcon, BD Biosciences) and equilibrated for 5 min with 100 μ L ddH₂O per gel plug. This and all the following destaining, reduction and alkylation steps were done at 42°C (Shevchenko et al., 1996). In order to destain the protein plugs, 100 μ L acetonitrile were added to the gel plugs (first destaining step). The supernatants were removed after 5 min of equilibration. 100 μ L of freshly prepared 10 mM ammonium bicarbonate (NH₄HCO₃) buffer were added to the gel plugs for 5 min. Another 100 μ L acetonitrile were added to the gel plugs and the supernatants were discarded after 5 min of incubation (second destaining step). Residual acetonitrile was evaporated for 15 min. Gel plugs were treated with 100 μ L DTT solution (10 mM DTT in 10 mM NH₄HCO₃ buffer) for 30 min (reduction step). 100 μ L 2-iodoacetamide solution (55 mM 2-iodoacetamide in 10 mM ammonium bicarbonate buffer) were added and gel plugs were equilibrated for 20 min (alkylation step). Then 100 μ L acetonitrile were added and supernatants were removed after 5 min incubation. Gel plugs were equilibrated with 100 μ L 10 mM ammonium bicarbonate buffer for 10 min. 100 μ L acetonitrile were added. After 5 min of incubation, the supernatants were removed. Gel plugs were dehydrated by treating them twice with 100 μ L acetonitrile for 5 min. Residual acetonitrile was removed by evaporation for 5 min. Sequence-dependent in-gel proteolysis was performed overnight at 37°C under humid conditions using 100 ng trypsin (Sequencing grade, Promega) per gel plug in 10 μ L 1 mM ammonium bicarbonate buffer.

An alternative accelerated protocol was used for the protein identification using the ABI 4700 mass spectrometer (see 2.1.8.2). Excised protein spots (gel plugs) were washed twice in 100 μ L HPLC-grade water for 10 min at RT. Colloidal Coomassie stained gel plugs were destained by incubating three times in 100 μ L 40% (v/v) acetonitrile for 15 min at RT. Gel plugs were dried for 30 min at RT. Sequence-dependent in-gel proteolysis was performed overnight at 37°C under humid conditions using 100 ng trypsin (Sequencing grade, Promega, Mannheim, Germany) per gel plug in 10 μ L 1 mM Tris buffer.

2.1.8.2 Maldi-TOF mass spectrometry

Resulting peptides were evaluated using mass spectrometers (MALDI/TOF Reflectron, Waters, Eschborn, Germany; Bruker Reflex III, Bruker Daltonics, Bremen, Germany; ABI 4700 Proteomics Analyzer, Applied Biosystems, Foster City, CA, USA) with time-of-flight (TOF) analyzers and the matrix-assisted laser desorption ionization (Maldi) technique for ionization of peptides.

For analyses using the MALDI/TOF Reflectron (Waters), peptides were spotted onto a steal target plate using the thinlayer method with α -cyano-4-hydroxycinnamic acid (HCCA) as matrix (10 mg/mL HCCA, 5 mg/mL nitrocellulose, 20% (v/v) isopropanol, 80% (v/v) acetone) (Shevchenko et al., 1996). Tryptic peptides of alcohol dehydrogenase (ADH, Sigma; 968.48, 1013.60, 1136.57, 1251.67, 1386.74, 1618.84, 2019.07, 2312.15, 2465.20, 2700.39 Da) were used as external standards and ACTH peptide (adenocorticotropic hormone clip 18-39, 2465.20 Da; Sigma) as internal standard. 1.0 μ L matrix per well was spotted onto the target. After crystallization 0.5 μ L ACTH solution (0.5 pmol) and 1.0 μ L tryptic peptides were pipetted per well. After drying, the plate was inserted into the mass spectrometer. Raw spectra were acquired using the MassLynx V.3.5 software (Waters) with the following settings: (i) mass range: 800 to 3000 Da, (ii) laser firing rate: 5 Hz, (iii) shots per spectrum: 10, (iv) ionization mode: LDI+, and (v) laser energy: 30 to 80% (depending on the quality of the laser). Processing of data (MassLynx V.3.5) was done as follows: (i) centering: min peak width at half height (channels): 4, centroid top: 75%, (ii) smoothing: Savitzky Golay algorithm, smooth window (channels): ± 3 , number of smooths: 2, (iii) background subtraction: polynomial order: 15, below curve: 30%, (iv) de-isotoping: tresh: 1, and (v) combining of single spectra.

For analyses using the Bruker Reflex III (Bruker), peptides were spotted onto a 400 μ m anchor steal target plate using the dried droplet method as spotting method with 2,5-dihydroxybenzoic acid (Sigma) (20 mg/mL in 20% (v/v) acetonitrile, 0.1% (v/v) trifluoroacetic acid (TFA)) and 2-hydroxy-5-methoxybenzoic acid (Fluka) (20 mg/mL in 20% (v/v) acetonitrile, 0.1% (v/v) TFA) in a 9:1 ratio (v/v) as matrix (Shevchenko et al., 1996). As external standards angiotensin-2-acetate (1046.54 Da), substance P (1347.74 Da), bombesin (1619.82 Da), and ACTH 18-39 (2465.20 Da) were used. 0.5 μ L matrix and 0.5 μ L standard solution or 0.5 μ L peptide solution, respectively, were spotted onto the target and mixed. After evaporation and co-crystalization the target was inserted into the mass spectrometer. Raw spectra were obtained in the positive ion reflector mode and were processed and analyzed using the Bruker-Daltonik X-ToF 5.1.0 software. 400 single spectra

were combined for each sample; combined spectra were then smoothed and background was subtracted (default settings). All monoisotopic peaks in the spectra were assigned manually using the centroidic peak picking mode. Mass spectra were internally calibrated referring to autoproteolytic trypsin fragments of 1045.56 and 2211.10 Da.

For analyses using the MALDI-TOF/TOF tandem mass spectrometer (ABI 4700 Proteomics Analyzer) peptides were spotted onto a target plate using the dried droplet method with α -cyano-4-hydroxycinnamic acid (HCCA) as matrix (2.5 mg/mL HCCA, 70% (v/v) acetonitrile, 0.1% (v/v) TFA) as matrix. As external standards angiotensin-2-acetate (1046.54 Da), substance P (1347.74 Da), bombesin (1619.82 Da), and ACTH 18-39 (2465.20 Da) were used. 0.5 μ L matrix and 0.5 μ L standard solution or 0.5 μ L peptide solution, respectively, were spotted onto the target and mixed. After evaporation and co-crystallization the target was inserted into the mass spectrometer. Raw spectra were obtained in the positive ion reflector mode with 2500 laser shots and were averaged and processed by GPS Explorer 2.0 software (Applied Biosystems). No smoothing or background subtraction was applied to the averaged MS spectra. Monoisotopic peak masses were automatically determined within the mass range 800-4000 Da with a signal to noise ratio minimum set to 5 and the local noise window width m/z 200. Up to seven of the most intense ion signals with signal to noise ratio above 30 were selected as precursors for MS/MS acquisition excluding common trypsin autolysis peaks and matrix ion signals. In MS/MS positive ion mode 4000 spectra were averaged; collision energy was 1 kV, collision gas air was at a pressure of 1.6×10^{-6} torr and default calibration was set. Monoisotopic peak masses were automatically determined with a signal to noise ratio minimum set to 10 and the local noise window width m/z 200.

2.1.8.3 Peptide mass finger printing (PMF) and database searching

Trypsin cleaves proteins specifically at the C-terminus of lysine and arginine residues, generating a fingerprint of peptide masses (PMF) that can be located on database searches.

Database searches from data acquired with the MALDI/TOF Reflectron were done in SwissProt (release October 2002) using the ProteinLynx Globalserver V.1.1 software (PLGS, Waters) with the following parameters: (i) trypsin cleavage, (ii) organisms: unrestricted, (iii) fixed modifications: carbamidomethyl, (iv) variable modifications: oxidations, (v) mass values: monoisotopic, (vi) protein mass: unrestricted, (vii) peptide mass tolerance: ± 150 ppm, (viii) peptide charge state: 1+, and (ix) maximum number of missed cleavages: 1. Protein identification was considered successful if four of the following five criteria were met: (i)

sequence coverage $\geq 20\%$, (ii) PLGS 1.1 score ≥ 10 , (iii) difference of PLGS 1.1 score of the most likely to the next likely protein hit out of the correct organism (*i.e.*, *S. cerevisiae*) ≥ 5 , (iv) consistent isoelectric point and (v) molecular mass.

Database searches from data acquired with the Bruker Reflex III were done in the metadatabase MSDB (release 20030429: 1165316 sequences and 37026491 residues, thereof eukaryotes 548831 sequences) using the Mascot 1.7 search engine (Matrix Science, London, UK) with the following parameters: (i) trypsin cleavage, (ii) organisms: eukarya sequences, (iii) fixed modifications: carbamidomethyl, (iv) variable modifications: oxidations, (v) mass values: monoisotopic, (vi) protein mass: unrestricted, (vii) peptide mass tolerance: ± 200 ppm, (viii) peptide charge state: 1+, and (ix) maximum number of missed cleavages: 1. Protein identification was considered successful if the following criteria were met: (i) Mowse scores ≥ 70 , (ii) sequence coverage $\geq 20\%$, (iii) consistent molecular weight, and (iv) the matched peptide masses were abundant in the spectrum. The probability based Mowse score (Pappin, 1997; Perkins et al., 1999) was significant for values greater than 70 ($p < 0.05$).

Database searches from data acquired with the ABI 4700 Proteomics Analyzer were done in the SwissProt database (release 20051206; 201594 sequences and 73123101 residues) with combined PMF and MS/MS queries using the Mascot 1.9 search engine (Pappin, 1997; Perkins et al., 1999) embedded in GPS-Explorer 2.0 software. The following parameter settings were used: (i) trypsin cleavage, (ii) organisms: all entries, (iii) fixed modifications: carbamidomethyl, (iv) variable modifications: oxidations, (v) mass values: monoisotopic, (vi) protein mass: unrestricted, (vii) peptide mass tolerance: ± 65 ppm, (viii) peptide charge state: 1+, (ix) maximum number of missed cleavages: 1, and (x) MS/MS fragment tolerance: 0.3 Da. A protein was regarded as identified, if the following criteria are met: (i) Mowse scores ≥ 66 , (ii) consistent molecular weight, and (iii) the matched peptide masses were abundant in the spectrum. The probability based Mowse score (Pappin, 1997; Perkins et al., 1999) was significant for values greater than 66 ($p < 0.05$).

2.2 Molecular biology

2.2.1 *E. coli* cultures

2.2.1.1 Liquid cultures

LB medium (Luria-Bertani; 1% (w/v) tryptone, 0.5% (w/v) yeast extract, 1% (w/v) sodium chloride, pH adjusted to 7.0 with 5 M sodium hydroxide solution) supplemented with the appropriate antibiotics (*e.g.*, ampicillin, kanamycin, chloramphenicol; see 1.4.6, Table 4) was inoculated either with an *E. coli* colony grown on LB plates or with small amounts of an *E. coli* cryo culture. Cultures were grown overnight at 37°C under shaking with 130 rpm in baffled flasks or with 225 rpm in 14 mL Falcon tubes.

2.2.1.2 Plating cultures

Plating cultures were streaked out from cryo cultures onto LB plates (LB medium with 1.5 (w/v) agar supplemented with the appropriate antibiotics; see 2.2.1.1). Plates were incubated overnight at 37°C and could then be stored at 4°C for several days.

2.2.1.3 Cryo cultures

Cryo cultures were obtained by mixing 500 µL of an overnight *E. coli* culture with 500 µL 80% (v/v) glycerol. Cryo cultures could be stored at -80°C for several years.

2.2.1.4 Generation of chemically competent *E. coli*

E. coli competent for chemical transformation according to the rubidium chloride (RbCl₂) method were generated from the *E. coli* strains DH10B (Invitrogen) and TOP10 (Invitrogen). DH10B and TOP10 cryo cultures were streaked out on LB plates without antibiotics and incubated overnight at 37°C. A single colony was expanded in 2.5 mL LB medium overnight at 37°C in a 14 mL Falcon tube under shaking with 225 rpm. The overnight culture was diluted 1:100 in LB medium supplemented with 20 mM MgSO₄. The culture was grown to an optical density (OD₆₀₀) of 0.4 to 0.6 (usually 2-3 h) and centrifuged (5 min, 10000 g, 4°C). The cell pellet was then gently resuspended in 100 mL ice-cold TFB1 buffer (30 mM potassium acetate, 100 mM rubidium chloride, 10 mM calcium chloride, 50 mM manganese chloride, 15% (v/v) glycerol, pH was adjusted to 5.8 with acetic acid) and incubated on ice for 5 min. The suspension was centrifuged (5 min, 10000 g, 4°C), and the cell pellet was gently resuspended in 10 mL TFB2 buffer (10 mM MOPS [3-(*N*-morpholino)propanesulfonic acid], 75 mM calcium chloride, 10 mM rubidium chloride, 15% (v/v) glycerol, pH was adjusted to 6.5 with potassium hydroxide solution). The

suspension was incubated on ice for 15 to 60 min and subsequently portioned in 100 μ L aliquots. The tubes were then shock frozen with liquid nitrogen and stored at -80°C prior use for transformation (see 2.2.2).

2.2.2 Chemical transformation of *E. coli*

Chemically competent *E. coli* were thawed on ice. 10 ng plasmid DNA (see 2.2.3) or 5 μ L ligation reaction (see 2.2.8) were added to a 50 μ L aliquot of competent *E. coli*, mixed and incubated for 30 to 60 min on ice. The *E. coli* were treated with a heat shock at 42°C for 45 sec and subsequently cooled down on ice for 2 min. The heat shock initiated the incorporation of DNA-salt complexes into the bacteria. 450 μ L SOC medium without antibiotics (2% (w/v) tryptone, 0.5% (w/v) yeast extract, 0.05% (w/v) sodium chloride, 20 mM glucose) were added and the *E. coli* were grown for 1 h at 37°C under shaking with 225 rpm. *E. coli* were sedimented (1 min, 16000 g, RT), and 400 μ L of the supernatant were discarded. The pellet was resuspended in the remaining supernatant and plated onto a LB plate supplemented with the appropriate antibiotics (see 2.2.1.2). The LB plate was incubated overnight at 37°C . Single colonies were expanded in LB medium supplemented with the appropriate antibiotic (see 2.2.1.1). Cultures were subsequently used for plasmid DNA preparation (see 2.2.3) and cryo cultures (see 2.2.1.3).

2.2.3 Plasmid DNA preparation

Single transformed *E. coli* colonies (see 2.2.2) were expanded in LB medium supplemented with the appropriate antibiotic (see 2.2.1.1). When applying the QIAprep Spin Plasmid Miniprep Kit (Qiagen), 2-5 mL of an overnight culture were sedimented (10 min, 10000 g, RT) and the pellets were used for plasmid DNA preparation according to manufacturer's protocol. For preparative purposes applying the PureYield Plasmid Midiprep System (Promega), 50-200 mL of an overnight culture were sedimented (10 min, 10000 g, RT) and the pellets were used for preparation of plasmid DNA as described in the manufacturer's protocol. Both kits (QIAprep Spin Plasmid Miniprep Kit and Promega Midi Kit) are based on the alkaline lysis of *E. coli* and on subsequent binding of plasmid DNA to DNA-binding columns. In both cases, plasmid DNA was eluted with hot ddH₂O (60°C , 50 μ L and 600 μ L, respectively). The concentration and purity of plasmid DNA preparations was determined photometrically. 200 μ L of a 1:100 to 1:200 dilution of plasmid DNA in ddH₂O were pipetted into a quartz cuvette and the absorption at 260 and 280 nm was measured with an Ultraspec 3300 pro photometer (GE Healthcare). A 260 nm/280 nm absorption ratio of 1.8

indicated a pure DNA preparation. DNA concentration was determined as follows: DNA concentration [$\mu\text{g/mL}$] = absorption at 260 nm x 50 x dilution factor.

2.2.4 DNA sequencing

DNA sequencing was performed in a capillary-based automated sequencer (ABI Prism 3100 Genetic Analyser, Applied Biosystems), after a cycle-sequence reaction using the BigDye-Terminator v3.1 Cycle Sequencing Kit (Applied Biosystems). Here, the DNA template is amplified linearly by a DNA polymerase using a sequence-specific primer (Zimmermann, 2006). The dNTP mixture is supplemented with dideoxynucleotides (ddNTPs) tagged with four different fluorescence labels referring to the four different bases (A, T, G, C). Upon incorporation of a ddNTP, the extension of the DNA stretch is prohibited, resulting in a DNA fragment with a certain length labeled with a base-specific fluorescence tag. The mixture of labeled DNA fragments generated during the cycle process were separated according to their length using capillary electrophoresis and analyzed for their tag. From these data the DNA sequence can be delineated. 200 ng of plasmid-DNA template were mixed with 2 μL BigDye Terminator Mix containing the DNA polymerase and the fluorescence-labeled dideoxynucleotides, 0.5 μL primer (10 pmol/ μL) and ddH₂O up to an end volume of 10 μL . Oligonucleotides used as primer for sequencing should have a melting temperature of about 50°C (see 1.4.5, Table 3). The PCR DNA Engine Tetrad Gradient Cycler PTC-225 (MJ Research, Bio-Rad) was used with the following cycling program with 30 cycles from step 2 to 4:

1. 96°C 2 min for first denaturation of the double-stranded DNA template
2. 96°C 30 sec for denaturation of the DNA template
3. 50°C 15 sec for annealing of the primer to the DNA template
4. 60°C 4 min for elongation of the primer catalyzed by the polymerase
5. 60°C 4 min for final elongation

After the cycle-sequence reaction, the DNA was precipitated by adding 8 μL HPLC-grade H₂O and 32 μL 95% (v/v) ethanol (p.A.). After 15 min incubation at RT in the dark, the reaction mixtures were centrifuged (15 min, 16000 g, RT). The DNA pellet was then washed in 200 μL 70% (v/v) ethanol in HPLC-grade H₂O and centrifuged (10 min, 16000 g, RT). The DNA pellet was dried at RT in a speed vac (SpeedVac SPD111V, Savant, Fisher Scientific) for 3 min and was dissolved in 75 μL HPLC-grade H₂O. 25 μL of dissolved DNA were transferred onto a microtiter plate, which was placed into the automated sequencer. The

resulting data were analyzed using ContigExpress in the Vector NTI Suite 9.0 software package (Invitrogen).

2.2.5 Agarose gel electrophoresis

DNA fragments were separated, identified and purified by agarose gel electrophoresis. 1% (w/v) DNA agarose (Biozym, Oldendorf, Germany) in TAE buffer (40 mM Tris-acetate, 1 mM ethylenediaminetetraacetate (EDTA), pH 8) was dissolved by boiling in a microwave. The agarose solution supplemented with 0.5 µg/mL of the fluorescent DNA-intercalating ethidium bromide was poured into the gel trays (gel trays for SubCell GT chambers, Bio-Rad) and the combs were inserted. After solidification of the gels, combs were removed and the trays were put into the electrophoresis chamber (SubCell GT chambers, Bio-Rad) and gels were overlaid with TAE buffer. DNA samples were treated with gel loading buffer (6x: 0.25% (w/v) bromophenol blue, 40% (w/v) sucrose) and loaded onto the gel. Electrophoresis was performed with 50-100 V until the bromophenol blue dye front reached the end of the gel. DNA fragments were visualized by an UV transilluminator (Herolab). To determine the size of the DNA fragments a 1 kb and a 100 bp DNA standard (New England Biolabs) were used. For purification, DNA fragments were excised with a scalpel and eluted from the gel plugs by the QIAquick Gel Extraction Kit (Qiagen) according to the manufacturer's protocol.

2.2.6 Polymerase chain reaction (PCR)

PCR was essentially done essentially according to a standard procedure (Saiki et al., 1988). Here, the DNA template is amplified exponentially by a DNA polymerase using two sequence specific primer that bind to the sense and antisense strand of the DNA template, respectively. Oligonucleotides used as primer are described in 1.4.5 (Tables 1 and 3). The reaction mixture (20 µL) contained 20-50 ng cDNA template, 1x PCR buffer (incl. ammonium sulfate, w/o MgCl₂; New England Biolabs), 1.5 mM MgCl₂, 200 µM dNTPs, 0.5 µM sense and 0.5 µM antisense oligonucleotide primer and 5 U Taq DNA polymerase (New England Biolabs) in ddH₂O. PCR reaction was performed in a thermal cycler (PCR DNA Engine Tetrad Gradient Cycler PTC-225, MJ Research, Bio-Rad) with the following amplification program:

1. 96°C 1 min for first denaturation of the double-stranded DNA template
2. 96°C 30 sec for denaturation of the DNA template
3. (*)°C 30 sec for annealing of the primer to the DNA template
4. 72°C (**) sec for elongation of the primer catalyzed by the polymerase

5. 72°C 5 min for final elongation

The amplification stage comprised 30 cycles from step 2 to 4. The annealing temperature (*) was set as the mean value of the melting temperatures of sense and antisense primer (see 1.4.5, Table 1). Sense and antisense primer were designed with the Vector NTI Suite 9.0 software so that (i) the melting temperatures of the primer was between 50 and 65°C, (ii) the difference in the melting temperatures of the chosen primer was below 3°C and (iii) hairpin structures and dimerization were unfavorable. The time required for elongation (***) depended on the length of the desired PCR product. For Taq DNA polymerase 1 min elongation was sufficient for a 1 kb PCR fragment.

2.2.7 DNA restriction

Empty plasmid vectors (3 µg), cDNA-containing plasmid vectors (3 µg) and purified cDNA PCR amplicates (200 to 500 ng) were digested for 2 h with 30 U of the appropriate sequence-specific restriction enzymes (New England Biolabs) in a 40 µL reaction mixture for further cloning (see 2.2.10). The manufacturer specifies the reaction buffer and the optimum temperature (usually 37°C) for the digestion. Restricted plasmid DNA was analyzed by agarose gel electrophoresis (see 2.2.5) and the fragments of interest were excised with a scalpel and were purified using the QIAquick Gel Extraction Kit (Qiagen) according to the manufacturer's protocol. Restricted cDNA PCR amplicates were purified using the QIAquick PCR Purification Kit (Qiagen) according to the manufacturer's protocol.

2.2.8 DNA ligation

Purified restricted DNA insert (about 30 fmol, see 2.2.7) and purified restricted plasmid vector (about 30 fmol, *i.e.*, 100 ng, see 2.2.7), treated with the same pair of restriction enzymes, were ligated overnight at 16°C in a 10 µL ligation reaction containing 0.5 µL T4 DNA ligase (400 U/µL, MBI Fermentas) and 1 µL 10x T4 DNA ligase buffer (MBI Fermentas) in ddH₂O. 5 µL of the ligation reaction was transformed into competent *E. coli* (see 2.2.2). As negative control (vector control), 5 µL of a ligation reaction lacking the insert were transformed. For best results, for each ligation several ratios of insert to vector were used.

2.2.9 TOPO cloning

TOPO cloning was done using the TOPO TA Cloning Kit (Invitrogen). This kit allows the incorporation of PCR fragments containing A-overhangs (provided by the Taq DNA

polymerase) into the pCR2.1-TOPO plasmid vector via recombination. 4 μ L of agarose gel-purified PCR amplicate (see 2.2.6 and 2.2.5) were equilibrated with 1 μ L TOPO salt solution and 1 μ L TOPO vector solution for 30 min at 37°C. 3 μ L of the reaction mixture were then transformed (see 2.2.2) into 50 μ L OneShot TOP10 competent cells. 40 μ L of a 40 mg/mL X-gal (5-bromo-4-chloro-3-indoyl- β -D-galactopyranoside) solution in dimethylformamide were spread on LB plates containing 50 μ g/mL kanamycin, and cells were then plated and grown overnight at 37°C. White but not blue colonies incorporated the PCR fragment resulting in the disruption of β -galactosidase reporter gene in the pCR2.1-TOPO vector. Plasmid DNA was isolated from white colonies expanded in LB medium supplemented with 100 μ g/mL ampicillin (see 2.2.3) and validated by DNA sequencing (see 2.2.4). The pCR2.1-TOPO-cDNA was then used for further cloning (see 2.2.10).

2.2.10 DNA cloning

2.2.10.1 Subcloning

cDNA of interest was subcloned from one plasmid vector into another as follows: cDNA of interest was excised by DNA restriction (see 2.2.7). The target vector was treated with the same restriction enzymes (see 2.2.7). Both cDNA fragment and target vector were purified by agarose gel electrophoresis (see 2.2.5). cDNA fragment and target vector were then ligated (see 2.2.8) and transformed into *E. coli* (see 2.2.2). Plasmid DNA was isolated (see 2.2.3) and constructs were validated by restriction analysis (see 2.2.7) and DNA sequencing (see 2.2.4).

2.2.10.2 PCR-based cloning

If the cDNA of interest could not be subcloned directly from one plasmid into another due to lack of appropriate DNA restriction sites, the cDNA was amplified by PCR (see 2.2.6) using primer with overhangs containing appropriate restriction sites (see 1.4.5, Table 1). The PCR amplicates were purified by agarose gel electrophoresis (see 2.2.5), treated with restriction enzymes (see 2.2.7) and purified with QIAquick PCR Purification Kit (Qiagen) (see 2.2.7). Subsequent ligation, transformation, plasmid DNA isolation and validation was done as described in 2.2.10.1.

2.2.10.3 TOPO-based cloning

TOPO-based cloning was performed if direct PCR-based cloning (see 2.2.10.2) was not successful. The PCR amplicate (see 2.2.10.2) was incorporated into the pCR2.1-TOPO

vector (see 2.2.9). The cDNA was then validated by DNA sequencing (see 2.2.4) and subsequently subcloned into the target vector as described in 2.2.10.1.

2.2.11 Site-directed mutagenesis

Point-mutated VCP constructs (VCP-R155H, VCP-S555G, VCP-K524A) were generated from the wild-type construct by site-directed mutagenesis using the QuikChange II Site-Directed Mutagenesis Kit (Stratagene). Mutagenesis primer pairs (see 1.4.5, Table 2) were designed considering the manufacturer's recommendations with a melting temperature of $> 78^{\circ}\text{C}$. Both primer (sense and antisense) comprised the nucleotide exchange. The whole plasmid was amplified by PCR with the *PfuUltra* High-Fidelity DNA polymerase, resulting in amplified plasmid harboring the mutation of interest. 10 ng cDNA template were used for a 50 μL reaction mixture containing 5 μL 10x reaction buffer, 125 ng oligonucleotide primer #1, 125 ng oligonucleotide primer #2, 1 μL dNTP mix and 1 μL *PfuUltra* High-Fidelity DNA polymerase (2.5 U/ μL) in ddH₂O. PCR reaction was performed in a thermal cycler (PCR DNA Engine Tetrad Gradient Cycler PTC-225, MJ Research, Bio-Rad) with the following settings:

1. 95°C 30 sec for first denaturation of the double-stranded DNA template
2. 95°C 30 sec for denaturation of the DNA template
3. 55°C 1 min for annealing of the primer to the DNA template
4. 68°C 1 min/kb of plasmid length for elongation
5. 68°C 5 min for final elongation

The amplification stage comprised from step 2 to 4 12 and 16 cycles for point mutations and dinucleotide mutations, respectively. The non-mutated methylated DNA template was selectively degraded by *DpnI* endonuclease by adding 1 μL *DpnI* (10 U/ μL) per reaction mixture and incubation at 37°C for 1 h. The non-methylated amplified mutation-harboring plasmid was then transformed (see 2.2.2) into XL1-Blue Supercompetent Cells by using 1 μL of *DpnI* treated DNA to 50 μL competent cells. Plasmid DNA was isolated from the transformed colonies (see 2.2.3) and validated by DNA sequencing (see 2.2.4).

2.2.12 Generation of VCP constructs

Three full-length VCP cDNA clones (in pOTB7 library vector) were ordered from the German Resource Center for Genome Research (RZPD, Berlin, Germany). VCP cDNA sequence was verified by sequencing (see 2.2.4) and resulted in the identification of a mutation in the 3' side of VCP cDNA in the clones A and B (IRALp962J231Q2 and

IRALp962O029Q2, respectively), whereas the 5' side of VCP was missing in the clone C (IRALp962D0522Q2). In order to obtain a full-length VCP clone, the 5' side of VCP in clone B was subcloned into the clone C using the internal *EcoRI* restriction site and the *EcoRI* restriction site of the 5' multiple cloning site of the pOTB7 vector, replacing the 5' fragment of VCP in clone C (see 2.2.10.1). The resulting complete VCP cDNA in the pOTB7 library vector was used as template for PCR-based cloning.

The complete VCP cDNA was amplified using primers with overhangs containing appropriate restriction sites for cloning into the pcDNA3 vector (Invitrogen) suitable for expression in mammalian cell cultures (see 2.2.10.2). The forward primer contained the restriction site *BamHI* and the Kozak sequence GCCACCATGG to ensure optimal expression of VCP. The reversed primer contained the restriction site *NotI* and the stop codon was omitted to allow C-terminal tagging of VCP for future studies (see below). Direct subcloning of the PCR fragment (*BamHI*-Kozak-VCP-NoStop-*NotI*) into the pcDNA3 vector was not successful. Therefore, a TOPO-based cloning approach (see 2.2.10.3) was performed. The PCR fragment (2.4 kb) should be incorporated by topoisomerases into the pCR2.1-TOPO vector (Invitrogen), sequenced (see 2.2.4) to check for completeness of the cDNA and correct restriction sites and subsequently subcloned (see 2.2.10.1) into the pcDNA3 vector. Since the TOPO reaction failed to incorporate the complete PCR fragment, a TOPO-based cloning approach (see 2.2.10.3) with smaller PCR fragments was performed. The 5' VCP cDNA (1.1 kb) was amplified with the forward primer containing the restriction site *BamHI* and the Kozak sequence and a reversed primer that specifically binds 3' of the internal *EcoRI* restriction site of the VCP cDNA. The 3' VCP cDNA (1.3 kb) was amplified with a forward primer that specifically binds 5' of the internal *EcoRI* restriction site of the VCP cDNA and the reversed primer containing the *NotI* restriction site and omitting the stop codon. Both PCR fragments were successfully incorporated into the pCR2.1-TOPO vector. The 5' PCR fragment (*BamHI*-Kozak-VCP-*EcoRI*) was subcloned (see 2.2.10.1) with the restriction sites *BamHI* and *EcoRI* into a proprietary pcDNA3 vector containing an in-frame stop codon 3' of the *NotI* restriction site (kindly provided by C. J. Gloeckner, GSF, Munich-Neuherberg). The 3' PCR fragment (*EcoRI*-VCP-NoStop-*NotI*) was subsequently subcloned (see 2.2.10.1) with the restriction sites *EcoRI* and *NotI* into the pcDNA3 vector containing the 5' PCR fragment. The pcDNA3 vector containing the complete VCP cDNA (in which the stop codon was moved 3' of the *NotI* restriction site leading to additional three alanine-coding codons) was evaluated by sequencing (see 2.2.4), resulting in a single base substitution in the VCP cDNA that was removed by site-directed mutagenesis (see 2.2.11).

The K524A, S555G and R155H variants of VCP were generated from the pcDNA3-VCP-WT construct by site-directed mutagenesis (see 2.2.11). The constructs were verified by sequencing (see 2.2.4). The VCP wild-type and its variants (pcDNA3-WT, K524A, S555G, R155H) could efficiently be expressed in mammalian cell culture (HEK293, see 2.4.2). VCP wild-type and its variants were then subcloned into the pcDNA3-Strep-GFP vector (kindly provided by C. J. Gloeckner), in order to obtain C-terminal GFP-tagged VCP for fluorescence microscopy.

2.3 Analysis of yeast cultures

2.3.1 Yeast culture

2.3.1.1 Liquid cultures

S. cerevisiae wild-type strain KFY417 and mutant strain KFY437 (Madeo et al., 1997) (see 1.5.3.1, Table 6) were used in all experiments, where the genomic *CDC48* gene is disrupted and replaced by *CDC48* wild-type or a *cdc48*^{S565G} mutation, under control of a (leaky) *GALI* promoter on a YEp52 plasmid. Since *CDC48* is essential for cellular function, selection for maintenance of the Yep52 plasmid was not necessary. Yeast cultures were inoculated from plating cultures and were either grown in YPGal (1% (w/v) yeast extract, 2% (w/v) bacto peptone, Difco, Otto Nordwald, Germany, 4% (w/v) galactose) medium (high expression of *CDC48* and *cdc48*^{S565G}, respectively) or in YPGlc (1% (w/v) yeast extract, 2% (w/v) bacto peptone, 4% (w/v) glucose) medium (residual expression of *CDC48* and *cdc48*^{S565G}, respectively) at 28°C under shaking with 130 rpm in baffled flasks if not otherwise stated.

2.3.1.2 Plating cultures

Plating cultures (KFY417 and KFY437, respectively) were streaked out from cryo cultures onto YPGal plates (1% (w/v) yeast extract, 2% (w/v) bacto peptone, 4% (w/v) galactose, 1.5% (w/v) agar). Plates were incubated at RT until colonies were formed and could then be stored at 4°C for up to three months.

2.3.1.3 Cryo cultures

Cryo cultures were obtained by mixing 500 µL of a stationary overnight culture with 500 µL 50% (v/v) glycerol. Cryo cultures could be stored for years at -80°C.

2.3.1.4 Determination of cell density

Cell density of yeast cultures was determined by the measurement of the optical density at 600 nm (OD₆₀₀) with medium used as blank. Absolute cell density of yeast cultures (in number of cells per mL culture) was determined using a Malassez chamber. Here, a 20 µL aliquot of the culture in an appropriate dilution was pipetted into the chamber and the number of yeast cells was counted in the different squares. Cell density of the original culture (in cells per mL) was calculated as follows: average number of cells per square x dilution factor x 10⁵.

2.3.2 Generation of ρ^0 strains

ρ^0 strains (yeast strains lacking functional mitochondria due to loss of mitochondrial DNA) were generated from the respective ρ^+ strains (KFY417, KFY437) by growing and inoculating cells in YPGlc media containing 10 $\mu\text{g}/\text{mL}$ ethidium bromide for three days. The resulting respiratory deficiency was confirmed by complete lack of growth on obligatory respiratory media (glycerol).

2.3.3 Culture conditions for the induction of apoptosis

Cells (*CDC48* wild-type: KFY417 and *cdc48*^{S565G} mutant: KFY437) were grown at least 36 h at 28°C in baffled flasks on YPGal, and were referred to as ‘galactose pre-cultures’. As cells reached a density of 1.5 (OD_{600}), they were sedimented and washed twice in YPGlc in order to remove galactose quantitatively. Following resuspension, YPGlc cultures were inoculated at a ratio of 1:3 wild-type (KFY417, $\text{OD}_{600} = 0.1$) to mutant (KFY437, $\text{OD}_{600} = 0.3$), in order to ensure comparable cell density at harvesting. For induction of apoptosis, cells were either grown for 12 h at 28°C in baffled flasks with 130 rpm and harvested after an additional hour of heat shock at 37°C (total 13 h, early apoptotic growth conditions) or grown for 16 h and then stressed by four additional hours of heat shock (total 20 h, late apoptotic growth conditions).

In ρ^0/ρ^+ experiments, cells were grown and treated as described for KFY417 and KFY437 with the modification that pre-cultures were grown in YPGal/Glc (1% (w/v) yeast extract, 2% (w/v) bacto peptone, 3% (w/v) galactose, 1% (w/v) glucose), since the generated ρ^0 strains were unable to grow in YPGal.

2.3.4 Viability of yeast cultures

2.3.4.1 Survival plating assay

Viability of yeast cultures (KFY417 and KFY437) was quantified using a survival plating assay (Madeo et al., 2002b). 1000 cells of each strain and condition were plated onto YPGal plates. After three days incubation at RT, the numbers of colonies (colony forming units, CFU) were determined. CFU was a measure of viability of the respective plated culture. Three plates were evaluated per culture and experiment. In ρ^0/ρ^+ experiments, 500 cells of each strain and condition were plated on YPGlc plates that were treated and evaluated as described above.

2.3.4.2 Differential plating assay

For analysis of respiratory deficiency, YPGal pre-cultures and YPGlc cultures (13 and 20 h) of both wild-type and mutant strains were plated on YP plates (1% (w/v) yeast extract, 2% (w/v) bacto peptone, 1.5% (w/v) agar) containing (i) 4% (w/v) glucose (YPGlc, fermentative selective medium) or (ii) 2% (w/v) lactate (YPLac, respiratory selective medium) or (iii) 4% (w/v) galactose (YPGal, viability control medium). Cultures were spotted on agar plates in dilution series (from 5×10^6 cells to 50 cells in tenfold dilution steps) clockwise on six distinct sections. After 5 days of incubation at RT, the sections were evaluated for growth.

2.3.5 Test for apoptosis

2.3.5.1 TUNEL Assay

The T4 terminal deoxynucleotidyl transferase-mediated dUTP nick end labeling (TUNEL) assay was used to visualize DNA fragmentation, a late marker of apoptosis. DNA fragmentation leads to free 3'-OH groups that are recognized by the enzyme T4 terminal deoxynucleotidyl transferase, which attaches fluorescence-labeled dUTPs, resulting in fluorescence-labeled DNA fragments in the nuclei.

Yeast cultures were sedimented in Eppendorf cups (1 min, 5000 g, RT) to obtain a pellet with 2-3 mm in diameter. Cells were washed in 500 μ L fixation buffer (35 mM KPB pH 6.8, 0.5 mM $MgCl_2$) and sedimented (1 min, 5000 g, RT). Cells were resuspended in 1 mL fixation buffer and fixed for 1 h at RT by adding 120 μ L 37% formaldehyde followed by 15 sec vortexing. Formaldehyde was removed by washing three times in 500 μ L digestion buffer (35 mM KPB pH 6.8, 0.5 mM $MgCl_2$, 1.2 M sorbitol) and sedimentation (1 min, 5000 g, RT). Removal of cell wall was done with 20 U lyticase (Sigma) for 2 h at 30°C in 330 μ L digestion buffer. Cells were gently sedimented (3 min, 1000 g, RT), washed in 500 μ L digestion buffer, resuspended in 30 μ L digestion buffer and 15 μ L were pipetted onto gelatinized slides (Superfrost slides (VWR) were dipped in a warm solution containing 0.5% (w/v) gelatine and 0.05% (w/v) chromic potassium sulfate and subsequently dried overnight at 37°C). Slides could be stored at 4°C until further use.

TUNEL reaction was performed using the *in situ* cell death detection kit (Roche Applied Sciences) and Chromatide Bodipy™ (Molecular Probes, Invitrogen) as fluorescence-labeled dUTP. Cells on the slides were washed twice with 50 μ L PBS per sample in order to remove sorbitol. Slides were put onto ice and 50 μ L ice-cold permeabilization solution (0.1 % Triton X-100, 0.1% (w/v) sodium citrate, freshly prepared) was added per sample for 2 min.

After removal of permabilization solution, cells were washed twice with 50 μ L PBS at RT. TUNEL reaction was induced by adding 30 μ L TUNEL reaction mix (enzyme solution (Roche) and Chromatide BodipyTM FL-dUTP (Molecular Probes) diluted 1:10 and 1:100 with label solution (Roche), respectively) per sample. Slides were incubated for 1 h at 37°C under humidified conditions. Slides were then washed six times with 50 μ L PBST per sample. Cells were embedded in one droplet FluorSave (Calbiochem, VWR) and slides were stored at 4°C overnight. Images were obtained by fluorescence microscopy using a fluorescein isothiocyanate (FITC) and Nomarski optical filter sets (40x/0.75, Axioskop 2, AxioCam HRc, AxioVision 4, Zeiss, Göttingen, Germany) and adjusted using the AxioVision 4 software package. The percentage of cells showing stained nuclei (TUNEL positive cells) to all cells was determined. As positive control, cells were treated with 30 μ L *DNaseI* (1 mg/mL *DNaseI* in DMEM/0.1 (w/v) BSA) prior the TUNEL reaction. As negative control, TUNEL reaction was performed without T4 terminal deoxynucleotidyl transferase.

2.3.5.2 Staining of reactive oxygen species (ROS) in yeast cells

Cellular ROS were detected with dihydrorhodamine 123 (DHR 123, Sigma) according to Madeo et al. (1999). DHR 123 is oxidized by cellular ROS to the red fluorescence dye rhodamine. Cells were stained for 30 min at 30°C by adding DHR 123 from a 2.5 mg/mL stock solution in ethanol to a final concentration of 5 μ g/mL to the yeast cultures. Cells were washed in PBS and embedded in pre-warmed (37°C) 0.5% (w/v) agarose in PBS. Images were obtained by fluorescence microscopy using rhodamine and Nomarski optical filter sets (40x/0.75, Axioskop 2, AxioCam HRc, AxioVision 4, Zeiss, Göttingen, Germany). Images were adjusted using the Min/Max function of the AxioVision 4 software package. The percentage of stained cells to all cells (red) was determined by counting at least 1000 cells per experiment.

In order to check for mitochondrial contribution to ROS production, yeast cultures were grown in the presence of inhibitors of the mitochondrial cytochrome *bc₁* complex (myxothiazol and stigmatellin, respectively, 1 μ M) at the 13 h time point (see 2.3.3) and tested for accumulation of ROS as described in the preceding paragraph.

In ρ^0/ρ^+ experiments, ROS were detected with the mitochondrial membrane potential-independent stain dihydroethidium (DHE, Sigma) according to Madeo et al. (1999). 5×10^6 cells were pelleted in 96-well microtiter plates (Microlon Fluorotrac 600, Greiner, Austria), washed twice with PBS, resuspended in 250 μ L of 2.5 μ g/mL DHE in PBS and incubated for 10 min at RT. Relative fluorescence units (RFU) were determined using a fluorescence reader

(GENios ProTM, Tecan, Grödig, Austria; excitation 515 nm, emission 595 nm, RT). As blank DHE in PBS was used. Additionally, cells were evaluated for staining by fluorescence microscopy using a rhodamine optical filter set.

2.3.5.3 *In vivo* measurement of caspase-like enzymatic activity in yeast cells

In vivo measurement of caspase-like activity by flow cytometric analysis was done according to Madeo et al. (2002b). Cells (5×10^6 cells) were harvested, washed in PBS and resuspended in 200 μ L staining solution containing FITC-VAD-FMK (CaspACETM, Promega). After incubation for 20 min at 30°C, cells were washed and resuspended in PBS. Stained cells were counted using a FACS Calibur (BD Biosciences) and Cell Quest analysis software (BD Biosciences). CaspACETM FITC-VAD-FMK *in situ* marker is a fluoroisothiocyanate (FITC) conjugate of the cell permeable caspase inhibitor VAD-FMK. This structure allows delivery of the inhibitor into the cell where it binds to activated caspase, serving as an *in situ* marker for apoptosis. The bound marker is localized by fluorescence detection.

2.3.6 *In vivo* fluorescence microscopy

For *in vivo* fluorescence labeling, cells were stained for 30 min at 30°C with MitoTrackerTM and ER-TrackerTM (Molecular Probes, Invitrogen) by adding 400 nM and 800 nM dye solution, respectively, to the yeast cultures. Cells were washed in PBS and embedded in pre-warmed (37°C) 0.5% (w/v) agarose in PBS. Images were obtained at RT by ApoTomeTM fluorescence microscopy (Zeiss, Göttingen, Germany) using Cy3 and Dapi optical filter sets (C-Apochromat 40x/1.20, optical section thickness 1 μ m, AxioCam, AxioVision 4, Zeiss) and adjusted using the AxioVision software package. The obtained images provide an axial resolution comparable to confocal microscopy (Garini et al., 2005) (for principle of ApoTome modus see 2.4.5). Cells that demonstrated both ER and mitochondrial staining were counted. The percentage of these cells showing overlap between both stainings within the optical section thickness of the image was determined. For quantification approximately 1000 cells per strain and experiment were evaluated for overlap between ER and mitochondrial staining.

2.3.7 Electron microscopy (EM)

EM analysis of yeast cells to visualize membrane structures was done essentially according to Byers (1991). Cells were harvested and incubated for 8 min in fixative (4% (w/v)

formaldehyde, 2% (v/v) glutaraldehyde, 4% (w/v) sucrose, 2 mM calcium acetate, 50 mM sodium cacodylate, pH 7.2) at RT. Cells were stored in fixative overnight at 4°C and subsequently prepared for cell wall removal by incubation in pretreatment solution (0.2 M Tris-HCl pH 9, 100 mM β -mercaptoethanol) for 10 min at RT. Removal of cell wall was done with 30 U lyticase (Sigma) and 0.6 U arylsulfatase (Roche) for 90 min at 30°C in digestion buffer (35 mM KPB pH 6.8, 0.5 mM MgCl₂, 1.2 M sorbitol). Cells were washed in cacodylate buffer (0.1 M sodium cacodylate, 5 mM CaCl₂), postfixed (0.5% osmium tetroxide, 0.8% potassium ferrocyanide), washed in distilled water, stained *en bloc* (1% aqueous uranyl acetate), dehydrated in ascending alcohol series and embedded in Araldite. The preparations were sectioned at 50 nm on an ultramicrotome (Ultratom III; LKB, Bromma, Sweden) and EM micrographs were obtained on a Zeiss EM 10 electron microscope (Oberkochen, Germany).

Ultrastructural analysis was done with the AxioVision LE V.4.2 software (Zeiss) to determine the distance between mitochondria and NE-ER membranes. A maximum distance of 100 nm was defined as high proximity between these subcellular structures. In order to quantify mitochondrial enlargement, the cellular area and the mitochondrial portion within this cellular area was determined using the AxioVision software package.

2.3.8 Preparation of cell extracts and cell fractionation

2.3.8.1 Preparation of cell extracts

Cell extracts for 2-DE were prepared as follows: Yeast cultures were harvested (5 min, 2000 g, RT), washed in dH₂O, resuspended in dH₂O and transferred into a test tube. After sedimentation (5 min, 2000 g, RT), supernatant was discarded. The same amount of glass beads was added (No. 854 179/1 Braun, Melsungen) to the cell pellet. Test tubes were incubated on ice and protease inhibitors were added in surplus (Protease Inhibitor Cocktail (PI) For Fungal and Yeast Cells, Sigma). After 4 min of vortexing, the resulting cell lysate became viscous. Ice-cold dH₂O (incl. 10 μ L/mL PI, Sigma) was added. The suspension was pipetted up and down and transferred into an Eppendorf tube. Cell lysates were separated from glass beads, intact cells and large cell remnants by centrifugation (5 min, 13000 g, 4°C), shock frozen in liquid nitrogen and stored at -80°C. Bradford assay was used to determine protein concentration (see 2.1.1).

Cell extracts for Western blot analysis were prepared as follows: Yeast cultures were harvested (5 min, 5000 g, RT), washed once in dH₂O, resuspended in dH₂O (incl. Complete Protease Inhibitor Cocktail, Roche Applied Sciences) and transferred into a mortar. Cell

suspension was shock frozen by adding liquid nitrogen. Frozen suspension was thoroughly grinded using a pistil. Suspension was transferred into an Eppendorf tube and stored at -80°C. Prior use, suspension was thawed on ice and intact cells and large cell remnants were removed by centrifugation (5 min, 16000 g, 4°C). Bradford assay was used to determine protein concentration (see 2.1.1).

2.3.8.2 Cell fractionation

Isolation of mitochondria was done according to Herrmann et al. (1994) and Rickwood et al. (1988) with minor modifications:

2.3.8.2.1 Enzymatic digestion of the yeast cell wall

Yeast cultures were harvested (5 min, 5000 g, RT), washed twice with dH₂O and the wet weight of the pellets was determined. Pellets were resuspended in 2 mL DTT buffer (10 mM DTT in 100 mM Tris-H₂SO₄ pH 9.4) per gram wet weight and incubated for 15 min at 28°C under shaking. In this step, disulfide bonds in the cell walls were reduced. Cells were washed once in 1.2 M sorbitol (5 min, 3000 g, RT), in order to remove surplus DTT. Cell pellets were resuspended in 7 mL lyticase buffer (1.2 M sorbitol, 20 mM KPB pH 7.4) per gram wet weight containing 5 mg lyticase (Sigma) or Zymolyase 20T (Seikagaku, AMS Biotechnology, Frankfurt a.M., Germany). Enzymatic digestion of cell walls was done under shaking at 28°C for 45 to 90 min for lyticase and 20 to 40 min for Zymolyase 20T depending on the density of the yeast cultures. Enzymatic digestion of stationary yeast cultures was less efficient due to rigid cell walls. Progression of cell wall digestion could be followed by adding 50 µL cell suspension into 2 mL dH₂O and measuring the OD at 578 nm. In contrast to intact yeast cells, spheroplasts (yeast cells without cell walls) lyzed under these hypoosmotic conditions, resulting in a decrease of the OD. Digestion was stopped when the OD was 20% of the OD prior to the addition of the enzyme. The cell suspension was gently centrifuged (5 min, 1000 g, 4°C) and the resultant pellet was washed once in 1.2 M sorbitol, in order to remove the lyticase/zymolyase. Spheroplasts were used to isolate mitochondria, cytosol and microsomes.

2.3.8.2.2 Isolation of mitochondria, cytosol and microsomes

Lysis of cell membranes was done under hypoosmotic conditions by resuspension of spheroplasts in 7 mL homogenization buffer (0.6 M sorbitol, 10 mM Tris-HCl pH 7.4, 5 mM EDTA, 2 mM phenylmethylsulfonylfluorid (PMSF)) per gram wet weight. Homogenization

was done using either a smooth-fitting glass pestle and a douncer with 40 strokes or a motor-driven smooth-fitting Teflon pestle and a potter with 10 strokes at 800 rpm. During homogenization, foaming of the suspension had to be avoided. Mitochondria, cytosol and microsomes were obtained from the resulting cell lysate by differential centrifugation. In a first step, intact cells, large cell remnants and nuclei were removed by centrifugation (5 min, 1700 g, 4°C). The supernatant was carefully removed and centrifuged again. In the next step, the first mitochondrial fraction was obtained from the supernatant by centrifugation (12 min, 17000 g, 4°C). The supernatant was removed and used for isolation of cytosol and microsomes (see below). The mitochondrial pellet was resuspended in SET buffer (0.25 M sucrose, 5 mM EDTA, 10 mM Tris-HCl pH 7.4, 2 mM PMSF) and centrifuged at low speed (5 min, 4500 g, 4°C) in order to remove mitochondrial aggregates. Mitochondria were harvested from the supernatant by centrifugation (12 min, 17000 g, 4°C), resuspended in SET buffer, shock frozen in liquid nitrogen and stored at -80°C until further analysis by SDS-PAGE (see 2.1.3), Western blot (see 2.1.5), 16-BAC/SDS-PAGE (see 2.1.7) and ZE-FFE analysis (see 2.3.9). For 2-DE analysis (see 2.1.6), mitochondria were sedimented (12 min, 16000 g, 4°C) and resuspended in ice-cold ddH₂O supplemented with Complete Protease Inhibitor Cocktail (Roche Applied Sciences) before shock freezing in liquid nitrogen. Determination of protein concentration was done using the Bradford assay (see 2.1.1). For further purification applying a linear sucrose gradient (see 2.3.8.2.3) freshly prepared mitochondria were used.

Cytosol and microsomes were obtained by ultracentrifugation from the supernatant of the first mitochondrial pellet (90 min, 170000 g, 4°C). Microsomal pellets were resuspended in SET buffer. Cytosol and microsomes were shock frozen in liquid nitrogen and stored at -80°C. Determination of protein concentration was done using the Bradford assay (see 2.1.1).

2.3.8.2.3 Purification of mitochondria applying gradient centrifugation

Mitochondria freshly isolated by differential centrifugation could further be purified applying a linear sucrose gradient (Rickwood et al., 1988). Mitochondria were resuspended in ice-cold gradient buffer (0.8 M sucrose, 1 mM EDTA, 10 mM Tris-HCl pH 7.4, 1 mM PMSF) and carefully laid on top of a linear sucrose gradient (1 to 2 M sucrose, 1 mM EDTA, 10 mM Tris-HCl pH 7.4, 1 mM PMSF, 4°C). Mitochondria were separated according to differential density by isopycnic centrifugation (90 min, 80000 g, 4°C) using a swinging-out rotor (SW40 rotor, Beckman Coulter). According to Rickwood et al. (1988), three brownish mitochondrial bands should appear: Mitochondria with the lowest density (1.14 g/mL)

showed damaged outer and inner membranes, the middle band (highly diffuse, 1.18 g/mL) contained intact mitochondria, whereas the lower band (often sedimented, 1.22 g/mL) comprised mitochondria with damaged outer membranes. Intact mitochondria were isolated by carefully removing the middle part of the gradient using a Pasteur pipette. After diluting in SET buffer, mitochondria were obtained by centrifugation (12 min, 17000 g, 4°C) and washed once in SET buffer. The mitochondrial pellet was resuspended in SET buffer to a final concentration of 2-5 mg/mL (see 2.1.1), shock frozen in liquid nitrogen and stored at -80°C until further use.

2.3.9 Analysis of mitochondria by zone-electrophoresis in a free-flow device

2.3.9.1 Principle of zone-electrophoresis in a free-flow device (ZE-FFE)

In ZE-FFE, mitochondria are transported with a continuous laminar buffer flow through a separation chamber. A perpendicular oriented electric field leads to specific deflection of mitochondria resulting in a major mitochondrial fraction with high purity (Hannig and Heidrich, 1990; Zischka et al., 2003). The FFE chamber used in this study (Octopus, Dr. Weber GmbH, see Results 1.4.3, Fig. 18) consisted of a front and back plate separated by a 0.5 mm spacer. Within this intermediate space a laminar buffer flow was created by a constant injection of separation media (10 mM acetic acid, 10 mM triethanolamine, 0.28 M sucrose, pH 7.4) via the media tubes 2-6 at the starting side of the chamber. The separation buffer was blocked by the counterflow (media tube 8) injected at the end side of the chamber and deviated via the fraction collector into a 96-well plate. The electrodes (cathode and anode), parallel oriented to this buffer stream, were flushed by electrode solution (100 mM acetic acid, 100 mM triethanolamine, pH 7.4) and separated from the separation chamber by electrophoresis membranes. To protect these membranes, stabilization medium (100 mM acetic acid, 100 mM triethanolamine, 0.28 M sucrose, pH 7.4) was flushed around the electrode chambers via media tubes 1 and 7.

2.3.9.2 Quality tests for correct instrument assembly and flow profile

ZE-FFE is a carrier free electrophoresis. This implies that any disturbance of the laminar buffer stream through the separation device had to be carefully avoided because a direct effect on the separation will occur. The stripe test revealed disturbances of the uniform laminar buffer stream and was done after the FFE setup. An aqueous solution of the red dye sulfanilazochromotrop (Sigma) was injected through the media tubes 2, 4 and 6 and dH₂O was pumped through the tubes 1, 3, 5, 7 and 8. Upon correct setup, alternate colorless and red

stripes of identical width and with sharp boundaries would flow in parallel along the separation chamber.

The sample inlet test revealed disturbances in the sample application setup. The aqueous solution of the red dye sulfanilazochromotrop was injected through the sample inlet pump. Upon correct assembly a narrow red stripe spanning 1-3 fractions would flow in a straight line parallel along the separation chamber.

2.3.9.3 Analysis of mitochondria by ZE-FFE

Mitochondria isolated by differential centrifugation (see 2.3.8.2.2) were used for the subsequent ZE-FFE purification. After thawing on ice, mitochondria were washed twice in ZE-FFE separation medium by centrifugation (12 min, 16000 g, 4°C). The mitochondrial pellet was carefully resuspended in ZE-FFE separation medium at a concentration of 1-3 mg/mL. The separation chamber was filled and equilibrated with stabilization medium (media tubes 1 and 7) and separation medium (media tubes 2-6) with a rate of media delivery of 300-400 mL/h. Voltage was set to 750 V. Mitochondrial suspension was applied into the separation chamber via the cathodal sample inlet using a sample pump with a rate of 2 mL/h. The mitochondrial sample entered the laminar buffer flow resulting in a visible major line that deflects towards the anode, since mitochondria are negatively charged particles at neutral pH (Ericson, 1974). At the end of the separation chamber the sample was collected in a 96-well format and the separation profile was visualized by measuring OD_{260nm} with the Synergy HT microplate reader (Biotek). Data were evaluated using MS Excel 2002. According to the separation profile mitochondrial main fractions (main peaks) and side fractions were pooled. Mitochondria were subsequently obtained by centrifugation (12 min, 17000 g, 4°C) and resuspended in SET buffer to a final concentration of 2-5 mg/mL. Samples were shock frozen in liquid nitrogen and stored at -80°C. Protein concentration was determined by the Bradford assay (see 2.1.1). In order to ensure maximal comparability, the ZE-FFE analysis of mitochondrial preparations (*i.e.*, CDC48-WT vs. *cdc48*^{S565G}) was done on the same day with the same FFE setup.

2.4 Analysis of mammalian cell cultures

2.4.1 Growth and maintenance of mammalian cell cultures

Cell cultures (human embryonic kidney cells, HEK293, see 1.5.3.2, Table 7) were started from cryo cultures. Cryo cultures were thawed quickly in a water bath at 37°C and transferred into a 10 cm cell culture dish (Nunc, Wiesbaden, Germany). 9 mL of pre-warmed medium (37°C, Dulbecco's modified Eagle medium (DMEM incl. L-glutamine and pyruvate; Gibco, Invitrogen) supplemented with 5% (v/v) heat-inactivated fetal calf serum (FCS, Gibco) and 0.1% (v/v) antibiotics, Penicillin-Streptomycin 10000 U/mL) were carefully added to the culture and the culture dish was gently shaken. Cells were cultured at 37°C in a humidified and 5% CO₂ containing atmosphere (CO₂ incubator, Sanyo). Confluent cultures were splitted into different cell culture dishes with a ratio of 1:5 to 1:10 as follows. Medium was removed and the adherent culture was washed with 5 mL of pre-warmed PBS (37°C, Gibco). The culture was then treated for 5 min at 37°C with 4 mL pre-warmed trypsinization solution (1x Trypsin-EDTA, Gibco). The detached cells were transferred into a 15 mL Falcon tube (BD Biosciences). The plate was rinsed with 4 mL pre-warmed PBS and the resultant suspension was then transferred into the 15 mL Falcon tube as well. Cells were sedimented (3 min, 180 g, RT), the supernatant was discarded and the cell pellet was gently resuspended in fresh medium. The cell suspension was then transferred into new cell culture dishes (10 mL suspension per 10 cm dish).

For the preparation of cryo cultures, cells of a confluent 10 cm dish were trypsinized as described above. Cells were sedimented, resuspended in 2 mL pre-warmed cryo medium (9.1% (v/v) supplemented medium, 0.9% (v/v) dimethylsulfoxide (DMSO), 37°C) and transferred into two cryo tubes (CryoTube Vials, Nunc). The tubes were placed at 4°C for 30 min, at -20°C for 1 h and at -80°C overnight. Long-term storage of cryo cultures was done in a cryo tank (-196°C, Messer) filled with liquid nitrogen.

2.4.2 Transient transfection of mammalian cell cultures

Transient transfection of cell cultures was done by lipofection using the Effectene Transfection Reagent (Qiagen). Here, the DNA constructs (cDNA cloned into a mammalian expression vector) bind to artificial membrane vesicles (liposomes) that adhere and subsequently fuse with the negatively charged plasma membranes, eventually leading to cells expressing the respective cDNAs (Felgner et al., 1994).

Transfection was done in a 6-well and 12-well format, respectively. Cells of a confluent 10 cm dish were trypsinized (see 2.4.1) and transferred into 6-well or 12-well plates (Nunc),

respectively, with a splitting ratio of 1:10 to 1:30. Cells were cultured overnight (37°C, 5% CO₂, humidified atmosphere). For transfection in a 6-well format, 1 µg total plasmid DNA was added to 150 µL EC buffer. After supplementing with 8 µL Enhancer solution, the solution was vortexed for 30 sec and incubated for 5 min at RT. Liposome formation was initiated by adding 25 µL Effectene. The solution was mixed and equilibrated at RT for 10 min. The medium was removed from the wells, and 1 mL fresh medium was added per well. The liposome solution was gently pipetted onto the medium, and lipofection was done for 6 h (37°C, 5% CO₂, humidified atmosphere). Medium was then removed and replaced by 3 mL fresh medium per well. After 2 d cultures were evaluated by fluorescence microscopy (see 2.4.4) or protein extracts were prepared for Western blot analysis (see 2.4.3).

2.4.3 Generation of protein extracts

Medium was completely removed from the cells. Plates were placed on ice and 330 µL of freshly prepared ice-cold lysis buffer (1 mL 10x PBS, 200 µL 100 mM orthovanadate, 100 µL 10x Complete Protease Inhibitor Cocktail (Roche Applied Sciences), 110 µL Nonidet-P40, 1.3 mL 80% (v/v) glycerol, ad 10 mL with ddH₂O) were added per well (6-well format). Cells were detached from the surface of the dishes using a cell scraper (Sarstedt, Nümbrecht, Germany). Cell lysates were transferred into Eppendorf cups and lysis was continued for 1 h on a vertical rotator at 4°C. The lysate was then centrifuged (15 min, 16000 g, 4°C), in order to remove intact cells and large cell debris. The supernatants were transferred into Eppendorf cups, and the protein concentrations were determined by the Bradford protein assay (see 2.1.1). Supernatants were shock frozen in liquid nitrogen and stored at -80°C until further use for Western blot analysis (see 2.1.5).

2.4.4 Fluorescence microscopy

Living cells were evaluated by *in vivo* fluorescence microscopy using the Leica inverse fluorescence microscope (DMIRE2/CTRMic with camera DC250; filter sets: DAPI, FITC, Rhodamine, and Nomarski).

2.4.5 Immunofluorescence microscopy

For immunofluorescence microscopy cells were grown and transfected on glass cover slips. To avoid cell detachment, cover slips were coated with poly-D-lysine (Sigma, 2 µg/cm²) and laminin (Sigma, 1 µg/cm²). First, cover slips were laid into a 10 cm dish containing 9 mL pre-warmed PBS (37°C) and 150 µL poly-D-lysine (1 µg/mL) and were incubated for 2 h at

37°C in an incubator. Then, cover slips were transferred into a 10 cm dish containing 9 mL pre-warmed PBS (37°C) and 75 µL laminin (1 µg/mL) and were equilibrated overnight at 37°C in an incubator. Up to 6 cover slips were put into a well (6-well format, Nunc) containing 1 mL medium with the coated side facing to the lid of the plate. The medium was then removed, the cell suspension was added and cells were cultured overnight (37°C, 5% CO₂, humidified atmosphere). Subsequently, cells were transfected as described in 2.4.2. 2 d after transfection, the medium was removed and the cells were fixed by adding 3 mL pre-warmed (37°C) 4% (w/v) paraformaldehyde in PBS. Plates were incubated at RT for 15 min. Paraformaldehyde was discarded and replaced by pre-warmed (37°C) PBS. Plates were then stored at 4°C until further use.

For immunostaining, fixed cells were permeabilized with 100 µL permeabilization solution (0.1% Triton X-100 in PBS) per cover slip for 5 min at RT. Cells were washed with 100 µL PBS per cover slip. Unspecific antibody binding was prohibited by blocking with 100 µL 1% (w/v) BSA in PBST (PBS supplemented with 0.1% (v/v) Tween-20) per cover slip for 1 h at RT. Cells were incubated for 3 h at RT with the primary antibody against the protein of interest in an appropriate dilution (see 1.5.4, Table 7) in 1% (w/v) BSA in PBST. Cells were then washed five times for 5 min with PBS and were then incubated for 1 h at RT with an Alexa Fluor-coupled secondary antibody (see 1.5.4, Table 8) in a 1:1000 dilution in 1% (w/v) BSA in PBST containing 1 µg/mL 4,6-diaminodiphenyl-2-phenylindole (DAPI) for nuclear staining. After five times washing for 5 min with PBS, cover slips were briefly rinsed in ddH₂O and mounted up-side-down onto a droplet FluorSave (Calbiochem, VWR) on a glass slide. After solidification of the fluorsave, immunostained cells were evaluated for staining by fluorescence microscopy. Mounted cover slips were stored at 4°C.

Images were obtained by the AxioScope 2 fluorescence microscope (Zeiss) using a FITC optical filter set for Alexa Fluor 488 staining, a Rhodamine optical filter set for Alexa Fluor 568 staining, a DAPI optical filter set for DAPI staining and a Nomarski optical filter set (Plan-Neofluar 40x/0.75 objective, AxioCam HRc, AxioVision 4, Zeiss). Images were adjusted using the AxioVision 4 software package.

For high resolution microscopy, images were obtained at RT by the ApoTome™ fluorescence microscope (Zeiss) using a Cy3 optical filter for Alexa 568 staining, a FITC optical filter for Alexa Fluor 488 staining, a DAPI optical filter for DAPI staining and a Nomarski optical filter (C-Apochromat 40x/1.20 objective with an optical section thickness of 1 µm and C-Apochromat 63x/1.20 objective with an optical section thickness of 1 µm; AxioCam, AxioVision 4, Zeiss). Images were adjusted using the AxioVision 4 software

package. The obtained images provide an axial resolution comparable to confocal microscopy (Garini et al., 2005). In the ApoTome mode, a grid was inserted into the field diaphragm plane of the reflected light beam path. The grid pattern was sharply projected into the object plane and was clearly visible through the eyepiece and in the live image. A high-precision scanning mechanism moved the grid pattern in defined steps in the sample plane. Images were acquired at each grid position. A single resulting image was calculated using a fast mathematical algorithm resulting in a precise optical section through the specimen. With this technique it was possible to acquire information from a z-plane of the sample and display it with enhanced resolution and increased contrast with no blurring.

2.4.6 Cell viability assay (Live-Dead Assay)

Cell viability of cell cultures was assessed in a 96-well format (Falcon, BD Biosciences) by a Live-Dead Assay. Here, cells were equilibrated with calcein AM (Molecular Probes, Invitrogen) and ethidium homodimer-1 (Molecular Probes). Viable cells but not dead cells modify calcein AM to the green-fluorescent dye calcein. In contrast, dead cells with porous cell membranes but not viable cells incorporate the DNA-intercalating red-fluorescent dye ethidium homodimer-1. The ratio of green to red fluorescence, *i.e.*, the relative number of viable to the relative number of dead cells, describes the viability of the respective culture.

Cultures were seeded with 6000 cells per well (96-well format) and grown overnight at 37°C in a humidified and 5% CO₂ containing atmosphere. Cells were transfected with 50 ng DNA construct per well (see 2.4.2). 2 d after transfection Live-Dead Assay was performed. Medium was removed from the wells and cells were optionally washed with 100 µL pre-warmed PBS per well. 100 µL staining solution (pre-warmed PBS (37°C) supplemented with 5 µM calcein AM and 2.5 µM ethidium homodimer-1; 4 mM calcein AM stock solution in DMSO, 2 mM ethidium homodimer-1 stock solution in DMSO/ddH₂O (1:4, v/v)) were added per well. Plates were incubated exactly for 30 min in the incubator (37°C, 5% CO₂, humidified atmosphere). Green and red fluorescence was then determined using the Synergy HT microplate reader (Biotek) with the following settings: endpoint measurement, optics position: bottom, Falcon 96 flat bottom, for measurement of calcein fluorescence: excitation 485/20, emission 528/20, sensitivity 50, for measurement of ethidium homodimer-1 fluorescence: excitation 530/25, emission 590/35, sensitivity 75. For every condition eight wells were measured. Staining solution was used as blank.

F. Results

1. Analysis of *Cdc48p* variants in yeast

Apoptosis in the *cdc48*^{S565G} yeast strain was first described by Madeo et al. (1997), but the cellular mechanisms underlying cell death in this strain upon *CDC48* mutation remained unknown. In order to detect alterations on the protein level associated with the genetic mutation (*cdc48*^{S565G}) as well as the apoptotic condition, a functional proteome analysis was performed starting with differential two-dimensional gel electrophoresis (2-DE).

1.1 Cell viability and apoptosis in the *cdc48*^{S565G} strain

1.1.1 Cell viability is decreased and susceptibility for apoptotic cell death is increased upon *CDC48* mutation in yeast

As a prerequisite for such a differential 2-DE analysis, growth conditions were adjusted such that the majority of *cdc48*^{S565G} cells undergo apoptotic cell death. This was achieved through specific growth conditions as well as increase in temperature. As described by Madeo et al. (1997, 1999), the percentage of apoptotic cells (i) is higher on glucose medium (YPGlc) than on galactose medium (YPGal), (ii) is increased during stationary phase compared to logarithmic and early-stationary growth phase, and (iii) apoptosis can be induced in the *cdc48*^{S565G} strain by heat shock at 37°C. Therefore, apoptotic cell death in the *cdc48*^{S565G} strain was induced by inoculating galactose pre-cultures (YPGal) into glucose medium with a subsequent heat shock at 37°C. In order to analyze both early and late events at the proteome level, two different apoptotic growth conditions were selected: (i) 13 h growth in YPGlc (early-stationary growth phase) incl. 1 h heat shock at 37°C, and (ii) 20 h growth in YPGlc (stationary growth phase) incl. 4 h heat shock at 37°C.

In order to validate the applied growth conditions, cell viability under these different growth conditions was determined by a survival plating assay (Fig. 5). In this assay equal numbers of cells were plated and the numbers of formed colonies were determined. Cell viability of *cdc48*^{S565G} cells was significantly decreased upon inoculation in YPGlc medium and heat shock (Fig. 5). Whereas after 13 h growth in YPGlc medium, the viability of the *cdc48*^{S565G} culture was only slightly decreased (16% decrease) compared to the YPGal pre-culture, at the 20 h time point cell viability was found to be severely and significantly affected (42% decrease) compared to the YPGal pre-culture. In contrast, loss of cell viability of wild-type cultures was rather weak after growth in YPGlc medium and heat shock (Fig. 5) with 4% and 14% decrease at the 13 h and 20 h time points, respectively, compared to the YPGal pre-

cultures. Thus, both wild-type and *cdc48*^{S565G} strains are progressively affected by inoculation in YPGlc medium and heat shock with the *cdc48*^{S565G} strain much more severely impaired.

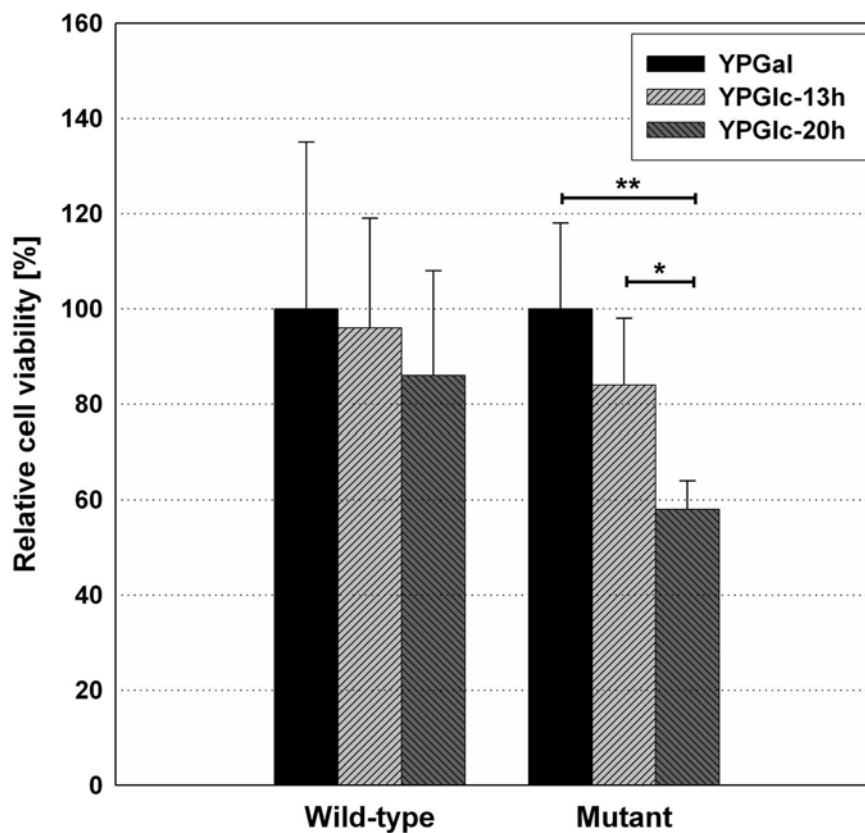


Figure 5: Viability in the *cdc48*^{S565G} strain is significantly decreased upon growth in glucose medium and heat shock. Galactose pre-cultures (YPGal) of both wild-type and *cdc48*^{S565G} strain were used for inoculation of glucose medium (YPGlc). YPGlc cultures were grown for 13 h (incl. 1 h heat shock at 37°C) and 20 h (incl. 4 h heat shock at 37°C), respectively. YPGal pre-cultures and YPGlc cultures, both 13 h and 20 h, were tested for cell viability by a survival plating assay. 1000 cells of each culture were plated onto YPGal plates and the numbers of formed colonies were determined. Four independent experiments were performed and the mean values of the YPGal pre-cultures for wild-type and mutant strain, respectively, were set to 100%. *p<0.05, **p<0.01, Student's t-test (unpaired). Error bars: s.d.

In order to confirm whether the observed loss of cell viability in the *cdc48*^{S565G} strain is associated with increased susceptibility for apoptotic cell death, cells were evaluated for DNA fragmentation, a hallmark of apoptosis, by performing a TUNEL assay. The 20 h time point was chosen for the TUNEL assay since at that time point cell viability of the *cdc48*^{S565G} strain was most severely affected (Fig. 5). At the 20 h time point, 53% of *cdc48*^{S565G} cells but only 20% of wild-type cells demonstrated DNA fragmentation (Fig. 6). Thus, the applied growth conditions allow the induction of apoptotic cell death in the majority of *cdc48*^{S565G} cells, thereby enabling differential 2-DE analysis.

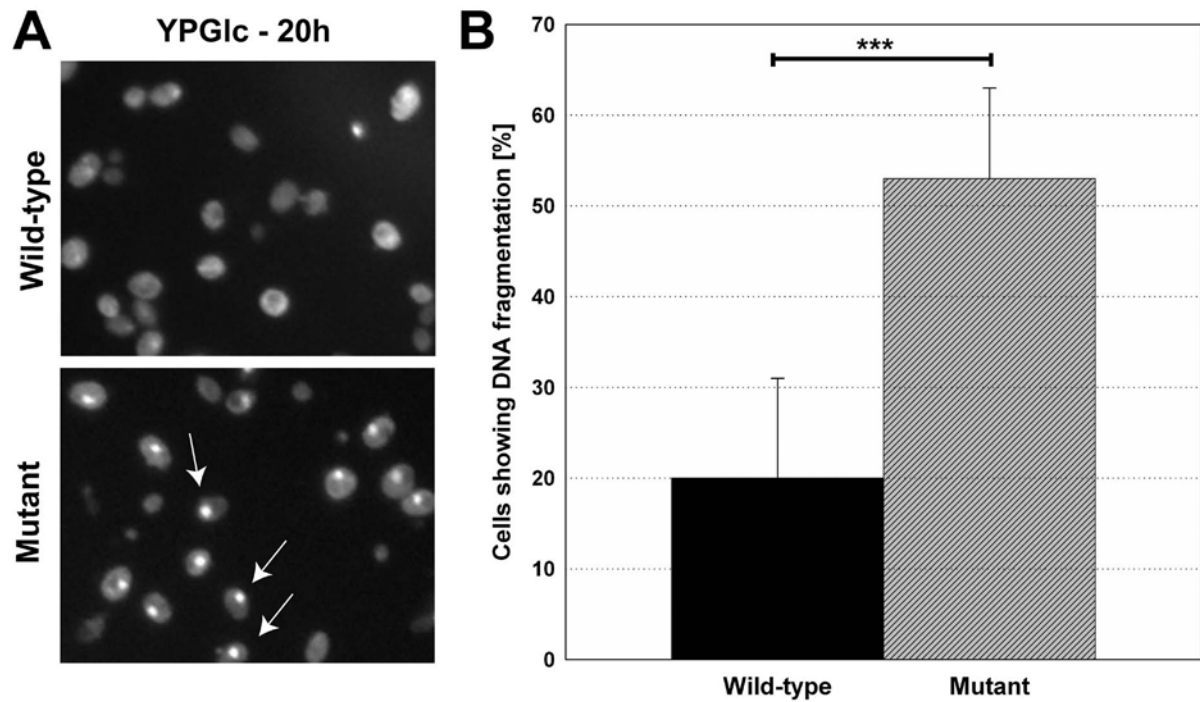


Figure 6: DNA fragmentation can be induced in the majority of *cdc48*^{S565G} cells.

Glucose medium (YPGlc) was inoculated with galactose pre-cultures (YPGal). TUNEL assay was performed after 20 h growth in YPGlc incl. 4 h heat shock at 37°C.

(A) DNA fragmentation, visualized by TUNEL staining, is increased in *cdc48*^{S565G} cells compared to wild-type cells. Representative micrographs of wild-type and *cdc48*^{S565G} cells. Arrows: stained nuclei of TUNEL-positive yeast cells.

(B) Quantification reveals a 2.6 fold increase in *cdc48*^{S565G} cells showing DNA fragmentation compared to wild-type cells. n=4, ***p<0.001, Student's t-test (unpaired). Error bars: s.d.

1.2 Differential 2-DE analysis of the *cdc48*^{S565G} strain

1.2.1 Distinct alterations are observed in mitochondrial extracts of *cdc48*^{S565G} cells compared to wild-type cells under apoptotic growth conditions

Differential 2-DE analysis was performed by comparing protein extracts of wild-type and *cdc48*^{S565G} strain. Beside total cell extracts, protein samples of mitochondrial and cytosolic extracts were examined. Since reactive oxygen species (ROS) are not only a by-product but a fully integrated component of the cell death process in the *cdc48*^{S565G} strain (Madeo et al., 1999), mitochondrial extracts were analyzed, as their involvement in apoptosis seemed probable. Cytosolic extracts were examined for apoptosis-associated alterations, since the recently identified yeast caspase (Madeo et al., 2002b) might process cytosolic protein substrates.

Differential 2-DE analysis of total cell extracts of wild-type and *cdc48*^{S565G} strain under apoptotic growth conditions, both YPGlc 13 h and 20 h, revealed no marked protein spot alterations (Braun, 2002). These data underline the identical genetic background of both strains and the high stability of the cellular proteome as illustrated as protein spot pattern on 2D gels even under apoptotic growth conditions.

Differential 2-DE analysis of mitochondrial extracts of wild-type and *cdc48*^{S565G} strain at the 20 h time, *i.e.*, the growth condition associated with a significant decrease in cell viability in the *cdc48*^{S565G} strain (Fig. 5) and the emergence of DNA fragmentation in the majority of *cdc48*^{S565G} cells (Fig. 6), resulted in 40 significant protein spot alterations out of 1400 protein spots per gel (Fig. 7A, gels 3 and 4, Table 16). In contrast, only 6 protein spots out of 1600 protein spots per gel were found to be altered between wild-type and *cdc48*^{S565G} strain when comparing cytosolic extracts at the 20 h time point (Fig. 7A, gels 1 and 2). 2-DE analysis of mitochondrial extracts at the 13 h time point, *i.e.*, the growth condition associated with a less severe decrease in cell viability in the *cdc48*^{S565G} strain compared to the 20 h time point (Fig. 5), revealed markedly fewer and less pronounced protein spot alterations between wild-type and *cdc48*^{S565G} strain (Fig. 7B, gels 1 and 2). At the 13 h time point, only 11 of the 40 protein spots altered at the 20 h time point, were found to be significantly altered (Table 16). However, additional 21 protein spots revealed the same tendency at the 13 h time point as observed in the 20 h time point, but with very low statistic significance (Table 16). Thus, mitochondria are a major site of alterations at the proteome level associated with apoptotic cell death, whereas the cytosol remains largely unaffected. Moreover, mitochondrial protein spot alterations are noticeable at the 13 h time point but become significant not until the cell viability in the *cdc48*^{S565G} strain significantly decreases at the 20 h time point.

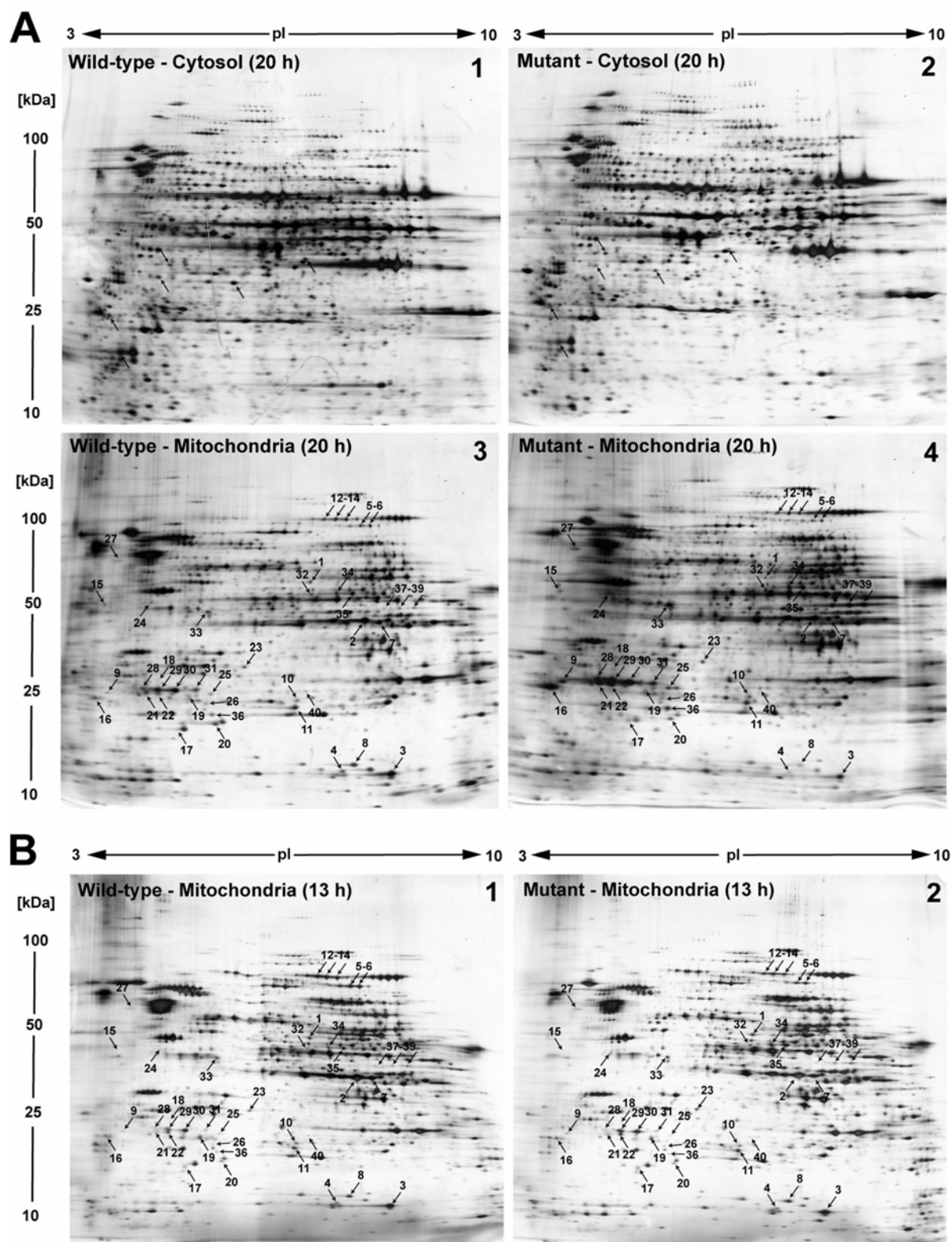


Figure 7: Differential 2-DE analysis of mitochondrial and cytosolic extracts from wild-type and *cdc48*^{S565G} cells under apoptotic growth conditions (13 h and 20 h).

(A) 2-DE comparison of cytosolic extracts (gels 1 and 2) and mitochondrial extracts (gels 3 and 4) at the 20 h time point. 6 reproducible differences (arrows) out of 1600 protein spots per gel were found in cytosolic extracts (gels 1 and 2, n=6). In contrast, 40 (arrows) out of 1400 protein spots per gel were found to be significantly altered in mitochondrial extracts (gels 3 and 4, n=7). Identified proteins and results of quantification (ProteomWeaver™) are listed in Table 16.

(B) 2-DE comparison of mitochondrial extracts (gels 1 and 2) at the 13 h time point. Protein spots significantly altered at the 20 h time point (A) were evaluated for alterations at the 13 h time point. Results of quantification (ProteomWeaver™) are listed in Table 16. Note that 31 out of the 40 significant variations observed at the 20 h time point have the same tendency at the 13 h time point, however, with very low statistic significance.

1.2.2 Mitochondrial proteins and proteins linked to mitochondrial motility and oxidative stress are altered in mitochondrial extracts of *cdc48^{S565G}* cells

Mass spectrometry (MS) analysis of the 40 altered protein spots in mitochondrial extracts identified 28 unique proteins (Table 16), eleven of which were established as mitochondrial proteins (spots 1 to 16, Table 16). Increased (‘enrichment’) and decreased (‘depletion’) amounts of mitochondrial proteins in mitochondrial extracts of *cdc48^{S565G}* cells were observed (*e.g.*, ‘mitochondrial 40S ribosomal protein 8’ (Mrp8p) Fig. 8, panel E, spot 9 and ‘maintenance of mitochondrial function 1 protein’ (Mmf1p) Fig. 8, panel A, spot 3, respectively; for quantification of protein spot alterations see Table 16).

The majority of the altered mitochondrial proteins (seven out of ten) is depleted in mitochondrial extracts in the *cdc48^{S565G}* strain under apoptotic growth conditions (Table 16). Depletion of ‘ARG5,6 protein’ (Arg5,6p, Fig. 8, panel C, spot 1), ‘ketol-acid reductoisomerase’ (Ilv5p, Fig. 8, panel B, spot 2), ‘maintenance of mitochondrial function 1 protein’ (Mmf1p, Fig. 8, panel A, spot 3), homoaconitase (spots 5-6, Table 16), ‘homoisocitrate dehydrogenase’ (Lys12p, Fig. 8, panel B, spot 7), cyclophilin C (Cyp. C, Fig. 8, panel A, spot 8), and ‘putative aconitase’ (spots 12-14, Table 16) suggest mitochondrial damage resulting in the release of these soluble proteins. Especially, the observed depletion of Mmf1p and Ilv5p, two proteins fundamental for the stability of mitochondrial DNA (Oxelmark et al., 2000; Zelenaya-Troitskaya et al., 1995), hints to reduced mitochondrial functionality under apoptotic

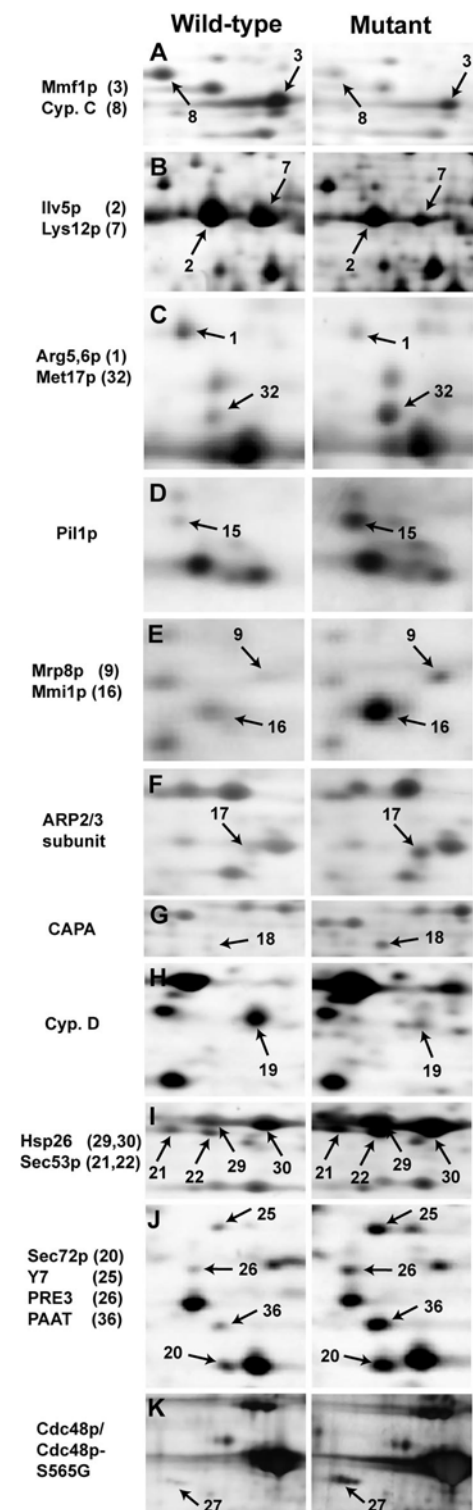


Figure 8: Protein spot alterations between wild-type and *cdc48^{S565G}* strains in mitochondrial extracts under apoptotic growth conditions (20 h).

Selected representative protein spot alterations observed in the 2-DE comparison of mitochondrial extracts at the 20 h time point (*e.g.*, Fig. 7A, gels 3 and 4). Results of quantification (ProteomWeaver™) are listed in Table 16.

growth conditions.

Accumulation of the ‘F-actin capping protein alpha subunit’ (CAPA, Fig. 8, panel G, spot 18) and of the ‘ARP2/3 complex 20 kDa subunit’ (Fig. 8, panel F, spot 17) was detected. The ARP2/3 complex is associated with the actin cytoskeleton and is involved in mitochondrial motility in yeast (Boldogh et al., 2001). Accumulation of these proteins may suggest an altered mitochondrial motility in *cdc48*^{S565G} cells.

Enrichment of the cytoplasmic protein ‘O-acetyl(homo)serine sulfhydrylase’ (Met17p) (Fig. 8, panel C, spot 32) and of the ‘microtubule and mitochondria interacting protein’ (Mmi1p), the highly conserved yeast orthologue of the human ‘translationally controlled tumor protein’ (TCTP) (Rinnerthaler et al., 2006; Yarm, 2002) was observed (Fig. 8, panel E, spot 16). Met17p is a protein central for sulfur metabolism and synthesis of glutathione (Miyake et al., 1999), a known antioxidant in yeast (Drakulic et al., 2005; Madeo et al., 1999). Mmi1p is a cytoplasmic microtubule-binding protein that upon mild oxidative stress translocates to mitochondria (Rinnerthaler et al., 2006). Accumulation of these proteins in mitochondrial extracts hints to an increased oxidative stress in *cdc48*^{S565G} cells.

Distinct changes of mitochondrial proteins and proteins linked to mitochondrial motility and oxidative stress suggest that mitochondria in *cdc48*^{S565G} cells are affected under apoptotic growth conditions. Mitochondria play a crucial role in many apoptotic pathways in both mammalian cells and in yeast (Green and Kroemer, 2004; Ludovico et al., 2002; Newmeyer and Ferguson-Miller, 2003). Therefore, further studies were performed to validate mitochondrial impairment and to elucidate if these organelles crucially contribute to apoptotic cell death in the *cdc48*^{S565G} yeast strain (see Results 1.3).

1.2.3 *Cdc48p-S565G* and other proteins associated with the NE-ER accumulate in mitochondrial extracts of *cdc48*^{S565G} cells

Interestingly, nine proteins associated with the NE-ER, a continuous membrane system consisting of the endoplasmic reticulum (ER) and the ER-related nuclear envelope (NE) (Baumann and Walz, 2001; Enenkel et al., 1998; Hepler, 1981), were found to show altered levels in mitochondrial extracts of the *cdc48*^{S565G} strain (spots 19-31, Table 16). In this context, ER luminal proteins, proteins integrated in or associated with the NE-ER membrane, and nuclear proteins are referred to as ‘NE-ER-associated’. In fact, the majority (eight out of nine) were clearly enriched in mitochondrial extracts (Table 16).

Table 16: Identified proteins differentially found in mitochondrial extracts under apoptotic growth conditions (13 h and 20 h time points)

Maldi-TOF Mass Spectrometry: Protein spots of interest were subjected to trypsin treatment. Resulting peptides were analyzed using a Maldi-TOF Reflectron mass spectrometer. Spectra were annotated applying the MassLynx 3.5 software and subsequent database searches in SwissProt with peptide mass fingerprinting queries were done using the ProteinLynx Globalserver 1.1 software (PLGS 1.1) as described in Material and Methods.

2-DE Analysis of Mitochondrial Extracts: Image analysis of the gels was performed visually assisted by ProteomWeaver™ image analysis software. For the analysis of mitochondrial extracts under apoptotic growth conditions (13 h and 20 h time points) data were determined by taking into account four independent mitochondrial preparations analyzed by five independent 2-DE separations sets (each consisting of several gels per condition). Quantification of protein spot alterations was done using ProteomWeaver™ V.2.2 software. For the analysis of the 13 h time point in total six 2D gels for wild-type and six 2D gels for mutant were considered for quantification and statistics. For the analysis of the 20 h time point in total seven 2D gels for wild-type and seven 2D gels for mutant were considered for quantification and statistics.

Protein Spot No. (Figs. 7, 8)	Swiss-Prot Accession No. (a)	PLGS 1.1 Score of Identified Protein/Score of Next Yeast Hit (b)	Sequence Coverage [%]	Molecular Weight [kDa]	Calculated Isoelectric Point (pI)	Gene Name (c)	Protein Name	Factor M vs. WT at the 13 h Time Point (d)	p-Value (Student's t-test) at the 13 h Time Point	Factor M vs. WT at the 20 h Time Point (d)	p-Value (Student's t-test) at the 20 h Time Point	Localization (e)	Function (e)
1	Q01217	54/26	42	94.9	8.6	YER069w	ARG5,6 protein (Arg5,6p)/ N-acetyl gamma glutamyl-phosphate reductase	1.1	0.14689	0.5	0.00200	Mitochondria, matrix	Amino acid metabolism
2	P06168	201/57	96	44.4	9.3	YLR355c	Ketol-acid reductoisomerase (Ilv5p)	0.8	0.11306	0.6	0.00332	Mitochondria	Amino acid metabolism, mtDNA stability
3,4	P40185	82/-	82	15.9	9.5	YIL051c	Maintenance of mitochondrial function 1 (Mmf1p)	0.9	0.32722	0.4	0.00361	Mitochondria, matrix	Amino acid metabolism, mtDNA stability
5,6	P49367	37/-	60	75.1	7.4	YDR234w	Homoaconitase	0.5	0.00232	0.5	0.01723	Mitochondria	Amino acid metabolism
7	P40495	60/-5	60	40.0	8.4	YIL094c	Homoisocitrate dehydrogenase (Lys12p)	1.0	0.48291	0.4	0.00054	Mitochondria	Amino acid metabolism
8	P25719	49/14	65	19.9	9.1	YML078w	Cyclophilin C (Cyp C)/ mitochondrial peptidyl-prolyl cis-trans isomerase C	0.9	0.32271	0.7	0.00247	Mitochondria, matrix	Protein folding
9	P35719	32/34	48	59.5	8.6	YKL142w	Mitochondrial 40S ribosomal protein (Mrp8p)	1.3	0.13469	4.0	0.01214	Mitochondria, ribosomes	Protein biosynthesis
10,11	P08067	74/47	78	23.3	8.5	YEL024w	Ubiquinol-cytochrome <i>c</i> reductase iron-sulfur subunit (UCRI)/ Rieske iron-sulfur protein (RISP)	1.2/ 1.2	0.0825/ 0.09815	0.65/ 1.2	0.04284/ 0.17448	Mitochondria, inner membrane	Energy metabolism, cytochrome <i>bc₁</i> complex
12-14	P39533	82/30	39	86.6	6.9	YJL200c	Putative aconitase	0.8	0.02749	0.5	0.00098	Mitochondria, cytosol, nucleus	Unknown
15	P53252	21/3	69	38.3	4.6	YGR086c	Sphingolipid long chain base responsive protein PIL1 (Pil1p)	1.0	0.48167	3.5	0.00007	Lipid particles, mitochondria	Negative regulator of cell wall integrity in unstressed cells
16	P35691	13/12	49	18.7	4.4	YKL056c	Microtubule and mitochondria interacting protein (Mmi1p) (f)/ Translationally controlled tumor protein homolog (TCTP)	1.3	0.09035	3.3	0.00037	Cytoskeleton, mitochondria (f)	Interacts with microtubule and translocates to mitochondria upon oxidative stress (f)
17	P33204	28/10	78	19.9	5.4	YKL013c	ARP2/3 complex 20 kDa subunit	1.4	0.18096	3.5	0.00038	Cytoskeleton	Mitochondrial motility (g)
18	P28495	31/12	35	30.7	5.2	YKL007w	F-actin capping protein alpha subunit (CAPA)	1.7	0.04537	2.8	0.00020	Cytoskeleton	Actin cytoskeleton

Results

19	P35176	22/-1	75	25.3	5.5	YDR304c	Cyclophilin D (Cyp D)/ Peptidyl cis-trans isomerase D	0.8	0.14735	0.5	0.00291	ER lumen	Protein folding
20	P39742	11/7	55	21.5	5.6	YLR292c	Translocation protein Sec72p	1.2	0.23605	1.8	0.00460	ER membrane	Protein biosynthesis, secretory pathway
21,22	P07283	46/-	49	29.0	5.2	YFL045c	Phosphomannomutase Sec53p	1.2	0.17007	1.8	0.00014	ER-associated (h)	Protein biosynthesis, secretory pathway
23	P38011	0/-6	69	34.8	6.1	YMR116c	Guanine nucleotide-binding beta subunit-like protein	0.8	0.21297	2.1	0.00154	Ribosome, NE- ER-associated (i)	Protein biosynthesis
24	P10081	70/22	71	44.5	5.1	YKR059w	Eukaryotic initiation factor 4A	1.1	0.41105	1.6	0.05509	Ribosome, NE- ER-associated (i)	Protein biosynthesis
25	P23639	10/4	35	48.1	9.2	YML092c	Proteasome component Y7	1.1	0.42593	3.6	0.00089	Proteasome, NE-ER- associated (j)	Protein degradation
26	P28624	10/-	60	23.5	5.8	YJL001w	Proteasome component PRE3	0.9	0.39001	2.4	0.01128	Proteasome, NE-ER- associated (j)	Protein degradation
27	P25694	29/3	20	92.0	4.8	YDL126c	Cell division cycle protein 48 (Cdc48p)	1.3	0.26942	5.8	0.00002	ER-associated, nucleus, cytosol	Protein degradation, membrane fusion, spindle apparatus
28-31	P15992	28/20	53	23.7	5.4	YBR072w	Heat shock protein 26 (Hsp26)	1.3	0.19396	1.7	0.00106	Nucleus, cytoplasm	Protein folding, stress response
32	P06106	32/8	60	48.5	6.3	YLR303w	MET17 protein (Met17p)/ O-acetyl(homo)serine sulfhydrylase	1.2	0.27838	1.5	0.00630	Cytoplasm	Amino acid metabolism
33	P04173	48/16	41	39.0	5.5	YCL018w	3-isopropylmalate dehydrogenase	1.1	0.28576	1.4	0.00615	Cytoplasm	Amino acid metabolism
34,35	P00924	23/-2	57	46.7	6.5	YGR254w	Enolase 1	1.6	0.01036	2.2	0.00199	Cytoplasm	Energy metabolism, glycolysis
36	Q12447	38/20	75	21.9	5.8	YDR071c	Polyamine acetyltransferase (PAAT)	0.9	0.26069	3.2	0.00070	Cytoplasm	Acetylation of polyamines
37-39	P38219	27/1	70	44.2	7.6	YBR025c	Putative GTP binding protein YBR025c	1.9	0.00572	2.4	0.00803	Cytoplasm	Unknown
40	Q05016	22/-6	76	29.1	6.8	YMR226c	Putative oxidoreductase YMR226c	0.9	0.37337	2.8	0.01019	Unknown	Unknown

(a) Accession number in Swiss-Prot database: <http://expasy.org/sprot/>; (b) PLGS 1.1 score of the identified protein/PLGS 1.1 score of the next yeast hit within the first 50 hits; (c) Gene name in MIPS database: <http://mips.gsf.de/>; (d) Factor in differential 2-DE analysis: intensity of a protein spot in mitochondrial extracts of mutant (M: *cdc48^{S565G}*) versus intensity of the same protein spot in mitochondrial extracts of wild-type strain (WT): <1 for depletion, >1 for accumulation of protein; (e) Localization and function according to Swiss-Prot database (<http://expasy.org/sprot/>) and Mitop2 database (<http://ihg.gsf.de/mitop2/start.jsp>) if not other stated; (f) According to Rinnerthaler et al. (2006), (g) According to Boldogh et al. (2001); (h) According to Ruohola and Ferro-Novick (1987); (i) According to Nicchitta, (2002); (j) According to Enenkel et al. (1998)

Cyclophilin D, an ER luminal protein involved in protein folding as peptidyl-prolyl cis-trans isomerase (Frigerio and Pelham, 1993), was the only protein of this class whose level was depleted in the mutant strain (Fig. 8, panel H, spot 19). In contrast, the remaining NE-ER-associated proteins were clearly enriched in mitochondrial extracts. Among these, two proteins associated with ribosomes that are predominately NE-ER-associated in yeast (Nicchitta, 2002) could be identified: ‘guanine nucleotide-binding beta subunit-like protein’ (spot 23, Table 16) and ‘eukaryotic initiation factor 4A’ (spot 24, Table 16). Moreover, enrichment of two proteins involved in the secretory pathway was noted: First, Sec72p (Fig. 8, panel J, spot 20), which has been described as a component of the integral ER membrane SEC complex allowing protein translocation from the cytosol into the ER lumen (Willer et al., 2003); and second, Sec53p (Fig. 8, panel I, spots 21-22), an ER-associated phosphomannomutase necessary in an early step of the glycosylation pathway (Ruohola and Ferro-Novick, 1987). Furthermore, accumulation of two subunits of the proteasome that are predominantly NE-ER-associated in yeast (Enenkel et al., 1998), namely the proteasome component Y7 (Fig. 8, panel J, spot 25) and the proteasome component PRE3 (Fig. 8, panel J, spot 26), was observed.

Most interestingly, Cdc48p-S565G itself, the protein causative for the facilitated induction of apoptotic cell death (Fig. 6), was found to be the NE-ER protein demonstrating the strongest enrichment in mitochondrial extracts of *cdc48^{S565G}* cells compared to wild-type (*i.e.*, 5.8 fold; Fig. 8, panel K, spot 27, Table 16). This finding was rather unexpected, since neither Cdc48p nor its mutated variant had been previously described as having a functional relationship with mitochondria. Instead, key functions of this protein are linked to the NE-ER, especially its essential role in ubiquitin-dependent ER-associated protein degradation (ERAD) (Elkabetz et al., 2004; Richly et al., 2005; Ye et al., 2001).

It has been shown that in the *cdc48^{S565G}* strain the ER is expanded (Madeo et al., 1997) and the ERAD pathway is impaired (Jarosch et al., 2002). Enrichment of Cdc48p-S565G and other NE-ER-associated proteins in mitochondrial extracts, especially the two proteasomal components Y7 and PRE3, might reflect that ERAD dysfunction is conferred to mitochondria, subsequently leading to mitochondrial damage. Therefore, further experiments were performed to address this hypothesis (see Results 1.4).

1.3 Crucial mitochondrial impairment in the *cdc48*^{S565G} strain

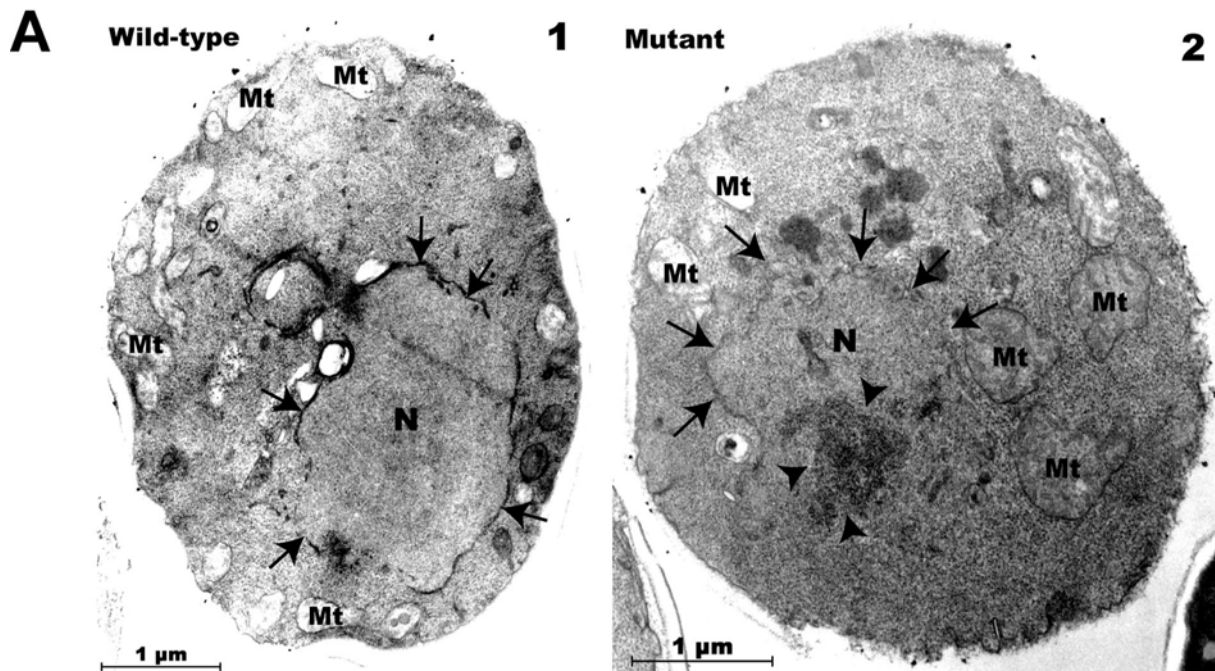
Depletion of proteins necessary for mitochondrial function and accumulation of proteins linked to mitochondrial motility and oxidative stress in mitochondrial extracts (Figs. 7 and 8, Table 16) suggest mitochondrial impairment in *cdc48*^{S565G} cells under apoptotic growth conditions. Therefore, further experiments were conducted to elucidate mitochondrial impairment and a possible role of mitochondria during cell death in the *cdc48*^{S565G} yeast strain.

1.3.1 Mitochondria in *cdc48*^{S565G} cells are enlarged compared to wild-type cells under apoptotic growth conditions

In order to evaluate morphological alterations of mitochondria, ultrastructural analysis (electron microscopy, EM) of yeast cells grown under apoptotic growth conditions (20 h) was performed. Preparation of EM sections and EM micrographs were done in collaboration by Dietmute Büringer (Max-Planck-Institute of Neurobiology, Martinsried, Germany). In *cdc48*^{S565G} cells a significant enlargement of mitochondria compared to wild-type cells was observed (Fig. 9A, for quantification see Fig. 9B). Determination of mitochondrial and total cellular area revealed, that in *cdc48*^{S565G} cells 10% of the cellular area was composed of mitochondria compared to 7% in wild-type cells. Since the average number of mitochondria per cell was highly similar between the *cdc48*^{S565G} and wild-type strains (1.1 for wild-type and 1.2 for *cdc48*^{S565G} cells), these data hint towards a swelling of mitochondria in the *cdc48*^{S565G} strain, which is a known feature in pathophysiological processes (Bernardi et al., 1999; Boya et al., 2002; Farber, 1994; Wakabayashi, 1999).

1.3.2 *Cdc48*^{S565G} cells show respiratory deficiency under apoptotic growth conditions

Mitochondrial swelling (Fig. 9) and depletion of proteins necessary for mitochondrial function (Figs. 7 and 8, Table 16) propose mitochondrial damage and subsequent loss of mitochondrial respiratory capacity in *cdc48*^{S565G} cells under apoptotic growth conditions. Therefore, the adaptability of both wild-type and *cdc48*^{S565G} cells to conditions, which challenge the respiratory capacity of their mitochondria was investigated. Only respiratory sufficient *S. cerevisiae* cells, in contrast to respiratory deficient cells, form colonies on media containing a principal carbon and energy source, which is obligatory aerobic (lactate) for growth (Ogur and St John, 1956). Consequently, cells with respiratory incompetent mitochondria cannot metabolize lactate, *i.e.*, they are unable to proliferate and do not form



B

Percentage of Mitochondrial Area within Cells		
WT	M	
7%	10%	
1%	2%	StDev
p=0.02		Student's t-Test

Figure 9: Mitochondria are enlarged in *cdc48^{S565G}* cells.

(A) EM analysis of wild-type and *cdc48^{S565G}* cells grown under apoptotic growth conditions (20 h). Wild-type cells (1) show intact nuclei (arrows: nuclear envelope) with mitochondria predominantly distributed near the plasma membrane. *Cdc48^{S565G}* cells (2) frequently demonstrate chromatin condensation (arrowheads), nuclear fragmentation and enlarged mitochondria. Mt: mitochondria, N: nucleus, arrows: nuclear envelope, arrowheads: chromatin condensation). Preparation of EM sections and EM micrographs were done in collaboration by Dietmute Büringer (Max-Planck-Institute of Neurobiology, Martinsried, Germany).

(B) Quantification of mitochondrial enlargement. Mitochondrial and total cellular area was determined using AxioVision Software LE V.4.2 (Zeiss). In order to exclude artifacts due to the fixation procedure, mitochondrial area was normalized to total cellular area. The obtained percentage of the mitochondrial area within cells was significantly increased in *cdc48^{S565G}* (10%) compared to wild-type cells (7%) ($p < 0.02$, Student's t-test, unpaired). These figures mean enlargement of mitochondria in *cdc48^{S565G}* cells, since the average number of mitochondria within $1 \mu\text{m}^2$ of cellular area remained unchanged (1.1 for wild-type and 1.2 for *cdc48^{S565G}* cells). For quantification and statistics 62 and 128 mitochondria for wild-type and *cdc48^{S565G}* strain, respectively, were evaluated.

colonies. Therefore, a differential plating assay was conducted (Ogur and St John, 1956), in which proliferation of wild-type and *cdc48^{S565G}* cultures grown under apoptotic growth conditions, both YPGlc 13 h and 20 h, was analyzed on agar plates. YPLac (lactate) plates were used as selective respiratory medium and YPGlc (glucose) plates as selective fermentative medium. Cultures were spotted on the plates in dilution series, clockwise on six

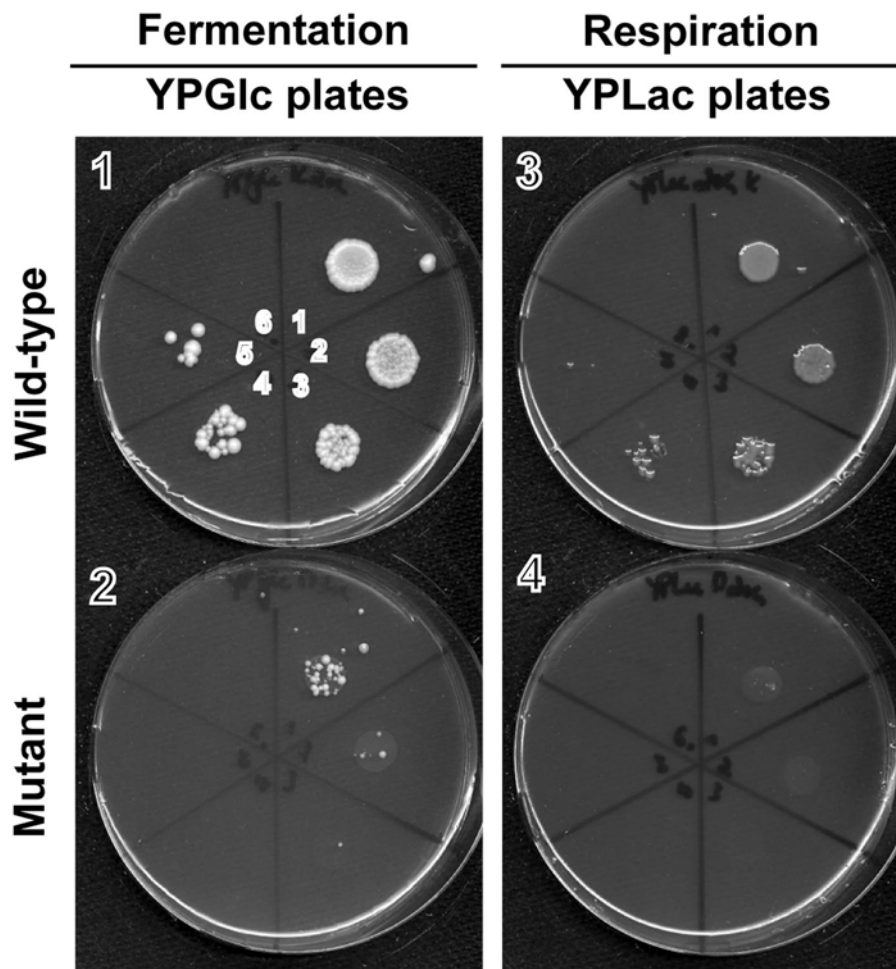


Figure 10: Respiratory deficiency of *cdc48*^{S565G} cells.

Wild-type and *cdc48*^{S565G} cultures grown under apoptotic growth conditions (20 h) were plated on YPLac (respiratory selective medium) and YPGlc (fermentative selective medium) agar plates. Cultures were spotted on the plates in logarithmic dilution series (from 5×10^6 cells to 5×10^1 cells) clockwise on six distinct sections. Section 1: 5×10^6 , section 2: 5×10^5 , section 3: 5×10^4 , section 4: 5×10^3 , section 5: 5×10^2 , section 6: 5×10^1 cells plated. Treated sections were evaluated for growth. Proliferation of *cdc48*^{S565G} cells (YPGlc) was low on YPGlc plates (plate 2) and almost completely abolished on YPLac plates (plate 4); (n=3).

distinct sections (Fig. 10, e.g., plate 1), and the proliferation of the plated cultures was subsequently evaluated.

Cdc48^{S565G} cells grown under apoptotic growth conditions (20 h) showed a markedly reduced proliferation on YPGlc plates compared to wild-type cells (Fig. 10, plates 1 and 2), demonstrating the induction of apoptotic cell death in this strain under these conditions (Fig. 6). However, the lowest level of proliferation was found on YPLac plates (Fig. 10, plate 4). The almost complete absence of proliferation of *cdc48*^{S565G} cells on obligatory respiratory YPLac plates and low but marked proliferation of *cdc48*^{S565G} cells on fermentative YPGlc plates (Fig. 10, plates 2 and 4) suggests respiratory deficiency of *cdc48*^{S565G} cells probably due to their progressed state of impaired mitochondrial functionality. Such

impairment was not detectable in wild-type cells under the same growth conditions (Fig 10, plates 1 and 3).

1.3.3 Cytochrome c accumulates in the cytosol of $cdc48^{S565G}$ cells under early apoptotic growth conditions

Cytochrome *c* is a mitochondrial protein essential for the transfer of electrons from the cytochrome *bc₁* complex to the cytochrome *c* oxidase complex of the respiratory chain (Voet and Voet, 1990). Depletion of cytochrome *c* leads to respiratory chain dysfunction and accumulation of reactive oxygen species (ROS) in yeast (Barros et al., 2003). It is a comparatively small and basic protein (12 kDa, isoelectric point of 9.5) and therefore hardly analyzable by the applied 2-DE analysis. Hence, amounts of cytochrome *c* in the cytosol under apoptotic growth conditions, both 13 h and 20 h, were evaluated using Western blot analysis. At the 13 h time point, a 2.3 fold increase of cytochrome *c* was observed in the cytosol of $cdc48^{S565G}$ cells compared to wild-type cells (Fig. 11A Western blots, for quantification see Fig. 11B). At the 20 h time point, higher amounts of cytochrome *c* were observed in the cytosol of both wild-type and $cdc48^{S565G}$ strains compared to the 13 h time point. Cytosolic cytochrome *c* amounts were found to be markedly increased also in the wild-type strain upon prolonged growth in glucose medium and sustained heat shock (20 h), however, cytosolic cytochrome *c* level of the $cdc48^{S565G}$ strain remained slightly but significantly higher (1.2 fold) compared to the wild-type strain. These data suggest a noticeably lowered threshold for cytochrome *c* release into the cytosol of $cdc48^{S565G}$ cells, since in the $cdc48^{S565G}$ strain high amounts of cytochrome *c* were already observed at the 13 h time point but in the wild-type strain not before the 20 h time point. Thus, release of cytochrome *c* into the cytosol preceded protein alterations in mitochondrial extracts observed by differential 2-DE (Figs. 7 and 8, Table 16) that became significant predominantly not until the 20 h time point. These data point to cytochrome *c* release being an early event taking place in the $cdc48^{S565G}$ strain under apoptotic growth conditions.

1.3.4 Reactive oxygen species (ROS) accumulate in $cdc48^{S565G}$ cells under early apoptotic growth conditions

Since Barros et al. have demonstrated that release of cytochrome *c* from mitochondria causes accumulation of ROS in yeast (Barros et al., 2003), it was of particular interest whether ROS accumulation occurs concomitantly with cytochrome *c* release. Cells with

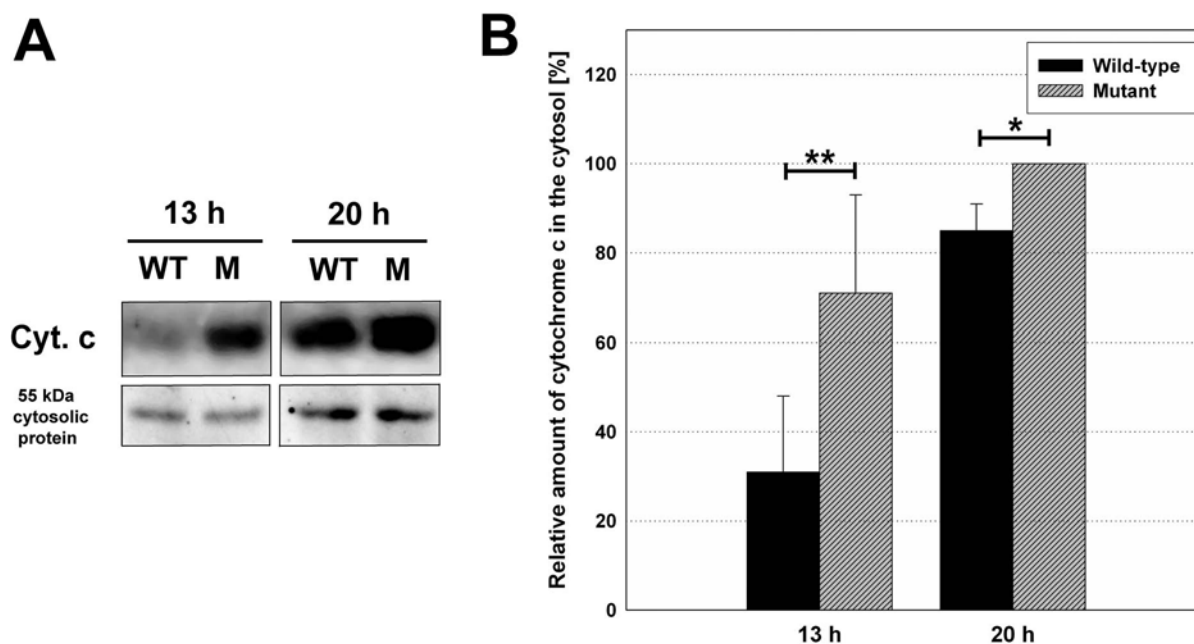


Figure 11: Release of cytochrome *c* into the cytosol of *cdc48*^{S565G} cells.

Increased amounts of cytochrome *c* were found in the cytosol in *cdc48*^{S565G} compared to wild-type cells under apoptotic growth conditions (13 h and 20 h, respectively).

(A) Representative Western blot of cytochrome *c* in cytosolic extracts (10 µg protein load per lane). The 55 kDa cytosolic protein was used as loading control. SDS-PAGE and Western transfer of provided cytosolic extracts was done in collaboration by Silvia Engelhardt (Prof. Frank Madeo, University of Tübingen, Germany).

(B) Histogram showing levels of cytochrome *c* in the cytosol. The level of cytochrome *c* in the cytosol of *cdc48*^{S565G} cells at the 20 h time point was set to 100% in every single experiment. At the 13 h time point, a 2.3 fold higher amount of cytochrome *c* was observed in the cytosol of *cdc48*^{S565G} compared to wild-type cells. At the 20 h time point, 1.2 fold more cytochrome *c* was detected in *cdc48*^{S565G} compared to wild-type cells. Note that yeast cultures grown on (fermentative) glucose medium contain relatively fragile mitochondria. The significantly increased amounts of cytochrome *c* levels in the cytosol of *cdc48*^{S565G} cells suggest for higher fragility of mitochondria compared to wild-type cells. The data shown here are percent change values of five independent experiments. Western blot quantification was done using QuantityOne® software. **p*<0.05, ***p*<0.01, Student's *t*-test (paired). Error bars: s.d.

increased levels of ROS were identified by their capability to oxidize dihydrorhodamine 123 to the red fluorescent dye rhodamine. In fact, a highly similar progression for ROS accumulation and occurrence of cytochrome *c* in the cytosol was observed (compare Figs. 11B and 12B). At the 13 h time point, a 2.5 fold higher number of *cdc48*^{S565G} cells demonstrated accumulation of ROS compared to wild-type cells (Fig. 12A and 12B). 48% of *cdc48*^{S565G} cells but only 19% of wild-type cells showed elevated levels of ROS under these growth conditions. At the 20 h time point, the number of ROS accumulating cells was found to be considerably increased in the wild-type strain upon prolonged growth in glucose medium and sustained heat shock (20 h), however, the number of cells with elevated levels of ROS remained significantly higher (1.6 fold) in the mutant strain (Fig. 12B). 59% of mutant cells but only 36% of wild-type cells accumulated ROS at the 20 h time point. These data suggest a markedly lowered threshold for ROS accumulation in the *cdc48*^{S565G} strain, since

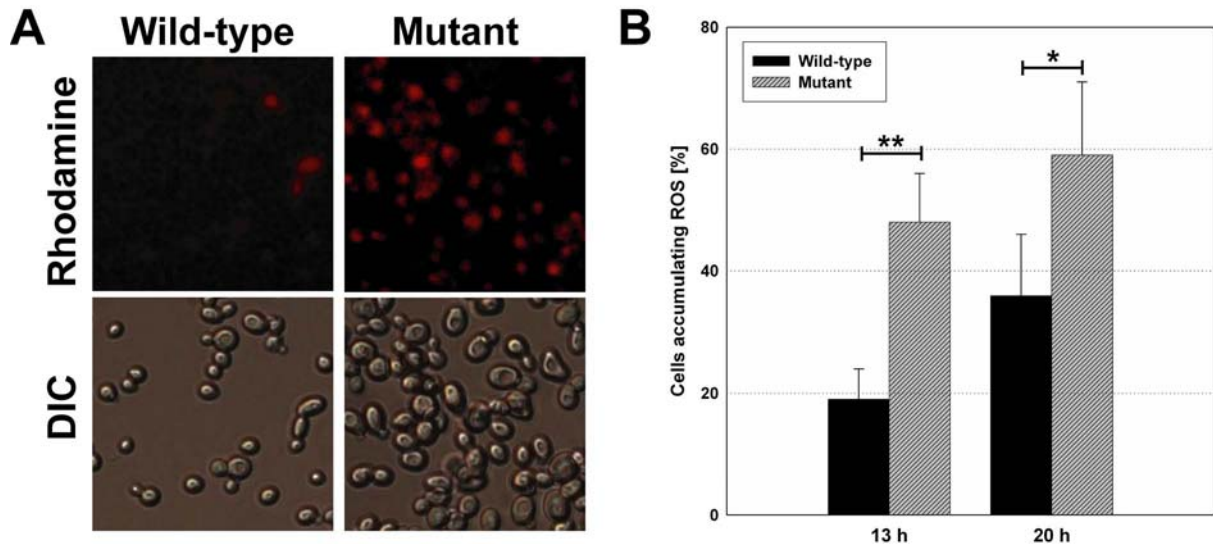


Figure 12: Reactive oxygen species accumulate in *cdc48*^{S565G} cells.

A higher number of *cdc48*^{S565G} cells demonstrated elevated levels of ROS compared to wild-type cells under apoptotic growth conditions (13 h and 20 h, respectively). Yeast cells were incubated with dihydrorhodamine 123 (DHR 123). Cells accumulating ROS oxidize DHR 123 to the red fluorescence dye rhodamine resulting in red fluorescent yeast cells.

(A) Representative micrographs of wild-type and *cdc48*^{S565G} cells at the 13 h time point.

(B) Histogram showing the number of ROS accumulating cells under apoptotic growth conditions (13 h and 20 h). At the 13 h time point, 2.5 fold more mutant cells show elevated levels of ROS compared to wild-type cells. At the 20 h time point, a 1.6 fold higher number of mutant cells accumulate ROS compared to wild-type cells. The data shown here are mean values of three independent experiments for the 13 h time point and four independent experiments for the 20 h time point. * $p < 0.05$.

high numbers of cells with elevated levels of ROS were found in the *cdc48*^{S565G} strain at the 13 h time point but in the wild-type strain not before the 20 h time point. Thus, emergence of ROS is, concomitant to cytochrome *c* release (Fig. 11), an early event under apoptotic growth conditions in the *cdc48*^{S565G} strain.

1.3.5 Accumulating ROS are predominantly produced by the mitochondrial cytochrome *bc*₁ complex

The observed respiratory deficiency of *cdc48*^{S565G} cells (Fig. 10), the release of cytochrome *c* into the cytosol (Fig. 11) paralleled by the emergence of ROS (Fig. 12) and the protein spot alterations of the ‘ubiquinol-cytochrome *c* reductase iron-sulfur subunit’ (UCRI, Table 16), a component of the cytochrome *bc*₁ complex of the inner mitochondrial membrane, suggest a disturbance of the respiratory chain. It is known that the cytochrome *bc*₁ complex, upon dysfunction, is a major cellular producer of ROS (Fang and Beattie, 2003). In order to elucidate if this complex significantly contributes to the observed elevated ROS levels in the *cdc48*^{S565G} strain, yeast cells were grown under apoptotic growth conditions (13 h) in presence of inhibitors of this complex, myxothiazol and stigmatellin (Crofts et al., 1999; Fang and Beattie, 2003; Pozniakovsky et al., 2005). Both inhibitors interrupt the electron transfer within

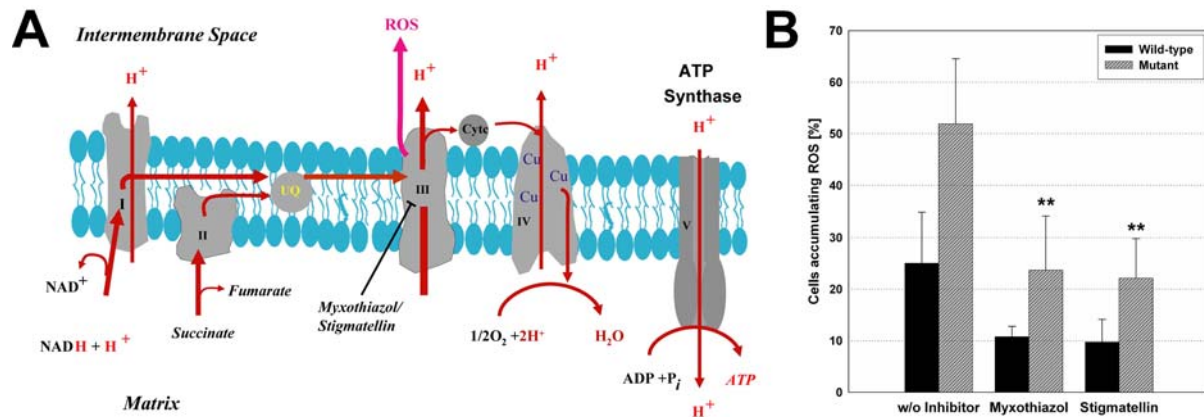


Figure 13: The cytochrome bc_1 complex is a major producer of ROS in $cdc48^{S565G}$ cells.

(A) Respiratory chain. The respiratory chain located in the inner mitochondrial membrane consists of five complexes (I-V). Complex III, also known as cytochrome bc_1 complex, is upon impairment of the inner mitochondrial membrane a major producer of ROS. ROS production in the cytochrome bc_1 complex can be inhibited using specific inhibitors that prevent the transfer of electrons to O_2 (see text). This figure is essentially based on a presentation of Prof. Osiewacz (University of Frankfurt a.M., Germany).

(B) Inhibition of the cytochrome bc_1 complex. Cultures were grown under apoptotic growth conditions (13 h) in the presence of inhibitors of the cytochrome bc_1 complex (myxothiazol and stigmatellin, respectively, 1 μ M) and tested for accumulation of ROS as described in Fig. 12 ($n=4$ for myxothiazol, $n=3$ for stigmatellin). In the case of the $cdc48^{S565G}$ strain, the number of ROS accumulating cells decreased from 52% to 24% for myxothiazol ($p<0.01$) and 22% for stigmatellin ($p<0.01$). The number of wild-type cells showing ROS accumulation was reduced from 25% to 11% ($p<0.05$) and 10% ($p<0.05$), respectively. For quantification >1000 cells per strain and experiment were evaluated. ** $p<0.01$, Student's t-test (unpaired). Error bars: s.d.

the cytochrome bc_1 complex (Fig. 13A) (Crofts et al., 1999; Fang and Beattie, 2003). Applying these inhibitors, a significant reduction in the number of cells showing ROS accumulation was observed. In the $cdc48^{S565G}$ strain the proportion of ROS-positive cells was reduced from 52% to 24% and 22% for myxothiazol and stigmatellin, respectively (Fig. 13B). These data suggest that the mitochondrial cytochrome bc_1 complex is a major site of ROS production in the $cdc48^{S565G}$ strain. Quenching of ROS production was also observed in the wild-type strain treated with inhibitors of the cytochrome bc_1 complex. However, the significant higher number of cells with elevated levels of ROS in the $cdc48^{S565G}$ strain compared to the wild-type strain, point to a higher susceptibility of mitochondria in the $cdc48^{S565G}$ strain to produce the detrimental ROS.

1.3.6 ρ^0 strains generated from wild-type and $cdc48^{S565G}$ strains are unable to produce ROS and demonstrate highly similar viability under apoptotic growth conditions

Mitochondrial contribution to the accumulation of ROS in the $cdc48^{S565G}$ strain suggests that the observed impairment of mitochondria may lead to cellular damage. In order to validate such a destructive role of mitochondria, the $CDC48$ wild-type and the $cdc48^{S565G}$ mutant strains (ρ^+ strains) were converted into yeast strains lacking functional mitochondria (ρ^0 strains) by overnight growth on media containing ethidium bromide, resulting in the loss

of mitochondrial DNA. Lack of mitochondrial functionality was confirmed by complete lack of growth on media containing obligatory respiratory carbon sources (glycerol). The generation of the ρ^0 strains and all the experiments with these strains (this chapter and Fig. 14) were performed in collaboration by Tobias Eisenberg and Sabrina Büttner (Prof. Frank Madeo, University of Graz, Austria).

ρ^0 and ρ^+ strains were evaluated for the emergence of ROS under apoptotic growth conditions (13 h). In both ρ^0 strains (wild-type and *cdc48*^{S565G} mutant), cells accumulating ROS were present only sporadically (Fig. 14A). Further analysis revealed a highly significant decrease in the production of ROS in both ρ^0 strains compared to the respective ρ^+ strains (Fig. 14B), *i.e.*, 88% and 62% reduction of ROS production in *cdc48*^{S565G} and in wild-type, respectively. These data confirm the considerable involvement of mitochondria in both wild-type and *cdc48*^{S565G} strains in the production of ROS as was already suggested by the decrease of ROS production via inhibition of the cytochrome *bc₁* complex of the respiratory chain (Fig. 13). Notably, ROS production between the wild-type ρ^0 and the *cdc48*^{S565G} ρ^0 strains assimilated at very low levels (Fig. 14B), further arguing that in the *cdc48*^{S565G} strain impaired mitochondria are responsible for the elevated levels of ROS.

In order to assess the viability of both ρ^+ and ρ^0 cultures under apoptotic growth conditions (13 h), a survival plating assay was applied. In this assay equal numbers of cells were plated onto YPGlc plates and the numbers of formed colonies were determined. The *cdc48*^{S565G} ρ^+ strain showed a significant lower viability (30% decrease) than the wild-type ρ^+ strain (Fig. 14C), as evidenced by the decreased number of formed colonies. In contrast, the viabilities of the *cdc48*^{S565G} ρ^0 and the wild-type ρ^0 strains became highly similar (Fig. 14C). Notably, the viability of the *cdc48*^{S565G} ρ^0 strain lacking functional mitochondria was slightly higher (16% increase) than the viability of the *cdc48*^{S565G} ρ^+ strain. These data hint to a deleterious role of the impaired mitochondria in the mutant *cdc48*^{S565G} strain.

1.3.7 Caspase-like enzymatic activity emerges in *cdc48*^{S565G} cells under early apoptotic growth conditions

Recently, a yeast protein demonstrating caspase-like enzymatic activity upon applied oxidative stress has been described (Madeo et al., 2002b). Since accumulation of ROS was observed in *cdc48*^{S565G} cells even under early apoptotic growth conditions (13 h, Fig. 12), wild-type and *cdc48*^{S565G} cells were evaluated for caspase-like enzymatic activity *in vivo* under these conditions. The analysis of wild-type and *cdc48*^{S565G} cells for caspase-like

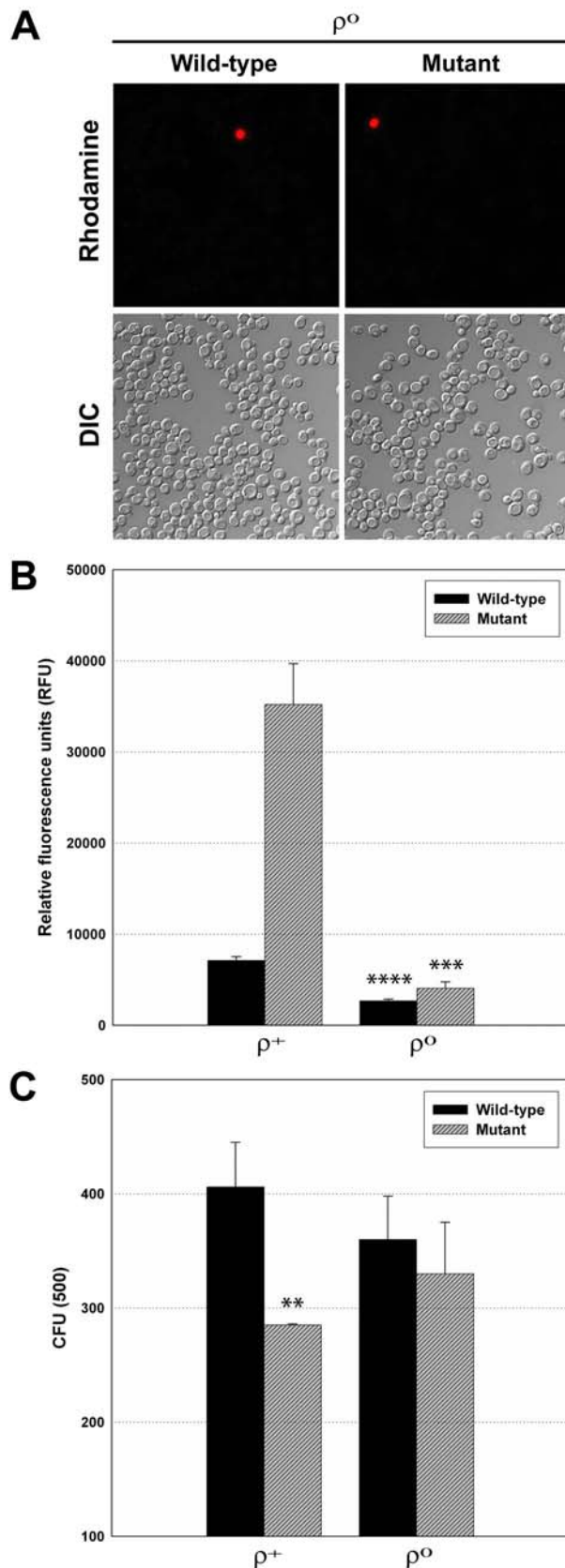


Figure 14: Wild-type ρ^0 and $cdc48^{S565G}$ ρ^0 strains showed very low levels of ROS production and highly similar viability.

CDC48 wild-type and *cdc48^{S565G}* mutant strains (ρ^+ strains) were converted into yeast strains lacking functional mitochondria (ρ^0 strains). ρ^+ and ρ^0 strains were grown under apoptotic growth conditions (13 h) and evaluated for the emergence of ROS and for cell viability. The generation of the ρ^0 strains and all the experiments with these strains were performed in collaboration by Tobias Eisenberg and Sabrina Büttner (Prof. Frank Madeo, University of Graz, Austria).

(A) ρ^0 strains are unable to accumulate ROS. Representative micrographs of wild-type ρ^0 and *cdc48^{S565G}* ρ^0 cells stained with dihydroethidium.

(B) Quantification of ROS accumulation in ρ^0 and ρ^+ strains. ROS accumulation was measured in a fluorescence reader after staining with dihydroethidium. In the case of the *cdc48^{S565G}* strains, ROS accumulation was decreased by 88% in the ρ^0 strain compared to the ρ^+ strain (from 35200 RFU to 4100 RFU, *** $p < 0.001$). ROS accumulation in the wild-type ρ^0 strain was found to be reduced by 62% compared to the wild-type ρ^+ strain (from 7100 RFU to 2700 RFU, **** $p < 0.0001$). Note that ROS production in the *cdc48^{S565G}* ρ^0 and wild-type ρ^0 strains assimilated at very low levels. In contrast, the *cdc48^{S565G}* ρ^+ strain showed significant higher levels of ROS compared to the wild-type ρ^+ strain. The data shown here are mean values of three independent experiments. p -values: Student's t -test (unpaired). Error bars: s.d.

(C) *Cdc48^{S565G}* ρ^0 strain shows highly similar viability compared to the wild-type ρ^0 strain. For each culture, ρ^0 and ρ^+ , 500 cells were plated on YPGlc plates and the number of formed colonies (colony forming unit, CFU) was determined. The viability of the *cdc48^{S565G}* ρ^0 strain was highly similar when compared to the wild-type ρ^0 strain (8% lower viability of the *cdc48^{S565G}* ρ^0 strain compared to the wild-type ρ^0 strain, $p = 0.42$). In contrast, the *cdc48^{S565G}* ρ^+ strain revealed a significant decreased viability compared to the wild-type ρ^+ strain (30% decrease, $p < 0.01$). Notably, the viability of the *cdc48^{S565G}* ρ^0 strain was found to be increased compared to the *cdc48^{S565G}* ρ^+ strain. The data shown here are mean values of three independent experiments. p -values: Student's t -test (unpaired). Error bars: s.d.

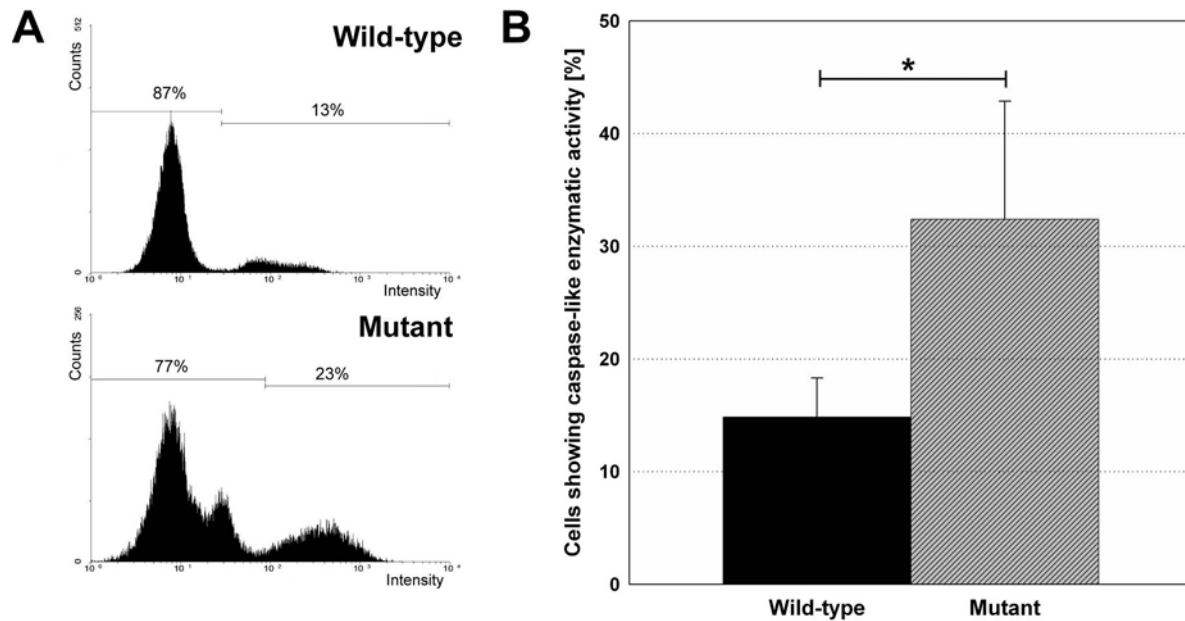


Figure 15: Emergence of caspase-like enzymatic activity in the *cdc48*^{S565G} strain.

Wild-type and *cdc48*^{S565G} cells were grown under apoptotic growth conditions (13 h) and labeled for active caspase by the cell permeable fluorescence-labeled caspase inhibitor FITC-VAD-FMK and analyzed by flow cytometry. The analysis of wild-type and *cdc48*^{S565G} cells for caspase-like enzymatic activity was performed in collaboration by Silke Wissing (Prof. Frank Madeo, University of Tübingen, Germany).

(A) Representative flow cytometric diagrams of wild-type and *cdc48*^{S565G} strain. The nature of the second peak in the flow cytometric diagram of the *cdc48*^{S565G} strain remained unknown.

(B) Quantification of caspase activity. A 2.2 fold increase in caspase activity was observed in the *cdc48*^{S565G} compared to the wild-type strain. The data shown here are mean values of three independent experiments. **p*<0.05, Student's t-test (unpaired). Error bars: s.d.

enzymatic activity (this chapter and Fig. 15) was performed in collaboration by Silke Wissing (Prof. Frank Madeo, University of Tübingen, Germany). Cells were labeled for active caspase with the fluorescence-tagged and cell permeable caspase inhibitor FITC-VAD-FMK and analyzed by flow cytometry. A significantly higher portion of *cdc48*^{S565G} cells compared to wild-type cells (2.2 fold) demonstrated caspase-like enzymatic activity under early apoptotic growth conditions (13 h) (Fig. 15A, for quantification see Fig. 15B). Thus, the emergence of caspase-like enzymatic activity paralleled the accumulation of ROS (Fig. 14), suggesting that caspase activity is triggered by endogenous oxidative stress.

In summary, mutation of *CDC48* (*cdc48*^{S565G}) is correlated with distinct alterations of mitochondrial proteins in mitochondrial extracts under apoptotic growth conditions (Figs. 7 and 8, Table 16) that are associated with mitochondrial swelling (Fig. 9), respiratory deficiency of the yeast cells (Fig. 10), release of cytochrome *c* into the cytosol (Fig. 11), and accumulation of ROS (Fig. 12) produced by the mitochondrial cytochrome *bc*₁ complex of the respiratory chain (Fig. 13). Mitochondria play a deleterious role since the mitochondria-

deficient *cdc48*^{S565G} (ρ^0) yeast strain is nearly unable to produce ROS (Fig. 14) and shows higher viability than the *cdc48*^{S565G} (ρ^+) strain under apoptotic growth conditions (Fig. 14). These cellular events are correlated with the induction of apoptotic cell death as evidenced by the emergence of caspase-like enzymatic activity (Fig. 15) and DNA fragmentation (Fig. 6).

1.4 Cdc48p-S565G dysfunction in ERAD is paralleled by increased association of NE-ER and mitochondria

Differential 2-DE analysis of mitochondrial extracts from *CDC48* wild-type and *cdc48^{S565G}* mutant yeast strain revealed accumulation of several NE-ER-associated proteins, especially Cdc48p-S565G itself, under apoptotic growth conditions (Figs. 7 and 8, Table 16). Cdc48p is an essential component of the ubiquitin-dependent ER-associated protein degradation (ERAD) pathway (Dai and Li, 2001; Elkabetz et al., 2004; Jarosch et al., 2002; Richly et al., 2005; Ye et al., 2001). Since it has been shown that the activity of the ERAD pathway is reduced in the *cdc48^{S565G}* strain (Jarosch et al., 2002), enrichment of Cdc48p-S565G and other NE-ER-associated proteins, especially of the two proteasomal components PRE3 and Y7, in mitochondrial extracts under apoptotic growth conditions (Figs. 7 and 8, Table 16) suggests that ERAD dysfunction affects mitochondria. This could then subsequently lead to the observed mitochondrial impairment described in Results 1.3. To address this hypothesis, dysfunction of the ubiquitin-proteasome-dependent ERAD pathway was explored and the way how such a dysfunction may impair mitochondria was investigated.

1.4.1 CDC48 mutation (*cdc48^{S565G}*) leads to accumulation of polyubiquitinated proteins and ER stress

In order to investigate whether the ubiquitin-dependent protein degradation pathway was impaired in the *cdc48^{S565G}* strain, the cellular amount of polyubiquitinated proteins was examined by Western blot. Accumulation of polyubiquitinated proteins was observed in total cell extracts of *cdc48^{S565G}* cells compared to wild-type cells (Fig. 16, panel 2). These data suggest that the *CDC48* mutation (*cdc48^{S565G}*) leads to dysfunction of this protein in the ubiquitin-dependent protein degradation pathway.

Wild-type Cdc48p was described to be essential for the degradation of ER luminal and ER membrane proteins in the ER-associated protein degradation (ERAD) pathway (Elkabetz et al., 2004; Jarosch et al., 2002; Richly et al., 2005; Ye et al., 2001). The observed dysfunction of

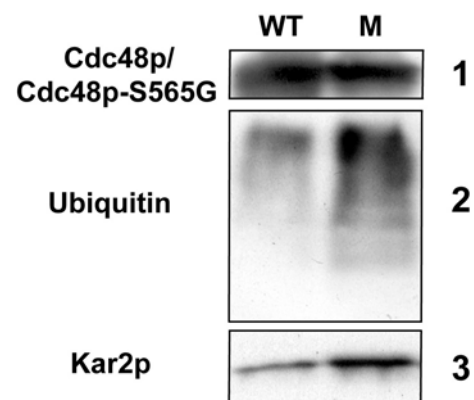


Figure 16: *CDC48* mutation (*cdc48^{S565G}*) leads to accumulation of polyubiquitinated proteins and ER stress.

The content of polyubiquitinated proteins of total cell extracts from galactose cultures was determined, applying Western blot analysis using an ubiquitin antibody (panel 2). The ER stress and proliferation marker Kar2p was enriched 5 fold (panel 3, $n=4$, $p=0.02$, Student's t-test paired, QuantityOne[®] software). Cdc48p and Cdc48p-S565G, respectively, demonstrate equal expression levels (panel 1). Protein load of total cell extracts per lane was 15 μ g.

Cdc48p-S565G in protein degradation (Fig 16, panel 2) may result in stress for the ER. Therefore the amount of the ER stress marker Kar2p (Kohno et al., 1993; Menzel et al., 1997) was measured, and indeed a 5 fold enrichment of this protein in the *cdc48*^{S565G} compared to the wild-type strain was observed (Fig. 16, panel 3). These data in combination with the overall increase of polyubiquitinated proteins suggest that dysfunctional Cdc48p-S565G causes ERAD malfunction, resulting in the induction of ER stress.

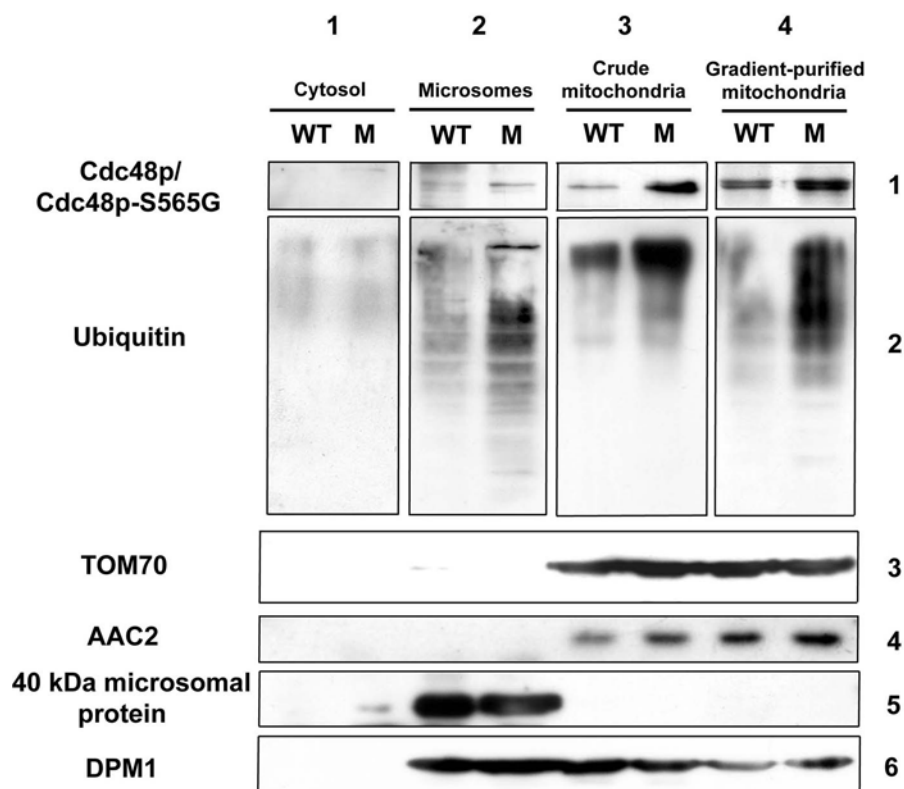
*1.4.2 Polyubiquitinated proteins, Cdc48p-S565G and microsomes stably co-migrate with mitochondria in the *cdc48*^{S565G} strain under apoptotic growth conditions*

In order to analyze which cellular compartments are affected by ERAD dysfunction under apoptotic growth conditions (20 h), subcellular fractions were evaluated for the content of polyubiquitinated proteins. Due to the observed linkage between *CDC48* mutation and the occurrence of polyubiquitinated proteins in total cell extracts these fractions were also probed for the presence of Cdc48p/Cdc48p-S565G.

Neither polyubiquitinated proteins nor Cdc48p/Cdc48p-S565G were found in cytosolic extracts (Fig. 17, column 1, panels 1 and 2). However, in microsomal extracts a 3.2 fold higher amount of Cdc48p-S565G compared to Cdc48p and markedly higher amounts of polyubiquitinated proteins in *cdc48*^{S565G} compared to wild-type strain were observed (Fig. 17, column 2, panels 1 and 2, for quantification see Table inset). Accumulation of polyubiquitinated proteins and Cdc48p-S565G in the microsomal fraction paralleled by the absence of these proteins in the cytosol underlines ERAD dysfunction due to *CDC48* mutation (Fig. 16).

Interestingly, a strong accumulation of polyubiquitinated proteins and Cdc48p-S565G was also observed in mitochondrial fractions (Fig. 17, column 3, panels 1 and 2). Similar to the microsomal extracts, mitochondrial fractions comprised a 2.5 fold higher amount of Cdc48p-S565G compared to Cdc48p and markedly higher amounts of polyubiquitinated proteins in *cdc48*^{S565G} compared to the wild-type strain. These data show that ERAD dysfunction in the *cdc48*^{S565G} strain under apoptotic growth conditions affects both microsomal and mitochondrial fractions.

In order to analyze the connection of ERAD dysfunction and mitochondria in the *cdc48*^{S565G} strain under apoptotic growth conditions (20 h), crude mitochondria, *i.e.*, mitochondria isolated by differential centrifugation, were further purified by sucrose gradient centrifugation. There again, a stable co-migration of both polyubiquitinated proteins and



Western Blot Quantification

Anti-body	Cytosol		Microsomes		Crude mitochondria		Gradient-purified mitochondria		Panel
	WT	M	WT	M	WT	M	WT	M	
Cdc48p	-	-	0.13	0.40	0.31	0.78	0.50	1.00	1
TOM70	-	-	<0.10	<0.10	0.83	1.01	0.93	1.00	3
AAC2	-	-	-	-	0.63	0.84	0.87	1.00	4
40 kDa	<0.10	<0.10	0.98	1.00	-	-	-	-	5
DPM1	-	-	0.96	1.00	0.90	0.75	0.45	0.58	6

Figure 17: Polyubiquitinated proteins and Cdc48p-S565G co-migrate with microsomes and mitochondria in the *cdc48^{S565G}* strain.

Subcellular fractions of wild-type (WT) and *cdc48^{S565G}* mutant (M) strain under apoptotic growth conditions were analyzed by Western blot for Cdc48p/Cdc48p-S565G (panel 1) and the content of polyubiquitinated proteins (panel 2). Compared to Cdc48p, Cdc48p-S565G was increased in microsomes, crude mitochondria, and gradient-purified mitochondria by 3.2, 2.5 and 2.0 fold, respectively (n=3, p<0.05, Student's t-test, unpaired). High levels of polyubiquitinated proteins were found in fractions with high amounts of Cdc48p-S565G. Cytosolic (column 1), microsomal (column 2) and crude mitochondrial extracts (column 3) were obtained by differential centrifugation; gradient-purified mitochondria (column 4) were obtained by further purification by linear sucrose gradient centrifugation. TOM70 (outer mitochondrial membrane) and AAC2 (inner mitochondrial membrane) were used as marker for mitochondria, 40 kDa microsomal protein and DPM1 as marker for light and heavy microsomes, respectively. Protein load per lane: 10 µg. Western blot quantification was done using QuantityOne[®] software. Signal intensities of gradient-purified mitochondria from mutant were set to 1.00 for Cdc48p/TOM70/AAC2. For 40 kDa and DPM1 signal intensities of microsomes from mutant were set to 1.00

Cdc48p-S565G with gradient-purified mitochondria was observed (Fig. 17, column 4, panels 1 and 2, for quantification see Table inset). Similar to crude mitochondria, in gradient-purified mitochondria a 2.0 fold higher amount of Cdc48p-S565G compared to Cdc48p and markedly higher amounts of polyubiquitinated proteins in *cdc48^{S565G}* compared to the wild-type strain were observed. Microsomal content, as evidenced by the heavy microsomal marker DPM1, was decreased in mitochondria purified by sucrose gradient centrifugation

(Fig. 17, column 4, panel 6, Table inset). However, in the *cdc48*^{S565G} strain markedly more DPM1 remained associated with mitochondria compared to the wild-type strain. Thus, in the *cdc48*^{S565G} strain under apoptotic growth conditions mitochondria are stably co-migrating with polyubiquitinated proteins, Cdc48p-S565G and microsomes.

1.4.3 Zone-electrophoresis in a free-flow device (ZE-FFE) allows the separation of a NE-ER-containing mitochondrial side fraction from the mitochondrial main fraction in wild-type and *cdc48*^{S565G} strain

The observed stable co-migration of polyubiquitinated proteins and Cdc48p-S565G with mitochondria in the *cdc48*^{S565G} strain under apoptotic growth conditions (Fig. 17) could be a result of ubiquitination of mitochondrial proteins. Alternatively, ERAD dysfunction due to *CDC48* mutation could result in microsomes with increased levels of polyubiquitinated proteins that demonstrate an augmented association with mitochondria under apoptotic growth conditions. In order to distinguish these two hypotheses, crude mitochondria, obtained by differential centrifugation, were further analyzed by zone-electrophoresis (ZE) using a free-flow electrophoresis device (FFE) that separates mitochondria according to their surface charge and hydrodynamic properties (Hannig and Heidrich, 1990; Zischka et al., 2006; Zischka et al., 2003). In ZE-FFE, crude mitochondria were continuously applied at the cathodal side of the separation chamber and transported with a continuous laminar buffer flow through the separation chamber (Fig. 18A). An electric field oriented perpendicular to the buffer flow led to specific deflection of mitochondria and associated organelles. Mitochondria strongly associated with microsomes should have different surface properties and therefore deflect differently in this device compared to purified mitochondria.

In separation profiles of both wild-type and mutant samples, a main peak was found in a fraction with equal deflection in ZE-FFE (Fig. 18B, fraction #53 in the displayed example). Beside the main fractions, side fractions (#54-59) were obtained in both wild-type and mutant strains (Fig. 18B). In this study, the terms ‘main fraction’ and ‘side fraction’ are referred to these mitochondrial fractions obtained by ZE-FFE of crude mitochondria. Interestingly, a depletion of the protein amount of the main fraction in the *cdc48*^{S565G} strain under apoptotic growth conditions (20 h) was observed. The amount of protein contained in the main fractions of the *cdc48*^{S565G} strain was only 80% of that observed in the main fractions of the wild-type strain (373 µg and 462 µg protein, respectively, from 2 mg crude mitochondrial starting material each). In contrast, a corresponding increase of protein amount was observed in the

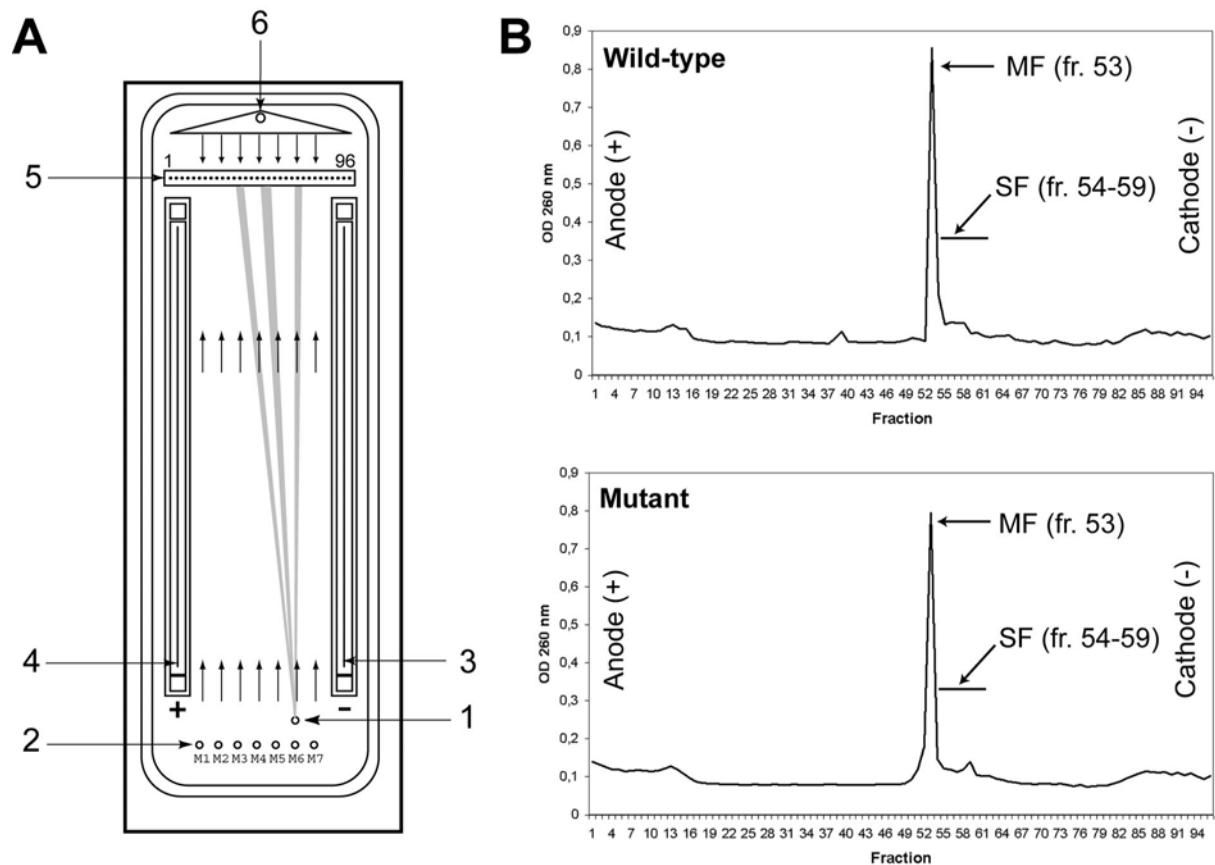


Figure 18: Crude mitochondria can be separated in a main and a side fraction by zone electrophoresis in a free-flow device (ZE-FFE).

(A) Crude mitochondria, *i.e.*, mitochondria isolated by differential centrifugation, were injected into the separation chamber via the sample inlet (no. 1) at the cathodal side (no. 3) of the chamber. They were transported with the laminar buffer flow produced by continuous input of separation media via the media inlets (no. 2) and deflected towards the anode (no. 4). At the end of the separating chamber, the laminar buffer flow was blocked via the counter flow (no. 6) and samples were fractionated in a 96-well format (no. 5). Separation was monitored by measuring the OD₂₆₀ of 200 μ L aliquots of the collected 96 fractions and illustrated as separation profile (see (B)). ZE-FFE separation conditions: (i) separation voltage: 750 V; (ii) media velocity: 400 mL/h; (iii) sample concentration: 2 mg/mL; (iv) sample velocity: 2 mL/h (v) separation temperature: 4°C.

(B) ZE-FFE separation profiles of mitochondrial preparations isolated from wild-type and *cdc48*^{S565G} strains under apoptotic growth conditions (20 h), showing main (MF, #53) and side (SF, #54-59) fractions for each strain. Mitochondria were obtained from the ZE-FFE fractions by centrifugation. (n=4).

side fractions under apoptotic growth conditions. A 30% higher protein amount in the side fractions of the *cdc48*^{S565G} strain compared to the side fractions of the wild-type strain was detected (150 μ g vs. 115 μ g protein, from 2 mg crude mitochondrial starting material each). Thus, the analyzed crude mitochondrial fractions of wild-type and *cdc48*^{S565G} strains grown under apoptotic growth conditions differed in their composition, since the side fractions are more prominent in the *cdc48*^{S565G} strain compared to the wild-type strain.

In order to analyze the protein contents of the mitochondrial fractions (crude mitochondria, main and side fractions) of wild-type and *cdc48*^{S565G} strain, mitochondrial protein extracts were separated by SDS-PAGE and protein bands were identified by MS

Table 17: Identified proteins of ZE-FFE-purified mitochondria

Protein bands of interest (SDS-PAGE of ZE-FFE main fractions) were subjected to trypsin treatment. Resulting peptides were analyzed using a Reflex III mass spectrometer. Spectra were annotated using the X-tof 5.1.0 software and subsequent database searches in the metadatabase MSDB were done with peptide mass fingerprinting queries using the Mascot 1.7 search engine as described in Material and Methods.

Protein Band No. (Fig. 19A)	Swiss-Prot Accession No. (a)	Mowse Score	Sequence Coverage [%]	Matched/ Searched Mass Values	Apparent/ Nominal Mass [kDa]	Gene Name (b)	Protein Name	Localization	Function
1	Q01852	89	22	11/35	38/49	YIL022w	Import inner membrane translocase subunit TIM44	Mitochondria, inner membrane	Protein translocation
2	P17505	131	52	14/43	32/36	YKL085w	Malate dehydrogenase	Mitochondria, matrix	Krebs cycle
2	P32473	77	36	10/43	32/40	YBR221c	Pyruvate dehydrogenase E1 component subunit beta	Mitochondria, matrix	Krebs cycle
3	P38077	101	41	11/37	28/34	YBR039w	ATP synthase gamma chain	Mitochondria, inner membrane	Respiratory chain
3	P49017	88	31	10/37	28/35	YML110c	Ubiquinone biosynthesis methyltransferase COQ5	Mitochondria	Ubiquinone biosynthesis
4	P18239	147	36	15/42	26/34	YBL030c	ADP,ATP carrier protein 2 (AAC2)	Mitochondria, inner membrane	ADP,ATP translocation
5	P09457	90	44	8/25	18/23	YDR298c	ATP synthase subunit 5	Mitochondria, inner membrane	Respiratory chain
6	P30902	151	48	11/24	17/20	YKL016c	ATP synthase D chain	Mitochondria, inner membrane	Respiratory chain

(a) Accession number in Swiss-Prot database: <http://expasy.org/sprot/>; (b) Gene name in MIPS database: <http://mips.gsf.de/>

Table 18: Identified proteins in the ZE-FFE side fractions

Protein spots (16-BAC/SDS-PAGE of ZE-FFE side fractions [Protein spots 1-35, Fig. 19B]) and protein bands (SDS-PAGE of ZE-FFE side fractions [Protein bands A-G, *e.g.*, Fig. 19A]) of interest were subjected to trypsin treatment. Resulting peptides from 16-BAC/SDS-PAGE were analyzed by the ABI 4700 Proteomics Analyser mass spectrometer. Spectra were annotated using the GPS-Explorer 2.0 software and subsequent database searches were done in the Swiss-Prot database with combined peptide mass fingerprinting (PMF) and MS/MS queries using the Mascot 1.9 search engine as described in Material and Methods. Resulting peptides from SDS-PAGE were analyzed by the Reflex III mass spectrometer. Spectra were annotated using the X-tof 5.1.0 software and subsequent database searches were done in the metadatabase MSDB with peptide mass fingerprinting queries using the Mascot 1.7 search engine as described in Material and Methods.

Protein Spot/Band No. (<i>e.g.</i> , Fig. 19)	Swiss-Prot Accession No. (a)	Mowse Score	Sequence Coverage [%]	Matched Mass Values (b)	Total Ion Score	Apparent/Nominal Mass [kDa]	Gene Name (c)	Protein Name	Localization	Function
1	P33416	69	16	11	0	72/92	YDR258c	Heat shock protein 78	Mitochondria, matrix	Protein folding
2	P12398	218	45	21	47	70/71	YJR045c	Heat shock protein SSC1	Mitochondria, matrix	Protein folding, protein translocation
3	Q00711	138	31	13	30	68/71	YKL148c	Succinate dehydrogenase flavoprotein subunit	Mitochondria, matrix	Respiratory chain
4	P32316	273	44	20	97	65/59	YBL015w	Acetyl-CoA hydrolase	Mitochondria, cytoplasm	Regulated intracellular acetyl-CoA pool
5	P19882	432	47	27	163	65/61	YLR259c	Heat shock protein 60	Mitochondria, matrix	Protein folding, protein translocation
6	P09624	213	35	15	58	60/57	YFL018c	Dihydrolipoyl dehydrogenase, pyruvate dehydrogenase complex E3 component	Mitochondria, matrix	Krebs cycle, glycine metabolism
7	P32340	100	28	13	0	60/57	YML120c	Rotenone-insensitive NADH-ubiquinone oxidoreductase	Mitochondria, inner membrane	Respiratory chain
8	P07251	549	58	27	287	58/57	YBL099w	ATP synthase alpha chain	Mitochondria, inner membrane	Respiratory chain
9	P46367	85	31	9	15	62/57	YOR374w	Potassium-activated aldehyde dehydrogenase	Mitochondria, matrix	Converts aldehydes into acids
10	P19262	76	15	5	50	55/51	YDR148c	Dihydrolipoyllysine-residue succinyltransferase component of 2-oxoglutarate dehydrogenase complex	Mitochondria, matrix	Krebs cycle
11	P00830	406	50	19	238	53/55	YJR121w	ATP synthase beta chain	Mitochondria, inner membrane	Respiratory chain
12	P00890	194	34	14	99	50/53	YNR001c	Citrate synthase	Mitochondria, matrix	Krebs cycle
13	P48015	187	31	10	96	45/45	YDR019c	Aminomethyltransferase	Mitochondria	Glycine metabolism
14	P19882	418	46	26	165	50/61	YLR259c	Heat shock protein 60	Mitochondria, matrix	Protein folding, protein translocation
15	P21954	81	24	10	0	42/48	YDL066w	Isocitrate dehydrogenase [NADP]	Mitochondria	Regulation of Krebs cycle
16	P16387	163	29	13	69	50/47	YER178w	Pyruvate dehydrogenase E1 component alpha subunit	Mitochondria, matrix	Krebs cycle
17	P28834	128	35	10	39	40/39	YNL037c	Isocitrate dehydrogenase [NAD] subunit 1	Mitochondria	Krebs cycle
18	P28241	209	38	11	118	40/40	YOR136w	Isocitrate dehydrogenase [NAD] subunit 2	Mitochondria, matrix	Krebs cycle
19	P06168	368	67	26	81	40/45	YLR355c	Ketol-acid reductoisomerase Ilv5p	Mitochondria	Amino acid metabolism, mtDNA stability
20	P07257	238	51	17	65	40/41	YPR191w	Ubiquinol-cytochrome <i>c</i> reductase complex core protein 2	Mitochondria, inner membrane	Respiratory chain
21	P32473	150	36	12	23	36/40	YBR221c	Pyruvate dehydrogenase E1 component beta subunit	Mitochondria, matrix	Krebs cycle

Results

22	P04840	349	78	18	136	33/30	YNL055c	Voltage-dependent anion-selective channel protein 1 (VDAC 1)	Mitochondria, outer membrane	Porin in the outer mitochondrial membrane
23	P18239	140	38	10	37	35/35	YBL030c	ADP,ATP carrier protein 2	Mitochondria, inner membrane	ADP,ATP translocation
24	P05626	104	39	9	12	33/27	YPL078c	ATP synthase subunit 4	Mitochondria, inner membrane	Respiratory chain
25	P09457	136	27	5	85	24/23	YDR298c	ATP synthase subunit 5	Mitochondria, inner membrane	Respiratory chain
A	P53252	110	32	10/22	-	28/38	YGR086c	Sphingolipid long chain base responsive protein PIL1 (Pil1p)	Lipid particles, mitochondria	Negative regulator of cell wall integrity in unstressed cells
B	P35691	82	39	8/38	-	18/19	YKL056c	Microtubule and mitochondria interacting protein (Mmi1p)/ (d) Translationally controlled tumor protein homolog (TCTP)	Cytoskeleton, mitochondria (d)	Interacts with microtubule and translocates to mitochondria upon oxidative stress (d)
26	P06634	209	35	20	51	72/66	YOR204w	ATP-dependent RNA helicase DED1	Ribosome, NE-ER-associated (e)	Protein biosynthesis
27	P40150	158	23	10	88	68/67	YNL209w	Heat shock protein SSB2	Ribosome, NE-ER-associated (e)	Protein biosynthesis
28	P02994	63*	21	7	12	62/50	YPR080w/ YBR118w	Elongation factor 1-alpha	Ribosome, NE-ER-associated (e)	Protein biosynthesis
29	P02992	69	24	7	15	42/48	YOR187w	Elongation factor Tu	Ribosome, NE-ER-associated (e)	Protein biosynthesis
30	P33767	208	39	14	78	52/50	YEL002c	Dolichyl-diphosphooligosaccharide-protein glycosyltransferase subunit WBP1	ER-associated	Protein biosynthesis, secretory pathway
31	P07283	87	38	8	19	25/29	YFL045c	Phosphomannomutase Sec53p	ER-associated (f)	Protein biosynthesis, secretory pathway
C	P16474	287	37	26/34	-	71/75	YJL034w	78 kDa Glucose regulated protein (GRP78/Kar2p)	ER lumen	Protein folding, protein translocation
D	Q04697	78	33	11/48	-	40/46	YML048w	Glucose signaling factor GSF2	ER membrane	Protein folding, protein translocation
E	P38911	98	21	11/31	-	58/47	YML074c	FK506-binding nuclear protein	Nucleus	Protein folding
F	P15992	111	57	10/32	-	25/24	YBR072w	Heat shock protein 26 (HSP26)	Nucleus, cytoplasm	Protein folding, stress response
32	P16140	218	46	17	44	62/58	YBR127c	Vacuolar ATP synthase subunit B	Vacuole, membrane	Acidification of vacuoles
33	P38219	187	45	14	33	42/45	YBR025c	Putative GTP-binding protein YBR025c	Cytoplasm	Unknown

(a) Accession number in Swiss-Prot database: <http://expasy.org/sprot/>; (b) Matched peptides in PMF-MS/MS queries for 16-BAC/SDS-PAGE spots; matched peptides to total peptides searched in PMF queries for SDS-PAGE bands; (c) Gene name in MIPS database: <http://mips.gsf.de/>; (d) According to (Rinnerthaler et al., 2006); (e) According to (Nicchitta, 2002); (f) According to (Ruohola and Ferro-Novick, 1987)

analysis. The protein band patterns of all fractions were highly similar, illustrating the mitochondrial content in these fractions (Fig. 19A). Moreover, protein bands comprising mitochondrial proteins (Fig. 19A, bands 1-6, Table 17), both membrane proteins (*e.g.*, TIM44 and AAC2 [Fig. 19A, bands 1 and 4]) and soluble proteins (*e.g.*, pyruvate and malate dehydrogenase [Fig. 19A, band 2]), were more pronounced in the main fractions of both wild-type and *cdc48*^{S565G} strain compared to crude mitochondria. These data indicate an enrichment of mitochondrial proteins and thus purification of mitochondria by ZE-FFE. In line with previous results (Zischka et al., submitted; Zischka et al., 2003), these purified mitochondria were obtained from the ZE-FFE main fractions.

In the ZE-FFE side fractions of both wild-type and *cdc48*^{S565G} strain, protein bands comprising mitochondrial proteins were less pronounced compared to the ZE-FFE main fractions (Fig. 19A, bands 1-6, Table 17), suggesting a decreased mitochondrial content in the side fractions. However, two mitochondria-associated proteins accumulated in the mitochondrial side fractions. The ‘sphingolipid long chain base responsive protein PIL1’ (Pil1p) (Fig. 19A, band A, Table 18) with known localization in both lipid particles and highly pure mitochondrial fractions (Sickmann et al., 2003b; Walther et al., 2006; Zhang et al., 2004), was clearly present in the side fractions of both wild-type and *cdc48*^{S565G} strains, whereas in the main fractions this protein was hardly detectable. The protein ‘microtubule and mitochondria interacting protein’ (Mmi1p) that translocates upon apoptosis-associated oxidative stress to mitochondria (Rinnerthaler et al., 2006) was found in the side fractions of the *cdc48*^{S565G} strain (Fig. 19A, band B, Table 18). Accumulation of these mitochondria-associated proteins in the side fractions suggests that these fractions may represent a subpool of mitochondria.

Therefore, the side fractions of the *cdc48*^{S565G} strain were further characterized by SDS-PAGE and 16-BAC/SDS-PAGE followed by MS analysis for identification of proteins. 16-BAC/SDS-PAGE was performed because of its lower bias against the analysis of membrane proteins compared to 2-DE analysis, allowing the separation of the mitochondrial and the potential microsomal membrane proteins within the crude mitochondrial samples (Braun et al., submitted; Hartinger et al., 1996; Islinger et al., 2006; Zahedi et al., 2005).

Beside membrane and soluble mitochondrial proteins (Fig. 19B, spots 1-25), and mitochondria-associated proteins (Fig. 19A, bands A and B), the side fractions of the *cdc48*^{S565G} strain comprised the cytoplasmic ‘putative GTP binding protein YBR025c’ (Fig. 19B, spot 32), the protein ‘vacuolar ATP synthase subunit B’ (Fig. 19B, spot 33) and

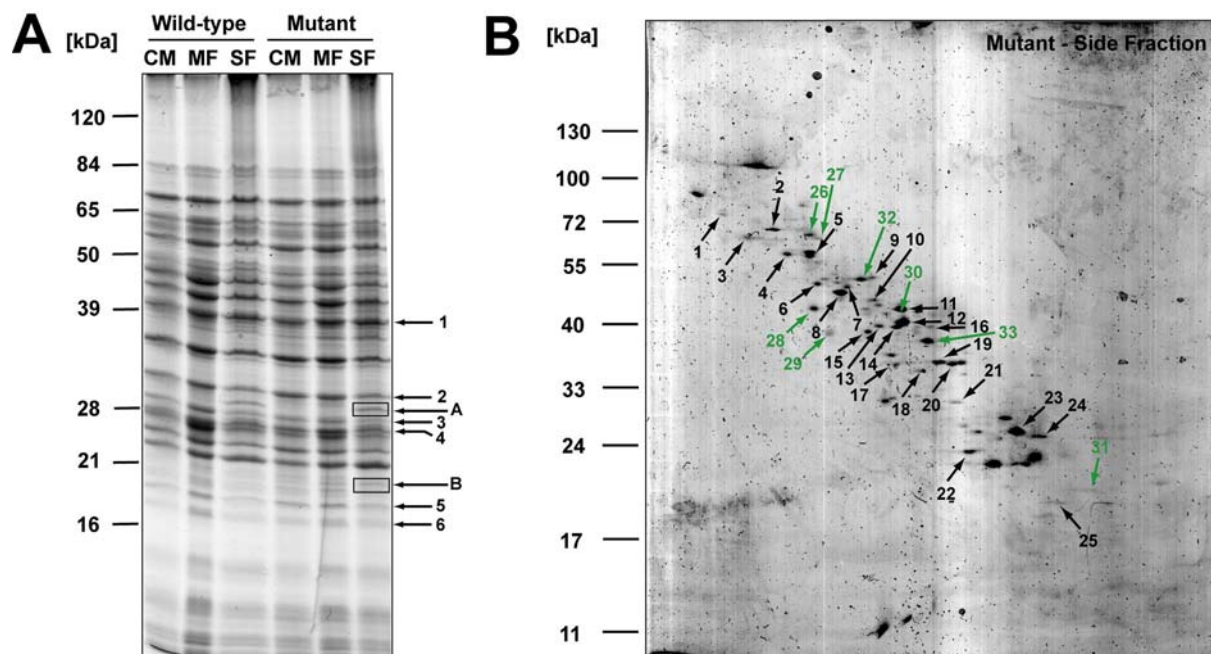


Figure 19: The ZE-FFE main fractions contain purified mitochondria, whereas the ZE-FFE side fractions represent a mitochondrial fraction enriched with NE-ER-associated proteins.

(A) SDS-PAGE analysis of crude mitochondria and mitochondria separated by ZE-FFE. Crude mitochondria (CM) from *cdc48*^{S565G} cells and wild-type cells under apoptotic growth conditions (20 h) were isolated by differential centrifugation and subjected to ZE-FFE, resulting in the separation into ZE-FFE main fractions (MF) and ZE-FFE side fractions (SF) (see Fig. 18). SDS-PAGE of CM, MF and SF resulted in highly similar protein band patterns among these different fractions. Mitochondrial proteins were identified from protein bands of the ZE-FFE main fractions by MALDI/TOF-MS (Bruker Reflex III) (bands 1-6 see Table 17). Accumulation of these proteins was observed in the MFs compared to the CMs of both *cdc48*^{S565G} and wild-type cells, indicating that MFs contained purified mitochondria. SFs, in contrast to MFs, comprised the mitochondria and lipid particle-associated protein Pil1p and the ‘mitochondria and microtubule-associated protein’ Mmi1p (bands A+B, respectively, see Table 18). 40 µg protein load per lane, Coomassie Brilliant Blue stain.

(B) 16-BAC/SDS-PAGE analysis of mitochondrial side fractions of the *cdc48*^{S565G} strain. Proteins were identified from protein spots by MALDI/TOF-MS (ABI 4700 Proteomics Analyser) (spots 1-33, see Table 18). Protein spots containing mitochondrial proteins are in black (spots 1-25), whereas protein spots containing non-mitochondrial proteins are in green (spots 26-33). The majority of non-mitochondrial proteins (spots 26-31) are known to be associated with the NE-ER. 5 µg protein load, improved colloidal Coomassie stain.

several NE-ER-associated proteins (Table 18, *e.g.*, Fig. 19B spots 26-31). The latter class included six proteins involved in protein biosynthesis (*e.g.*, the ER-associated phosphomannomutase Sec53p) and four proteins involved in protein folding in the ER lumen (‘78 kDa glucose regulated protein’, GRP78/Kar2p), ER membrane (‘glucose signaling factor’ GSF2), and the nucleus (*e.g.*, FK506-binding nuclear protein) (Table 18). Thus, protein analysis revealed that the ZE-FFE side fractions of the *cdc48*^{S565G} strain comprised a mitochondrial fraction co-migrating with NE-ER-associated proteins.

These data show that ZE-FFE analysis of crude mitochondria from wild-type and *cdc48*^{S565G} strains allowed the separation of a mitochondrial side fraction co-migrating with NE-ER-associated proteins from the mitochondrial main fraction containing mitochondria with increased purity.

1.4.4 Polyubiquitinated proteins and Cdc48p-S565G accumulate in the mitochondrial side fraction enriched with NE-ER-derived microsomes

Performing Western blot analysis, polyubiquitinated proteins and Cdc48p/Cdc48p-S565G were predominantly found in the NE-ER-comprising mitochondrial side fractions, whereas only small amounts were present in the mitochondrial main fractions (Fig. 20, columns 1 and 2, panels 1 and 2). Specific enrichment of NE-ER content (DPM1, Kar2p) in the side fractions compared to the respective main fractions, and the lower content of mitochondria (TOM70, AAC2) in these fractions (Fig. 20, columns 1 and 2, panels 3-6, for quantification see legend of Fig. 20) was confirmed. Thus, the majority of mitochondria is not affected by polyubiquitination.

Comparing the ZE-FFE side fractions of wild-type and *cdc48*^{S565G} strain grown under apoptotic growth conditions revealed increased amounts of polyubiquitinated proteins and Cdc48p-S565G in the side fraction of the *cdc48*^{S565G} strain concomitantly to enrichment of NE-ER (DPM1, Kar2p) and depletion of mitochondrial content (TOM70, AAC2) (Fig. 20, column 3, panels 1-6, for quantification see legend of Fig. 20). These data suggest that the observed elevated amounts of polyubiquitinated proteins and Cdc48p-S565G in the side fraction of the *cdc48*^{S565G} strain is due to an increased NE-ER content in this fraction.

In order to evaluate the data obtained on protein level on a morphological level, EM analysis of ZE-FFE main and side fractions of both wild-type and *cdc48*^{S565G} strain was performed. Preparation of EM sections and EM micrographs were done in collaboration by Dietmute Büringer (Max-Planck-Institute of Neurobiology, Martinsried, Germany). Whereas the main fractions were characterized as containing intact mitochondria with a high degree of purity (Fig. 21), the side fractions comprised in addition to mitochondria, a higher portion of membranous structures and microsomal vesicles (Fig. 21). Importantly, EM comparisons of the side fractions of *cdc48*^{S565G} and wild-type strains showed a significantly higher number of mitochondria-associated microsomal vesicles for the *cdc48*^{S565G} strain under apoptotic growth conditions (Fig. 21, magnified inlet). Indeed, microsomes were found only sporadically in the side fraction of wild-type cells but became a major part in *cdc48*^{S565G} cells grown under apoptotic growth conditions.

Thus, in the *cdc48*^{S565G} strain, as evidenced by (i) SDS-PAGE and 16-BAC/SDS-PAGE analysis (Fig. 19), (ii) Western blot analysis (Fig. 20) and (iii) EM analysis (Fig. 21), increased amounts of NE-ER-derived microsomes stably co-migrate with a subset of mitochondria obtained as ZE-FFE side fraction. In this side fraction, polyubiquitinated

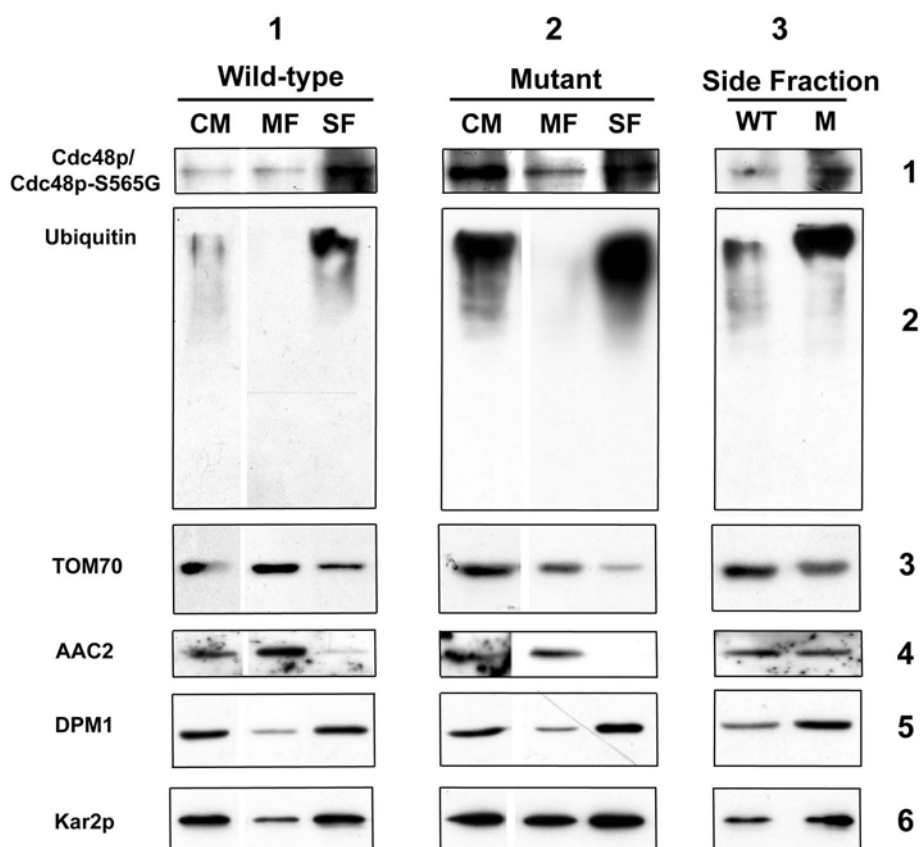


Figure 20: Polyubiquitinated proteins and Cdc48p-S565G accumulate in mitochondrial side fractions enriched with NE-ER-associated proteins obtained by ZE-FFE.

ZE-FFE fractions were further characterized by Western blot analysis. Crude mitochondrial (CM) protein extracts and ZE-FFE main (MF) and side fractions (SF) for both wild-type (WT) and mutant (M) strains grown under apoptotic growth conditions were analyzed. Fractions were tested for Cdc48p/Cdc48p-S565G and the content of polyubiquitinated proteins. TOM70 and AAC2 were used as markers for mitochondria, DPM1 as marker for heavy microsomes and Kar2p as marker for the NE-ER. Protein load per lane: 10 μ g. Western blot quantification was done using QuantityOne[®] software. (n=3).

Increased amounts of the mitochondrial proteins TOM70 (1.7 fold for wild-type, 1.5 fold for mutant) and AAC2 (4.0 fold for wild-type, 4.2 fold for mutant) were noted in the main fractions compared to the side fractions (main fraction vs. side fraction) of both strains. In contrast, less amounts of the microsomal proteins DPM1 (0.4 fold for wild-type, 0.3 fold for mutant), Kar2p (0.4 fold for wild-type, 0.5 fold for mutant) and Cdc48p/Cdc48p-S565G (0.4 fold for wild-type, 0.3 fold for mutant) were found in the main fractions compared to the side fractions.

The comparison of the side fractions of wild-type and mutant (wild-type vs. mutant) revealed increased amounts of the mitochondrial proteins TOM70 (1.2 fold) and AAC2 (1.2 fold) but decreased amounts of the microsomal proteins DPM1 (0.6 fold), Kar2p (0.5 fold) and Cdc48p/Cdc48p-S565G (0.3 fold).

proteins, Cdc48p-S565G and the ER stress marker Kar2p accumulate. These data suggest that *CDC48* mutation results in the accumulation of polyubiquitinated proteins in microsomes that show an increased association with mitochondria.

1.4.5 In *cdc48^{S565G}* cells NE-ER and mitochondria demonstrate a significantly increased spatial proximity

Subcellular fractionation (Fig. 17), protein (Fig. 19), Western (Fig. 20) and EM analysis (Fig. 21) of mitochondria separated by ZE-FFE (Fig. 19) suggest an increased

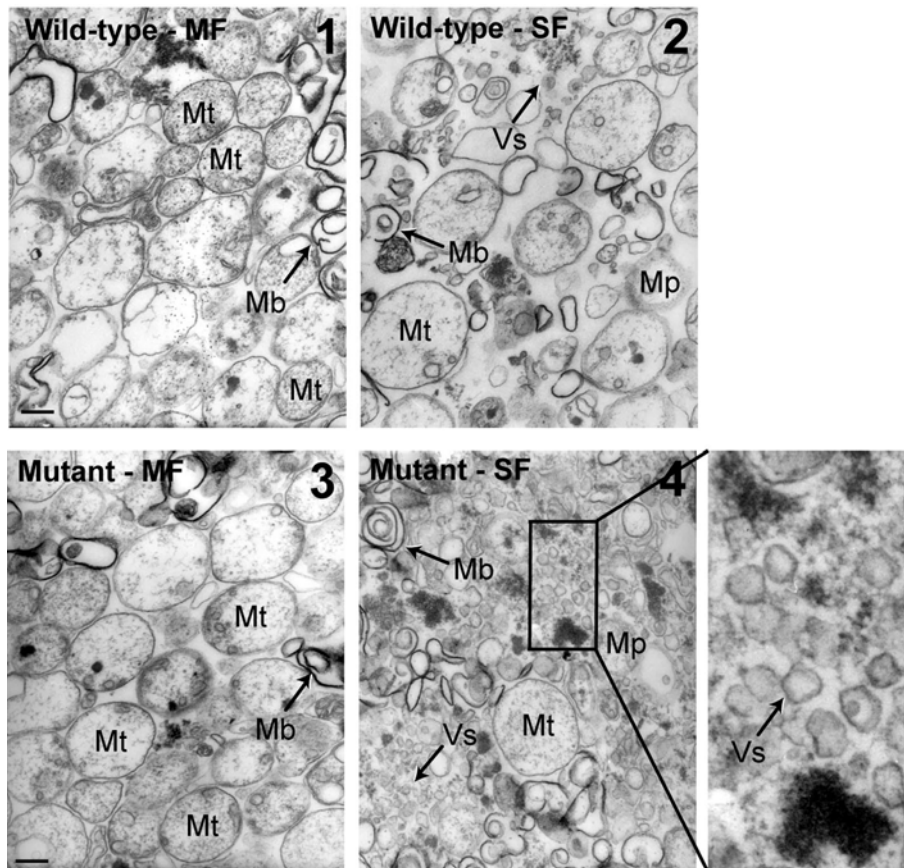


Figure 21: Microsomal vesicles stably co-migrate with mitochondria in ZE-FFE side fractions of the *cdc48*^{S565G} strain. Analysis of ZE-FFE samples by electron microscopy. Homogeneous intact mitochondria (Mt) can be observed in main fractions of both wild-type (micrograph 1) and *cdc48*^{S565G} strains (micrograph 3). Marked differences are evident in the side fractions of both strains (micrographs 2 and 4) under apoptotic growth conditions (20 h) containing intact mitochondria (Mt), mitoplasts (Mp), high-contrast membranous structures (Mb) and a low-contrast microsomal vesicle fraction (Vs). Vesicles are substantially enriched in the *cdc48*^{S565G} mutant strain as compared to wild-type (micrograph 4 and magnified section). Bar: 0.2 μ m. Preparation of EM sections and EM micrographs were done in collaboration by Dietmute Büringer (Max-Planck-Institute of Neurobiology, Martinsried, Germany).

association of microsomes and mitochondria in the *cdc48*^{S565G} strain, resulting in a stable co-migration of these organelles during the separation procedures. Therefore, yeast cells grown under apoptotic growth conditions (20 h) were directly investigated for this association by *in vivo* fluorescence microscopy and electron microscopy (EM).

In vivo double fluorescence-labeling of mitochondria and ER in *cdc48*^{S565G} and wild-type cells was done using ER-Tracker and Mito-Tracker, respectively. Due to the fact that yeast cells are small unicellular organisms ($\sim 6 \mu$ m in diameter for haploid cells) the resolution of the obtained images was very low, even when applying high resolution microscopy (Fig. 22A). However, evaluating high number of cells revealed that 37% of wild-type but 47% of *cdc48*^{S565G} cells showed an overlap between these two organelle-specific stainings (Fig. 22A, for quantification and statistics see Fig. 22C), suggesting an increased spatial proximity between mitochondria and ER in *cdc48*^{S565G} cells.

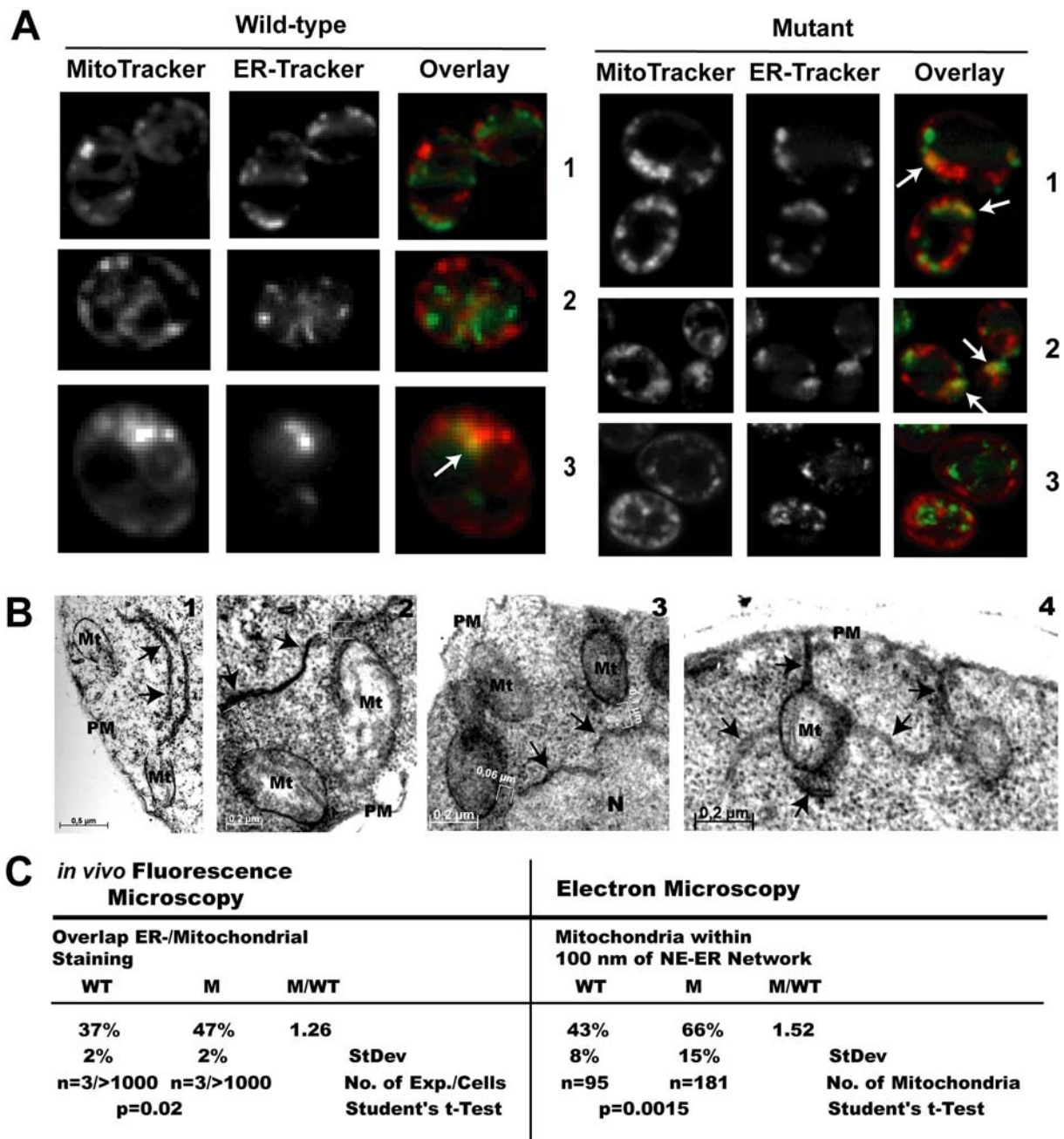


Figure 22: Mitochondria show markedly increased proximity to the NE-ER in *cdc48^{S565G}* cells.

(A) *In vivo* double fluorescence labeling of mitochondria and ER under apoptotic growth conditions (20 h). *Cdc48^{S565G}* and wild-type cells were stained with MitoTracker™ and ER-Tracker™. Image acquisition was done using a Zeiss ApoTome™ high resolution fluorescence microscope (C-Apochromat 40x/1.20, optical section thickness: 1 μm, AxioVision V.4.2). A higher number of cells, which demonstrated overlap between ER and mitochondrial staining were found in the *cdc48^{S565G}* mutant (right) strain compared to wild-type (left). Note that the obtained low resolution of the images was due to the fact that yeast cells are comparatively small unicellular organisms (~6 μm in diameter) when compared to cells from metazoans. MitoTracker™, red; ER-Tracker™, green (pseudocolor for better visualization); overlapping areas, yellow (white arrows). For quantification and statistics see (C).

(B) EM analysis of wild-type and *cdc48^{S565G}* strains under apoptotic growth conditions (20 h). Electron micrographs of *cdc48^{S565G}* cells are shown (1-4). Mitochondria are adjacent to the ER (1, 2, and 4), and NE (3). AxioVision LE V.4.2 (Zeiss) was used for distance determination between mitochondria and NE-ER membranes. For quantification see (C). PM: plasma membrane. Mt: mitochondria, N: nucleus, arrows: NE and ER.

(C) Quantitative analysis of fluorescence (A) and EM data (B). For fluorescence data, approximately 1000 cells per strain and experiment were evaluated for overlap between ER and mitochondrial staining. The p-value (Student's t-test) refers to three independent experiments (n=3). To quantify the proximity of mitochondria to NE-ER, distances between mitochondria and NE-ER were determined using AxioVision LE V.4.2 (Zeiss). The percentages of mitochondria in micrographs of both wild-type (n=6) and mutant (n=13) within close proximity (≤100 nm) to NE-ER were determined. In total, 95 and 181 mitochondria for wild-type and mutant strain, respectively, were evaluated for NE-ER proximity.

Ultrastructural analysis by EM was done in an attempt to quantify the changes in the spatial proximity between mitochondria and ER membranes, as well as the connected structures of the nuclear envelope (NE). For this purpose the distance between these structures was measured on electron micrographs of wild-type and mutant cells (Fig. 22B-C). This analysis showed that a significantly higher percentage of mitochondria in *cdc48*^{S565G} cells were in close spatial proximity (*i.e.*, ≤ 100 nm) to membranes of the NE-ER network compared to wild-type cells under apoptotic growth conditions (Fig. 22B, for quantification and statistics see Fig. 22C).

Enhanced overlap between mitochondria and ER (Fig. 22A and 22C) and increased proximity between mitochondrial and NE-ER membranes (Fig. 22B and 22C) sustain the notion of a deleterious link between these two organelles under apoptotic growth conditions.

Thus, this study proposes that in *S. cerevisiae* upon mutation of *CDC48* (*cdc48*^{S565G}), dysfunction of ER-associated protein degradation (ERAD) results in mitochondrial impairment caused by increased association of NE-ER and mitochondria. This may subsequently lead to the observed induction of mitochondria-dependent apoptotic cell death (see Results 1.3).

2. Analysis of VCP variants in mammalian cell culture

Mutation of *CDC48* in yeast (*cdc48*^{S565G} strain) leads to impairment of ER-associated protein degradation (ERAD), resulting in a high tendency to undergo mitochondria-dependent apoptotic cell death (see Results 1. and Discussion 1.). Valosin-containing protein (VCP), the highly conserved human orthologue of Cdc48p, has been proposed as a sensor for several misfolded and aggregated proteins associated with human disease (Hirabayashi et al., 2001; Mizuno et al., 2003). Upon mutation human VCP is an inductor of ‘inclusion body myopathy associated with Paget disease of bone and frontotemporal dementia’ (IBMPFD), a dominant progressive disorder characterized by protein deposits in either myofibrils or brain (Forman et al., 2006; Guyant-Marechal et al., 2006; Haubenberger et al., 2005; Kimonis and Watts, 2005; Watts et al., 2004). In order to analyze the influence of human VCP on cell viability and cell death in correlation with its functionality in the ubiquitin-dependent degradation of proteins, a mammalian cell culture system expressing human VCP variants was established.

2.1 Selection of VCP variants and generation of constructs suitable for expression in mammalian cell culture

Similar to the analysis of the *CDC48* mutation *cdc48*^{S565G} in yeast, the cellular role of VCP can be evaluated by expressing VCP variants carrying function-relevant mutations in mammalian cell cultures. For this purpose, several VCP variants were selected and cloned into a vector suitable for expression in mammalian cell cultures.

The homohexamer VCP is a type II AAA-ATPase (ATPases associated with various cellular activities). Each subunit consists of four domains, the N-terminal domain, the ATPase domains D1 and D2 comprising the conserved AAA motifs Walker A, Walker B and the ‘second region of homology’ (SRH), and the C-terminal domain (Fig. 23A), (Wang et al., 2004). The major ATPase activity of VCP is located in the D2 domain, whereas the D1 domain has only residual ATPase activity but is crucially involved in the formation of the VCP homohexamer (Song et al., 2003; Wang et al., 2004). The exchange of the amino acid lysine 524 to alanine (K524A) in the Walker A motif of the D2 domain drastically reduces the ATPase activity and functionality of VCP (Kobayashi et al., 2002; Wang et al., 2003b). It is a dominant mutation, since incorporation of only one mutated VCP subunit into the VCP hexamer is sufficient to markedly reduce the ATPase activity of the hexamer (Wang et al., 2003a; Wang et al., 2003b). Therefore, VCP-K524A was selected as a dominant loss-of-(ATPase)function variant of VCP.

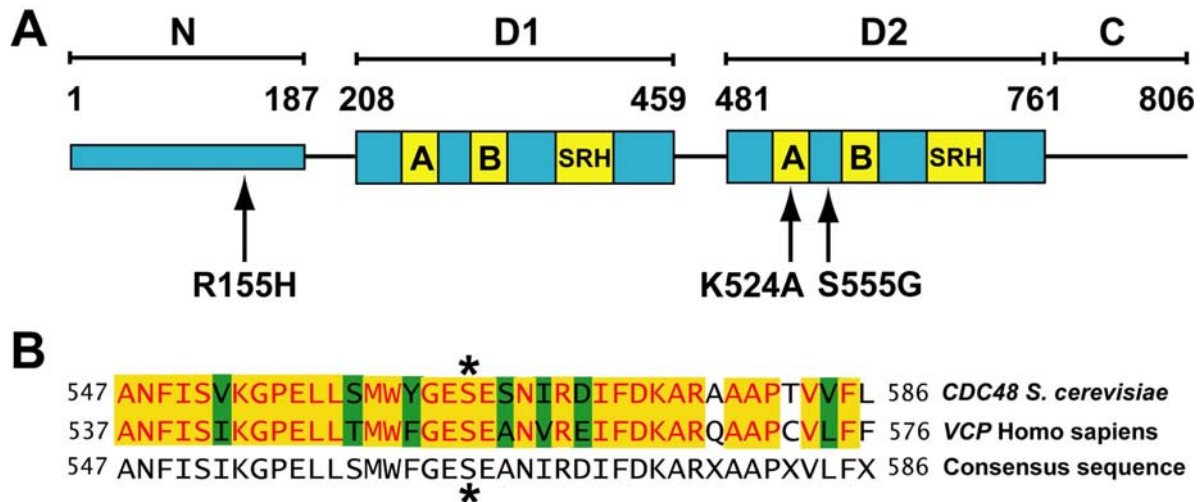


Figure 23: VCP variants used in this study.

(A) VCP domain structure and VCP mutations. VCP consists of four domains, the N-terminal domain (N), the ATPase domains D1 and D2 comprising the motifs Walker A, Walker B and the ‘second region of homology’ (SRH) motif, and the C-terminal domain (C). In VCP the major ATPase activity is located in the D2 domain. Mutation of the lysine 524 to alanine (K524A) in the Walker A motif of the D2 domain results in a VCP variant with significantly impaired ATP binding capacity and eventually in drastically reduced ATPase activity of VCP complexes. Mutation of the serine 555 to glycine (S555G) is the orthologous mutation to the serine 565 to glycine (S565G) in the *cdc48*^{S565G} mutant yeast strain (see B). The mutation of the arginine 155 to histidine (R155H) is the most frequent mutation causative for the dominant human disorder ‘inclusion body myopathy associated with Paget disease of bone and frontotemporal dementia’ (IBMPFD).

(B) Protein sequence alignment of yeast Cdc48p and human VCP. Alignment was done with Vector NTI Suite V.10. Amino acids marked yellow are conserved from yeast to humans. Green marks demonstrate the exchange of an amino acid by an amino acid with similar chemical properties during evolution. Unmarked amino acids are exchanged during evolution by a amino acids with different chemical properties. The asterisks mark the serine 565 to glycine (S565G) mutation in the *cdc48*^{S565G} mutant yeast strain and its orthologous human mutation serine 555 to glycine (S555G).

Yeast cells expressing a mutated form of *CDC48* (*cdc48*^{S565G} strain), the yeast orthologue of VCP, demonstrated malfunction of Cdc48p/VCP-dependent ERAD pathway, leading to a high tendency for apoptosis (see Results 1. and Discussion 1.). Protein sequence alignment of yeast Cdc48p and human VCP revealed that the serine residue 565 exchanged in the mutant yeast strain to a glycine residue (S565G) is conserved in human VCP as serine 555 (Fig. 23B), a residue between the Walker A and B motifs of the D2 domain of VCP (Fig. 23A). In order to correlate the results obtained in the *cdc48*^{S565G} yeast model, the orthologous mutation in VCP, *i.e.*, VCP-S555G, was selected.

The most frequent VCP mutation leading to IBMPFD is the exchange of the amino acid arginine 155 to histidine (R155H) located in the N-terminal domain of VCP (Watts et al., 2004). VCP-R155H was selected as VCP variant, because it is associated with a human disorder and because its mutation is outside of the ATPase domains of VCP, potentially leading to other cellular effects than VCP-K524A or VCP-S555G when expressed in mammalian cell cultures.

Full-length VCP cDNA was cloned into a mammalian expression vector applying various cloning techniques, and the VCP variants were then generated by site-directed mutagenesis (for details of the cloning strategy see Methods 2.2.12).

2.2 Influence of the expression of VCP variants on cell viability and cell death in mammalian cell culture

2.2.1 Expression of ATPase-deficient VCP-K524A and of VCP-S555G but not of the IBMPFD-associated mutation VCP-R155H has severe effects on cell viability

Wild-type VCP and its variants VCP-K524A, VCP-S555G and VCP-R155H were overexpressed in the ‘human embryonic kidney cell’ line HEK293 and analyzed for their effects on cell morphology by fluorescence microscopy. Overexpressing wild-type and IBMPFD-associated VCP-R155H did not show any marked alterations compared to the vector control (Fig. 24, columns 1 and 4 vs. column 5). The cells showed normal shape, cell extensions and had contact to other cells. In contrast, overexpressing the variants VCP-K524A (ATPase-deficient variant) and VCP-S555G (homologous variant to Cdc48p-S565G) resulted in marked morphological alterations compared to the vector control (Fig. 24, columns 2 and 3 vs. column 5). A large portion of cells lost contact to neighboring cells, their extensions were reduced or disappeared, the cells got a round shape and tended to detach from the culture dishes – characteristics of dying cells.

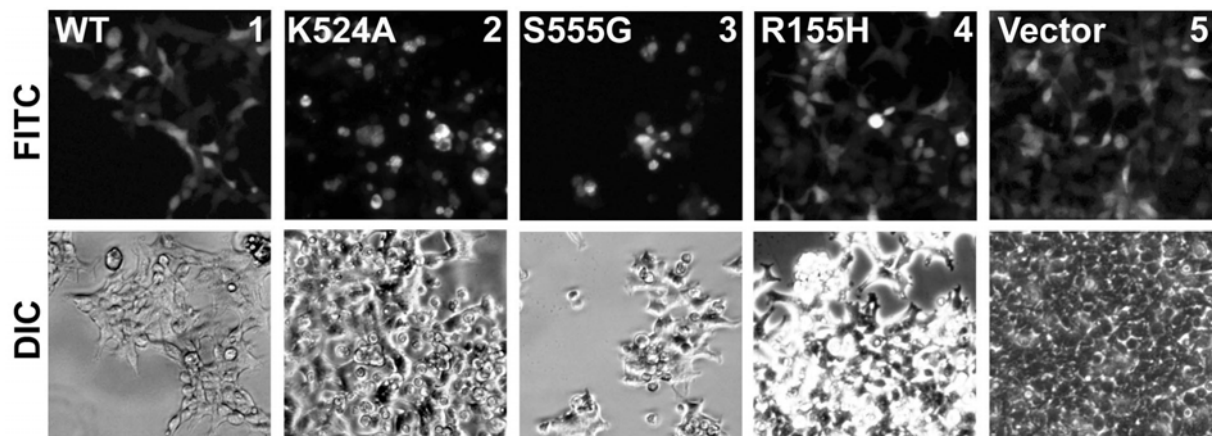


Figure 24: Expression of ATPase-deficient VCP-K524A and of VCP-S555G leads to severe morphological alterations. Expression of VCP in human embryonic kidney cells (HEK293). HEK293 cultures were transiently co-transfected with pcDNA3 constructs containing VCP-WT, VCP-K524A, VCP-S555G, and VCP-R155H, respectively, and pcDNA3-Strep-GFP in a ratio of 10:1. Transfected cultures were grown for 2 d and were then evaluated in the culture dishes by an inverse fluorescence microscope (Leica) using a 20x objective and FITC and Nomarski (DIC) optical filter sets.

In order to quantify the effects of the VCP variants on cell viability, a Live/Dead assay was performed. In this assay cells were incubated with calcein AM and ethidium homodimer-1. Viable cells incorporate calcein AM and modify this substrate to the green-fluorescent dye calcein. In contrast, dead cells with porous cell membranes incorporate the DNA-intercalating red-fluorescent dye ethidium homodimer-1 in the nucleus. The ratio of green to red fluorescence, *i.e.*, the relative number of viable to the relative number of dead cells, describes the viability of the respective culture. Overexpression of VCP-K524A and VCP-S555G in

HEK293 cells decreased the cell viability significantly (43% decrease for VCP-K524A and 23% decrease for VCP-S555G) compared to overexpression of VCP wild-type (Fig. 25). In contrast, overexpression of VCP-R155H did not lead to a decrease but rather to a small increase in cell viability (13% increase) compared to overexpression of VCP wild-type. Thus, mutations in the major ATPase domain of VCP (VCP-K524A, VCP-S555G) are highly detrimental for cells expressing these variants, as evidenced by severe morphological alterations (Fig. 24) and significantly decreased cell viability (Fig. 25).

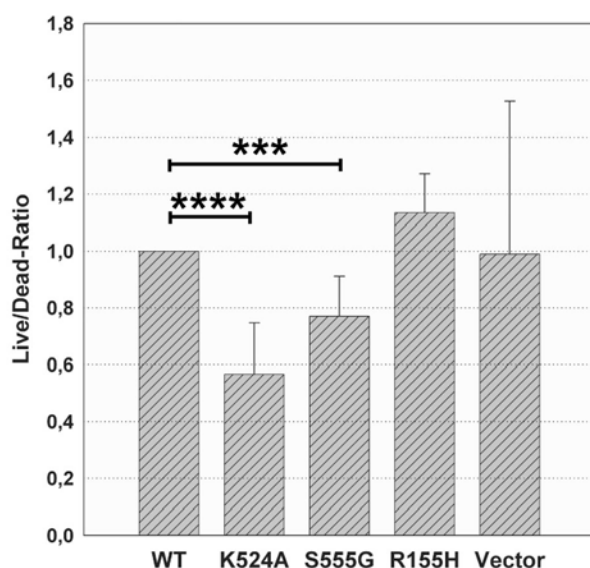


Figure 25: Expression of ATPase-deficient VCP-K524A and of VCP-S555G but not of the IBMPFD-causing VCP-R155H results in decreased cell viability.

Viability of HEK293 cells upon expression of VCP. HEK293 cultures were transiently transfected with pcDNA3 constructs containing VCP-WT, VCP-K524A, VCP-S555G, and VCP-R155H, respectively. After growth for 2 d, cell viability was assessed by a Live/Dead assay. Viable but not dead cells are able to incorporate calcein AM and to modify this substrate to the green-fluorescent dye calcein. In contrast, dead cells with porous cell membranes but not viable cells incorporate the DNA-intercalating red-fluorescent dye ethidium homodimer-1. The ratio of green to red fluorescence, *i.e.*, the relative number of viable to the relative number of dead cells, describes the viability of the respective culture. The data shown here are percent change values of six independent experiments. * $p < 0.05$, ** $p < 0.01$, *** $p < 0.001$, **** $p < 0.0001$, Student's t-test (unpaired), error bars: s.d.

2.2.2 Expression of VCP-K524A and VCP-S555G leads to cytoplasmic vacuolization and condensation and fragmentation of nuclei

In order to further characterize the observed morphological alterations (Fig. 24), immunofluorescence microscopy was performed. HEK293 cells overexpressing 'green-fluorescence protein' (GFP)-tagged VCP wild-type and VCP variants were immunostained for β -tubulin to visualize cellular morphology and nuclei were stained with DAPI (Fig. 26).

Overexpression of wild-type VCP resulted in a cytoplasmic distribution of VCP (Fig. 26, panel 2), as has been observed for endogenous VCP (data not shown). Within these cells the microtubule cytoskeleton formed a network structure, similar to cells transfected with the empty vector (Fig. 26, panel 1).

The expression of ATPase-deficient VCP-K524A led to marked morphological alterations (Fig. 26, panels 3 and 4). In contrast to expression of wild-type VCP, VCP-K524A was not equally distributed within the cytoplasm (Fig. 26, panels 2 vs. 3). Both VCP-K524A and β -tubulin were allocated in a cytoplasmic network structure with wide meshes enclosing

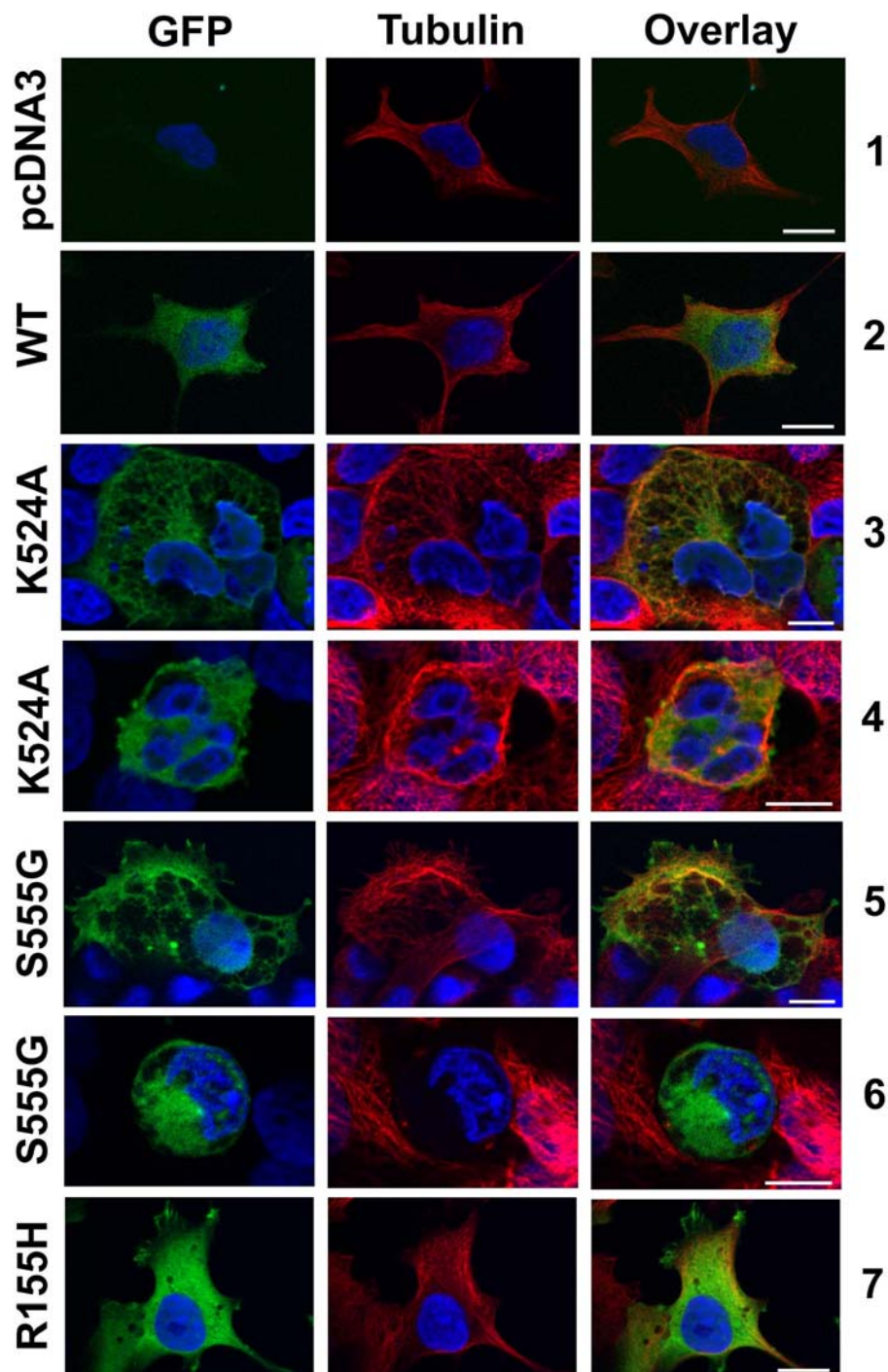


Figure 26: Expression of VCP-K524A and VCP-S555G leads to cytoplasmic vacuolization, nuclear condensation and cell death.

HEK293 cultures were transiently transfected with pcDNA3-Strep-GFP constructs containing VCP-WT, VCP-K524A, VCP-S555G, and VCP-R155H, respectively. After transfection cells expressing C-terminally GFP-tagged VCP (green) were grown for 2 d, fixed and immunostained with a specific antibody against the cytoskeletal protein β -tubulin (red). Nuclei were stained with DAPI (blue). Image acquisition was done using a Zeiss ApoTome™ high resolution fluorescence microscope with Cy3, FITC, and DAPI optical filter sets (C-Apochromat 63x/1.20 objective, optical section thickness: 1 μ m; AxioCam, AxioVision 4, Zeiss). Bar: 10 μ m.

black ‘cellular holes’ (Fig. 26, panel 3). These data hint to the emergence of vacuoles in the cytoplasm of cells expressing VCP-K524A, as was already demonstrated in a previous study (Hirabayashi et al., 2001). In a more progressed state of cells expressing detrimental VCP-K524A, cells rounded up and nuclei were often found to be condensed and fragmented (Fig. 26, panel 4). Whereas the nuclei were predominantly round when overexpressing VCP wild-type (Fig. 26, panel 2), they demonstrated an abnormal shape, often sickle-shaped, when overexpressing VCP-K524A (Fig. 26, panel 4). Quantification revealed that 27% of cells overexpressing VCP-K524A but only 8% of cells overexpressing VCP wild-type showed nuclei with abnormal shape, a hallmark of apoptotic cell death. Thus, expression of pathophysiological VCP-K524A results in cell death that is preceded by subcellular rearrangements, such as cytoplasmic vacuolization.

Expression of VCP-S555G, the homologous variant to yeast Cdc48p-S565G, caused highly similar morphological alterations observed in cells expressing VCP-K524A: (i) rearrangement of VCP and β -tubulin in a network structure with wide meshes enclosing ‘black holes’ indicating cytoplasmic vacuolization (Fig. 26, panel 5), and (ii) rounding of cells and increased emergence of abnormally shaped nuclei (Fig. 26, panel 6). Thus, expression of VCP-S555G has the same effect than expression of ATPase-deficient VCP-K524A. This is consistent with the fact that both variants harbor a mutation within the major ATPase domain of VCP (Fig. 23A).

In contrast, expression of VCP-R155H, an IBMPFD-causing VCP variant with functional ATPase activity, did not show any marked morphological alterations compared to wild-type VCP (Fig. 26, panels 2 vs. 7). VCP remained equally distributed within the cytoplasm and the microtubule cytoskeleton was shown to be unaltered (Fig. 26, panel 7). Only after increasing the amount of transfected DNA, cells expressing VCP-R155H but not cells expressing wild-type VCP demonstrated cytoplasmic VCP aggregates or vacuoles (data not shown). Thus, mutations in the major ATPase domain of VCP (VCP-K524A, VCP-S555G) have a much more severe effect on cell morphology and cell viability compared to the N-terminal VCP mutation VCP-R155H.

2.2.3 Increased cell death upon ATPase domain mutations in VCP is paralleled by accumulation of polyubiquitinated proteins

Analysis of the *cdc48*^{S565G} yeast strain that has a high tendency to undergo apoptotic cell death (Fig. 6) revealed that mutation of *CDC48* leads to accumulation of polyubiquitinated proteins (Fig. 16). Therefore, it should be evaluated whether increased cell

death in HEK293 cells when overexpressing VCP variants is accompanied by dysfunction of the ubiquitin-proteasome system. Cell lysates were analyzed by Western blot for the level of the cleaved form of the nuclear protein Poly-[ADP-ribose]-polymerase (PARP), a substrate of caspases during apoptotic cell death (Lazebnik et al., 1994; Nosseri et al., 1994) and for cellular amounts of polyubiquitinated proteins. In HEK293 cells overexpressing VCP-K524A and VCP-S555G the cleaved form of PARP was found (Fig. 27, columns 1 and 2, panel 2), underlining the induction of apoptotic cell death that was already suggested by condensation of nuclei (Fig. 26). Accumulation of polyubiquitinated proteins in cells expressing VCP-K524A and VCP-S555G (Fig. 27, columns 1 and 2, panel 3) suggest dysfunction of the ubiquitin-dependent ER-associated protein degradation pathway (ERAD), in which VCP is crucially involved (Ye, 2005; Ye, 2006). Thus, HEK293 cells overexpressing VCP-K524A and VCP-S555G demonstrate highly similar phenotypes as described for the *cdc48*^{S565G} yeast strain, *i.e.*, induction of (apoptotic) cell death and dysfunction of ubiquitin-dependent ERAD.

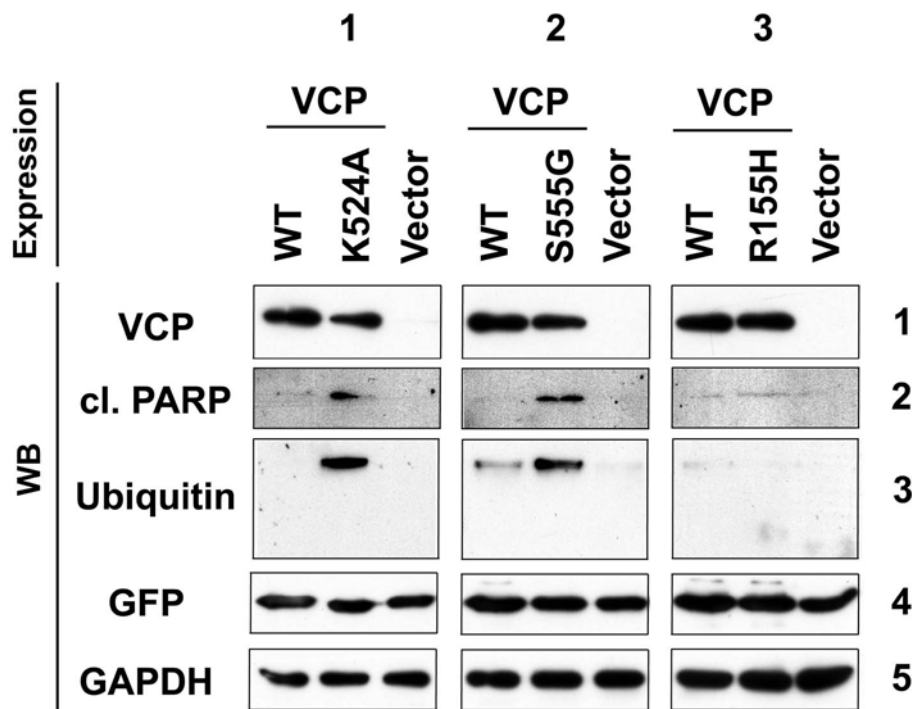


Figure 27: Apoptotic cell death upon expression of VCP-K524A and VCP-S555G is paralleled by accumulation of polyubiquitinated proteins.

HEK293 cultures were transiently co-transfected with pcDNA3 constructs containing VCP-WT, VCP-K524A, VCP-S555G and VCP-R155H, respectively, and pcDNA3-Strep-GFP in a ratio of 10:1. Transfected cells were grown for 1-2 d, cells were lysed, protein extracts were separated by SDS-PAGE and proteins were blotted onto PVDF membranes. VCP (panel 1), cleaved PARP – a marker of apoptotic cell death (panel 2), ubiquitin (panel 3), GFP (panel 4), and GAPDH (panel 5), were detected using specific antibodies. GFP was used as transfection control, GAPDH as loading control. 15 µg protein per lane. WB: Western blot.

In contrast, expression of VCP-R155H did result only in a faint accumulation of cleaved PARP (Fig. 27, column 3, panel 2) and no accumulation of polyubiquitinated proteins could be observed (Fig. 27, column 3, panel 3). These data are consistent with the observed weak cellular phenotype when overexpressing VCP-R155H (Fig. 26).

2.3 Dysfunction of VCP variants in the degradation of rhodopsin – a potential ERAD substrate

Accumulation of polyubiquitinated proteins in HEK293 cells overexpressing the ATPase mutants VCP-K524A and VCP-S555G (Fig. 27) suggest dysfunction of the ubiquitin-dependent ERAD pathway in these cells. In order to validate ERAD dysfunction, the VCP variants were co-expressed with a substrate of the ERAD pathway. Increased cellular levels of this substrate hint to dysfunction of the respective VCP variant in the ERAD pathway. As potential substrate of ERAD and VCP the membrane protein rhodopsin was selected.

2.3.1 Rhodopsin and rhodopsin-P23H, a frequent variant causative for the human disorder retinitis pigmentosa, can be efficiently expressed in mammalian cell cultures

Both ER luminal and ER membrane proteins are substrates of the VCP-dependent ERAD pathway (Ye, 2005; Ye, 2006). Membrane proteins of the secretory pathway are synthesized at the ER membrane and are co- or post-translationally inserted into the ER membrane (Alberts et al., 1994a). A significant portion of newly synthesized membrane proteins fails to fold correctly and has to be degraded shortly after synthesis by the ERAD pathway as part of the cellular protein quality control (Meusser et al., 2005; Wu et al., 2006; Ye, 2005). Rhodopsin is a highly hydrophobic membrane protein of the secretory pathway with seven transmembrane domains (Garriga and Manyosa, 2002). It is the visual pigment of rods in the retina of vertebrates and is the most abundant protein in photoreceptors (Garriga and Manyosa, 2002). The variant rhodopsin-P23H is causative for the human degenerative retinal disorder retinitis pigmentosa (Chapple et al., 2001; Naash et al., 1993; Olsson et al., 1992; Sung et al., 1993). Rhodopsin-P23H has a high tendency for aggregation and has been described to stack within the ER and Golgi but also to form perinuclear inclusion bodies (Frederick et al., 2001; Illing et al., 2002; Saliba et al., 2002).

Rhodopsin wild-type was efficiently expressed in HEK293 cells (Fig. 28). As evidenced by immunofluorescence microscopy and consistently with earlier results (Illing et al., 2002; Saliba et al., 2002), rhodopsin was found in the plasmamembrane (Fig. 28A). However, few cytoplasmic rhodopsin aggregates could also be observed. SDS-PAGE and Western blot analysis of cell lysates revealed that the major portion of cellular wild-type rhodopsin could be separated by this denaturing electrophoretic method in its monomeric form (Fig. 28B). In line with previous results (Illing et al., 2002; Saliba et al., 2002), monomeric rhodopsin appeared in different glycosylated states resulting in a smear from 35-

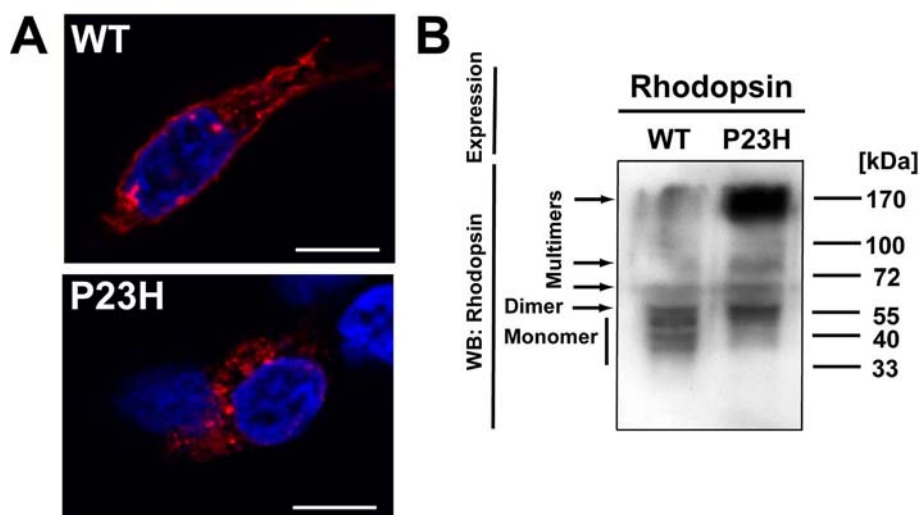


Figure 28: Expression of rhodopsin in HEK293 cells.

(A) Cellular localization of rhodopsin. HEK293 cells were transiently transfected with pRC/CMV constructs containing rhodopsin-WT and rhodopsin-P23H, respectively. Transfected cells were grown for 2 d, cells were fixed and immunostained with antibodies against rhodopsin (red; 4D2 for rhodopsin-WT, ABR for rhodopsin-P23H). Nuclei were stained with DAPI (blue). Image acquisition was done using a Zeiss ApoTome™ high resolution fluorescence microscope with Cy3 and DAPI optical filter sets (C-Apochromat 63x/1.20 objective, optical section thickness: 1 μ m; AxioCam, AxioVision 4). Note that rhodopsin-WT is partially inserted into the plasma membrane, whereas aggregation-prone rhodopsin-P23H remains cytoplasmic and forms increased number of cellular rhodopsin aggregates.

(B) Separation of rhodopsin by SDS-PAGE. HEK293 cells were transiently transfected with pRC/CMV constructs containing rhodopsin-WT and rhodopsin-P23H, respectively. Transfected cells were grown for 2 d, cells were lysed and protein extracts were separated by SDS-PAGE. Proteins were blotted onto PVDF membranes. Rhodopsin was detected using specific antibodies (ABR for rhodopsin-WT and rhodopsin-P23H). 20 μ g protein per lane. The rhodopsin monomer forms a smear from 35 to 50 kDa due to different states of glycosylation. Note that aggregation-prone rhodopsin-P23H (and to a certain extent rhodopsin-WT) forms dimers and high molecular SDS-insoluble aggregates visible by Western blot (WB) analysis (see text). Bar: 10 μ m.

50 kDa. Also accordingly to earlier data (Illing et al., 2002; Saliba et al., 2002), part of the wild-type rhodopsin formed SDS-insoluble dimers (60 kDa) and multimers due to its high hydrophobicity (Fig. 28B).

Expression of rhodopsin-P23H in HEK293 cells resulted in the accumulation of cellular rhodopsin aggregates (Fig. 28). In contrast to wild-type rhodopsin, rhodopsin-P23H was not able to enter the plasmamembrane but remained cytoplasmic (Fig. 28A). Underlining previous results (Illing et al., 2002; Saliba et al., 2002), rhodopsin-P23H formed cytoplasmic peri-nuclear aggregates (Fig. 28A). SDS-PAGE and Western blot analysis of cell lysates demonstrated accumulation of SDS-insoluble high molecular rhodopsin aggregates and rhodopsin dimers (Fig. 28B), demonstrating the high tendency of rhodopsin-P23H for aggregation.

Thus, wild-type rhodopsin and rhodopsin-P23H can efficiently be expressed in HEK293 cells. Consistently with previous results (Illing et al., 2002; Saliba et al., 2002), rhodopsin-P23H has a high tendency for aggregation as evidenced by cytoplasmic aggregates in immunofluorescence and SDS-insoluble aggregates in SDS-PAGE. In contrast, wild-type rhodopsin is inserted into the plasmamembrane and has a weaker tendency for aggregation.

2.3.2 Mutation of VCP leads to accumulation and increased aggregation of the ERAD substrate rhodopsin

ERAD dysfunction of cells expressing VCP variants can be evaluated by measuring the cellular amount and analyzing the protein separation pattern of the ERAD substrate rhodopsin using Western blot analysis (Fig. 29). Co-expression of the ATPase-deficient variant VCP-K524A with both wild-type rhodopsin and rhodopsin-P23H resulted in increased amounts of high molecular SDS-insoluble rhodopsin aggregates (Fig. 29A, columns 1 and 2, panel 1). These data demonstrate dysfunction of ERAD in VCP-K524A-expressing cells.

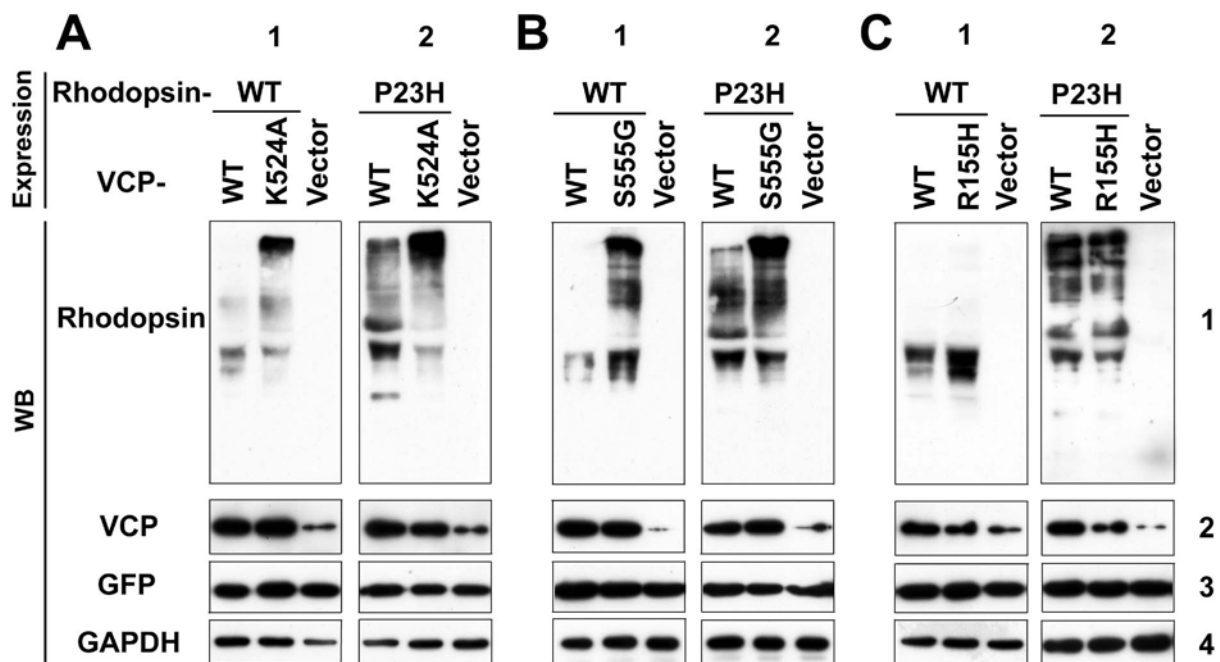


Figure 29: VCP mutation leads to accumulation of rhodopsin.

HEK293 cultures were transiently co-transfected with pcDNA3 constructs containing VCP-WT (A, B, C), VCP-K524A (A), VCP-S555G (B), and VCP-R155H (C), respectively, and pRC/CMV constructs containing rhodopsin-WT, and rhodopsin-P23H, respectively (A, B, C). For expression control, pcDNA3-Strep-GFP vector was co-transfected in a ratio of 10:1 (VCP/Rhodopsin vs. pcDNA3-Strep-GFP). Cultures were grown for 1-2 d, and cell lysates were separated by SDS-PAGE (15 µg protein per lane) and blotted to PVDF membranes. Rhodopsin (panels 1), VCP (panels 2), GFP (panel 3) and GAPDH (panel 4) were detected using specific antibodies (1D4 for rhodopsin). GFP was used as expression control and GAPDH as loading control. The data shown here are representative for three independent experiments.

(A, B) Expression of ATPase-deficient VCP-K524A and of Cdc48p-S565G-homologous VCP-S555G results in increased formation of high-molecular SDS-insoluble aggregates of rhodopsin.

(B) Expression of IBMPFD-associated VCP-R155H results in an accumulation of rhodopsin-WT but not of rhodopsin-P23H.

Highly similar to VCP-K524A, in cells expressing VCP-S555G the cellular levels of high molecular rhodopsin aggregates was markedly increased (Fig. 29B, columns 1 and 2, panel 1), showing dysfunction of VCP-S555G in ERAD. Thus, VCP-K524A and VCP-S555G-expressing cells behave highly similar consistent to the fact that both variants harbor a mutation in the major ATPase domain of VCP. Expression of both variants results in (i) reduced cell viability (Figs. 24 and 25), (ii) severe morphological alterations, such as

cytoplasmic vacuolization and nuclear fragmentation (Fig. 26), (iii) apoptotic cell death and accumulation of polyubiquitinated proteins (Fig. 27), and (iv) ERAD dysfunction (Fig. 29).

When expressing VCP-R155H markedly increased levels of monomeric rhodopsin but not of high molecular SDS-insoluble rhodopsin aggregates were found in the case of co-expression with wild-type rhodopsin (Fig. 29C, column 1, panel 1). However, co-expressing VCP-R155H with aggregation-prone rhodopsin-P23H did not result in a clear accumulation of rhodopsin (Fig. 29C, column 2, panel 1). Thus, VCP-R155H-expressing cells demonstrated a comparatively weak impairment of ERAD, when compared with cells expressing VCP variants harboring mutations in the major ATPase domain of VCP, namely VCP-K524A and VCP-S555G. This might explain that cell viability and cell morphology was not affected in VCP-R155H cells at least under unstressed conditions (Figs. 24-26).

G. Discussion

Cdc48p/VCP is an evolutionary highly conserved ubiquitin-controlled AAA-ATPase involved in a variety of cellular mechanisms such as protein degradation, ERAD, membrane fusion, cell cycle control, transcriptional control, and DNA repair (Wang et al., 2004; Woodman, 2003; Ye, 2006). Human VCP is involved in the pathogenesis of various human degenerative diseases (Hirabayashi et al., 2001; Mizuno et al., 2003; Watts et al., 2004). However, the mechanisms of cell death in these disorders have remained unknown. This study aimed at elucidating the cellular consequences of pathophysiological mutations of Cdc48p/VCP. This was done applying a functional proteome analysis of the apoptotic *cdc48*^{S565G} mutant yeast strain (see Discussion 1.) and analyzing mammalian cell cultures expressing different human VCP variants (see Discussion 2.).

1. Analysis of Cdc48p variants in yeast

1.1 Functional proteome analysis of apoptotic *cdc48*^{S565G} yeast

Upon mutation of *CDC48* (*cdc48*^{S565G}), yeast cells have a high susceptibility to undergo apoptotic cell death (Madeo et al., 1997). In order to reveal the unknown molecular mechanisms of apoptotic cell death in the *cdc48*^{S565G} strain a functional proteomics approach was performed. Here, the proteome of apoptotic *cdc48*^{S565G} mutant cells was compared with isogenic *CDC48* wild-type cells applying differential two-dimensional gel electrophoresis (2-DE).

Decreased cell viability and induction of apoptotic cell death in *cdc48*^{S565G} cells could be controlled very efficiently applying a shift of the major carbon source from galactose to glucose as initial synchronizing apoptotic stimulus. Growth in glucose medium for 13 h and 20 h, respectively, and heat shock were used to obtain two different apoptotic growth conditions with increased stringency. Under prolonged apoptotic conditions (20 h), an apoptotic phenotype in more than 50% of *cdc48*^{S565G} cells could be reached. However, the overall proteome as illustrated by the applied 2-DE remained highly stable and hardly marked protein spot alterations were observed under these conditions (Braun, 2002). *S. cerevisiae* contains about 6000 protein-coding genes (Cherry et al., 1997), and the number of individual protein species is additionally multiplied by various co- and post-translational modifications. 2-DE resolves robustly up to 2000 of these protein species as protein spots (Görg et al., 2004) and allows therefore only the description of a part of the resulting complex cellular proteome. Highly abundant proteins encoded by house-keeping genes are thus overrepresented on 2-DE. Moreover, proteins present in low-copy numbers within a cell, which are often involved in

regulatory mechanisms (*e.g.*, transcription factors and apoptosis-regulating proteins), are hardly detectable with this method, since they are covered by highly abundant proteins, below detection threshold of the gel staining method or not identifiable by mass spectrometry (Stasyk and Huber, 2004). Thus, the observed very high stability of the total cellular proteome under apoptotic growth conditions might be due to the background of unaltered high-copy number proteins that are not involved in the progression of the apoptotic cell death program.

The separation capability of 2-DE can be considerably extended by separating the same sample on different 2D gels using immobilized pH gradient (IPG) strips with overlapping pH gradients (Görg et al., 2004). Alternatively, coupling of the gel-based 2-DE technique with gel-free approaches like LC-MS/MS can give access to a more complete analysis of the total cellular proteome. These approaches could result in the identification of apoptosis-associated protein alterations at a cellular level that were not detectable with the 2-DE technique applied in this study.

Instead of increasing the separation range to analyze a given proteome in more detail, here, an alternative approach was taken. The complexity of the proteome was markedly reduced by analyzing subcellular fractions, namely mitochondrial and cytosolic fractions, of apoptotic *cdc48*^{S565G} cells. Yeast mitochondria are believed to comprise 700-800 different proteins (Prokisch et al., 2006; Prokisch et al., 2004), and mitochondrial extracts are therefore significantly less complex than the overall yeast proteome with 6000 protein-coding genes (Cherry et al., 1997). 2-DE as performed in this study is able to separate up to 2000 different protein species referring to several hundred individual proteins. Thus, the applied 2-DE is expected to cover a major portion of the mitochondrial proteome. Conducting this approach, significant protein alterations between apoptotic *cdc48*^{S565G} cells and wild-type cells were observed in mitochondrial extracts, whereas in the more complex cytosolic extracts only minor changes were observed. In mitochondrial extracts increased and decreased amounts of mitochondrial proteins were revealed, suggesting for the first time that mitochondria are involved in apoptotic cell death triggered by *CDC48* mutation (see Discussion 1.2). Based on these results, further studies confirmed a crucial role of mitochondria during apoptosis in *cdc48*^{S565G} cells (see Discussion 1.2). Beside alterations of mitochondrial proteins, accumulation of proteins associated with the NE-ER, a continuous membrane system consisting of the endoplasmic reticulum (ER) and the ER-related nuclear envelope (NE) (Baumann and Walz, 2001; Enenkel et al., 1998; Hepler, 1981), was observed in mitochondrial extracts of apoptotic *cdc48*^{S565G} cells. Additional experiments demonstrated increased association of NE-ER and mitochondria accompanied with dysfunctional ER-

associated protein degradation (ERAD) upon *CDC48* mutation (see Discussion 1.3). The complexity of mitochondrial extracts was further reduced by zone electrophoresis using a free flow device (ZE-FFE). Applying this method, a mitochondrial side fraction associated with NE-ER-derived microsomes and increased amounts of polyubiquitinated proteins was separated from purified mitochondria. These data are finalized in the description of a model of apoptosis in *cdc48*^{S565G} cells (see Discussion 1.4, Fig. 30). This model proposes that detrimental processes taking place in the ER upon *CDC48* mutation result in the damage of associated mitochondria that subsequently initiate apoptotic cell death. Thus, differential proteome analysis using 2-DE of subcellular proteomes with decreased complexity, compared to total cell extracts, allowed the description of pathophysiological markers and thus provide basis for further insights into the molecular and functional mechanisms of apoptotic cell death in *cdc48*^{S565G} cells.

1.2 Crucial mitochondrial impairment upon *CDC48* mutation in apoptotic yeast

This study demonstrates that mutation of *CDC48* (*cdc48*^{S565G}) results in mitochondrial impairment in yeast cells:

First, mitochondria are a specific site for qualitative as well as quantitative protein alterations in *cdc48*^{S565G} cells. Both “enrichment” and “depletion” of distinct proteins were observed. In particular, depletion of the mitochondrial proteins Mmf1p, Ilv5p, homoaconitase and putative aconitase was revealed. Mmf1p is a mitochondrial matrix factor that upon depletion (Δ *mmf1*) results in cells that lose mitochondrial DNA (mtDNA) (Oxelmark et al., 2000). Ilv5p is a bifunctional protein required for branched-chain amino acid biosynthesis and for the maintenance of mtDNA (Zelenaya-Troitskaya et al., 1995). Aconitase, a protein with high homology to homoaconitase and putative aconitase, is a mtDNA-associated protein that, independent of its catalytic activity in the Krebs cycle, is essential for mtDNA maintenance (Chen et al., 2005). Depletion of Mmf1p, Ilv5p, homoaconitase and putative aconitase in mitochondrial extracts of *cdc48*^{S565G} yeast therefore hints to a decreased mitochondrial functionality under apoptotic growth conditions. A recent transcriptome analysis of *cdc48*^{S565G} cells under apoptotic growth conditions demonstrated genes coding for proteins involved in mitochondrial functionality to be the largest group of differentially regulated genes, both up- and down-regulation of gene expression was observed (Laun et al., 2005). Thus, the observed distinct alterations at the mitochondrial protein level suggest that mitochondria are a pivotal site of changes on the protein level associated with *CDC48* mutation.

Second, mitochondrial enlargement and release of cytochrome *c* into the cytosol in the *cdc48*^{S565G} strain compared to the wild-type strain was observed, hinting to a loss of mitochondrial integrity possibly due to damaged mitochondrial membranes.

Third, the deficit of *cdc48*^{S565G} cells to adapt to respiratory growth conditions as well as accumulation of ROS produced by the mitochondrial cytochrome *bc₁* complex suggest dysfunction of the mitochondrial respiratory chain.

Mitochondrial damage and dysfunction, release of cytochrome *c* into the cytosol and emergence of ROS are characteristic features of most mitochondria-dependent apoptotic pathways in both mammalian cells and in yeast (Green and Kroemer, 2004; Ludovico et al., 2002; Newmeyer and Ferguson-Miller, 2003). Consistently to previous studies (Laun et al., 2005; Madeo et al., 1997; Madeo et al., 1999), apoptotic cell death in the *cdc48*^{S565G} strain was observed as evidenced by DNA fragmentation. In contrast to significant protein alterations at the mitochondrial proteome level, release of cytochrome *c* into the cytosol and

accumulation of ROS was revealed already under early apoptotic growth conditions (13 h) concomitantly to the emergence of caspase-like enzymatic activity. In mammalian cells, cytochrome *c*, when translocated into the cytosol, is an essential component of the so-called apoptosome (Zou et al., 1999). In this complex, pro-caspase 9 is cleaved and activated to caspase 9 triggering the apoptotic cell death cascade (Zou et al., 1999). In yeast, such an essential role of cytochrome *c* during mitochondria-mediated apoptosis has not been evaluated yet. However, ROS appear to play a central role in the progression of apoptosis in yeast (Madeo et al., 1999; Madeo et al., 2004). Specifically, the yeast caspase Yca1p is activated upon exogenously applied oxidative stress (Madeo et al., 2002b). Thus, it is likely that the observed endogenously accumulating ROS in the *cdc48*^{S565G} strain induce caspase activity that precedes and subsequently triggers DNA fragmentation and cell death (see Discussion 1.4, Fig. 30).

In a previous study, ROS have been demonstrated to be essential for the progression of cell death in the *cdc48*^{S565G} strain (Madeo et al., 1999). Therefore, the increased production of ROS by the mitochondrial cytochrome *bc₁* complex suggests a mitochondrial contribution in apoptotic cell death in the *cdc48*^{S565G} strain. Consistently, generation of yeast strains lacking functional mitochondria (ρ^0 strains) revealed that the *cdc48*^{S565G} ρ^0 strain was found to be highly similar to the wild-type ρ^0 strain in both cell viability (Fig. 14) and growth rates (data not shown). In contrast, the *cdc48*^{S565G} ρ^+ strain showed significantly lower cell viability (Fig. 14) and a markedly decreased growth rate (data not shown) compared to the wild-type ρ^+ strain. In line with the assumption that mitochondria do play a pivotal role in *cdc48*^{S565G}-mediated apoptotic cell death, a complete loss of functional mitochondria in *cdc48*^{S565G} ρ^0 cells resulted in a higher viability compared to *cdc48*^{S565G} ρ^+ cells containing damaged ROS-producing mitochondria.

Proteome alterations in mitochondrial extracts of *cdc48*^{S565G} cells compared to wild-type cells further support mitochondrial involvement in apoptotic cell death. Increased amounts of the glycolytic enzyme enolase 1 suggests increased glycolytic ATP production, confirming previous results of apoptosis in *cdc48*^{S565G} cells being an ATP-dependent active programmed cell death (Madeo et al., 1999). Elevated amounts of the mitochondrial ribosomal subunit Mrp8p were observed. Transcriptome analysis of apoptotic *cdc48*^{S565G} cells revealed upregulation of several components of the mitochondrial protein translation machinery (Laun et al., 2005). These data may therefore hint to active protein alterations in mitochondria during the cell death program.

Depletion of cyclophilin C in mitochondrial extracts of apoptotic yeast cells was found. Mitochondrial cyclophilin in mammalian cells has been described as a repressor of mitochondria-dependent apoptosis (Schubert and Grimm, 2004). Depletion of its homologue during apoptosis suggests a similar role in yeast. The actin cytoskeleton proteins ‘ARP2/3 complex 20 kDa subunit’ and ‘F-actin capping protein alpha subunit’ (CAPA) were found to be accumulated. Recently, a connection between yeast apoptosis and actin dynamics has been made (Breitenbach et al., 2005; Gourlay et al., 2004). These authors demonstrated that decreased actin dynamics caused depolarization of the mitochondrial membrane and an increase in ROS production resulting in cell death. Since I observed mitochondrial damage and ROS production in the *cdc48*^{S565G} strain, accumulation of proteins of the actin cytoskeleton (CAPA, ARP2/3) in mitochondrial extracts might hint to an altered actin dynamic in apoptotic *cdc48*^{S565G} cells.

Accumulation of the yeast orthologue of the human ‘translationally controlled tumor protein’ (TCTP) was demonstrated in mitochondrial extracts of the *cdc48*^{S565G} mutant strain under apoptotic growth conditions. Based on this finding and since human TCTP was proposed to have anti-apoptotic functions in mitochondria-dependent apoptosis in mammalian cells (Li et al., 2001; Zhang et al., 2002), our collaboration partners in the laboratory of Dr. Laun at the University of Salzburg (Austria) initiated further studies on the yeast orthologue of TCTP. They revealed that yeast TCTP, like human TCTP, is a microtubule-binding cytoplasmic protein (Rinnerthaler et al., 2006; Yarm, 2002). Notably, yeast TCTP translocates to mitochondria upon mild oxidative stress or replicative ageing of yeast cells (Rinnerthaler et al., 2006) that is known to be associated with the accumulation of ROS (Laun et al., 2001). These authors therefore named this yeast protein ‘microtubule and mitochondria interacting protein 1’ (Mmi1p) (Rinnerthaler et al., 2006). Deletion of the *MMI1* gene results in yeast cells with markedly increased resistance to oxidative stress and increased lifespan of individual yeast cells (Rinnerthaler et al., 2006). Thus, Mmi1p may play an important role in ROS-dependent apoptotic cell death in yeast. Enrichment of Mmi1p in mitochondrial extracts of *cdc48*^{S565G} cells, which accumulate ROS predominantly produced by mitochondria, suggests a role of this protein in mitochondria-mediated cell death in the *cdc48*^{S565G} strain.

1.3 CDC48 mutation is paralleled by increased association of ubiquitinated NE-ER and mitochondria

Accumulation of polyubiquitinated proteins and of the protein Kar2p, an ER stress marker (Kohno et al., 1993; Menzel et al., 1997), was observed in total cell extracts of *cdc48*^{S565G} cells by Western blot analysis. Others have screened different *cdc48* mutants for ERAD activity and revealed that the efficiency of Cdc48p-S565G in the degradation pathway is decreased in the *cdc48*^{S565G} compared to the wild-type strain (Jarosch et al., 2002). Accordingly, I observed enrichment of polyubiquitinated proteins and of Kar2p, underlining dysfunction of the Cdc48p-S565G variant in ERAD. It has been shown that dysfunction of the ubiquitin-proteasome system or more specifically the ERAD pathway may lead to apoptotic cell death in mammalian cells (Meriin and Sherman, 2005; Paschen, 2004; Shah et al., 2001). Thus, the lower efficiency of the highly conserved and crucial cellular protein quality control mechanism ERAD might be the reason for the observed increased susceptibility of the *cdc48*^{S565G} yeast strain to undergo apoptotic cell death.

Differential 2-DE analysis revealed that several proteins associated with the NE-ER were found to be enriched in mitochondrial extracts in the *cdc48*^{S565G} strain, suggesting an increased NE-ER content in mitochondrial fractions upon *CDC48* mutation. Interestingly, the strongest accumulation was observed for Cdc48p-S565G itself. Western blot analysis confirmed increased amounts of Cdc48p-S565G in mitochondrial extracts and demonstrated concomitant accumulation of polyubiquitinated proteins. Since Cdc48p-S565G and polyubiquitinated proteins remained stably associated with mitochondria after further purification applying sucrose gradient centrifugation, these data show that mitochondrial fractions are affected by dysfunctional ERAD upon *CDC48* mutation.

Analysis of mitochondrial extracts by ZE-FFE allowed the separation of purified mitochondria (ZE-FFE main fractions) and mitochondria associated with NE-ER-derived microsomes (ZE-FFE side fractions) as characterized by SDS-PAGE/MS, 16-BAC/SDS-PAGE/MS, Western blot and EM. The association between mitochondria and NE-ER-derived microsomes must be very stringent, since it remained stable during both ZE-FFE separation upon high voltages and subsequent centrifugation and washing steps. Associations between mitochondria and the NE-ER are well established. Stable interactions between a mitochondrial subpopulation and the ER in mammalian cells that allow exchange of calcium have been demonstrated (Filippin et al., 2003; Goetz and Nabi, 2006). An ER-like membrane fraction, termed the 'mitochondria-associated membrane' (MAM) has been characterized as a membrane bridge between the ER and mitochondria necessary in synthesis and interorganelle

transport of phospholipids in both mammalian cells and yeast (Achleitner et al., 1999; Goetz and Nabi, 2006; Schumacher et al., 2002; Vance, 1990). Therefore, the ZE-FFE side fractions containing both mitochondria and NE-ER could represent a functional relevant fraction involved in the renewal of mitochondrial membranes. This is of high interest, since in apoptotic *cdc48*^{S565G} cells the NE-ER-association of mitochondria is increased (see below), possibly resulting in a disturbed turnover of mitochondrial membranes.

Polyubiquitinated proteins were predominantly found in ZE-FFE side fractions of the *cdc48*^{S565G} strain but not in the ZE-FFE main fractions. These data suggest that the majority of purified mitochondria (ZE-FFE main fractions) were not affected by the disturbed protein degradation due to *CDC48* mutation. In the ZE-FFE side fractions of the *cdc48*^{S565G} strain significantly more NE-ER-derived microsomes were observed compared to the ZE-FFE side fractions of the wild-type strain as evidenced by SDS-PAGE/MS, 16-BAC/SDS-PAGE/MS, Western blot and EM. These data hint to an increased association of the NE-ER to mitochondria in the *cdc48*^{S565G} strain compared to the wild-type strain. *In vivo* double fluorescence-labeling of mitochondria and ER showed enhanced overlap in *cdc48*^{S565G} compared to wild-type cells. In addition, the ultrastructural analysis (EM) of yeast cells revealed a significantly increased proximity between mitochondria and NE-ER membranes in this strain. Thus, an increased proximity between the NE-ER and mitochondria demonstrated by these morphological studies could be observed in intact cells of the *cdc48*^{S565G} strain, underlining the observed increased association of the NE-ER to mitochondria in *cdc48*^{S565G} cells.

Moreover, the ZE-FFE side fractions of the *cdc48*^{S565G} strain always comprised the highest amounts of (i) polyubiquitinated proteins, (ii) Cdc48p-S565G, (iii) the protein Kar2p, and (iv) the protein Mmi1p. The ER luminal chaperone Kar2p has been described as an indicator for ER stress and proliferation (Kohno et al., 1993; Menzel et al., 1997). Mmi1p is a regulator of ROS-dependent apoptosis in yeast that translocates from the cytoplasm (ER?) to mitochondria upon oxidative stress (Rinnerthaler et al., 2006). Accumulation of these proteins together with mutated Cdc48p-S565G and polyubiquitinated proteins in this mitochondrial side fraction markedly enriched with NE-ER-derived microsomes strongly implies a deleterious link between mitochondria and the NE-ER in the *cdc48*^{S565G} strain.

1.4 Model of Cdc48p-mediated apoptosis in yeast

Following the observations of this study, a model for Cdc48p-S565G-induced apoptosis can be proposed (Fig. 30):

Mutation in *CDC48* (*cdc48*^{S565G}) results in a lowered efficiency of ER-associated protein degradation (ERAD), leading to an enrichment of polyubiquitinated proteins at the ER (microsomes). Concomitantly, an expansion of ER and related structures such as the NE occurs, as was already observed in earlier studies with this strain (Madeo et al., 1997). These deleterious processes may be transferred to mitochondria via association of the NE-ER (microsomes) with mitochondrial membranes.

First, the stress exerted on mitochondrial membranes may be of physical nature, *i.e.*, shearing forces or pressure by proliferating ER. Similar to the ER, mitochondria form a branched mitochondrial reticulum in both mammalian cells and in yeast (Hermann and Shaw, 1998; Vandecasteele et al., 2001). Since both cellular structures are known to interact with each other (Goetz and Nabi, 2006; Vance, 2003; Voelker, 2003), an expanding NE-ER might apply forces to the mitochondrial reticulum, resulting in damaged mitochondrial membranes.

Second, ER stress might lead to impairment of the turnover of mitochondrial membranes affecting membrane integrity. Phospholipids are synthesized within the ER or ER-derived mitochondria-associated membranes (MAMs) and are then transported in a membrane-mediated fashion to mitochondria to renew the mitochondrial membranes (Vance, 2003; Voelker,

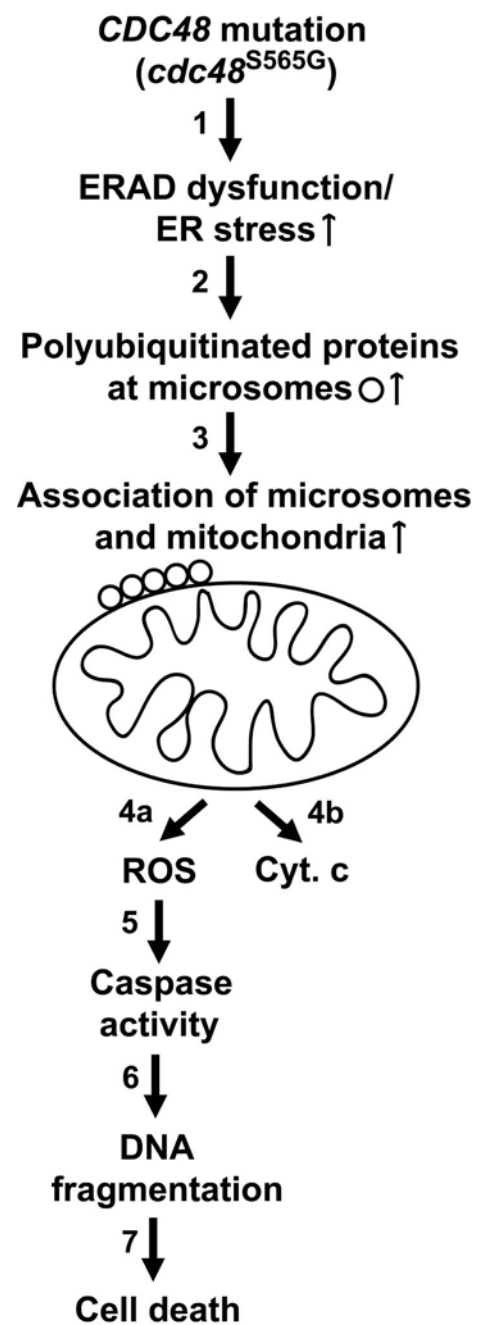


Figure 30: Model of apoptosis in *cdc48*^{S565G} yeast. Expression of Cdc48p-S565G leads to dysfunction of ERAD and induction of ER stress (1). Consequently, polyubiquitinated proteins accumulate at microsomes (2). Increased association of polyubiquitinated microsomes and mitochondrial fractions result in the damage of mitochondrial membranes (3) via an unknown mechanism (for discussion see text). Impaired mitochondria produce ROS (4a) and release cytochrome *c* into the cytosol (4b). ROS trigger caspase activity (5) that ultimately may result in DNA fragmentation (6) and cell death (7).

2003). This process is regulated in yeast, at least in the case of the phospholipid phosphatidylserine, by ubiquitination (Schumacher et al., 2002). Cdc48p is known to be involved in ER membrane fusion processes in yeast (Latterich et al., 1995) that has been proposed to be regulated by ubiquitination as well (Ye, 2006). Thus, mutation of *CDC48* might affect membrane transport from the ER to mitochondria.

Third, ROS produced in the ER under ER stress may damage nearby mitochondrial membranes, resulting in a boost of mitochondrially produced ROS. In an ERAD-deficient yeast model, overexpression of a single misfolded model protein leads to ER stress and ultimately apoptotic cell death (Haynes et al., 2004). The authors suggest that initial pathological pre-settings in the ER lead to accumulation of ER-derived ROS. Using ZE-FFE, I showed an enhanced association of NE-ER-derived microsomes with mitochondria in mitochondrial fractions of the *cdc48*^{S565G} strain and, applying a combination of EM and fluorescence microscopy, an increased proximity between these two organelles in *cdc48*^{S565G} yeast cells. Since the *cdc48*^{S565G} strain is characterized by dysfunctional ERAD (Fig. 16 and Jarosch et al., 2002), this raises the question whether potential ER-derived ROS in *cdc48*^{S565G} cells damage nearby mitochondrial membranes. This could result in deficiency of the respiratory chain, leading to a strong accumulation of detrimental ROS produced by mitochondria.

In either scenario, damaged mitochondrial membranes could lead to the release of cytochrome *c* into the cytosol, to the loss of mitochondrial functionality and to the mitochondrial production of ROS. According to previous results obtained in other apoptotic yeast strains, accumulation of ROS could mediate the induction of caspase-like enzymatic activity (Madeo et al., 2002b), resulting in events that initiate DNA fragmentation and apoptotic cell death (Fig. 30).

Involvement of wild-type VCP, the human orthologue of Cdc48p, has been demonstrated in neurodegenerative disorders displaying ubiquitin-containing inclusion bodies and aggregates, such as Huntington, Alzheimer, Creutzfeldt-Jakob and Parkinson disease, as well as motor neuron disease with dementia (Hirabayashi et al., 2001; Mizuno et al., 2003). Especially for polyglutamine disorders, wild-type VCP has been proposed as a modulator of both apoptotic cell death (Higashiyama et al., 2002) and protein aggregation (Yamanaka et al., 2004). Point mutations of VCP are causative for IBMPFD, a dominant human disorder (Schröder et al., 2005; Watts et al., 2004). There, VCP co-localizes with both nuclear inclusions in neuronal cells (Schröder et al., 2005) and protein deposits in muscle fibers (Watts et al., 2004), leading to frontotemporal dementia and myopathy, respectively.

Notably, strong similarities exist between apoptosis in *cdc48*^{S565G} yeast and these VCP-mediated human pathologies:

First, a drastic increase in the amount of polyubiquitinated proteins concomitant with apoptosis in the *cdc48*^{S565G} strain was observed. A growing body of evidence describes the disturbance of the ubiquitin-proteasome system as one crucial feature in the pathogenesis of many neurodegenerative diseases (Bossy-Wetzel et al., 2004; Goellner and Rechsteiner, 2003). Depletion of wild-type VCP or expression of dominant loss-of-function variant of VCP in mammalian cell cultures resulted in accumulation of polyubiquitinated proteins and apoptotic cell death (Hirabayashi et al., 2001; Kobayashi et al., 2002; Wojcik et al., 2004). Thus, results obtained in yeast in the course of this study are, at least in part, conferrable to homologous mammalian systems.

Second, a strong attachment of NE-ER-derived membranes to mitochondria in the *cdc48*^{S565G} strain was demonstrated. Similar subcellular rearrangements have been demonstrated in studies of human neurodegenerative disorders, *e.g.*, mitochondria becoming attached predominantly to perinuclear inclusions containing ER proteins in a Huntington disease cell culture model (Waelter et al., 2001). Similarly, Stenoien and co-authors have reported that mutant androgen receptors accumulate in cytoplasmic and nuclear aggregates that sequester mitochondria (Stenoien et al., 1999). Thus, augmented association between mitochondria and NE-ER-derived structures might be a characteristic attribute in both VCP-related disorders in humans and in *cdc48*^{S565G} yeast.

Third, a mitochondria-dependent progression of apoptosis was observed in the *cdc48*^{S565G} strain. This finding strikingly correlates with the proceeding of cell death observed in neurodegenerative diseases, that show typical hallmarks of mitochondria-dependent apoptosis, *e.g.*, depolarization of mitochondria, emergence of ROS and translocation of cytochrome *c* into the cytosol (Jana et al., 2001; Wyttenbach et al., 2002).

In the light of these observations, identification of the molecular mechanisms of degeneration and cell death associated with Cdc48p/VCP bears implications for a variety of diseases characterized by abnormal protein deposits. This study points at a crucial role of Cdc48p/VCP in common pathological mechanism of degeneration associated with the ERAD-ubiquitin-proteasome system.

2. Analysis of VCP variants in mammalian cell culture

Upon mutation of *CDC48* (*cdc48*^{S565G}), yeast cells show dysfunctional ERAD accompanied with increased association of NE-ER and mitochondria. The latter might be the cause for the increased susceptibility of *cdc48*^{S565G} cells to undergo mitochondria-dependent apoptotic cell death (see Discussion 1.4). Human VCP, the highly conserved orthologue of yeast Cdc48p, has been proposed as sensor for misfolded proteins associated with human degenerative disorders (Hirabayashi et al., 2001; Mizuno et al., 2003) and is associated upon mutation with the dominant progressive human disorder IBMPFD (Schröder et al., 2005; Watts et al., 2004). In order to correlate cellular mechanisms proposed for yeast cells expressing mutant *CDC48* (*cdc48*^{S565G}) with the potential role of human VCP in degenerative disorders, a mammalian cell culture system expressing wild-type VCP and several VCP variants was established. Beside wild-type VCP three different VCP variants were generated: (i) VCP-K524A, a dominant ATPase-deficient variant (Kobayashi et al., 2002; Wang et al., 2003a), (ii) VCP-S555G, a variant homologous to the yeast variant Cdc48p-S565G, and (iii) VCP-R155H, the most common variant causative for IBMPFD that bears the mutation in the N-terminal domain and not in the ATPase domain of VCP (Schröder et al., 2005; Watts et al., 2004).

2.1 VCP mutations in the major ATPase domain of VCP severely impair cell viability and cell morphology and result in cell death

Loss of VCP ATPase activity (overexpression of VCP-K524A) had drastic effects on both cell viability and cell morphology. Cells lost contact to neighboring cells, they rounded up and detached from the culture dish. Consistently, subcellular morphological alterations, such as cytoplasmic vacuolization, occurred. Nuclei from cells overexpressing VCP-K524A condensed, often resulting in sickle-shaped and fragmented nuclei. Beside these morphological alterations, on molecular level the processing of the nuclear protein PARP and accumulation of polyubiquitinated proteins were observed. Abnormally shaped nuclei and processing of the caspase substrate PARP are morphological and molecular characteristics of apoptotic cell death (Kuo et al., 2006; Lazebnik et al., 1994; Nosseri et al., 1994). Cellular enrichment of polyubiquitinated proteins is a characteristic for dysfunction of the ubiquitin-proteasome system (UPS) (Fortun et al., 2005; Piccinini et al., 2001). Emergence of these features therefore suggests induction of apoptotic cell death upon dysfunction of the UPS in cells expressing ATPase-deficient VCP-K524A. These data are in accordance to previous results that revealed that cells overexpressing ATPase-deficient VCP demonstrated

cytoplasmic vacuolization and cell death (Hirabayashi et al., 2001; Kobayashi et al., 2002). Thus, the observed decrease in cell viability and severe morphological alterations upon overexpression of mutant VCP-K524A sustain the essential cellular role of VCP and its ATPase activity for proper cellular function.

Overexpression of VCP-S555G, the homologous VCP variant of yeast Cdc48p-S565G that is causative for increased susceptibility for apoptotic cell death in *S. cerevisiae* (see Discussion 1.), led to similar but less severe phenotypes when compared to overexpression of VCP-K524A. Decreased cell viability, altered cellular morphology, PARP processing and accumulation of polyubiquitinated proteins was observed. The amino acid exchange in the S555G variant lies in between the highly conserved Walker A and Walker B motifs of the D2 domain that harbors the major ATPase activity of VCP. Thus, it is likely that overexpression of the VCP-S555G variant, similar to overexpression of VCP-K524A, also impairs ATPase activity of cellular VCP. This might also result in dysfunction of the UPS, ultimately leading to decreased cell viability and increased apoptotic cell death. Accumulation of polyubiquitinated proteins, decreased cell viability and increased susceptibility for apoptotic cell death was also observed in the *cdc48^{S565G}* yeast strain expressing Cdc48p-S565G. These similarities of yeast cells expressing Cdc48p-S565G and mammalian cells expressing VCP-S555G strongly support the relevance of the *cdc48^{S565G}* yeast strain used as a model for VCP-mediated pathophysiological processes (see Discussion 1.4).

VCP-R155H, the most frequent mutation causing the human disorder IBMPFD (Haubenberger et al., 2005; Schröder et al., 2005; Watts et al., 2004), does not lead to a decrease in cell viability, to marked morphological alterations or to an increase in apoptotic cell death upon overexpression. However, it should be noted that, consistent to very recently published data (Weihl et al., 2006), transfection of a higher amount of VCP-R155H but not of wild-type VCP resulted in the emergence of VCP-containing cellular aggregates (data not shown). It has been shown that in VCP-R155H ATPase activity is not impaired (Weihl et al., 2006). The mutation affects the N-terminal domain of VCP known to be involved in substrate and co-factor binding (Wang et al., 2004). Notably, all VCP mutations causing IBMPFD are localized in the N-terminal domain of this protein and none is localized within the two ATPase domains (Haubenberger et al., 2005; Schröder et al., 2005; Watts et al., 2004). Thus, ATPase activity of VCP is essential for cell survival. In contrast, although causative for the human degenerative disorder IBMPFD, mutation of the N-terminal domain of VCP appears to be tolerable for cells, at least under unstressed conditions.

2.2 VCP mutations in the ATPase domain and the most common IBMPFD-causing mutation result in impairment of ERAD

Wild-type VCP and the VCP variants VCP-K524A, VCP-S555G and VCP-R155H were evaluated for their functionality in the ERAD pathway applying co-expression studies with the ERAD substrate rhodopsin. The visual pigment rhodopsin is a highly hydrophobic membrane protein synthesized via the secretory pathway (Alberts et al., 1994a). Rhodopsin-P23H is causative for the retinal disorder retinitis pigmentosa (Chapple et al., 2001; Naash et al., 1993; Olsson et al., 1992; Sung et al., 1993). It is prone to misfold and aggregate within the ER membrane and the Golgi (Frederick et al., 2001; Illing et al., 2002; Saliba et al., 2002). Wild-type rhodopsin and its variants are substrates of the ER-associated protein quality control and are therefore degraded via the ERAD pathway upon misfolding (Saliba et al., 2002; Ye, 2005). Co-expression of the ATPase-deficient VCP variant VCP-K524A with wild-type rhodopsin and rhodopsin-P23H resulted in the accumulation of high-molecular rhodopsin aggregates. The same was true for the potential ATPase-deficient VCP variant VCP-S555G. ATPase activity of VCP has been suggested to be essential for retrotranslocation of ERAD substrates into the cytosol (Ye, 2005; Ye, 2006). Thus, loss of VCP ATPase activity impairs both ERAD and cell viability, further sustaining the importance of ATPase activity for proper cellular function.

Interestingly, co-expression of VCP-R155H with the ERAD substrates wild-type rhodopsin resulted in a marked accumulation of cellular rhodopsin. However, compared to the effects of VCP-K524A and VCP-S555G, the effects of VCP-R155H were comparatively weak. Very recently, it has been shown that co-expression of the ERAD substrate CFTR- Δ F508 with VCP-R155H resulted in the accumulation of cellular CFTR- Δ F508 (Weihl et al., 2006). Mutation of the multipass membrane protein ‘cystic fibrosis transmembrane regulator’ (CFTR- Δ F508) is the most frequent cause for cystic fibrosis, a human multisystem disorder affecting predominantly the respiratory tract (Riordan, 1999). As a protein of the secretory pathway it is synthesized into the ER membrane, processed in the Golgi and finally transported into the plasma membrane where it forms a chloride channel (Marcet and Boeynaems, 2006). Upon mutation (CFTR- Δ F508), CFTR is prone for misfolding in the ER membrane and, like rhodopsin, a membrane substrate of ERAD and of VCP (Vij et al., 2006; Weihl et al., 2006). The enrichment of CFTR- Δ F508 upon co-expression of VCP-R155H was proposed to be due to dysfunction of VCP-R155H in the ERAD pathway (Weihl et al., 2006). Thus, the observed accumulation of the ERAD substrate rhodopsin upon co-expression of VCP-R155H, sustains dysfunction of this variant in the ERAD pathway.

The amino acid exchange in the VCP-R155H variant is harbored, like all IBMPFD-associated mutations (Haubenberger et al., 2005; Schröder et al., 2005; Watts et al., 2004), in the N-terminal domain of VCP involved in substrate and co-factor binding (Wang et al., 2004). Since ATPase activity is not impaired in VCP-R155H (Weihl et al., 2006), ERAD deficiency upon VCP mutation may be caused by altered binding of VCP to its substrates or to co-factors involved in the transfer of ubiquitinated substrates via VCP to the proteasome. The resulting lower activity of the VCP complex in the ERAD pathway appears to be tolerated by the cells under normal conditions. However, upon stress, *e.g.*, overexpression of ERAD substrates (rhodopsin), the lower ERAD efficiency becomes evident.

IBMPFD is characterized by the emergence of ubiquitinated protein deposits in brain, muscle or bone tissue (Haubenberger et al., 2005; Schröder et al., 2005; Watts et al., 2004). The comparatively late-onset of this disease (42 years for inclusion body myopathy and Paget disease of bone, 53 years for frontotemporal dementia, Watts et al., 2004) might be a result of the slow but steady accumulation of misfolded and aggregated proteins upon ageing. This might challenge the ER protein quality control system that has a lower efficiency due to VCP mutations, leading to enrichment of toxic aggregated protein species, eventually resulting in cell death and tissue degeneration.

Various human degenerative disorders, such as polyglutamine disorders and Parkinson disease, are characterized by cellular protein deposits that are built up by misfolded and aggregated proteins (Bossy-Wetzel et al., 2004; Goellner and Rechsteiner, 2003). Protein aggregates are often comprised of a mutated protein that has a high tendency for misfolding and is causative for the respective disease (*e.g.*, huntingtin for Huntington diseases and α -synuclein for Parkinson disease) (Bossy-Wetzel et al., 2004; Goellner and Rechsteiner, 2003). VCP has been proposed as sensor for such misfolded and aggregated proteins (Hirabayashi et al., 2001; Mizuno et al., 2003). Therefore, it is tempting to speculate that endogenous wild-type VCP is sequestered by accumulation of protein aggregates. This might result in an overwhelming of the ER protein quality control system, leading to an increased susceptibility to apoptotic cell death. This hypothesis might explain the role of VCP in human degenerative disorders that has been proposed in the case of polyglutamine disorders (Higashiyama et al., 2002; Hirabayashi et al., 2001; Mizuno et al., 2003; Yamanaka et al., 2004).

3. Perspectives

A yeast strain expressing mutant *CDC48* (*cdc48*^{S565G}) has an increased susceptibility to undergo apoptotic cell death (Madeo et al., 1997). Starting from a differential proteome analysis, I revealed that upon ERAD dysfunction due to *CDC48* mutation (*cdc48*^{S565G}), mitochondria are crucially involved in apoptotic cell death in yeast. Several of the observed altered mitochondrial proteins are implicated as regulators of mitochondrial functionality and mitochondria-mediated apoptotic cell death. Independent of its enzymatic activity in the Krebs cycle, aconitase has been demonstrated to be essential for maintenance of mtDNA in yeast (Chen et al., 2005). It might be of interest if the homologous proteins homoaconitase and putative aconitase, two proteins significantly depleted in mitochondrial extracts of apoptotic *cdc48*^{S565G} cells, play a similar role for mitochondrial functionality. Furthermore, the mitochondrial cyclophilin is a known regulator of the mitochondrial permeability transition pore complex in mammalian cells (Schubert and Grimm, 2004). A similar role of this protein during yeast apoptosis might be feasible, because the yeast homologue was markedly depleted in mitochondrial extracts. Further studies have to evaluate the potential roles of these mitochondrial proteins during apoptosis in *cdc48*^{S565G} cells.

Upon *CDC48* mutation (*cdc48*^{S565G}) yeast cells demonstrate ER stress and impaired functionality of the ERAD pathway. Concomitantly, I could show an increased spatial proximity between NE-ER and mitochondria on cellular level and augmented association of NE-ER-derived microsomes and mitochondria in mitochondrial extracts in this strain under apoptotic growth conditions. Based on these data, I propose a model of apoptotic cell death in the *cdc48*^{S565G} strain, where upon *CDC48* mutation subsequent emergence of ER stress is transferred to a close-by mitochondrial fraction that eventually triggers mitochondria-mediated cell death. Further studies have to evaluate the mechanism of the interorganelle transfer of cellular stress. Analysis of the transport of phospholipids from the ER to mitochondria and *vice versa* could clarify if this cellular process essential for the renewal of mitochondrial membranes is disturbed upon ER stress and/or ERAD deficiency. Moreover, it is interesting if ROS emerge in yeast cells upon *CDC48* mutation (*cdc48*^{S565G}) aside mitochondria within the ER as it is described for another ERAD deficient yeast strain (Haynes et al., 2004). If this is the case, it appears attractive to investigate, whether ER-derived ROS are a causative first event, triggering the observed damage of mitochondrial membranes that then result in the observed boost of mitochondrially-produced ROS triggering cell death.

Consistently to the results obtained in yeast, I could demonstrate in mammalian cell culture that cells expressing the ATPase-deficient VCP variant VCP-K524A and the potential

ATPase-deficient variant VCP-S555G, the homologous variant to yeast Cdc48p-S565G, show features of apoptotic cell death. In further studies, mechanisms of VCP-mediated apoptotic cell death will be analyzed in more detail, especially concerning a potential crucial role of mitochondria in cell death as was demonstrated in the homologous *cdc48*^{S565G} yeast model. Therefore, I have employed the neuronal rat cell line PC12 to establish stable cell lines expressing wild-type VCP and VCP variants in a tetracycline-regulated fashion (data not shown). PC12 is a well characterized cell line concerning mechanisms of cell signaling and apoptosis (Mills et al., 1995; Valavanis et al., 2001) and should therefore be a good model system to analyze mechanisms of apoptotic cell death upon VCP mutation in the future.

In contrast to expression of ATPase-deficient VCP variants in mammalian cell culture, expressing the most prevalent VCP variant causing the human disorder IBMPFD (VCP-R155H) does not reduce cell viability. It is of high interest if cells expressing VCP-R155H (and other IBMPFD-associated variants) are more vulnerable when treated with different stressors. Induction of ER stress or protein misfolding stress (*e.g.*, via overexpression of aggregation-prone proteins) may challenge the impaired function of VCP upon mutation (see below) and therewith result in decreased cell viability and increased susceptibility to apoptotic cell death. Such a scenario might explain how accumulating stress upon ageing results in a comparatively late-onset induction of cell degeneration in IBMPFD.

Co-expression of the ERAD substrate rhodopsin and VCP resulted in a marked accumulation of rhodopsin for the IBMPFD-associated VCP variant VCP-R155H. Since all IBMPFD-associated VCP variants harbor a mutation in the N-terminal domain of VCP involved in substrate and co-factor binding (Haubenberger et al., 2005; Schröder et al., 2005; Watts et al., 2004), it is tempting to speculate that impaired binding of protein substrates or regulating co-factors might be the reason for the dysfunction of ERAD in IBMPFD. Determination of protein interactors of wild-type VCP and IBMPFD-associated VCP variants via pull-down, immunoprecipitation, blue native gel electrophoresis or yeast two-hybrid analyses might therefore give important insights in both the mechanisms triggering cell death in IBMPFD and the essential function of VCP and its cofactors in ERAD.

H. References

- Acharya, U., Jacobs, R., Peters, J. M., Watson, N., Farquhar, M. G., and Malhotra, V. (1995). The formation of Golgi stacks from vesiculated Golgi membranes requires two distinct fusion events. *Cell* 82, 895-904.
- Achleitner, G., Gaigg, B., Krasser, A., Kainersdorfer, E., Kohlwein, S. D., Perktold, A., Zellnig, G., and Daum, G. (1999). Association between the endoplasmic reticulum and mitochondria of yeast facilitates interorganelle transport of phospholipids through membrane contact. *Eur J Biochem* 264, 545-553.
- Alberts, B., Bray, D., Lewis, J., Raff, M., Roberts, K., and Watson, J. D. (1994a). Chapter 12: Intracellular Compartments and Protein Sorting; The Endoplasmic Reticulum. In *Molecular Biology of the Cell* (New York, Garland Publishing, Inc.). pp. 577-598.
- Alberts, B., Bray, D., Lewis, J., Raff, M., Roberts, K., and Watson, J. D. (1994b). Chapter 23: The Immune System. In *Molecular Biology of the Cell* (New York, Garland Publishing, Inc.). pp. 1196-1254.
- Anderson, L., and Seilhamer, J. (1997). A comparison of selected mRNA and protein abundances in human liver. *Electrophoresis* 18, 533-537.
- Asai, T., Tomita, Y., Nakatsuka, S., Hoshida, Y., Myoui, A., Yoshikawa, H., and Aozasa, K. (2002). VCP (p97) regulates NF κ B signaling pathway, which is important for metastasis of osteosarcoma cell line. *Jpn J Cancer Res* 93, 296-304.
- Baggerman, G., Vierstraete, E., De Loof, A., and Schoofs, L. (2005). Gel-based versus gel-free proteomics: a review. *Comb Chem High Throughput Screen* 8, 669-677.
- Barros, M. H., Netto, L. E., and Kowaltowski, A. J. (2003). H₂O₂ generation in *Saccharomyces cerevisiae* respiratory pet mutants: effect of cytochrome *c*. *Free Radic Biol Med* 35, 179-188.
- Baumann, O., and Walz, B. (2001). Endoplasmic reticulum of animal cells and its organization into structural and functional domains. *Int Rev Cytol* 205, 149-214.
- Bernardi, P., Scorrano, L., Colonna, R., Petronilli, V., and Di Lisa, F. (1999). Mitochondria and cell death. Mechanistic aspects and methodological issues. *Eur J Biochem* 264, 687-701.
- Beuron, F., Flynn, T. C., Ma, J., Kondo, H., Zhang, X., and Freemont, P. S. (2003). Motions and negative cooperativity between p97 domains revealed by cryo-electron microscopy and quantised elastic deformational model. *J Mol Biol* 327, 619-629.
- Bisle, B., Schmidt, A., Scheibe, B., Klein, C., Tebbe, A., Kellermann, J., Siedler, F., Pfeiffer, F., Lottspeich, F., and Oesterhelt, D. (2006). Quantitative profiling of the membrane proteome in a halophilic archaeon. *Mol Cell Proteomics* 5, 1543-1558.
- Bitterman, K. J., Medvedik, O., and Sinclair, D. A. (2003). Longevity regulation in *Saccharomyces cerevisiae*: linking metabolism, genome stability, and heterochromatin. *Microbiol Mol Biol Rev* 67, 376-399.

- Boldogh, I. R., Yang, H. C., Nowakowski, W. D., Karmon, S. L., Hays, L. G., Yates, J. R., 3rd, and Pon, L. A. (2001). Arp2/3 complex and actin dynamics are required for actin-based mitochondrial motility in yeast. *Proc Natl Acad Sci U S A* 98, 3162-3167.
- Bossy-Wetzel, E., Schwarzenbacher, R., and Lipton, S. A. (2004). Molecular pathways to neurodegeneration. *Nat Med* 10 *Suppl*, S2-9.
- Botstein, D., Chervitz, S. A., and Cherry, J. M. (1997). Yeast as a model organism. *Science* 277, 1259-1260.
- Boya, P., Cohen, I., Zamzami, N., Vieira, H. L., and Kroemer, G. (2002). Endoplasmic reticulum stress-induced cell death requires mitochondrial membrane permeabilization. *Cell Death Differ* 9, 465-467.
- Bradford, M. M. (1976). A rapid and sensitive method for the quantitation of microgram quantities of protein utilizing the principle of protein-dye binding. *Anal Biochem* 72, 248-254.
- Braun, R. J. (2002) Detaillierte Proteomanalyse des apoptotischen Programms der Hefemutante Cdc48^{S565G}, Diplomarbeit, Eberhard-Karls-Universität Tübingen, Tübingen.
- Braun, R. J., Kinkl, N., Zischka, H., and Ueffing, M. (submitted). 16-BAC/SDS-PAGE analysis of membrane proteins of yeast mitochondria purified by free flow electrophoresis. In *Methods in the Proteomics of Membrane Proteins*, M. Peirce, ed. (Humana Press).
- Breitenbach, M., Laun, P., and Gimona, M. (2005). The actin cytoskeleton, RAS-cAMP signaling and mitochondrial ROS in yeast apoptosis. *Trends Cell Biol* 15, 637-639.
- Brunger, A. T., and DeLaBarre, B. (2003). NSF and p97/VCP: similar at first, different at last. *FEBS Lett* 555, 126-133.
- Byers, B., and Goetsch, L. (1991). Guide to Yeast Genetics and Molecular Biology. In *Guide to Yeast Genetics and Molecular Biology*, C. Guthrie, ed. (San Diego, Academic Press), pp. 603-626.
- Candiano, G., Bruschi, M., Musante, L., Santucci, L., Ghiggeri, G. M., Carnemolla, B., Orecchia, P., Zardi, L., and Righetti, P. G. (2004). Blue silver: a very sensitive colloidal Coomassie G-250 staining for proteome analysis. *Electrophoresis* 25, 1327-1333.
- Cao, K., Nakajima, R., Meyer, H. H., and Zheng, Y. (2003). The AAA-ATPase Cdc48/p97 regulates spindle disassembly at the end of mitosis. *Cell* 115, 355-367.
- Chapple, J. P., Grayson, C., Hardcastle, A. J., Saliba, R. S., van der Spuy, J., and Cheetham, M. E. (2001). Unfolding retinal dystrophies: a role for molecular chaperones? *Trends Mol Med* 7, 414-421.
- Chen, X. J., Wang, X., Kaufman, B. A., and Butow, R. A. (2005). Aconitase couples metabolic regulation to mitochondrial DNA maintenance. *Science* 307, 714-717.
- Cherry, J. M., Ball, C., Weng, S., Juvik, G., Schmidt, R., Adler, C., Dunn, B., Dwight, S., Riles, L., Mortimer, R. K., and Botstein, D. (1997). Genetic and physical maps of *Saccharomyces cerevisiae*. *Nature* 387, 67-73.

- Crofts, A. R., Barquera, B., Gennis, R. B., Kuras, R., Guergova-Kuras, M., and Berry, E. A. (1999). Mechanism of ubiquinol oxidation by the *bc*₁ complex: different domains of the quinol binding pocket and their role in the mechanism and binding of inhibitors. *Biochemistry* 38, 15807-15826.
- Dai, R. M., Chen, E., Longo, D. L., Gorbea, C. M., and Li, C. C. (1998). Involvement of valosin-containing protein, an ATPase co-purified with I κ B α and 26 S proteasome, in ubiquitin-proteasome-mediated degradation of I κ B α . *J Biol Chem* 273, 3562-3573.
- Dai, R. M., and Li, C. C. (2001). Valosin-containing protein is a multi-ubiquitin chain-targeting factor required in ubiquitin-proteasome degradation. *Nat Cell Biol* 3, 740-744.
- Del Carratore, R., Della Croce, C., Simili, M., Taccini, E., Scavuzzo, M., and Sbrana, S. (2002). Cell cycle and morphological alterations as indicative of apoptosis promoted by UV irradiation in *S. cerevisiae*. *Mutat Res* 513, 183-191.
- DeLaBarre, B., and Brunger, A. T. (2003). Complete structure of p97/valosin-containing protein reveals communication between nucleotide domains. *Nat Struct Biol* 10, 856-863.
- DeLaBarre, B., and Brunger, A. T. (2005). Nucleotide dependent motion and mechanism of action of p97/VCP. *J Mol Biol* 347, 437-452.
- DeLaBarre, B., Christianson, J. C., Kopito, R. R., and Brunger, A. T. (2006). Central pore residues mediate the p97/VCP activity required for ERAD. *Mol Cell* 22, 451-462.
- Domon, B., and Broder, S. (2004). Implications of new proteomics strategies for biology and medicine. *J Proteome Res* 3, 253-260.
- Drakulic, T., Temple, M. D., Guido, R., Jarolim, S., Breitenbach, M., Attfield, P. V., and Dawes, I. W. (2005). Involvement of oxidative stress response genes in redox homeostasis, the level of reactive oxygen species, and ageing in *Saccharomyces cerevisiae*. *FEMS Yeast Res* 5, 1215-1228.
- Dreveny, I., Pye, V. E., Beuron, F., Briggs, L. C., Isaacson, R. L., Matthews, S. J., McKeown, C., Yuan, X., Zhang, X., and Freemont, P. S. (2004). p97 and close encounters of every kind: a brief review. *Biochem Soc Trans* 32, 715-720.
- Dujon, B. (1998). European Functional Analysis Network (EUROFAN) and the functional analysis of the *Saccharomyces cerevisiae* genome. *Electrophoresis* 19, 617-624.
- Elkabetz, Y., Shapira, I., Rabinovich, E., and Bar-Nun, S. (2004). Distinct steps in dislocation of luminal endoplasmic reticulum-associated degradation substrates: roles of endoplasmic reticulum-bound p97/Cdc48p and proteasome. *J Biol Chem* 279, 3980-3989.
- Enenkel, C., Lehmann, A., and Kloetzel, P. M. (1998). Subcellular distribution of proteasomes implicates a major location of protein degradation in the nuclear envelope-ER network in yeast. *Embo J* 17, 6144-6154.
- Ericson, I. (1974). Determination of the isoelectric point of rat liver mitochondria by cross-partition. *Biochim Biophys Acta* 356, 100-107.

- Fabrizio, P., and Longo, V. D. (2003). The chronological life span of *Saccharomyces cerevisiae*. *Aging Cell* 2, 73-81.
- Fang, J., and Beattie, D. S. (2003). External alternative NADH dehydrogenase of *Saccharomyces cerevisiae*: a potential source of superoxide. *Free Radic Biol Med* 34, 478-488.
- Farber, J. L. (1994). Mechanisms of cell injury by activated oxygen species. *Environ Health Perspect* 102 Suppl 10, 17-24.
- Feiler, H. S., Desprez, T., Santoni, V., Kronenberger, J., Caboche, M., and Traas, J. (1995). The higher plant *Arabidopsis thaliana* encodes a functional *CDC48* homologue which is highly expressed in dividing and expanding cells. *Embo J* 14, 5626-5637.
- Felgner, J. H., Kumar, R., Sridhar, C. N., Wheeler, C. J., Tsai, Y. J., Border, R., Ramsey, P., Martin, M., and Felgner, P. L. (1994). Enhanced gene delivery and mechanism studies with a novel series of cationic lipid formulations. *J Biol Chem* 269, 2550-2561.
- Filippin, L., Magalhaes, P. J., Di Benedetto, G., Colella, M., and Pozzan, T. (2003). Stable interactions between mitochondria and endoplasmic reticulum allow rapid accumulation of calcium in a subpopulation of mitochondria. *J Biol Chem* 278, 39224-39234.
- Fink, G. R., and Guthrie, C. (1992). *Guide to Yeast Genetics and Molecular and Cell Biology* (San Diego, Academic Press).
- Forman, M. S., Mackenzie, I. R., Cairns, N. J., Swanson, E., Boyer, P. J., Drachman, D. A., Jhaveri, B. S., Karlawish, J. H., Pestronk, A., Smith, T. W., *et al.* (2006). Novel Ubiquitin Neuropathology in Frontotemporal Dementia With Valosin-Containing Protein Gene Mutations. *J Neuropathol Exp Neurol* 65, 571-581.
- Fortun, J., Li, J., Go, J., Fenstermaker, A., Fletcher, B. S., and Notterpek, L. (2005). Impaired proteasome activity and accumulation of ubiquitinated substrates in a hereditary neuropathy model. *J Neurochem* 92, 1531-1541.
- Frederick, J. M., Krasnoperova, N. V., Hoffmann, K., Church-Kopish, J., Ruther, K., Howes, K., Lem, J., and Baehr, W. (2001). Mutant rhodopsin transgene expression on a null background. *Invest Ophthalmol Vis Sci* 42, 826-833.
- Frigerio, G., and Pelham, H. R. (1993). A *Saccharomyces cerevisiae* cyclophilin resident in the endoplasmic reticulum. *J Mol Biol* 233, 183-188.
- Fröhlich, K. U., Fries, H. W., Rüdiger, M., Erdmann, R., Botstein, D., and Mecke, D. (1991). Yeast cell cycle protein CDC48p shows full-length homology to the mammalian protein VCP and is a member of a protein family involved in secretion, peroxisome formation, and gene expression. *J Cell Biol* 114, 443-453.
- Fu, X., Ng, C., Feng, D., and Liang, C. (2003). Cdc48p is required for the cell cycle commitment point at Start via degradation of the G1-CDK inhibitor Far1p. *J Cell Biol* 163, 21-26.

- Fujiki, Y., Hubbard, A. L., Fowler, S., and Lazarow, P. B. (1982). Isolation of intracellular membranes by means of sodium carbonate treatment: application to endoplasmic reticulum. *J Cell Biol* 93, 97-102.
- Garini, Y., Vermolen, B. J., and Young, I. T. (2005). From micro to nano: recent advances in high-resolution microscopy. *Curr Opin Biotechnol* 16, 3-12.
- Garriga, P., and Manyosa, J. (2002). The eye photoreceptor protein rhodopsin. Structural implications for retinal disease. *FEBS Lett* 528, 17-22.
- Gavin, A. C., Bosche, M., Krause, R., Grandi, P., Marzioch, M., Bauer, A., Schultz, J., Rick, J. M., Michon, A. M., Cruciat, C. M., *et al.* (2002). Functional organization of the yeast proteome by systematic analysis of protein complexes. *Nature* 415, 141-147.
- Ghislain, M., Dohmen, R. J., Levy, F., and Varshavsky, A. (1996). Cdc48p interacts with Ufd3p, a WD repeat protein required for ubiquitin-mediated proteolysis in *Saccharomyces cerevisiae*. *Embo J* 15, 4884-4899.
- Goellner, G. M., and Rechsteiner, M. (2003). Are Huntington's and polyglutamine-based ataxias proteasome storage diseases? *Int J Biochem Cell Biol* 35, 562-571.
- Goetz, J. G., and Nabi, I. R. (2006). Interaction of the smooth endoplasmic reticulum and mitochondria. *Biochem Soc Trans* 34, 370-373.
- Golbik, R., Lupas, A. N., Koretke, K. K., Baumeister, W., and Peters, J. (1999). The Janus face of the archaeal Cdc48/p97 homologue VAT: protein folding versus unfolding. *Biol Chem* 380, 1049-1062.
- Görg, A., Postel, W., and Gunther, S. (1988). The current state of two-dimensional electrophoresis with immobilized pH gradients. *Electrophoresis* 9, 531-546.
- Görg, A., Weiss, W., and Dunn, M. J. (2004). Current two-dimensional electrophoresis technology for proteomics. *Proteomics* 4, 3665-3685.
- Gourlay, C. W., Carpp, L. N., Timpson, P., Winder, S. J., and Ayscough, K. R. (2004). A role for the actin cytoskeleton in cell death and aging in yeast. *J Cell Biol* 164, 803-809.
- Green, D. R., and Kroemer, G. (2004). The pathophysiology of mitochondrial cell death. *Science* 305, 626-629.
- Guyant-Marechal, L., Laquerriere, A., Duyckaerts, C., Dumanchin, C., Bou, J., Dugny, F., Le Ber, I., Frebourg, T., Hannequin, D., and Campion, D. (2006). Valosin-containing protein gene mutations: Clinical and neuropathologic features. *Neurology* 67, 644-651.
- Gygi, S. P., Rochon, Y., Franza, B. R., and Aebersold, R. (1999). Correlation between protein and mRNA abundance in yeast. *Mol Cell Biol* 19, 1720-1730.
- Halawani, D., and Latterich, M. (2006). p97: The Cell's Molecular Purgatory? *Mol Cell* 22, 713-717.

Hannig, K., and Heidrich, H. G. (1990). *Free-Flow Electrophoresis*, 1 edn (Darmstadt, GIT Verlag).

Hartinger, J., Stenius, K., Hogemann, D., and Jahn, R. (1996). 16-BAC/SDS-PAGE: a two-dimensional gel electrophoresis system suitable for the separation of integral membrane proteins. *Anal Biochem* 240, 126-133.

Haubenberger, D., Bittner, R. E., Rauch-Shorny, S., Zimprich, F., Mannhalter, C., Wagner, L., Mineva, I., Vass, K., Auff, E., and Zimprich, A. (2005). Inclusion body myopathy and Paget disease is linked to a novel mutation in the VCP gene. *Neurology* 65, 1304-1305.

Haynes, C. M., Titus, E. A., and Cooper, A. A. (2004). Degradation of misfolded proteins prevents ER-derived oxidative stress and cell death. *Mol Cell* 15, 767-776.

Hepler, P. K. (1981). The structure of the endoplasmic reticulum revealed by osmium tetroxide-potassium ferricyanide staining. *Eur J Cell Biol* 26, 102-111.

Herker, E., Jungwirth, H., Lehmann, K. A., Maldener, C., Fröhlich, K. U., Wissing, S., Büttner, S., Fehr, M., Sigrist, S., and Madeo, F. (2004). Chronological aging leads to apoptosis in yeast. *J Cell Biol* 164, 501-507.

Hermann, G. J., and Shaw, J. M. (1998). Mitochondrial dynamics in yeast. *Annu Rev Cell Dev Biol* 14, 265-303.

Herrmann, J. M., Fölsch, H., Neupert, W., and Stuart, R. A. (1994). Isolation of Yeast Mitochondria and Study of Mitochondrial Protein Translation. In *Cell Biology: A Laboratory Handbook*, D. E. Celis, ed. (San Diego, Academic Press), pp. 538-544.

Hetzer, M., Meyer, H. H., Walther, T. C., Bilbao-Cortes, D., Warren, G., and Mattaj, I. W. (2001). Distinct AAA-ATPase p97 complexes function in discrete steps of nuclear assembly. *Nat Cell Biol* 3, 1086-1091.

Higashiyama, H., Hirose, F., Yamaguchi, M., Inoue, Y. H., Fujikake, N., Matsukage, A., and Kakizuka, A. (2002). Identification of ter94, *Drosophila* VCP, as a modulator of polyglutamine-induced neurodegeneration. *Cell Death Differ* 9, 264-273.

Hiller, M. M., Finger, A., Schweiger, M., and Wolf, D. H. (1996). ER degradation of a misfolded luminal protein by the cytosolic ubiquitin-proteasome pathway. *Science* 273, 1725-1728.

Hirabayashi, J. (2004). Lectin-based structural glycomics: glycoproteomics and glycan profiling. *Glycoconj J* 21, 35-40.

Hirabayashi, M., Inoue, K., Tanaka, K., Nakadate, K., Ohsawa, Y., Kamei, Y., Popiel, A. H., Sinohara, A., Iwamatsu, A., Kimura, Y., *et al.* (2001). VCP/p97 in abnormal protein aggregates, cytoplasmic vacuoles, and cell death, phenotypes relevant to neurodegeneration. *Cell Death Differ* 8, 977-984.

Hitchcock, A. L., Krebber, H., Fietze, S., Lin, A., Latterich, M., and Silver, P. A. (2001). The conserved npl4 protein complex mediates proteasome-dependent membrane-bound transcription factor activation. *Mol Biol Cell* 12, 3226-3241.

- Hubbard, M. J. (2002). Functional proteomics: The goalposts are moving. *Proteomics* 2, 1069-1078.
- Huh, G. H., Damsz, B., Matsumoto, T. K., Reddy, M. P., Rus, A. M., Ibeas, J. I., Narasimhan, M. L., Bressan, R. A., and Hasegawa, P. M. (2002). Salt causes ion disequilibrium-induced programmed cell death in yeast and plants. *Plant J* 29, 649-659.
- Huyer, G., Piluek, W. F., Fansler, Z., Kreft, S. G., Hochstrasser, M., Brodsky, J. L., and Michaelis, S. (2004). Distinct machinery is required in *Saccharomyces cerevisiae* for the endoplasmic reticulum-associated degradation of a multispinning membrane protein and a soluble luminal protein. *J Biol Chem* 279, 38369-38378.
- Huyton, T., Pye, V. E., Briggs, L. C., Flynn, T. C., Beuron, F., Kondo, H., Ma, J., Zhang, X., and Freemont, P. S. (2003). The crystal structure of murine p97/VCP at 3.6Å. *J Struct Biol* 144, 337-348.
- Illing, M. E., Rajan, R. S., Bence, N. F., and Kopito, R. R. (2002). A rhodopsin mutant linked to autosomal dominant retinitis pigmentosa is prone to aggregate and interacts with the ubiquitin proteasome system. *J Biol Chem* 277, 34150-34160.
- Imamura, S., Ojima, N., and Yamashita, M. (2003). Cold-inducible expression of the cell division cycle gene *CDC48* and its promotion of cell proliferation during cold acclimation in zebrafish cells. *FEBS Lett* 549, 14-20.
- Indig, F. E., Partridge, J. J., von Kobbe, C., Aladjem, M. I., Latterich, M., and Bohr, V. A. (2004). Werner syndrome protein directly binds to the AAA ATPase p97/VCP in an ATP-dependent fashion. *J Struct Biol* 146, 251-259.
- Islinger, M., Luers, G. H., Zischka, H., Ueffing, M., and Völkl, A. (2006). Insights into the membrane proteome of rat liver peroxisomes: microsomal glutathione-S-transferase is shared by both subcellular compartments. *Proteomics* 6, 804-816.
- Jana, N. R., Zemskov, E. A., Wang, G., and Nukina, N. (2001). Altered proteasomal function due to the expression of polyglutamine-expanded truncated N-terminal huntingtin induces apoptosis by caspase activation through mitochondrial cytochrome *c* release. *Hum Mol Genet* 10, 1049-1059.
- Jarosch, E., Taxis, C., Volkwein, C., Bordallo, J., Finley, D., Wolf, D. H., and Sommer, T. (2002). Protein dislocation from the ER requires polyubiquitination and the AAA-ATPase Cdc48. *Nat Cell Biol* 4, 134-139.
- Kerr, J. F., Wyllie, A. H., and Currie, A. R. (1972). Apoptosis: a basic biological phenomenon with wide-ranging implications in tissue kinetics. *Br J Cancer* 26, 239-257.
- Kimonis, V. E., Kovach, M. J., Waggoner, B., Leal, S., Salam, A., Rimer, L., Davis, K., Khardori, R., and Gelber, D. (2000). Clinical and molecular studies in a unique family with autosomal dominant limb-girdle muscular dystrophy and Paget disease of bone. *Genet Med* 2, 232-241.

Kimonis, V. E., and Watts, G. D. (2005). Autosomal dominant inclusion body myopathy, Paget disease of bone, and frontotemporal dementia. *Alzheimer Dis Assoc Disord* 19 Suppl 1, S44-47.

Klein, C., Garcia-Rizo, C., Bisle, B., Scheffer, B., Zischka, H., Pfeiffer, F., Siedler, F., and Oesterhelt, D. (2005). The membrane proteome of *Halobacterium salinarum*. *Proteomics* 5, 180-197.

Kobayashi, T., Tanaka, K., Inoue, K., and Kakizuka, A. (2002). Functional ATPase activity of p97/valosin-containing protein (VCP) is required for the quality control of endoplasmic reticulum in neuronally differentiated mammalian PC12 cells. *J Biol Chem* 277, 47358-47365.

Kohno, K., Normington, K., Sambrook, J., Gething, M. J., and Mori, K. (1993). The promoter region of the yeast KAR2 (BiP) gene contains a regulatory domain that responds to the presence of unfolded proteins in the endoplasmic reticulum. *Mol Cell Biol* 13, 877-890.

Koller, K. J., and Brownstein, M. J. (1987). Use of a cDNA clone to identify a supposed precursor protein containing valosin. *Nature* 325, 542-545.

Kondo, H., Rabouille, C., Newman, R., Levine, T. P., Pappin, D., Freemont, P., and Warren, G. (1997). p47 is a cofactor for p97-mediated membrane fusion. *Nature* 388, 75-78.

Kovach, M. J., Waggoner, B., Leal, S. M., Gelber, D., Khardori, R., Levenstien, M. A., Shanks, C. A., Gregg, G., Al-Lozi, M. T., Miller, T., *et al.* (2001). Clinical delineation and localization to chromosome 9p13.3-p12 of a unique dominant disorder in four families: hereditary inclusion body myopathy, Paget disease of bone, and frontotemporal dementia. *Mol Genet Metab* 74, 458-475.

Kuo, W. W., Liu, C. J., Chen, L. M., Wu, C. H., Chu, C. H., Liu, J. Y., Lu, M. C., Lin, J. A., Lee, S. D., and Huang, C. Y. (2006). Cardiomyoblast apoptosis induced by insulin-like growth factor (IGF)-I resistance is IGF-II dependent and synergistically enhanced by angiotensin II. *Apoptosis* 11, 1075-1089.

La Spada, A. R., and Taylor, J. P. (2003). Polyglutamines placed into context. *Neuron* 38, 681-684.

Laemmli, U. K. (1970). Cleavage of structural proteins during the assembly of the head of bacteriophage T4. *Nature* 227, 680-685.

Lamanda, A., Zahn, A., Roder, D., and Langen, H. (2004). Improved Ruthenium II tris (bathophenanthroline disulfonate) staining and destaining protocol for a better signal-to-background ratio and improved baseline resolution. *Proteomics* 4, 599-608.

Lamb, J. R., Fu, V., Wirtz, E., and Bangs, J. D. (2001). Functional analysis of the trypanosomal AAA protein TbVCP with trans-dominant ATP hydrolysis mutants. *J Biol Chem* 276, 21512-21520.

Latterich, M., Fröhlich, K. U., and Schekman, R. (1995). Membrane fusion and the cell cycle: Cdc48p participates in the fusion of ER membranes. *Cell* 82, 885-893.

- Laun, P., Pichova, A., Madeo, F., Fuchs, J., Ellinger, A., Kohlwein, S., Dawes, I., Fröhlich, K. U., and Breitenbach, M. (2001). Aged mother cells of *Saccharomyces cerevisiae* show markers of oxidative stress and apoptosis. *Mol Microbiol* 39, 1166-1173.
- Laun, P., Ramachandran, L., Jarolim, S., Herker, E., Liang, P., Wang, J., Weinberger, M., Burhans, D. T., Suter, B., Madeo, F., *et al.* (2005). A comparison of the aging and apoptotic transcriptome of *Saccharomyces cerevisiae*. *FEMS Yeast Res* 5, 1261-1272.
- Lazebnik, Y. A., Kaufmann, S. H., Desnoyers, S., Poirier, G. G., and Earnshaw, W. C. (1994). Cleavage of poly(ADP-ribose) polymerase by a proteinase with properties like ICE. *Nature* 371, 346-347.
- Li, F., Zhang, D., and Fujise, K. (2001). Characterization of fortilin, a novel antiapoptotic protein. *J Biol Chem* 276, 47542-47549.
- Loayza, D., Tam, A., Schmidt, W. K., and Michaelis, S. (1998). Ste6p mutants defective in exit from the endoplasmic reticulum (ER) reveal aspects of an ER quality control pathway in *Saccharomyces cerevisiae*. *Mol Biol Cell* 9, 2767-2784.
- Lottspeich, F. (2006). Proteomanalyse. In *Bioanalytik*, F. Lottspeich, and J. W. Engels, eds. (München, Spektrum Akademischer Verlag), pp. 995-1016.
- Ludovico, P., Madeo, F., and Silva, M. (2005). Yeast programmed cell death: an intricate puzzle. *IUBMB Life* 57, 129-135.
- Ludovico, P., Rodrigues, F., Almeida, A., Silva, M. T., Barrientos, A., and Corte-Real, M. (2002). Cytochrome *c* release and mitochondria involvement in programmed cell death induced by acetic acid in *Saccharomyces cerevisiae*. *Mol Biol Cell* 13, 2598-2606.
- Ludovico, P., Sousa, M. J., Silva, M. T., Leao, C., and Corte-Real, M. (2001). *Saccharomyces cerevisiae* commits to a programmed cell death process in response to acetic acid. *Microbiology* 147, 2409-2415.
- Lupas, A. N., and Martin, J. (2002). AAA proteins. *Curr Opin Struct Biol* 12, 746-753.
- Macfarlane, D. E. (1983). Use of benzyldimethyl-n-hexadecylammonium chloride ("16-BAC"), a cationic detergent, in an acidic polyacrylamide gel electrophoresis system to detect base labile protein methylation in intact cells. *Anal Biochem* 132, 231-235.
- Macfarlane, D. E. (1989). Two dimensional benzyldimethyl-n-hexadecylammonium chloride---sodium dodecyl sulfate preparative polyacrylamide gel electrophoresis: a high capacity high resolution technique for the purification of proteins from complex mixtures. *Anal Biochem* 176, 457-463.
- Madeo, F., Engelhardt, S., Herker, E., Lehmann, N., Maldener, C., Proksch, A., Wissing, S., and Fröhlich, K. U. (2002a). Apoptosis in yeast: a new model system with applications in cell biology and medicine. *Curr Genet* 41, 208-216.
- Madeo, F., Fröhlich, E., and Fröhlich, K. U. (1997). A yeast mutant showing diagnostic markers of early and late apoptosis. *J Cell Biol* 139, 729-734.

Madeo, F., Fröhlich, E., Ligr, M., Grey, M., Sigrist, S. J., Wolf, D. H., and Fröhlich, K. U. (1999). Oxygen stress: a regulator of apoptosis in yeast. *J Cell Biol* 145, 757-767.

Madeo, F., Herker, E., Maldener, C., Wissing, S., Lachelt, S., Herlan, M., Fehr, M., Lauber, K., Sigrist, S. J., Wesselborg, S., and Fröhlich, K. U. (2002b). A caspase-related protease regulates apoptosis in yeast. *Mol Cell* 9, 911-917.

Madeo, F., Herker, E., Wissing, S., Jungwirth, H., Eisenberg, T., and Fröhlich, K. U. (2004). Apoptosis in yeast. *Curr Opin Microbiol* 7, 655-660.

Madeo, F., Schlauer, J., Zischka, H., Mecke, D., and Fröhlich, K. U. (1998). Tyrosine phosphorylation regulates cell cycle-dependent nuclear localization of Cdc48p. *Mol Biol Cell* 9, 131-141.

Manon, S., Chaudhuri, B., and Guerin, M. (1997). Release of cytochrome *c* and decrease of cytochrome *c* oxidase in Bax-expressing yeast cells, and prevention of these effects by coexpression of Bcl-x_L. *FEBS Lett* 415, 29-32.

Marcet, B., and Boeynaems, J. M. (2006). Relationships between cystic fibrosis transmembrane conductance regulator, extracellular nucleotides and cystic fibrosis. *Pharmacol Ther* *Epub ahead of print*.

Martin, S. J., Reutelingsperger, C. P., McGahon, A. J., Rader, J. A., van Schie, R. C., LaFace, D. M., and Green, D. R. (1995). Early redistribution of plasma membrane phosphatidylserine is a general feature of apoptosis regardless of the initiating stimulus: inhibition by overexpression of Bcl-2 and Abl. *J Exp Med* 182, 1545-1556.

Matsuyama, S., Xu, Q., Velours, J., and Reed, J. C. (1998). The Mitochondrial F₀F₁-ATPase proton pump is required for function of the proapoptotic protein Bax in yeast and mammalian cells. *Mol Cell* 1, 327-336.

McNew, J. A., Parlati, F., Fukuda, R., Johnston, R. J., Paz, K., Paumet, F., Sollner, T. H., and Rothman, J. E. (2000). Compartmental specificity of cellular membrane fusion encoded in SNARE proteins. *Nature* 407, 153-159.

Menzel, R., Vogel, F., Kargel, E., and Schunck, W. H. (1997). Inducible membranes in yeast: relation to the unfolded-protein-response pathway. *Yeast* 13, 1211-1229.

Meriin, A. B., and Sherman, M. Y. (2005). Role of molecular chaperones in neurodegenerative disorders. *Int J Hyperthermia* 21, 403-419.

Meusser, B., Hirsch, C., Jarosch, E., and Sommer, T. (2005). ERAD: the long road to destruction. *Nat Cell Biol* 7, 766-772.

Meyer, H. H. (2005). Golgi reassembly after mitosis: the AAA family meets the ubiquitin family. *Biochim Biophys Acta* 1744, 108-119.

Meyer, H. H., Shorter, J. G., Seemann, J., Pappin, D., and Warren, G. (2000). A complex of mammalian ufd1 and npl4 links the AAA-ATPase, p97, to ubiquitin and nuclear transport pathways. *Embo J* 19, 2181-2192.

- Mills, B. G., and Singer, F. R. (1976). Nuclear inclusions in Paget's disease of bone. *Science* *194*, 201-202.
- Mills, J. C., Wang, S., Erecinska, M., and Pittman, R. N. (1995). Use of cultured neurons and neuronal cell lines to study morphological, biochemical, and molecular changes occurring in cell death. *Methods Cell Biol* *46*, 217-242.
- Miyake, T., Sammoto, H., Kanayama, M., Tomochika, K., Shinoda, S., and Ono, B. (1999). Role of the sulphate assimilation pathway in utilization of glutathione as a sulphur source by *Saccharomyces cerevisiae*. *Yeast* *15*, 1449-1457.
- Mizuno, Y., Hori, S., Kakizuka, A., and Okamoto, K. (2003). Vacuole-creating protein in neurodegenerative diseases in humans. *Neurosci Lett* *343*, 77-80.
- Moir, D., Stewart, S. E., Osmond, B. C., and Botstein, D. (1982). Cold-sensitive cell-division-cycle mutants of yeast: isolation, properties, and pseudoreversion studies. *Genetics* *100*, 547-563.
- Monti, M., Orru, S., Pagnozzi, D., and Pucci, P. (2005). Interaction proteomics. *Biosci Rep* *25*, 45-56.
- Naash, M. I., Hollyfield, J. G., al-Ubaidi, M. R., and Baehr, W. (1993). Simulation of human autosomal dominant retinitis pigmentosa in transgenic mice expressing a mutated murine opsin gene. *Proc Natl Acad Sci U S A* *90*, 5499-5503.
- Neuber, O., Jarosch, E., Volkwein, C., Walter, J., and Sommer, T. (2005). Ubx2 links the Cdc48 complex to ER-associated protein degradation. *Nat Cell Biol* *7*, 993-998.
- Neuhoff, V., Arold, N., Taube, D., and Ehrhardt, W. (1988). Improved staining of proteins in polyacrylamide gels including isoelectric focusing gels with clear background at nanogram sensitivity using Coomassie Brilliant Blue G-250 and R-250. *Electrophoresis* *9*, 255-262.
- Newmeyer, D. D., and Ferguson-Miller, S. (2003). Mitochondria: releasing power for life and unleashing the machineries of death. *Cell* *112*, 481-490.
- Nicchitta, C. V. (2002). A platform for compartmentalized protein synthesis: protein translation and translocation in the ER. *Curr Opin Cell Biol* *14*, 412-416.
- Nosseri, C., Coppola, S., and Ghibelli, L. (1994). Possible involvement of poly(ADP-ribosyl) polymerase in triggering stress-induced apoptosis. *Exp Cell Res* *212*, 367-373.
- Ogur, M., and St John, R. (1956). A differential and diagnostic plating method for population studies of respiration deficiency in yeast. *J Bacteriol* *72*, 500-504.
- Ohlmeier, S., Kastaniotis, A. J., Hiltunen, J. K., and Bergmann, U. (2004). The yeast mitochondrial proteome, a study of fermentative and respiratory growth. *J Biol Chem* *279*, 3956-3979.
- Olsson, J. E., Gordon, J. W., Pawlyk, B. S., Roof, D., Hayes, A., Molday, R. S., Mukai, S., Cowley, G. S., Berson, E. L., and Dryja, T. P. (1992). Transgenic mice with a rhodopsin

mutation (Pro23His): a mouse model of autosomal dominant retinitis pigmentosa. *Neuron* 9, 815-830.

Oxelmark, E., Marchini, A., Malanchi, I., Magherini, F., Jaquet, L., Hajibagheri, M. A., Blight, K. J., Jauniaux, J. C., and Tommasino, M. (2000). Mmf1p, a novel yeast mitochondrial protein conserved throughout evolution and involved in maintenance of the mitochondrial genome. *Mol Cell Biol* 20, 7784-7797.

Pamnani, V., Tamura, T., Lupas, A., Peters, J., Cejka, Z., Ashraf, W., and Baumeister, W. (1997). Cloning, sequencing and expression of VAT, a CDC48/p97 ATPase homologue from the archaeon *Thermoplasma acidophilum*. *FEBS Lett* 404, 263-268.

Pappin, D. J. (1997). Peptide mass fingerprinting using MALDI-TOF mass spectrometry. *Methods Mol Biol* 64, 165-173.

Partridge, J. J., Lopreiato, J. O., Jr., Latterich, M., and Indig, F. E. (2003). DNA damage modulates nucleolar interaction of the Werner protein with the AAA ATPase p97/VCP. *Mol Biol Cell* 14, 4221-4229.

Paschen, W. (2004). Endoplasmic reticulum dysfunction in brain pathology: critical role of protein synthesis. *Curr Neurovasc Res* 1, 173-181.

Patel, S., and Latterich, M. (1998). The AAA team: related ATPases with diverse functions. *Trends Cell Biol* 8, 65-71.

Pavlov, E. V., Priault, M., Pietkiewicz, D., Cheng, E. H., Antonsson, B., Manon, S., Korsmeyer, S. J., Mannella, C. A., and Kinnally, K. W. (2001). A novel, high conductance channel of mitochondria linked to apoptosis in mammalian cells and Bax expression in yeast. *J Cell Biol* 155, 725-731.

Perkins, D. N., Pappin, D. J., Creasy, D. M., and Cottrell, J. S. (1999). Probability-based protein identification by searching sequence databases using mass spectrometry data. *Electrophoresis* 20, 3551-3567.

Peters, J. M., Harris, J. R., Lustig, A., Muller, S., Engel, A., Volker, S., and Franke, W. W. (1992). Ubiquitous soluble Mg²⁺-ATPase complex. A structural study. *J Mol Biol* 223, 557-571.

Peters, J. M., Walsh, M. J., and Franke, W. W. (1990). An abundant and ubiquitous homo-oligomeric ring-shaped ATPase particle related to the putative vesicle fusion proteins Sec18p and NSF. *Embo J* 9, 1757-1767.

Piccinini, M., Tazartes, O., Mezzatesta, C., Ricotti, E., Bedino, S., Grosso, F., Dianzani, U., Tovo, P. A., Mostert, M., Musso, A., and Rinaudo, M. T. (2001). Proteasomes are a target of the anti-tumour drug vinblastine. *Biochem J* 356, 835-841.

Pinter, M., Jekely, G., Szepesi, R. J., Farkas, A., Theopold, U., Meyer, H. E., Lindholm, D., Nassel, D. R., Hultmark, D., and Friedrich, P. (1998). TER94, a Drosophila homolog of the membrane fusion protein CDC48/p97, is accumulated in nonproliferating cells: in the reproductive organs and in the brain of the imago. *Insect Biochem Mol Biol* 28, 91-98.

- Pozniakovsky, A. I., Knorre, D. A., Markova, O. V., Hyman, A. A., Skulachev, V. P., and Severin, F. F. (2005). Role of mitochondria in the pheromone- and amiodarone-induced programmed death of yeast. *J Cell Biol* 168, 257-269.
- Prokisch, H., Andreoli, C., Ahting, U., Heiss, K., Ruepp, A., Scharfe, C., and Meitinger, T. (2006). MitoP2: the mitochondrial proteome database--now including mouse data. *Nucleic Acids Res* 34, D705-711.
- Prokisch, H., Scharfe, C., Camp, D. G., 2nd, Xiao, W., David, L., Andreoli, C., Monroe, M. E., Moore, R. J., Gritsenko, M. A., Kozany, C., *et al.* (2004). Integrative analysis of the mitochondrial proteome in yeast. *PLoS Biol* 2, e160.
- Rabilloud, T., Adessi, C., Giraudel, A., and Lunardi, J. (1997). Improvement of the solubilization of proteins in two-dimensional electrophoresis with immobilized pH gradients. *Electrophoresis* 18, 307-316.
- Rabilloud, T., and Charmont, S. (2000). Detection of Proteins on Two-Dimensional Electrophoresis Gels. In *Proteome Research: Two-Dimensional Gel Electrophoresis and Identification Methods*, T. Rabilloud, ed. (Berlin, Springer), pp. 109-112.
- Rabilloud, T., Strub, J. M., Luche, S., van Dorsselaer, A., and Lunardi, J. (2001). A comparison between Sypro Ruby and ruthenium II tris (bathophenanthroline disulfonate) as fluorescent stains for protein detection in gels. *Proteomics* 1, 699-704.
- Rabouille, C., Levine, T. P., Peters, J. M., and Warren, G. (1995). An NSF-like ATPase, p97, and NSF mediate cisternal regrowth from mitotic Golgi fragments. *Cell* 82, 905-914.
- Rape, M., Hoppe, T., Gorr, I., Kalocay, M., Richly, H., and Jentsch, S. (2001). Mobilization of processed, membrane-tethered SPT23 transcription factor by CDC48(UFD1/NPL4), a ubiquitin-selective chaperone. *Cell* 107, 667-677.
- Reifschneider, N. H., Goto, S., Nakamoto, H., Takahashi, R., Sugawa, M., Dencher, N. A., and Krause, F. (2006). Defining the mitochondrial proteomes from five rat organs in a physiologically significant context using 2D blue-native/SDS-PAGE. *J Proteome Res* 5, 1117-1132.
- Reinders, J., and Sickmann, A. (2005). State-of-the-art in phosphoproteomics. *Proteomics* 5, 4052-4061.
- Richly, H., Rape, M., Braun, S., Rumpf, S., Hoegel, C., and Jentsch, S. (2005). A series of ubiquitin binding factors connects CDC48/p97 to substrate multiubiquitylation and proteasomal targeting. *Cell* 120, 73-84.
- Rickwood, D., Dujon, B., and Darley-Usmar, V. M. (1988). Yeast mitochondria. In *Yeast - a practical approach*, I. Campbell, Duffus, J.H., ed. (Oxford, Washington DC, IRL Press), pp. 219-221.
- Rinnerthaler, M., Jarolim, S., Heeren, G., Palle, E., Perju, S., Klinger, H., Bogengruber, E., Madeo, F., Braun, R. J., Breitenbach-Koller, L., *et al.* (2006). MMI1 (YKL056c, TMA19), the yeast orthologue of the translationally controlled tumor protein (TCTP) has apoptotic

functions and interacts with both microtubules and mitochondria. *BBA-Bioenergetics* 1757, 631-638.

Riordan, J. R. (1999). Cystic fibrosis as a disease of misprocessing of the cystic fibrosis transmembrane conductance regulator glycoprotein. *Am J Hum Genet* 64, 1499-1504.

Roggy, J. L., and Bangs, J. D. (1999). Molecular cloning and biochemical characterization of a VCP homolog in African trypanosomes. *Mol Biochem Parasitol* 98, 1-15.

Römisch, K. (2006). Cdc48p is UBX-linked to ER ubiquitin ligases. *Trends Biochem Sci* 31, 24-25.

Rothstein, R. (1991). Targeting, disruption, replacement, and allele rescue: integrative DNA transformation in yeast. *Methods Enzymol* 194, 281-301.

Rouiller, I., Butel, V. M., Latterich, M., Milligan, R. A., and Wilson-Kubalek, E. M. (2000). A major conformational change in p97 AAA ATPase upon ATP binding. *Mol Cell* 6, 1485-1490.

Rouiller, I., DeLaBarre, B., May, A. P., Weis, W. I., Brunger, A. T., Milligan, R. A., and Wilson-Kubalek, E. M. (2002). Conformational changes of the multifunction p97 AAA ATPase during its ATPase cycle. *Nat Struct Biol* 9, 950-957.

Roy, L., Bergeron, J. J., Lavoie, C., Hendriks, R., Gushue, J., Fazel, A., Pelletier, A., Morre, D. J., Subramaniam, V. N., Hong, W., and Paiement, J. (2000). Role of p97 and syntaxin 5 in the assembly of transitional endoplasmic reticulum. *Mol Biol Cell* 11, 2529-2542.

Rumpf, S., and Jentsch, S. (2006). Functional division of substrate processing cofactors of the ubiquitin-selective Cdc48 chaperone. *Mol Cell* 21, 261-269.

Ruohola, H., and Ferro-Novick, S. (1987). Sec53, a protein required for an early step in secretory protein processing and transport in yeast, interacts with the cytoplasmic surface of the endoplasmic reticulum. *Proc Natl Acad Sci U S A* 84, 8468-8472.

Saiki, R. K., Gelfand, D. H., Stoffel, S., Scharf, S. J., Higuchi, R., Horn, G. T., Mullis, K. B., and Erlich, H. A. (1988). Primer-directed enzymatic amplification of DNA with a thermostable DNA polymerase. *Science* 239, 487-491.

Sali, A., Glaeser, R., Earnest, T., and Baumeister, W. (2003). From words to literature in structural proteomics. *Nature* 422, 216-225.

Saliba, R. S., Munro, P. M., Luthert, P. J., and Cheetham, M. E. (2002). The cellular fate of mutant rhodopsin: quality control, degradation and aggresome formation. *J Cell Sci* 115, 2907-2918.

Santoni, V., Molloy, M., and Rabilloud, T. (2000). Membrane proteins and proteomics: un amour impossible? *Electrophoresis* 21, 1054-1070.

Schröder, R., Watts, G. D., Mehta, S. G., Evert, B. O., Broich, P., Fliessbach, K., Pauls, K., Hans, V. H., Kimonis, V., and Thal, D. R. (2005). Mutant valosin-containing protein causes a novel type of frontotemporal dementia. *Ann Neurol* 57, 457-461.

- Schubert, A., and Grimm, S. (2004). Cyclophilin D, a component of the permeability transition-pore, is an apoptosis repressor. *Cancer Res* 64, 85-93.
- Schubert, W. (2003). Topological proteomics, toponomics, MELK-technology. *Adv Biochem Eng Biotechnol* 83, 189-209.
- Schuberth, C., and Buchberger, A. (2005). Membrane-bound Ubx2 recruits Cdc48 to ubiquitin ligases and their substrates to ensure efficient ER-associated protein degradation. *Nat Cell Biol* 7, 999-1006.
- Schuberth, C., Richly, H., Rumpf, S., and Buchberger, A. (2004). Shp1 and Ubx2 are adaptors of Cdc48 involved in ubiquitin-dependent protein degradation. *EMBO Rep* 5, 818-824.
- Schumacher, M. M., Choi, J. Y., and Voelker, D. R. (2002). Phosphatidylserine transport to the mitochondria is regulated by ubiquitination. *J Biol Chem* 277, 51033-51042.
- Severin, F. F., and Hyman, A. A. (2002). Pheromone induces programmed cell death in *S. cerevisiae*. *Curr Biol* 12, R233-235.
- Shah, S. A., Potter, M. W., and Callery, M. P. (2001). Ubiquitin proteasome pathway: implications and advances in cancer therapy. *Surg Oncol* 10, 43-52.
- Sherman, M. Y., and Muchowski, P. J. (2003). Making yeast tremble: yeast models as tools to study neurodegenerative disorders. *Neuromolecular Med* 4, 133-146.
- Shevchenko, A., Wilm, M., Vorm, O., and Mann, M. (1996). Mass spectrometric sequencing of proteins silver-stained polyacrylamide gels. *Anal Chem* 68, 850-858.
- Shirogane, T., Fukada, T., Muller, J. M., Shima, D. T., Hibi, M., and Hirano, T. (1999). Synergistic roles for Pim-1 and c-Myc in STAT3-mediated cell cycle progression and antiapoptosis. *Immunity* 11, 709-719.
- Sickmann, A., Mreyen, M., and Meyer, H. E. (2003a). Mass spectrometry--a key technology in proteome research. *Adv Biochem Eng Biotechnol* 83, 141-176.
- Sickmann, A., Reinders, J., Wagner, Y., Joppich, C., Zahedi, R., Meyer, H. E., Schonfisch, B., Perschil, I., Chacinska, A., Guiard, B., *et al.* (2003b). The proteome of *Saccharomyces cerevisiae* mitochondria. *Proc Natl Acad Sci U S A* 100, 13207-13212.
- Song, C., Wang, Q., and Li, C. C. (2003). ATPase activity of p97-valosin-containing protein (VCP). D2 mediates the major enzyme activity, and D1 contributes to the heat-induced activity. *J Biol Chem* 278, 3648-3655.
- Stasyk, T., and Huber, L. A. (2004). Zooming in: fractionation strategies in proteomics. *Proteomics* 4, 3704-3716.
- Steller, H. (1995). Mechanisms and genes of cellular suicide. *Science* 267, 1445-1449.
- Stenoien, D. L., Cummings, C. J., Adams, H. P., Mancini, M. G., Patel, K., DeMartino, G. N., Marcelli, M., Weigel, N. L., and Mancini, M. A. (1999). Polyglutamine-expanded androgen

receptors form aggregates that sequester heat shock proteins, proteasome components and SRC-1, and are suppressed by the HDJ-2 chaperone. *Hum Mol Genet* 8, 731-741.

Stults, J. T., and Arnott, D. (2005). Proteomics. *Methods Enzymol* 402, 245-289.

Sung, C. H., Davenport, C. M., and Nathans, J. (1993). Rhodopsin mutations responsible for autosomal dominant retinitis pigmentosa. Clustering of functional classes along the polypeptide chain. *J Biol Chem* 268, 26645-26649.

Susin, S. A., Lorenzo, H. K., Zamzami, N., Marzo, I., Snow, B. E., Brothers, G. M., Mangion, J., Jacotot, E., Costantini, P., Loeffler, M., *et al.* (1999). Molecular characterization of mitochondrial apoptosis-inducing factor. *Nature* 397, 441-446.

Taylor, J. P., Hardy, J., and Fischbeck, K. H. (2002). Toxic proteins in neurodegenerative disease. *Science* 296, 1991-1995.

Tebbe, A., Klein, C., Bisle, B., Siedler, F., Scheffer, B., Garcia-Rizo, C., Wolfertz, J., Hickmann, V., Pfeiffer, F., and Oesterhelt, D. (2005). Analysis of the cytosolic proteome of *Halobacterium salinarum* and its implication for genome annotation. *Proteomics* 5, 168-179.

Thoms, S. (2002). Cdc48 can distinguish between native and non-native proteins in the absence of cofactors. *FEBS Lett* 520, 107-110.

Tickle, I., Sharff, A., Vinkovic, M., Yon, J., and Jhoti, H. (2004). High-throughput protein crystallography and drug discovery. *Chem Soc Rev* 33, 558-565.

Tortorella, D., Gewurz, B. E., Furman, M. H., Schust, D. J., and Ploegh, H. L. (2000). Viral subversion of the immune system. *Annu Rev Immunol* 18, 861-926.

Towbin, H., Staehelin, T., and Gordon, J. (1979). Electrophoretic transfer of proteins from polyacrylamide gels to nitrocellulose sheets: procedure and some applications. *Proc Natl Acad Sci U S A* 76, 4350-4354.

Uren, A. G., and Vaux, D. L. (1996). Molecular and clinical aspects of apoptosis. *Pharmacol Ther* 72, 37-50.

Valavanis, C., Hu, Y., Yang, Y., Osborne, B. A., Chouaib, S., Greene, L., Ashwell, J. D., and Schwartz, L. M. (2001). Model cell lines for the study of apoptosis in vitro. *Methods Cell Biol* 66, 417-436.

Vance, J. E. (1990). Phospholipid synthesis in a membrane fraction associated with mitochondria. *J Biol Chem* 265, 7248-7256.

Vance, J. E. (2003). Molecular and cell biology of phosphatidylserine and phosphatidylethanolamine metabolism. *Prog Nucleic Acid Res Mol Biol* 75, 69-111.

Vandecasteele, G., Szabadkai, G., and Rizzuto, R. (2001). Mitochondrial calcium homeostasis: mechanisms and molecules. *IUBMB Life* 52, 213-219.

- Vij, N., Fang, S., and Zeitlin, P. L. (2006). Selective inhibition of endoplasmic reticulum-associated degradation rescues Δ F508-cystic fibrosis transmembrane regulator and suppresses interleukin-8 levels: therapeutic implications. *J Biol Chem* *281*, 17369-17378.
- Vinarov, D. A., and Markley, J. L. (2005). High-throughput automated platform for nuclear magnetic resonance-based structural proteomics. *Expert Rev Proteomics* *2*, 49-55.
- Voelker, D. R. (2003). New perspectives on the regulation of intermembrane glycerophospholipid traffic. *J Lipid Res* *44*, 441-449.
- Voet, D., and Voet, J. G. (1990). Chapter 20: Electron Transport and Oxidative Phosphorylation. In *Biochemistry* (New York, John Wiley & Sons, Inc.) pp. 528-560.
- Waelter, S., Boeddrich, A., Lurz, R., Scherzinger, E., Lueder, G., Lehrach, H., and Wanker, E. E. (2001). Accumulation of mutant huntingtin fragments in aggresome-like inclusion bodies as a result of insufficient protein degradation. *Mol Biol Cell* *12*, 1393-1407.
- Wakabayashi, T. (1999). Structural changes of mitochondria related to apoptosis: swelling and megamitochondria formation. *Acta Biochim Pol* *46*, 223-237.
- Walther, T. C., Brickner, J. H., Aguilar, P. S., Bernales, S., Pantoja, C., and Walter, P. (2006). Eisosomes mark static sites of endocytosis. *Nature* *439*, 998-1003.
- Wang, Q., Song, C., and Li, C. C. (2003a). Hexamerization of p97-VCP is promoted by ATP binding to the D1 domain and required for ATPase and biological activities. *Biochem Biophys Res Commun* *300*, 253-260.
- Wang, Q., Song, C., and Li, C. C. (2004). Molecular perspectives on p97-VCP: progress in understanding its structure and diverse biological functions. *J Struct Biol* *146*, 44-57.
- Wang, Q., Song, C., Yang, X., and Li, C. C. (2003b). D1 ring is stable and nucleotide-independent, whereas D2 ring undergoes major conformational changes during the ATPase cycle of p97-VCP. *J Biol Chem* *278*, 32784-32793.
- Watts, G. D., Wymer, J., Kovach, M. J., Mehta, S. G., Mumm, S., Darvish, D., Pestronk, A., Whyte, M. P., and Kimonis, V. E. (2004). Inclusion body myopathy associated with Paget disease of bone and frontotemporal dementia is caused by mutant valosin-containing protein. *Nat Genet* *36*, 377-381.
- Weber, T., Zemelman, B. V., McNew, J. A., Westermann, B., Gmachl, M., Parlati, F., Sollner, T. H., and Rothman, J. E. (1998). SNAREpins: minimal machinery for membrane fusion. *Cell* *92*, 759-772.
- Weihl, C. C., Dalal, S., Pestronk, A., and Hanson, P. I. (2006). Inclusion body myopathy-associated mutations in p97/VCP impair endoplasmic reticulum-associated degradation. *Hum Mol Genet* *15*, 189-199.
- Weinberger, M., Ramachandran, L., and Burhans, W. C. (2003). Apoptosis in yeasts. *IUBMB Life* *55*, 467-472.

Wessel, D., and Flügge, U. I. (1984). A method for the quantitative recovery of protein in dilute solution in the presence of detergents and lipids. *Anal Biochem* *138*, 141-143.

Wilkins, M. R., Sanchez, J. C., Gooley, A. A., Appel, R. D., Humphery-Smith, I., Hochstrasser, D. F., and Williams, K. L. (1996). Progress with proteome projects: why all proteins expressed by a genome should be identified and how to do it. *Biotechnol Genet Eng Rev* *13*, 19-50.

Wilkins, M. R., Williams, K. L., Appel, R. D., and Hochstrasser, D. F. (1997). *Proteome Research: New Frontiers in Functional Genomics* (Heidelberg, Springer Verlag).

Willer, M., Jermy, A. J., Young, B. P., and Stirling, C. J. (2003). Identification of novel protein-protein interactions at the cytosolic surface of the Sec63 complex in the yeast ER membrane. *Yeast* *20*, 133-148.

Wissing, S., Ludovico, P., Herker, E., Buttner, S., Engelhardt, S. M., Decker, T., Link, A., Proksch, A., Rodrigues, F., Corte-Real, M., *et al.* (2004). An AIF orthologue regulates apoptosis in yeast. *J Cell Biol* *166*, 969-974.

Wojcik, C., Yano, M., and DeMartino, G. N. (2004). RNA interference of valosin-containing protein (VCP/p97) reveals multiple cellular roles linked to ubiquitin/proteasome-dependent proteolysis. *J Cell Sci* *117*, 281-292.

Woodman, P. G. (2003). p97, a protein coping with multiple identities. *J Cell Sci* *116*, 4283-4290.

Wu, D., Chen, P. J., Chen, S., Hu, Y., Nunez, G., and Ellis, R. E. (1999a). *C. elegans* MAC-1, an essential member of the AAA family of ATPases, can bind CED-4 and prevent cell death. *Development* *126*, 2021-2031.

Wu, J. C., Liang, Z. Q., and Qin, Z. H. (2006). Quality control system of the endoplasmic reticulum and related diseases. *Acta Biochim Biophys Sin (Shanghai)* *38*, 219-226.

Wu, X. Q., Lefrancois, S., Morales, C. R., and Hecht, N. B. (1999b). Protein-protein interactions between the testis brain RNA-binding protein and the transitional endoplasmic reticulum ATPase, a cytoskeletal gamma actin and Trax in male germ cells and the brain. *Biochemistry* *38*, 11261-11270.

Wyllie, A. H. (1980). Glucocorticoid-induced thymocyte apoptosis is associated with endogenous endonuclease activation. *Nature* *284*, 555-556.

Wytenbach, A., Sauvageot, O., Carmichael, J., Diaz-Latoud, C., Arrigo, A. P., and Rubinsztein, D. C. (2002). Heat shock protein 27 prevents cellular polyglutamine toxicity and suppresses the increase of reactive oxygen species caused by huntingtin. *Hum Mol Genet* *11*, 1137-1151.

Yamada, T., Okuhara, K., Iwamatsu, A., Seo, H., Ohta, K., Shibata, T., and Murofushi, H. (2000). p97 ATPase, an ATPase involved in membrane fusion, interacts with DNA unwinding factor (DUF) that functions in DNA replication. *FEBS Lett* *466*, 287-291.

- Yamanaka, K., Okubo, Y., Suzaki, T., and Ogura, T. (2004). Analysis of the two p97/VCP/Cdc48p proteins of *Caenorhabditis elegans* and their suppression of polyglutamine-induced protein aggregation. *J Struct Biol* 146, 242-250.
- Yarm, F. R. (2002). Plk phosphorylation regulates the microtubule-stabilizing protein TCTP. *Mol Cell Biol* 22, 6209-6221.
- Ye, Y. (2005). The role of the ubiquitin-proteasome system in ER quality control. *Essays Biochem* 41, 99-112.
- Ye, Y. (2006). Diverse functions with a common regulator: Ubiquitin takes command of an AAA ATPase. *J Struct Biol*.
- Ye, Y., Meyer, H. H., and Rapoport, T. A. (2001). The AAA ATPase Cdc48/p97 and its partners transport proteins from the ER into the cytosol. *Nature* 414, 652-656.
- Ye, Y., Shibata, Y., Kikkert, M., van Voorden, S., Wiertz, E., and Rapoport, T. A. (2005). Inaugural Article: Recruitment of the p97 ATPase and ubiquitin ligases to the site of retrotranslocation at the endoplasmic reticulum membrane. *Proc Natl Acad Sci U S A* 102, 14132-14138.
- Ye, Y., Shibata, Y., Yun, C., Ron, D., and Rapoport, T. A. (2004). A membrane protein complex mediates retro-translocation from the ER lumen into the cytosol. *Nature* 429, 841-847.
- Yuasa, T., Hayashi, T., Ikai, N., Katayama, T., Aoki, K., Obara, T., Toyoda, Y., Maruyama, T., Kitagawa, D., Takahashi, K., *et al.* (2004). An interactive gene network for securin-separase, condensin, cohesin, Dis1/Mtc1 and histones constructed by mass transformation. *Genes Cells* 9, 1069-1082.
- Zahedi, R. P., Meisinger, C., and Sickmann, A. (2005). Two-dimensional benzyldimethyl-n-hexadecylammonium chloride/SDS-PAGE for membrane proteomics. *Proteomics* 5, 3581-3588.
- Zahedi, R. P., Sickmann, A., Boehm, A. M., Winkler, C., Zufall, N., Schonfisch, B., Guiard, B., Pfanner, N., and Meisinger, C. (2006). Proteomic analysis of the yeast mitochondrial outer membrane reveals accumulation of a subclass of preproteins. *Mol Biol Cell* 17, 1436-1450.
- Zelenaya-Troitskaya, O., Perlman, P. S., and Butow, R. A. (1995). An enzyme in yeast mitochondria that catalyzes a step in branched-chain amino acid biosynthesis also functions in mitochondrial DNA stability. *Embo J* 14, 3268-3276.
- Zhang, D., Li, F., Weidner, D., Mnjoyan, Z. H., and Fujise, K. (2002). Physical and functional interaction between myeloid cell leukemia 1 protein (MCL1) and Fortilin. The potential role of MCL1 as a fortilin chaperone. *J Biol Chem* 277, 37430-37438.
- Zhang, H., Wang, Q., Kajino, K., and Greene, M. I. (2000a). VCP, a weak ATPase involved in multiple cellular events, interacts physically with BRCA1 in the nucleus of living cells. *DNA Cell Biol* 19, 253-263.

Zhang, X., Lester, R. L., and Dickson, R. C. (2004). Pil1p and Lsp1p negatively regulate the 3-phosphoinositide-dependent protein kinase-like kinase Pkh1p and downstream signaling pathways Pkc1p and Ypk1p. *J Biol Chem* 279, 22030-22038.

Zhang, X., Shaw, A., Bates, P. A., Newman, R. H., Gowen, B., Orlova, E., Gorman, M. A., Kondo, H., Dokurno, P., Lally, J., *et al.* (2000b). Structure of the AAA ATPase p97. *Mol Cell* 6, 1473-1484.

Zimmermann, J. (2006). DNA-Sequenzierung. In *Bioanalytik*, F. Lottspeich, and J. W. Engels, eds. (München, Spektrum Akademischer Verlag), pp. 777-803.

Zischka, H., Braun, R. J., Marantidis, E. P., Büringer, D., Bornhoevd, C., Hauck, S. M., Demmer, O., Gloeckner, C. J., Reichert, A. S., Madeo, F., and Ueffing, M. (2006). Differential analysis of *Saccharomyces cerevisiae* mitochondria by free-flow electrophoresis. *Mol Cell Proteomics E-Pub ahead of print*.

Zischka, H., Kinkl, N., Braun, R. J., and Ueffing, M. (submitted). Purification of *Saccharomyces cerevisiae* mitochondria by zone-electrophoresis in a free flow device (ZE-FFE). In *Methods in Molecular Biology: Organelle Proteomics*, D. Pflieger, and J. S. Rossier, eds.

Zischka, H., Weber, G., Weber, P. J., Posch, A., Braun, R. J., Büringer, D., Schneider, U., Nissum, M., Meitinger, T., Ueffing, M., and Eckerskorn, C. (2003). Improved proteome analysis of *Saccharomyces cerevisiae* mitochondria by free-flow electrophoresis. *Proteomics* 3, 906-916.

Zou, H., Li, Y., Liu, X., and Wang, X. (1999). An APAF-1/cytochrome *c* multimeric complex is a functional apoptosome that activates procaspase-9. *J Biol Chem* 274, 11549-11556.

Zwickl, P., and Baumeister, W. (1999). AAA-ATPases at the crossroads of protein life and death. *Nat Cell Biol* 1, E97-98.

I. Annex

1. Figure index

Figure	Title	Page
1	Structure of the AAA-ATPase Cdc48p/VCP	21
2	Specific disassembly of protein complexes by the AAA-ATPase Cdc48p/VCP	22
3	Role of Cdc48p/VCP in ER-associated protein degradation (ERAD)	25
4	VCP causes upon mutation the protein deposit disorder IBMPFD and endogenous VCP is a sensor of aggregated proteins causative for neurodegenerative disorders	30
5	Viability in the <i>cdc48^{S565G}</i> strain is significantly decreased upon growth in glucose medium and heat shock	88
6	DNA fragmentation can be induced in the majority of <i>cdc48^{S565G}</i> cells	89
7	Differential 2-DE analysis of mitochondrial and cytosolic extracts from wild-type and <i>cdc48^{S565G}</i> cells under apoptotic growth conditions (13 h and 20 h)	91
8	Protein spot alterations between wild-type and <i>cdc48^{S565G}</i> strains in mitochondrial extracts under apoptotic growth conditions (20 h)	92
9	Mitochondria are enlarged in <i>cdc48^{S565G}</i> cells	98
10	Respiratory deficiency of <i>cdc48^{S565G}</i> cells	99
11	Release of cytochrome <i>c</i> into the cytosol of <i>cdc48^{S565G}</i> cells	101
12	Reactive oxygen species accumulate in <i>cdc48^{S565G}</i> cells	102
13	The cytochrome <i>bc₁</i> complex is major producer of ROS in <i>cdc48^{S565G}</i> cells	103
14	Wild-type ρ^0 and <i>cdc48^{S565G}</i> ρ^0 strains showed very low levels of ROS production and highly similar viability	105
15	Emergence of caspase-like enzymatic activity in the <i>cdc48^{S565G}</i> strain	106
16	<i>CDC48</i> mutation (<i>cdc48^{S565G}</i>) leads to accumulation of polyubiquitinated proteins and ER stress	108
17	Polyubiquitinated proteins and Cdc48p-S565G co-migrate with microsomes and mitochondria in the <i>cdc48^{S565G}</i> strain	110
18	Crude mitochondria can be separated in a main and a side fraction by zone electrophoresis in a free-flow device (ZE-FFE)	112
19	The ZE-FFE main fractions contain purified mitochondria whereas the ZE-FFE side fractions represent a mitochondrial side fraction enriched with NE-ER-associated proteins	117
20	Polyubiquitinated proteins and Cdc48p-S565G accumulate in a mitochondrial side fraction enriched with NE-ER-associated proteins obtained by ZE-FFE	119
21	Microsomal vesicles stably co-migrate with mitochondria in ZE-FFE side fractions of the <i>cdc48^{S565G}</i> strain	120
22	Mitochondria show markedly increased proximity to the NE-ER in <i>cdc48^{S565G}</i> cells	121
23	VCP variants used in this study	124
24	Expression of ATPase-deficient VCP-K524A and of VCP-S555G leads to severe morphological alterations	126
25	Expression of ATPase-deficient VCP-K524A and of VCP-S555G but not of IBMPFD-causing VCP-R155H results in decreased cell viability	127
26	Expression of VCP-K524A and VCP-S555G leads to cytoplasmic vacuolization, nuclear condensation and cell death	128
27	Apoptotic cell death upon expression of VCP-K524A and VCP-S555G is paralleled by accumulation of polyubiquitinated proteins	130
28	Expression of rhodopsin in HEK293 cells	133
29	VCP mutation leads to accumulation of rhodopsin	134
30	Model of apoptosis in <i>cdc48^{S565G}</i> yeast	144

2. Table index

Table	Title	Page
1	Primer for cloning of VCP	41
2	Mutagenesis primer	41
3	Sequencing and PCR primer	41
4	Plasmids	41
5	Constructs	42
6	Yeast strains	43
7	Mammalian cell lines	43
8	Antibodies against yeast proteins	43
9	Antibodies against mammalian proteins	43
10	Secondary antibodies	44
11	Gel solution for SDS separating gel (60 mL)	47
12	Gel solution for SDS stacking gel (15 mL)	47
13	Gel solution for second dimension in 2-DE	55
14	Gel solution for 16-BAC separating gel (40 mL)	57
15	Gel solution for 16-BAC stacking gel (10 mL)	58
16	Identified proteins differentially found in mitochondrial extracts under apoptotic growth conditions (13 h and 20 h time points)	94
17	Identified proteins of ZE-FFE-purified mitochondria	113
18	Identified proteins in the ZE-FFE side fractions	114

3. Publications and presentations

Journals (peer-reviewed):

Zischka H., Braun R.J., Marantidis E.P., Büringer D., Bornhoevd C., Hauck S.M., Demmer O., Gloeckner C.J., Reichert A.S., Madeo F., Ueffing M. Differential analysis of *Saccharomyces cerevisiae* mitochondria by free-flow electrophoresis. Mol. Cell Proteomics 2006 August 17, E-pub ahead of print. #

Braun R.J.*, Zischka H.*, Madeo F., Engelhardt S.M., Wissing S., Büringer D., Ueffing M. Crucial mitochondrial impairment upon *CDC48* mutation in apoptotic yeast. J. Biol. Chem., 2006 July 10, E-pub ahead of print. #

Rinnerthaler M., Jarolim S., Heeren G., Palle E., Perju S., Klinger H., Bogengruber E., Madeo F., Braun R.J., Breitenbach-Koller L., Breitenbach M., Laun P. MMI1 (YKL056c, TMA19), the yeast orthologue of the translationally controlled tumor protein (TCTP) has apoptotic functions and interacts with both microtubules and mitochondria. Biochim Biophys Acta. 2006 May-June; **1757**(5-6):631-8. Epub 2006 May 20. #

Gloeckner C.J., Kinkl N., Schumacher A., Braun R.J., O'Neill E., Meitinger T., Kolch W., Prokisch H., Ueffing M. The Parkinson disease causing LRRK2 mutation I2020T is associated with increased kinase activity. Hum. Mol. Genet. 2006; **15**(2):223-32.

Zischka H., Weber G., Weber P.J., Posch A., Braun R.J., Büringer D., Schneider U., Nissum M., Meitinger T., Ueffing M., Eckerskorn C. Improved proteome analysis of *Saccharomyces cerevisiae* mitochondria by free-flow electrophoresis. Proteomics 2003; **3**(6):906-16.

Book sections:

Zischka H.*, Kinkl N.*, Braun R.J., Ueffing M. Purification of *Saccharomyces cerevisiae* mitochondria by zone-electrophoresis in free flow device (ZE-FFE). Organelle Proteomics, Methods Mol. Biol.; *in press*.

Braun R.J.*, Kinkl N.*, Zischka H., Ueffing, M. Analysis of membrane proteins of yeast mitochondria purified by free flow electrophoresis. Methods in the Proteomics of Membrane Proteins, Methods Mol. Biol.; *submitted*. #

Poster presentations:

Braun R.J., Zischka H., Ueffing M. Impaired functionality of mutated Cdc48p in the ER-associated protein degradation pathway triggers mitochondria-mediated cell death. NGFN meeting in Bonn, Germany, November 2005

Braun R.J.*, Zischka H.*, Madeo F., Engelhardt S.M., Wissing S., Büringer D., Ueffing M. Impaired functionality of mutated Cdc48p in the ER-associated protein degradation pathway triggers mitochondria-mediated cell death. 4th Annual World Congress of HUPO, Munich, Germany, August 2005

Braun R.J.*, Zischka H.*, Madeo F., Engelhardt S.M., Wissing S., Büringer D., Ueffing M. Impaired functionality of mutated Cdc48p in the ER-associated protein degradation pathway

triggers mitochondria-mediated cell death. BMBF Statusseminar Proteomics, Potsdam, Germany, May 2005

Oral presentations:

Braun R., Analysis of Cdc48p/VCP-Variants in Cell Death, 5. Human Brain Proteome Meeting, Schloss Rauschholzhausen near Marburg, Germany, November 2005

Wissing S., Ligr M., Braun R., Zischka H., Wolf H.-D., Fröhlich K.-U., Laun P., Breitenbach M., Madeo F., Potential Mechanisms of *cdc48*^{S565G} Induced Apoptosis. 2nd International Meeting on Yeast Apoptosis, Slomenice, Slovakia, September 2003

* These authors equally contributed to this work.

Part of the data presented in this PhD thesis were published.

4. Acknowledgments

Diese Arbeit wurde in der Arbeitsgruppe Dr. Marius Ueffing am Institut für Humangenetik (Leitung: Prof. Thomas Meitinger) des GSF-Forschungszentrums in München-Neuherberg durchgeführt. Die Betreuung an der GSF erfolgte durch Dr. Marius Ueffing und die Betreuung und Vertretung dieser Arbeit an der TU München erfolgte durch Prof. Jerzy Adamski.

Die Vorarbeiten zur vorliegenden Arbeit habe ich als Diplomand in der Arbeitsgruppe Dr. Frank Madeo am Physiologisch-chemischen Institut der Universität Tübingen und in der Arbeitsgruppe Dr. Marius Ueffing an der GSF unter Betreuung von Dr. Hans Zischka durchgeführt. Bei Marius möchte ich mich dafür bedanken, dass ich als Doktorand in seiner Arbeitsgruppe das angearbeitete Thema erfolgreich weiterführen und wesentlich weiterentwickeln konnte. Weiterhin, möchte ich mich für seine Kritiken zu dieser Arbeit und für die Unterstützung, insbesondere im letzten Jahr dieser Arbeit, bedanken. Desweiteren ermöglichte Marius mir einen ersten Einblick in die Funktionsweise des deutschen und europäischen Wissenschaftsbetriebs.

Bei Prof. Jerzy Adamski möchte ich mich herzlich für die Betreuung, das große Interesse an dieser Arbeit, und für seinen großen Einsatz als externer Doktorvater bedanken. Die konstruktiven Anmerkungen von Jurek und seine Unterstützung haben dieser Arbeit wesentlich geholfen. Den Mitgliedern seiner Arbeitsgruppe, insbesondere Dr. Gabriele Möller, danke ich für das Interesse an meiner Arbeit und für die geleistete Unterstützung.

Bei Dr. Hans Zischka möchte ich mich für die Betreuung während dem ersten Jahr meiner Doktorarbeit bedanken. Hans führte mich insbesondere in die proteomischen Techniken (2-DE Gelelektrophorese und Massenspektrometrie) ein und brachte mir das Paper-Schreiben bei. Bei letzterem hatten wir beide eine lange Durststrecke zu gehen, die wir jedoch mittlerweile erfolgreich überstanden haben.

Bei Prof. Frank Madeo möchte ich mich für die über die letzten Jahre geleistete Unterstützung bedanken. Frank hat nie an dieser Arbeit gezweifelt und mir Mut gemacht. Ich möchte mich insbesondere für die gewährte experimentelle Unterstützung bedanken, die es letztendlich ermöglicht haben, wesentliche Teile der vorliegenden Arbeit zu publizieren. Seinen Doktoranden Silvia Engelhardt (Cytochrom *c*), Silke Wissing (Caspase), Tobias Eisenberg (ρ_0 -Stämme) und Sabrina Büttner (ρ_0 -Stämme) danke ich daher sehr für ihre Hilfe und ihren Einsatz!

Bei Prof. Thomas Meitinger bedanke ich mich für das Interesse an meiner Arbeit und die direkte aber konstruktive Kritik.

Bei Dr. Norbert Kinkl bedanke ich mich für die vielfältige Unterstützung, die er mir während dieser Arbeit gewährt hat: Beginnend mit dem Beibringen experimenteller Fertigkeiten (z.B. Fluoreszenzmikroskopie und Zellkultur), mit dem kritischen Korrekturlesen verschiedenster Paper-Versionen und vor allem auch der vorliegenden Dissertation. Desweiteren bedanke ich mich bei Norbert für die ständigen wissenschaftlichen Diskussionen, die dieser Arbeit wesentlich genützt haben. Nicht zu vergessen sind jedoch auch die unzähligen Kaffeepausen und das Bereitstellen nicht-wissenschaftlicher Nervennahrung in Buchform (Terry Pratchett).

Bei Dr. Stefanie Hauck möchte ich mich für ihr Interesse und ihre Unterstützung für diese Arbeit, für wissenschaftliche und außer-wissenschaftliche Diskussionen bedanken. Insbesondere danke ich Steffi für das Korrekturlesen dieser Dissertation.

Bei Dr. Ch. Johannes Gloeckner möchte ich mich für seine Unterstützung, insbesondere was die Molekularbiologie und Computer betrifft, bedanken. Johannes' Hilfsbereitschaft ist einfach unbegrenzt!

Bei Dr. Ursula Olazabal möchte ich mich bedanken, dass sie es als Labor-Koordinatorin versteht, die wachsende Arbeitsgruppe zusammenzuhalten. Ohne Ursula und ihre guten Verbindungen wäre die Arbeitsgruppe schon lange im Chaos versunken; und wer sollte auch die Labmeetings im Biergarten oder im Oktoberfestzelt organisieren?

Bei Dr. Magdalena Swiatek-de Lange möchte ich für ihre Unterstützung bedanken. Insbesondere ist jedoch hervorzuheben, dass Magda Leben ins Labor gebracht hat, was uns schrecklich bewusst wurde, seit sie das Labor verlassen hat.

Meiner Praktikantin und späteren Diplomandin Katja Huemer danke ich für ihre Vorschläge, ihre Kritik und die zahlreichen Diskussionen. Katjas Arbeit, die sich aus der vorliegenden Dissertation entwickelt hat, wird die zukünftige Entwicklung des Projektes wesentlich erleichtern.

Meinem Hiwi Julian Bucher danke ich für seine technische Unterstützung im letzten dreiviertel Jahr meiner Arbeit. Julians Arbeitseinsatz und Zuverlässigkeit ist zu verdanken, dass die Arbeit am Ende noch einmal richtig an Fahrt gewinnen konnte.

Bei Matthias Bauer, Gabriele Dütsch, Elöd Kortvely, Stephanie Schöffmann, Annette Schumacher, bei meinen Mit-Doktoranden Monika Beer, Karsten Boldt, Ana Griciuc und Andrea Meixner sowie bei den ehemaligen Praktikanten/Diplomanden/TAs/Doktoranden Oliver Demmer, Nikki Kolb, Enrico Marantidis, Brigitte Haupt, Stefanie Willmann und Jordanos Kiflemariam bedanke ich mich für die sehr angenehme und kooperative Arbeitsatmosphäre in der Arbeitsgruppe. Bei Monika bewundere ich ihre ansteckende

Fröhlichkeit, die auch kein misslungenes Experiment beeinträchtigen kann, bei Annette und Karsten ihre Ruhe, bei Stephanie ihre Arbeitseffizienz. Bei Andrea bedanke ich mich für die Abwechslung bei den gemeinsamen Meetings (NGFN, „Human P...“, Neurotrain).

Bei Dietmute Büringer bedanke ich mich für ihre Kooperation in Sachen Elektronenmikroskopie und bei Dr. Peter Hutzler bedanke ich mich für die Hilfe bei der hochauflösenden Fluoreszenzmikroskopie.

Bei meinen Eltern und bei meinem Bruder bedanke ich mich für die über Jahre geleistete Unterstützung in jeglicher Form. Insbesondere muss ich mich aber bei meiner Freundin Angelika bedanken, die unter dem hohen Zeitaufwand der Arbeit zu leiden hatte, die mir aber trotzdem Halt gegeben hat und die Marotten eines gelegentlich etwas verwirrten Wissenschaftlers zu tolerieren weiß.

5. *Curriculum vitae*

Lebenslauf

Ralf J. Braun

*30.01.1977 in Oppenau/Schwarzwald

Ausbildung

- Seit 11/2002 Doktorarbeit in der Arbeitsgruppe Dr. Marius Ueffing am Institut für Humangenetik, GSF-Forschungszentrum für Umwelt und Gesundheit, Neuherberg bei München
- 08/2002-10/2002 Wissenschaftliche Hilfskraft in der Arbeitsgruppe Dr. Marius Ueffing am Institut für Humangenetik, GSF
- 07/2002 Abschluss des Studiums der Biochemie an der Eberhard-Karls-Universität Tübingen
Abschluss: Diplom-Biochemiker, Gesamtnote: „Sehr gut“
- 11/2001-07/2002 Diplomarbeit in der Arbeitsgruppe Dr. Frank Madeo am Physiologisch-chemischen Institut der Eberhard-Karls Universität Tübingen in Kooperation mit der Arbeitsgruppe Dr. Marius Ueffing am Institut für Humangenetik, GSF
Thema der Diplomarbeit:
„Detaillierte Proteomanalyse des apoptotischen Programms der Hefemutante Cdc48^{S565G}.“
- 04/2000-03/2001 Praktisches Jahr am Max-Planck-Institut für Biochemie, Martinsried bei München
- 10/1999-07/2002 Hauptstudium im Studienfach Biochemie an der Eberhard-Karls-Universität Tübingen
Hauptfächer: Biochemie und Physikalische Chemie, Wahlfach: Genetik
- 04/1997-09/1999 Grundstudium im Studienfach Biochemie an der Eberhard-Karls-Universität Tübingen
- 07/1996-04/1997 Wehrdienst im Jägerbataillon 292/Deutsch-Französische Brigade in Donaueschingen
- 1987-06/1996 Hans-Furler Gymnasium, Oberkirch/Baden
Abschluss: Allgemeine Hochschulreife
Gesamtnote: 1,1
- 1983-1987 Grund- und Hauptschule, Oppenau/Schwarzwald